CASCADE REALIZATION OF COMPLEX WAVE DIGITAL AND ANALOG NETWORKS

by

Gordon B. Scarth

A thesis presented to the Faculty of Graduate Studies
University of Manitoba
in partial fulfillment of the requirements for the degree
Doctor of Philosophy

February 1992, Winnipeg, Manitoba

National Library of Canada
Bibliothèque nationale du Canada

Acquisitions and Bibliographic Services Branch
Direction des acquisitions et des services bibliographiques

395 Wellington Street
Ottawa, Ontario
K1A 0N4

395, rue Wellington
Ottawa (Ontario)
K1A 0N4

Your file Votre référence

Our file Notre référence

The author has granted an irrevocable non-exclusive licence allowing the National Library of Canada to reproduce, loan, distribute or sell copies of his/her thesis by any means and in any form or format, making this thesis available to interested persons.

L'auteur a accordé une licence irrévocable et non exclusive permettant à la Bibliothèque nationale du Canada de reproduire, prêter, distribuer ou vendre des copies de sa thèse de quelque manière et sous quelque forme que ce soit pour mettre des exemplaires de cette thèse à la disposition des personnes intéressées.

The author retains ownership of the copyright in his/her thesis. Neither the thesis nor substantial extracts from it may be printed or otherwise reproduced without his/her permission.

L'auteur conserve la propriété du droit d'auteur qui protège sa thèse. Ni la thèse ni des extraits substantiels de celle-ci ne doivent être imprimés ou autrement reproduits sans son autorisation.

ISBN 0-315-77816-4

Canada

CASCADE REALIZATION OF COMPLEX WAVE DIGITAL AND ANALOG NETWORKS

BY

GORDON B. SCARTH

A thesis submitted to the Faculty of Graduate Studies of the University of Manitoba in partial fulfillment of the requirements for the degree of

DOCTOR OF PHILOSOPHY

© 1992

Permission has been granted to the LIBRARY OF THE UNIVERSITY OF MANITOBA to lend or sell copies of this thesis to the NATIONAL LIBRARY OF CANADA to microfilm this thesis and to lend or sell copies of the film, and UNIVERSITY MICROFILMS to publish an abstract of this thesis.

The author reserves other publication rights, and neither the thesis nor extensive extracts from it may be printed or otherwise reproduced without the author's written permission.

I hereby declare that I am the sole author of this thesis.

I authorize the University of Manitoba to lend this thesis to other institutions or individuals for the purpose of scholarly research.

Gordon B. Scarth

I further authorize the University of Manitoba to reproduce this thesis by photocopying or by other means, in total or in part, at the request of other institutions or individuals for the purpose of scholarly research.

Gordon B. Scarth

Abstract

Fettweis first proposed that a complex reference network can be implemented using real wave digital (WD) elements by requiring the property known as one-realness. A one-real network simply has a real driving-point impedance when evaluated at unity. This thesis developes a new theory for complex wave digital (WD) filters allowing the realization of general complex reference networks without alteration to make them one-real. Thus the networks do not require the property of one-realness and all quantities are allowed to be complex.

A port reference impedance is now allowed to be complex, containing a constant positive resistance and a constant reactance (imaginary resistor). The voltage wave incident and reflected wave variables, A and B, are redefined as

$$A = V + Z I$$

$$B = V - Z^* I$$

and the familiar concept of the WD mapping of analog networks is preserved. The generalization reduces to the known theory of real WD filters if all quantities are real and, furthermore, a stability theory exists. The resulting definition of power is the same as suggested by Fettweis. The existence of complex port impedances is necessary and sufficient for the computability of a complex WD network unless the network is composed of one-real sections, when the port impedances can be real. Thus, a motivation for the generalization is found in the additional degree of freedom in the choice of the imaginary part of the port reference (that is, there is an additional parameter), which can be used *simultaneously* to guarantee computability of the complex WD network and to simplify the CWD elements.

Many useful complex dynamic and non-dynamic one-ports, as well as non-dynamic two-ports that do not have a real WD equivalent can now be defined from the new definitions of the signal variables. The analog series connected imaginary resistor when viewed as a two-port has a complex WD equivalent as a simple pass-through connection. In contrast, the analog parallel connected imaginary resistor when viewed as a two-port has a WD equivalent of a pair of mutually inverse conjugate multipliers in the signal paths which is a hybrid form of scaling. Thus the definition of the voltage waves has a bias towards series connections. Similarly, the dual definition of complex current waves has a bias towards parallel connections.

The new definitions of the incident and reflected wave variables lead to new definitions for the complex n-port series and parallel adaptors which allow complex port references.

The complex series three-port adaptor with a reflection-free port has the same scattering matrix as the real case. Thus, no extra computations are needed, that is, there is no penalty for having free parameters in the port references. The complex three-port parallel adaptor is more complicated than the series adaptor. Equivalences between the three-port adaptors only exist when each adaptor contains a reflection-free port, in which case each adaptor can be decomposed into combinations of real two-port adaptors and pairs of mutually inverse conjugate multipliers.

The complex reference networks are designed using a new generalization of the synthesis algorithm, given in [16], to the complex domain. The algorithm is novel since it does not require the use of zero-finding or polynomial manipulation routines associated with the determination of intermediate polynomials, namely, it is based entirely on polynomial evaluations. Complex networks are derived with general first-order complex sections which are capable of independently realizing a transmission zero anywhere in the complex plane. It is found that a more judicious representation for a complex elementary section, from the viewpoint of network synthesis, is a set of canonic parameters rather than the set of lumped-element parameters. The canonic parameters completely characterize a section and are given by the location of the transmission zero, the reflectance evaluated at the transmission zero, and for reciprocal sections, the return group delay (or simply the delay) evaluated at the transmission zero.

A complex WD ladder network is realized from a complex reference filter using one of two methods. The first method maps a complex reciprocal reference network to the equivalent CWD network on an element-by-element basis. This inherently requires the use of complex three-port series and parallel adaptors. The second method maps a complex elementary section as a dynamic two-port to the CWD equivalent. This method requires at most two real normalized two-port adaptors and two unimodular multipliers for each dynamic section, which is referred to as the canonic cascade section. From the examples presented, the realization method using the cascade section appears less sensitive to binary quantizations than the method using three-port adaptors.

Acknowledgements

The author wishes to express his sincere gratitude to Professor G. O. Martens for his support, guidance and encouragement during the course of this work. He also wishes to thank his colleagues M. Jarmasz, R. Smith, V. Cheng and L. Leung for many informative discussions. Thanks are also given to the author's parents, family and friends for their support and to the many Engineering students who have encouraged the author during this work. Financial support from the Natural Sciences and Engineering Research Council and the University of Manitoba is greatly appreciated.

Table of Contents

Abstract iii

Acknowledgements v

List Of Figures ix

List Of Tables xii

I **Introduction** 1

II **Complex Analog Networks** 8
- 2.1 New Complex Elements 8
- 2.2 The Positive Function 10
- 2.3 Properties of A Complex Lossless Immittance 11
- 2.4 Canonic Polynomial Representation of A Complex Lossless Two-Port . . 13
- 2.5 Reflection-Free Port of A Complex Lossless Two-Port 18
- 2.6 Complex Elementary Sections 21
  - 2.6.1 Complex First-Order Reciprocal Sections 22
    - 2.6.1.1 Sections that Realize a Transmission Zero at Infinity 22
    - 2.6.1.2 Sections that Realize a Transmission Zero at the Origin 24
    - 2.6.1.3 Sections that Realize a Transmission Zero On the Finite $j\phi$ Axis . . 26
  - 2.6.2 Complex First-Order Non-Reciprocal Sections 30
    - 2.6.2.1 Sections that Realize a Transmission Zero Anywhere in ψ Plane . . 31
    - 2.6.2.2 Sections that Realize a Transmission Zero on the Real Axis . . . 33
  - 2.6.3 Complex Constant Sections 35
- 2.7 Real elementary Sections 39
  - 2.7.1 First Order Reciprocal Real Sections 39
  - 2.7.2 First Order Non-Reciprocal Real Sections 42
  - 2.7.3 Second Order Reciprocal Real Sections 44
- 2.8 Equivalences Between the Brune Section and the Complex Sections . . . 47
- 2.9 Equivalences Between the Complex Sections 50

III **Synthesis Of Complex Lossless Two-Ports** 53
3.1 Extraction of An Elementary Section via Factorization of the Scattering Transfer Matrix 54
3.2 Canonic Representation of Elementary Complex Sections 56
3.3 Recomputation for the Remaining Network 58
3.4 Calculation of the Reflectance and the Delay 61
3.5 Complex Synthesis Algorithm 65
3.6 Extraction of the Last (Constant Complex) Section 67
3.7 Recomputation Using a Constant Complex Section 68
3.8 Design Examples 69

IV **Introduction To Complex Wave Digital Networks** 72
4.1 Definition of the Complex Voltage and Power Wave Variables 72
4.2 Definition of Power 76
4.3 Two-Port Scattering Matrix 78
4.4 Impedances Mapped to the CWD Domain 80
4.4.1 One-port Impedances 80
4.4.2 Non-Dynamic Two-Ports 83
4.5 Interconnection of Ports 86
4.6 CWDF Adaptors 87
4.6.1 General n-port Complex Series Adaptor 87
4.6.1.1 Definition of the Complex Series Adaptor 88
4.6.1.2 Dependent Coefficient 90
4.6.1.3 Reflection-free Port 90
4.6.1.4 Symbols of the General n-port Complex Series Adaptor 92
4.6.1.5 Complex Three-port Series Adaptor 92
4.6.2 General n-port Complex Parallel Adaptor 95
4.6.2.1 Definition of the Complex Parallel Adaptor 95
4.6.2.2 Dependent Coefficient 97
4.6.2.3 Reflection-free Port 98
4.6.2.4 Symbols of the General n-port Complex Parallel Adaptor 99
4.6.2.5 Complex Three-port Parallel Adaptor 99
4.6.3 Equivalence Between the Reflection-free Three-port Adaptors 104
4.6.4 Complex Two-port Adaptor 106
4.6.5 Equivalence Between the Complex Two-port Adaptor and Complex Transformer 114
4.6.6 Complex Two-port and Three-port Adaptor Equivalences 116
4.7 Robustness of Complex Wave Digital Filters 119
4.7.1 Stability of Complex Wave Digital Filters 120

4.7.2 Robustness 123

V **Cascade and Ladder Realizations Using Complex Wave Digital Networks** 125
5.1 Ladder Realization Using three-port Adaptors 126
5.1.1 CWD Realization of Complex Reference Networks 126
5.1.2 Scaling the CWD Networks 129
5.1.2.1 L_∞-Norm Scaling 130
5.1.2.2 L_2-Norm Scaling 130
5.1.3 Quantization of A CWD Network 130
5.2 Design Examples Using 3-port Complex Adaptors 131
5.2.1 Non-canonic CWD Realization of Frequency Shifted Filters 131
5.2.2 Canonic CWD Realization of Complex Filters 133
5.2.2.1 Realization Using Complex Parallel Adaptors Exclusively 133
5.2.2.2 Realization Using Complex Series Adaptors Exclusively 136
5.2.2.3 Comments On the Two Equivalent Realizations 139
5.2.2.4 Elliptic Example of order 5 139
5.3 Cascade Realization of Complex Networks 142
5.3.1 Derivation of the Canonic Cascade Section 142
5.3.2 Canonic First-Order Complex Sections Mapped to the CWD Domain . 146
5.3.3 Complex Zero-Order (Constant) Complex Sections 153
5.3.4 CWD Ladder Realization 156
5.3.5 Canonic Cascade Section Using Real 2-port Adaptors 157
5.3.6 Minimum Multiplier Realization of CWD Filters 158
5.3.7 Quantization of the Minimal Form CWD Realization 164
5.4 Design Examples Using the Minimal Form of the First-Order Sections . . 164
5.4.1 Elliptic Filter of Order Four 165
5.4.2 Elliptic Filter of Order Five 168
5.4.3 Elliptic Filter of Order Eight 169
5.5 Comparison of the Two Realization Methods 171

VI **Conclusion** 174

Appendix A: Complex Analog Design Examples 176

Appendix B: Computer Software 214

References 226

List of Figures

Figure 1.1: Constant complex two-ports. 4
Figure 1.2: One-port source and imaginary resistor using real port references. 4
Figure 1.3: One-port inductor and imaginary resistor using real port references. . . . 5
Figure 2.1: Reflection-free two-port. 19
Figure 2.2: Complex constant two-port. 20
Figure 2.3: Equivalent of the T connection of imaginary resistors with $X_2 \neq -X_3$. . . 35
Figure 2.4: Equivalent of the T connection of imaginary resistors with $X_1 \neq -X_2$. . . 36
Figure 3.1: Doubly-terminated complex network. 53
Figure 3.2: Extraction of an elementary section. 55
Figure 3.3: Flow diagram of the N_a and N_R networks. 56
Figure 3.4: Flow diagram of the N_a and N_R networks evaluated at ψ_a. 57
Figure 3.5: Sample points for the sample characterization. 63
Figure 4.1: Complex one-ports in the analog and CWD domains. 73
Figure 4.2: CWD n-port. 75
Figure 4.3: Symbols used for the n-port complex series adaptor. 92
Figure 4.4: Wave-flow diagram of the complex three-port series adaptor without a RF port. 93
Figure 4.5: Wave-flow diagram of the complex three -port series adaptor with a RF port. 94
Figure 4.6: Symbols used for the three-port series adaptors. 95
Figure 4.7: Symbols used for the n-port complex parallel adaptor. 99
Figure 4.8: Wave-flow diagram of the complex three-port parallel adaptor without a RF port. 100
Figure 4.9: Wave-flow diagram of the complex three-port parallel adaptor with a RF port. 103
Figure 4.10: Symbols used for the three-port parallel adaptors. 104
Figure 4.11: Equivalence between the complex parallel and series 3-port adaptors. . . 105
Figure 4.12: Equivalence between the complex series and parallel 3-port adaptors. . . 106
Figure 4.13: Symbol of the complex two-port adaptor. 107
Figure 4.14: Wave flow diagram of the complex two-port adaptor. 108
Figure 4.15: Signal flow diagram of mutually inverse conjugate multipliers. 109
Figure 4.16: Analog equivalent of inverse conjugate multipliers. 109
Figure 4.17: Complex section with unimodular multipliers. 110
Figure 4.18: Equivalent of a complex two-port adaptor in terms of a real adaptor. . . . 112

Figure 4.19: A complex normalized two-port adaptor in terms of a real adaptor. . . . 114
Figure 4.20: Section composed of complex two-port adaptors. 117
Figure 4.21: Equivalent form of the complex series three-port adaptor. 118
Figure 4.22: Equivalent form of the complex parallel three-port adaptor. 119
Figure 4.23: Real or imaginary equivalent of the overflow truncation function. 122
Figure 4.24: Saturation overflow function. 122
Figure 4.25: Triangle overflow function. 123
Figure 5.1: Example of a complex analog network. 127
Figure 5.2: CWD equivalent of Figure 5.1. 128
Figure 5.3: CWD equivalent of the parallel inductor first-order complex section. . . . 128
Figure 5.4: CWD equivalent of the series capacitor first-order complex section. . . . 129
Figure 5.5: Stopband attenuation of the 8th order Elliptic filter. 132
Figure 5.6: Passband attenuation of the 8th order Elliptic filter. 132
Figure 5.7: Stopband of the 4th order Elliptic filter with external multipliers. 134
Figure 5.8: Passband of the 4th order Elliptic filter with external multipliers. 134
Figure 5.9: Stopband of the 4th order Elliptic filter without external multipliers. . . . 135
Figure 5.10: Passband of the 4th order Elliptic filter without external multipliers. . . . 135
Figure 5.11: Stopband of the 4th order Elliptic filter with external multipliers. 137
Figure 5.12: Passband of the 4th order Elliptic filter with external multipliers. 137
Figure 5.13: Stopband of the 4th order Elliptic filter without external multipliers. . . . 138
Figure 5.14: Passband of the 4th order Elliptic filter without external multipliers. . . . 138
Figure 5.15: Passband of the quantized 5th order Elliptic filter. 140
Figure 5.16: Stopband of the quantized 5th order Elliptic filter. 141
Figure 5.17: Passband of the quantized 5th order Elliptic filter. 141
Figure 5.18: General canonic cascade section. 143
Figure 5.19: Equivalent form of the general canonic cascade section. 144
Figure 5.20: Reciprocal canonic cascade section. 145
Figure 5.21: General form of a complex constant section. 154
Figure 5.22: Equivalent of the canonic cascade section using real two-port adaptors. . 158
Figure 5.23: General form of the canonic cascade section using real two-port adaptors. 159
Figure 5.24: Reciprocal form of the canonic cascade section using real two-port adaptors. 160
Figure 5.25: Minimal realization of the canonic cascade section. 162
Figure 5.26: The last constant section in a CWD network. 162
Figure 5.27: Minimal form of the last constant section in a CWD network. 163
Figure 5.28: Stopband attenuation plot of the 4th order Elliptic filter using 6 bits. . . . 166
Figure 5.29: Passband attenuation plot of the 4th order Elliptic filter using 6 bits. . . . 166
Figure 5.30: Stopband attenuation plot of the 4th order Elliptic filter using 8 bits. . . . 167
Figure 5.31: Passband attenuation plot of the 4th order Elliptic filter using 8 bits. . . . 167

Figure 5.32: Stopband attenuation plot of the 5th order Elliptic filter using 7 bits. . . . 168
Figure 5.33: Passband attenuation plot of the 5th order Elliptic filter using 7 bits. . . . 169
Figure 5.34: Stopband attenuation plot of the 8th order Elliptic filter using 9 bits. . . . 170
Figure 5.35: Passband attenuation plot of the 8th order Elliptic filter using 9 bits. . . . 170
Figure 5.36: General first-order complex sections. 171
Figure 5.37: General form of the transformation of a complex first-order section. . . . 172

List of Tables

Table 2.1: The CA1_∞ section that realizes a transmission zero at infinity. 23
Table 2.2: The CB1_∞ section that realizes a transmission zero at infinity. 24
Table 2.3: The CC1_0 section that realizes a transmission zero at the origin. 25
Table 2.4: The CD1_0 section that realizes a transmission zero at the origin. 26
Table 2.5: The CA1_$j\phi$ section that realizes a finite non-zero transmission zero. . . . 27
Table 2.6: The CB1_$j\phi$ section that realizes a finite non-zero transmission zero. . . . 28
Table 2.7: The CC1_$j\phi$ section that realizes a finite non-zero transmission zero. . . . 29
Table 2.8: The CD1_$j\phi$ section that realizes a finite non-zero transmission zero. . . . 30
Table 2.9: The CE1 section that realizes a transmission zero anywhere in the ψ plane. . 31
Table 2.10: The CF1 section that realizes a transmission zero anywhere in the ψ plane. 32
Table 2.11: The CG1 section that realizes a transmission zero on the finite real axis. . 33
Table 2.12: The CH1 section that realizes a transmission zero on the finite real axis. . . 34
Table 2.13: C0_π constant section. 36
Table 2.14: C0_T constant section. 37
Table 2.15: Series imaginary resistor and real transformer C0_1 constant section. . . 38
Table 2.16: Shunt imaginary resistor and real transformer C0_2 constant section. . . . 38
Table 2.17: Complex transformer T0 section. 39
Table 2.18: Real A1 section that realizes a transmission zero at infinity. 40
Table 2.19: Real B1 section that realizes a transmission zero at infinity. 40
Table 2.20: Real C1 section that realizes a transmission zero at the origin. 41
Table 2.21: Real D1 section that realizes a transmission zero at the origin. 41
Table 2.22: Real E1 section that realizes a transmission zero on the real axis. 42
Table 2.23: Real F1 section that realizes a transmission zero on the real axis. 43
Table 2.24: Real A2 section that realizes complex conjugate transmission zeros on $j\phi$ axis. 44
Table 2.25: Real B2 section that realizes complex conjugate transmission zeros on $j\phi$ axis. 45
Table 2.26: Real Brune section that realizes complex conjugate transmission zeros on $j\phi$ axis. 46
Table 2.27: Equivalence between the Brune section and two CA1_$j\phi$ complex sections. 47
Table 2.28: Equivalence between the Brune section and two CB1_$j\phi$ complex sections. 48
Table 2.29: Equivalence between the Brune section and two CC1_$j\phi$ complex sections. 49
Table 2.30: Equivalence between the Brune section and two CD1_$j\phi$ complex sections. 50

Table 2.31: Equivalence between the CA1_∞ and the CB1_∞ complex sections. . . . 51
Table 2.32: Equivalence between the CC1_0 and the CD1_0 complex sections. . . . 51
Table 2.33: Equivalence between the CA1_$j\phi$ and the CB1_$j\phi$ complex sections. . . 52
Table 2.34: Equivalence between the CC1_$j\phi$ and the CD1_$j\phi$ complex sections. . . 52
Table 4.1: Source and non-dynamic one-ports in the analog and CWD domains. . . . 81
Table 4.2: Inductive one-ports in the analog and CWD domains. 82
Table 4.3: Capacitive one-ports in the analog and CWD domains. 83
Table 4.4: Non-dynamic two-ports in the analog and CWD domains. 84
Table 5.1: CWD equivalent of the CA1_∞ and the CB1_∞ sections. 147
Table 5.2: CWD equivalent of the CC1_0 and the CD1_0 sections. 148
Table 5.3: CWD equivalent of the CA1_$j\phi$ and the CB1_$j\phi$ sections. 149
Table 5.4: CWD equivalent of the CC1_$j\phi$ and the CD1_$j\phi$ sections. 150
Table 5.5: CWD equivalent of the CE1 and the CF1 sections. 151
Table 5.6: CWD equivalent of the CG1 and the CH1 sections. 152
Table 5.7: Special case of the CG1 and the CH1 sections with $r = -1$. 153
Table 5.8: Special case of the CG1 and the CH1 sections with $r = 1$. 153
Table 5.9: CWD equivalent of the C0_π section. 154
Table 5.10: CWD equivalent of the C0_T section. 155
Table 5.11: CWD equivalent of the C0_1 section. 155
Table 5.12: CWD equivalent of the C0_2 section. 156
Table 5.13: CWD equivalent of the T0 section. 156

Chapter I

Introduction

The theory of complex networks has a rich history [35,40,43,45]. Until numerical algorithms operating on a sampled signal (ie. digital filters) became popular, this theory found little practical application. With the advent of the numerical computer, complex networks have been realized by several authors [26-31, 63-66] using complex digital filters. Applications include SSB-FDM modulation [65], transmultiplexer design [63-64,66], non-symmetric bandpass filters [35,43] and complex modulation (complex envelope representation) [75]. A more general application is the realization of a real transfer function using complex networks [53-55,70,74]. The usefulness is enhanced by special purpose digital signal processors (DSP) that are optimized for complex operations.

Many different design philosophies exist for the realization of a complex network with each having inherently different characteristics. The designer would logically wish to use the method of realization that contains the most attractive properties. Of the many classes, the class of wave digital (WD) filters as originated by Fettweis [1] is the most promising [18]. A properly designed WD filter inherits many of the beneficial properties of the analog filter it is derived from, henceforth known as the reference filter. These include low sensitivity to parametric deviations [6]. Other attractive properties under non-linear (digital) conditions include zero-input stability [3,6], forced-response stability [6,7], suppression of limit cycles [3,6], and a continuous input-output relationship [7].

Fettweis first introduced complex WDF in [26] where he stated that it may be possible to realize a complex reference network using real WD elements and unimodular multipliers if the reference network contains a property known as one-realness. A one-real network is composed of elements that have a real input impedance at $\Psi = 1$ in the Ψ plane. The necessity for the condition arises from using real port-reference impedances (discussed in the next chapter). For a computable WDF, there cannot exist a delay-free path. For a one-port, this translates into the condition that the reflectance ρ must be zero at $\Psi = 1$ [26]. The definition of the reflectance with real references is given by

$$\rho = \frac{Z(\psi) - R}{Z(\psi) + R} \tag{1.1}$$

where $Z(\psi)$ is the complex driving-point impedance of the one-port and R is the real port reference. This gives the condition that

$$Z(\psi)|_{\psi=1} = R \tag{1.2}$$

and thus the name "one-real".

Obviously, a general complex ladder network is not one-real since $Z(\psi = 1)$ is usually complex for each branch impedance, and thus it cannot be realized using real WD elements without alteration to make it one-real. Any complex impedance function in the ψ domain can be made externally one-real by introducing a constant phase change in the reflectance function. After a one-real impedance function has been derived from a general impedance, the problem then arises of how to extract one-real sections, or sections that have an impedance of the form [26]

$$Z(\psi) = R\left(\frac{1 + j\alpha\psi}{\psi + j\alpha}\right) \tag{1.3}$$

However, a one-real impedance function is not necessarily realizable as an interconnection of one-real branch impedances in a ladder configuration. Indeed, a trivial example of a doubly-terminated series inductor and imaginary resistor was made one-real, but sections could not be extracted in the form of a doubly-terminated one-real LCX lumped-element one-ports. This suggests that an externally one-real network does not imply internal one-realness in the ψ domain, analogous to the way external passivity does not imply internal passivity.

With real WD networks, a particular passive linear classical filter can always be realized with either two-port or three-port adaptors [6]. However, it is not known if a complex ladder WD filter in the Ψ domain can be realized using real three-port adaptors since no examples of cascade synthesis exist, and no indication of any method of realization has been proposed (excluding the case where a complex filter is decomposed into real filters with real arithmetic operations throughout [27, 28]). This leads to the question as to whether or not such a realization using the one-real theory is possible. It is not known if non-reciprocal filter sections with transmission zeros anywhere on the Ψ plane can be realized using one-realness.

A one-real complex ladder realization does exist if a *real* WD ladder network is frequency shifted in the s domain instead of the ψ domain [26] (the relation between the complex frequencies s and ψ is found in Section 4.1, equation (4.3)). It exists because the corresponding form of the ψ domain frequency variable, resulting from the shifting in the s domain, maps a real immittance into a one-real immittance as given by the form of (1.3). The shifting in the s domain introduces a unimodular multiplier in series with each delay and the port reference impedance remains real. However, the discussion given above implies that approximation methods used to induce desirable properties in the ψ domain

(for example, a filter with linear phase in the z domain) that result in a complex ladder filter cannot be realized using one-realness. Namely, any transformations on a ladder LC filter in order to create a complex one-real filter must be performed *after* the real wave digital LC filter has been realized.

Greater success has been found in the realization of one-real lattice WD filters [27,28,56]. It has been found that the one-real property is not restrictive when realizing complex lattice WD filters arising from real even-order classical filters [28]. This is because the function being realized is a complex one-port reflectance, which corresponds to a WD allpass function. The reflectance is made one-real by extracting a constant phase change in the form of a unimodular multiplier. When a constant phase is removed from an allpass function, another allpass function remains (which is now one-real). Thus a real two-port adaptor, a unimodular multiplier and delay can be extracted as a building block and the lattice is formed using a form of the Schur algorithm [32]. Another form of this section is the so-called Cross adaptor [56] which requires only two independent real quantizations in its implementation, however it is poorly scaled.

Non-WD complex lattices have also been developed [29-31]. All of the above lattice realizations are essentially equivalent to within a scaling transformation on the ports of the two-port building blocks; that is, simple scaling multipliers in the signal paths.

Another configuration for a network is the ladder realization, which realizes a transmittance rather than a reflectance. A transmittance has the input and output at different ports, while a reflectance has the input and output at the same port, and therefore is a one-port. Thus one-port synthesis realizes a reflectance. All the transmission zeros of a network are realized directly with a transmittance, whereas a reflectance realizes all transmission zeros of a network through cancellation (that is, in order to create a zero at the output port, two signals must cancel exactly, which is usually difficult to achieve in a finite-precision digital realization). This leads to higher stopband sensitivity for the reflectance compared to the transmittance and thus to higher stopband sensitivity for a one-port. Note that the property of low passband sensitivity is inherited from the analog doubly-terminated network. From these observations, the lattice approach will not be used, and the ladder realization will be implemented exclusively.

The use of real port impedances with common complex elements that are not one-real have a WD equivalent that may be either non-computable or unnecessarily complicated. This is a reason for not using real port impedances for complex networks which are not one-real. For example, consider either a series or parallel connection of an imaginary resistor viewed as a two-port as shown in Figure 1.1.

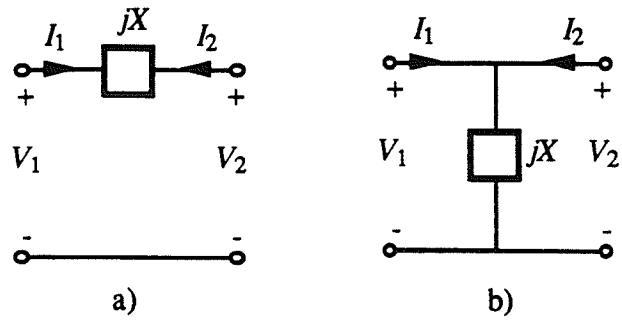

Figure 1.1: Constant complex two-ports: a) series-connected imaginary resistor b) parallel-connected imaginary resistor.

The diagonal elements of the scattering matrix (described in the next chapter) describing either the series-connected (1.4a) or the parallel-connected (1.4b) imaginary resistor

$$\mathbf{S} = \frac{1}{R_1 + R_2 + jX}\begin{bmatrix} -R_1 + R_2 + jX & 2R_1 \\ 2R_2 & R_1 - R_2 + jX \end{bmatrix}$$

$$\mathbf{S} = \frac{1}{R_1R_2 + jX\,(R_1 + R_2)}\begin{bmatrix} -R_1R_2 + jX(-R_1 + R_2) & 2jXR_1 \\ 2jXR_2 & -R_1R_2 + jX(R_1 - R_2) \end{bmatrix} \qquad (1.4a,b)$$

must be non-zero for real port references, and thus the ports cannot be made reflection-free. This will normally lead to delay-free loops within a structure containing the above elements. An analog one-port source with an imaginary resistor as shown in Figure 1.2

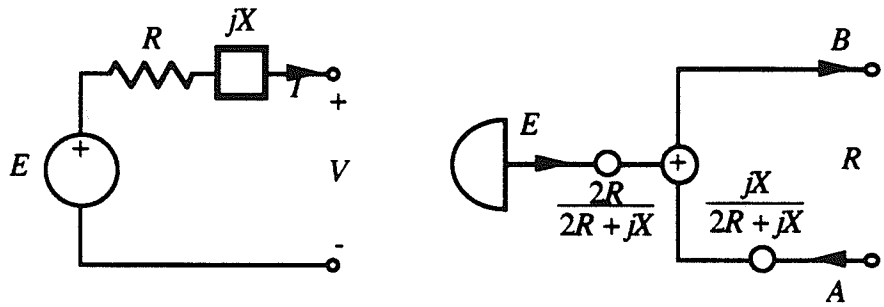

Figure 1.2: One-port source and imaginary resistor using real port references.

has the WD equivalent with real port impedances shown on the right in the above figure. This flow diagram is clearly not the usual combination of a source and sink. Consider as a last example a one-port inductor in series with an imaginary resistor as shown in Figure 1.3.

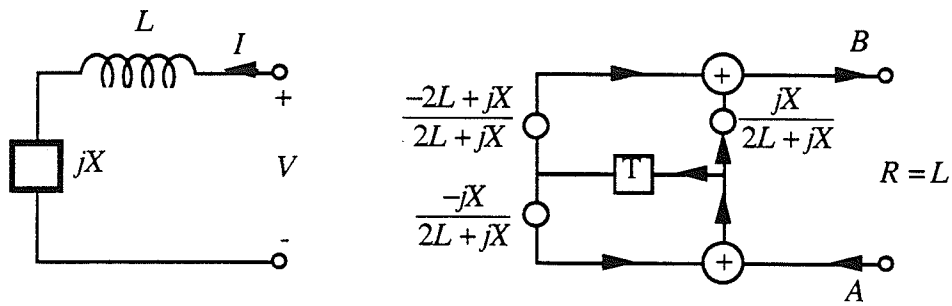

Figure 1.3: One-port inductor and imaginary resistor using real port references.

The WD equivalent is clearly more complicated than the real case ($X = 0$) since it requires three multiplications and two additions. Also, the interconnection of the above WD equivalent with a three-port adaptor will create a delay-free loop.

Other cascade filter structures can be found in the literature, including the orthogonal [29] and unitary filters [77]. These structures are based on signal flow diagrams that possess the unitary property which is associated with beneficial scaling characteristics. However, the structures are derived without the use of port impedances, and therefore they do not explicitly inherit the properties of analog networks. Thus, the conceptually pleasing characteristic that the synthesis in either the analog or the discrete domain (using WD filters) is equivalent, is not inherited by the structures without port impedances. Since no direct advantage has been identified for not transferring analog characteristics, and since Fettweis has shown that the orthogonal (unitary) filters are equivalent to normalized WD filters [18], the WD filters with the beneficial properties outlined earlier may be the preferred choice for a general complex digital filter structure.

In this thesis, the author will rederive the theory of WD filters in order to give a truly general theory of complex WD networks. The generalization to complex WD networks should reduce to the known theory of real WD networks if all quantities are restricted to be real. Clearly, the generalization is useless if either of the following cannot be guaranteed: first all of the familiar WD elements must be realizable, and second, a simple stability theory must exist and follow from the definition of power (similar to the real case).

In order to guarantee these two objectives, the definitions of the incident and reflected (voltage) wave quantities are redefined to allow complex port reference impedances. This new definition requires that all WD components must be rederived. It was found by the author [53-54] that this generalization allowed the realization of complex lattice WD networks using only the complex two-port adaptor and delays (no external multipliers), and a simple stability theory exists which gives the beneficial properties of zero-input and forced-response stability. The earlier work by the author [53] only supported a highly

restricted class of complex filters.

A motivation for the generalization is found in the additional degree of freedom in the choice of the imaginary part of the port impedance, that is, there is an additional parameter. The existence of the imaginary part of the port impedance (leading to the theory developed in this thesis) is necessary and sufficient to guarantee that a complex WD network is computable as shown by the following theorem.

Theorem 1.1:

In general, a complex WD cascade network is computable if and only if the port reference impedances are allowed to be complex; when the complex network is one-real, the port impedances can be chosen to be real.

Proof:

In order to show necessity, consider the interconnection of two adjacent complex WD dynamic or constant two-ports. At the interconnection, the reflectance of either port has the following form:

$$\rho = \frac{Z(\psi) - Z_0^*}{Z(\psi) + Z_0} \tag{1.5a}$$

where Z_0 is the real or complex port reference impedance with a positive real part, and $Z(\psi)$ is the input impedance of the appropriate port under consideration. Although it may difficult to identify the reference input impedance from the WD counterpart, the existence of $Z(\psi)$ is sufficient for the proof.

A computable network possesses the property that the total delay within every loop is a positive integer multiple of a basic delay [6,73] (the proof as given for the real case is based on graph theory and thus also applies for complex discrete networks). This implies that every loop must contain at least the term z^{-1} (a delay) as a factor. At the interconnection of two ports a loop is bisected, and thus the reflected signal from either the left port or the right port (or possibly both) must contain positive delay. Thus either the reflectance of the right port or the reflectance of the left port (or possibly both) must be zero regardless of the associated incident signal at $z = \infty$, that is, when $\psi = 1$. This is consistent with the need for reflection-free ports within a WD structure. Thus, for the complex WD network to be computable, it is clear from (1.5a) above and the observation that at least one reflectance must be zero at $\psi = 1$, that

$$Z(\psi = 1) = Z_0^* \tag{1.5b}$$

for one of the complex input impedances. If $Z(\psi = 1)$ is complex, which is true in general for complex networks, then at least one port impedance must be complex within the WD network for the flowgraph to be computable. A special case of this is an interconnection of one-real two-ports, where the evaluation of (1.5b) is a real constant. In this case the port reference impedance can be chosen to be real. In either case the port interconnection criterion was assumed to be satisfied.

The proof for the sufficiency of allowing complex port reference impedances will follow through construction from the development given in Chapters IV and V.

The purpose of this thesis is to derive the many remaining complex WD elements in order to realize complex ladder networks (as opposed to the complex lattice) and more general reference networks that have not yet been investigated. To this end the following will present the new definitions of all of the complex WD elements that are needed to realize general complex networks.

Complex analog networks will be reviewed in Chapter II along with the definition of the complex first-order and zeroth-order elementary sections. Equivalences between the real Brune section and two complex reciprocal sections are given as well as several equivalences between the complex sections.

The network synthesis algorithm given in [16] will be generalized to the complex domain in Chapter III. The motivation for the development of the algorithm as well as implementation considerations will be discussed.

Chapter IV introduces complex wave digital filters with the new definitions of the wave variables. Many useful dynamic and non-dynamic one-port as well as constant two-port equivalences are given. The new definitions for the series and parallel adaptors with complex impedances is given as well as the definition of the two-port adaptor. Several adaptor equivalences conclude the chapter.

Complex WD ladder filters are realized in Chapter V. First, the realization method employing three-port adaptors is outlined and examples are given. Finally, a new complex first-order section, known as the canonic cascade section, is derived and examples using the section are presented.

This thesis concludes with Chapter VI which states several observations and summarizes the thesis.

Chapter II

Complex Analog Networks

In order to justify the need for the generalization of wave digital filters to the complex domain, general complex networks will be discussed in the following. Many examples of complex analog networks exist [35,40,43,55], however, much of the pioneering work was done by Belevitch [40]. All work in this area has treated a complex element as an abstract lumped-element electrical device which is either physically unrealizable or very difficult to realize as an analog device. The present work will continue this point of view.

There are several theoretical advantages gained by including complex elements in the library of acceptable elements. Perhaps the greatest advantage is the existence of general first-order complex building blocks that are capable of independently realizing transmission zeros anywhere in the complex plane. Also, since the phase of the gain of the reflectance function is a free parameter when realizing a transmittance, the phase can be made any arbitrary value (this is in contrast to the one-real case given in the preceding Chapter when a unique phase is chosen in order to induce the one-real property). This leads to an infinite number of realizations of the same real voltage transfer function as opposed to the real case where the number of realizations of the same transfer function is finite. This introduces an extra degree of freedom that may be taken advantage of during the design process in order to derive appealing characteristics of the resulting network. Another theoretical advantage is found in the observation that many common elements can be generated from combinations of complex elements.

The zero-shifting process used to realize finite transmission zeros can also be extended to include the imaginary resistor as shown by Belevitch [40] and Humphreys [43].

2.1 New Complex Elements

The most common complex elements that are added to the library of acceptable elements are the imaginary resistor [40,43], the complex transformer [40], and the complex gyrator. A simple way of deriving a complex network from a real network is to shift the frequency response with the following transformation on the complex frequency variable ψ,

$$\psi \rightarrow \psi - j\phi_0 \tag{2.1}$$

which simply translates all of the poles and zeros in the imaginary axis direction by the

amount ϕ_o. This introduces an imaginary resistor in series with each inductor and in parallel with each capacitor. Non-symmetric bandpass filters were introduced [35] using this concept, since the lowpass prototype for the bandpass filter is first shifted using the above transformation to give a non-symmetric lowpass response about the origin. Other work in the area of non-symmetric bandpass filters can be found in [43], where actual networks are derived.

The imaginary resistor, which is also known as a constant reactance, is perhaps the most well-known complex element. The input impedance of an imaginary resistor is constant for all frequencies and complex, namely $Z = jX$. It is an ideal, physically unrealizable, reciprocal and lossless device [40].

The imaginary resistor, in different combinations, can replace common analog elements. This means that our "library" of components used to build networks, in its simplest form, contains only a resistor, an imaginary resistor and an inductor (or a capacitor). For example, imaginary resistors in a T-connection can be used to replace a dualizer with a real gyration resistance R when viewed as a one-port [40, p. 116]. A gyrator with an inductor (capacitor) connected to port two can be used to replace a capacitor (inductor). Other common analog elements can also be replaced with combinations with the imaginary resistor. For example, an exact equivalence exists for a transformer with a real turns ratio n [40, p. 118]. Although many elements are now not strictly required, no advantage is ordinarily found by limiting our possible selections of components, thus all of the common elements will be allowed.

The ideal complex transformer [40] is defined by the following voltage-current equations relating ports 1 and 2,

$$\begin{aligned} V_1 &= n^* V_2 \\ I_2 &= -n I_1 \end{aligned} \tag{2.2a,b}$$

It is ideal, lossless and non-reciprocal [40]. This contrasts with the real ideal transformer which is a reciprocal device.

Finally, the complex gyrator can be defined by imposing the lossless property upon the generalization of a real gyrator, giving the following

$$\begin{aligned} I_1 &= -\sigma Y V_2 \\ I_2 &= \sigma Y^* V_1 \end{aligned} \tag{2.3a,b}$$

where Y is a complex constant hereby known as the gyration admittance and $\sigma = \pm 1$. By the convention set for the real gyrator in [40], $\sigma = +1$. Note that the complex gyrator as defined above is a physically unrealizable, lossless and a non-reciprocal device when $\mathrm{Re}\{Y\} \neq 0$. In this thesis, no advantage will be gained from the added degree of freedom in

the imaginary part of Y and thus real gyrators will be used exclusively.

2.2 The Positive Function

The immittance function of a real passive network is known as a positive-real function. A similar result holds for complex networks, where the immittance of a complex passive network is known as a positive function (PF) [40,43,45]. Clearly, the positive real property is a special case of the PF property, where the function must also be real when the complex frequency variable ψ is real. The basic property of a positive rational function $Z(\psi)$ is given by [45, p. 129]

$$\mathrm{Re}\{Z(\psi)\} \geq 0, \quad \mathrm{Re}\{\psi\} \geq 0 \tag{2.4}$$

which can also be expressed as

$$Z(\psi) + Z^*(\psi) \geq 0, \quad \mathrm{Re}\{\psi\} \geq 0 \tag{2.5}$$

The asterisk operator denotes the complex conjugate. Other properties include:

- if there are any poles on the $j\phi$-axis, they must be simple and the residues of all poles on the $j\phi$-axis must be real and positive
- the denominator of $Z(\psi)$ must be at least modified Hurwitz
- since the inverse of a PF must be a PF, the zeros of $Z(\psi)$ must also be at least modified Hurwitz

The following theorem dealing with a complex passive network will give the correspondence between a PF (passive immittance) and its associated reflectance function as referenced to a complex immittance, and is an extension of the proof given in [43].

<u>Theorem 2.1:</u>

An immittance function $Z(\psi)$ is a PF if and only if the complex reflectance function defined by

$$\rho(\psi) = \frac{Z(\psi) - Z_r^*}{Z(\psi) + Z_r} \tag{2.6a}$$

satisfies the property

$$|\rho(\psi)| \leq 1, \quad \mathrm{Re}\{\psi\} \geq 0 \tag{2.6b}$$

for any finite constant immittance $Z_r = R_r + jX_r$ of the same immittance type as $Z(\psi)$

and $R_r > 0$.

Proof:

To prove necessity, assume $Z = R + jX$ is a PF. Thus Z is finite in the open RHP (right half plane) and has a finite number of simple poles on the $\psi = j\phi$ axis. Also $R \geq 0$ in the closed RHP. The magnitude of $\rho(\psi)$ is given by

$$|\rho(\psi)|^2 = \frac{(R - R_r)^2 + (X + X_r)^2}{(R + R_r)^2 + (X + X_r)^2} \tag{2.6c}$$

and since $R \geq 0$ and $R_r > 0$,

$$|\rho(\psi)|^2 \leq 1 \;\Rightarrow\; |\rho(\psi)| \leq 1 \tag{2.6d}$$

Thus $|\rho(\psi)| \leq 1$ for $\mathrm{Re}\{\psi\} \geq 0$, and since $\rho(\psi)$ is rational in polynomials in ψ, it is a bounded function. Note that $\rho(\psi) = 1$ at a pole of Z. To prove sufficiency, assume $|\rho(\psi)| \leq 1$ for $\mathrm{Re}\{\psi\} \geq 0$ (and thus analytic) in the closed RHP and solve for $Z(\psi)$ from (2.6a),

$$Z(\psi) = \frac{Z_r^* + Z_r\,\rho(\psi)}{1 - \rho(\psi)} \tag{2.6e}$$

and let $\rho(\psi) = \alpha + j\beta$. The real part of $Z(\psi)$ is thus,

$$\mathrm{Re}\{Z(\psi)\} = R_r\left(\frac{1 - |\rho(\psi)|^2}{(1 - \alpha)^2 + \beta^2}\right) \tag{2.6f}$$

and since $|\rho(\psi)| \leq 1$ and $R_r > 0$, it is clear that $\mathrm{Re}\{Z(\psi)\} \geq 0$ in $\mathrm{Re}\{\psi\} \geq 0$ for $\rho(\psi) \neq 1$. At a pole $\psi = j\phi_0$ of Z on the $\psi = j\phi$ axis (when $\rho(\psi) = 1$), the value of $\mathrm{Re}\{Z(\psi)\}$ evaluated in the RHP at $\psi = \phi_r + j\phi$ near but not at the pole (ie. $\phi_r \geq 0$) is approximately

$$\mathrm{Re}\{Z(\psi)\} \approx \mathrm{Re}\left\{\frac{A}{\psi - j\phi_0}\right\} \approx \mathrm{Re}\left\{\frac{A}{\phi_r + j(\phi - \phi_0)}\right\} \approx \frac{A\phi_r}{\phi_r^2 + (\phi - \phi_0)^2} \tag{2.6g}$$

which is positive since the residue A is positive and real. Thus, $\mathrm{Re}\{Z(\psi)\} \geq 0$ in $\mathrm{Re}\{\psi\} \geq 0$.

2.3 Properties of A Complex Lossless Immittance

In the preceding section, it was found that a passive immittance function must possess the characteristics of a PF. Now consider the specialized class of complex lossless networks where the following equality holds [40, p. 131]

$$Z(\psi) + Z_*(\psi) = 0, \;\; \mathrm{Re}\{\psi\} \geq 0 \tag{2.7}$$

and thus a lossless function is a para-odd function. The lower asterisk represents the para-conjugate (or the Hurwitz conjugate) defined by

$$Z_*(\psi) = Z^*(-\psi^*) \tag{2.8}$$

In the real case this reduces to the familiar definition $Z_*(\psi) = Z(-\psi)$. On the $\psi = j\phi$ axis the para-conjugate reduces to

$$Z_*(j\phi) = Z^*(j\phi) \tag{2.9}$$

which is simply the complex conjugate of the function. In particular, the following holds on the $\psi = j\phi$ axis

$$Z(j\phi) + Z^*(j\phi) = 0 \tag{2.10}$$

For the lossless case, $Z(\psi)$ of order n can be represented as

$$Z(\psi) = jX_0 + A_\infty \psi + \frac{A_0}{\psi} + \sum_{i=1}^{n} \frac{A_i}{\psi - j\phi_i} \tag{2.11}$$

where the A_i are real and positive for all values of i. It is clear that $Z(j\phi)$ can be represented as

$$Z(j\phi) = jX_0 + jA_\infty \phi - \frac{jA_0}{\phi} + \sum_{i=1}^{n} \frac{-jA_i}{\phi - \phi_i} \tag{2.12}$$

and thus

$$Z(j\phi) = j\,X(\phi) \tag{2.13}$$

where the real function $X(\phi)$ is given by

$$X(\phi) = X_0 + A_\infty \phi - \frac{A_0}{\phi} + \sum_{i=1}^{n} \frac{-A_i}{\phi - \phi_i} \tag{2.14}$$

The derivative of the function $X(\phi)$ is positive and real for all frequencies ϕ [71, p. 495] (note that the proof in [71] is given for a PRF, however, it is also valid for a PF)

$$\frac{d}{d\phi} X(\phi) > 0 \tag{2.15}$$

This can be restated to say that at a real part zero of the immittance on the $\psi = j\phi$ axis, the derivative of the immittance is strictly positive

$$\frac{d}{d\psi} Z(\psi) > 0 \tag{2.16}$$

Hereafter in this thesis, all relevant functions will be assumed to be lossless unless stated otherwise.

2.4 Canonic Polynomial Representation of A Complex Lossless Two-Port

In the earlier analysis, all quantities were given using voltage-current signals. An alternative representation is given by the so called scattering parameters. This representation will be used exclusively for the remainder of the thesis and in particular will be used to represent lossless two-ports.

The voltage-current signal variables V and I are replaced by the voltage-wave variables A and B as defined by the following transformation as referenced to an impedance of 1 Ω,

$$\begin{aligned} A(\psi) &= V(\psi) + I(\psi) \\ B(\psi) &= V(\psi) - I(\psi) \end{aligned} \tag{2.17}$$

where A is the incident (input) wave variable and B is the reflected (output) wave variable. This is a specific case of the general transformation as reference to a constant impedance Z with real part R as given by

$$A(\psi) = \frac{V(\psi) + Z\,I(\psi)}{\sqrt{R}}$$

$$B(\psi) = \frac{V(\psi) - Z^{*}I(\psi)}{\sqrt{R}} \tag{2.18}$$

Using the above transformation, a stable complex lossless two-port can be represented by the signal variables A_i and B_i, i=1,2 in the following matrix form

$$\begin{bmatrix} B_1 \\ B_2 \end{bmatrix} = \frac{1}{g}\begin{bmatrix} h & \sigma f_* \\ f & -\sigma h_* \end{bmatrix}\begin{bmatrix} A_1 \\ A_2 \end{bmatrix} \tag{2.19}$$

where the scattering matrix as defined by

$$\mathbf{S} = \frac{1}{g}\begin{bmatrix} h & \sigma f_* \\ f & -\sigma h_* \end{bmatrix} \tag{2.20}$$

is unitary. The polynomials f, h, and g are known as the canonic polynomials and satisfy

$$g g_* = f f_* + h h_* \tag{2.21}$$

which is the analytic continuation of the Feldtkeller equation. The polynomial g has all of its zeros strictly in the left-half plane (that is, it is Hurwitz) since the network is stable by assumption. The complex constant σ is unimodular and if the network is reciprocal, it is given by

$$\sigma = \frac{f}{f_*} \tag{2.22}$$

Another form often used is the transfer matrix defined by

$$\begin{bmatrix} B_1 \\ A_1 \end{bmatrix} = \frac{1}{f}\begin{bmatrix} \sigma g_* & h \\ \sigma h_* & g \end{bmatrix}\begin{bmatrix} A_2 \\ B_2 \end{bmatrix} \tag{2.23}$$

that is

$$\mathbf{T} = \frac{1}{f}\begin{bmatrix} \sigma g_* & h \\ \sigma h_* & g \end{bmatrix} \tag{2.24}$$

The f, h and g polynomials can be scaled by a complex constant K giving the new canonic polynomials

$$\begin{aligned} f &\rightarrow Kf \\ h &\rightarrow Kh \\ g &\rightarrow Kg \end{aligned} \tag{2.25a,b,c}$$

which changes the σ value to the unimodular quantity

$$\sigma \rightarrow \frac{K\sigma}{K^*} \tag{2.26}$$

Notice that if K is real then the σ value will not change with the scaling of the polynomials.

The scattering matrix can be represented in terms of the open-circuit impedance matrix

parameters

$$\mathbf{Z} = \begin{bmatrix} z_{11} & z_{12} \\ z_{21} & z_{22} \end{bmatrix} \tag{2.27}$$

as given by

$$\mathbf{S} = \frac{1}{z_{11} + z_{22} + 1 + \Delta_z} \begin{bmatrix} z_{11} - z_{22} - 1 + \Delta_z & 2z_{12} \\ 2z_{21} & -z_{11} + z_{22} - 1 + \Delta_z \end{bmatrix}$$

$$\Delta_z = z_{11}z_{22} - z_{12}z_{21} \tag{2.28a,b}$$

Similar, the scattering matrix given in terms of the short-circuit admittance matrix

$$\mathbf{Y} = \begin{bmatrix} y_{11} & y_{12} \\ y_{21} & y_{22} \end{bmatrix} \tag{2.29}$$

is given by

$$\mathbf{S} = \frac{1}{y_{11} + y_{22} + 1 + \Delta_y} \begin{bmatrix} -y_{11} + y_{22} + 1 - \Delta_y & -2y_{12} \\ -2y_{21} & y_{11} - y_{22} + 1 - \Delta_y \end{bmatrix}$$

$$\Delta_y = y_{11}y_{22} - y_{12}y_{21} \tag{2.30a,b}$$

A complex two-port can be defined using lumped element values as parameters. However, from the point of view of two-port synthesis using reciprocal elementary sections, a more judicious choice for the parameters of the section are the return group delay and the reflectance, both evaluated at the transmission zero of the section, and the location of the transmission zero. Note that for non-reciprocal sections the return group delay will not be needed.

The reflectance of a lossless complex two-port evaluated at the transmission zero ψ_0 is given by

$$\rho = \left.\frac{h(\psi)}{g(\psi)}\right|_{\psi = \psi_0} \tag{2.31}$$

Since the reflectance is evaluated at a transmission zero where $ff_*|_{\psi = \psi_0} = 0$, the analytic continuation of the Feldtkeller equation (2.21) reduces to

$$hh_*|_{\psi = \psi_0} = gg_*|_{\psi = \psi_0} \tag{2.32}$$

which gives

$$\left.\frac{h}{g}\right|_{\psi=\psi_0} = \left.\frac{g_*}{h_*}\right|_{\psi=\psi_0} \tag{2.33}$$

For a transmission zero ($\psi_0 = j\phi_o$) on the imaginary axis, the reflectance is unimodular, since (2.33) above is in the form of $x = 1/x^*$. Using this fact, the reflectance evaluated at $\psi_0 = j\phi_o$ can be expressed as

$$\rho = \frac{h}{g} = e^{j\theta}, \quad -\pi < \theta \leq \pi \tag{2.34}$$

The magnitude of the reflectance evaluated at a transmission zero not located on the imaginary axis is bounded by

$$\left|\frac{h}{g}(\psi_0)\right| < 1, \ \ \mathrm{Re}\{\psi_0\} > 0$$

$$\left|\frac{h}{g}(\psi_0)\right| > 1, \ \ \mathrm{Re}\{\psi_0\} < 0 \tag{2.35a,b}$$

as the reflectance represents a passive network, and is thus analytic in the closed right-half plane.

The return group delay evaluated at the transmission zero $j\phi_o$, hereafter called the delay D, is defined in a similar manner to the forward group delay and is defined by [58]

$$D = -\,\mathrm{Ev}\left\{\frac{d}{d\psi}\, ln\left(\frac{h(\psi)}{g(\psi)}\right)\right\}\Bigg|_{\psi=j\phi_o} \tag{2.36}$$

where the operator 'Ev' refers to the para-even function given by

$$\mathrm{Ev}\,\{P(\psi)\} = \frac{1}{2}(P(\psi) + P_*(\psi)) \tag{2.37}$$

Note that the forward group delay is defined by replacing $h(\psi)$ by $f(\psi)$ in (2.36) above. Consider the reflectance expressed in polar form

$$\frac{h}{g}(\psi) = \left|\frac{h}{g}(\psi)\right| e^{j\theta(\psi)} \tag{2.38}$$

where the phase of the reflectance is given by the real function $\theta(\psi)$. Substitute the above

into the definition of the delay in order to derive

$$D = -\,\mathrm{Ev}\left\{\frac{d}{d\psi}\,ln\left(\left|\frac{h}{g}(\psi)\right| e^{j\theta(\psi)}\right)\right\}\Bigg|_{\psi=j\phi_o} = -\,\mathrm{Ev}\left\{\frac{d}{d\psi}ln\left(\left|\frac{h}{g}(\psi)\right|\right) + \frac{d}{d\psi}\left(j\theta(\psi)\right)\right\}\Bigg|_{\psi=j\phi_o} \tag{2.39}$$

However, when ψ is restricted to the $\psi = j\phi$ axis, the above becomes

$$D = -\,\mathrm{Re}\left\{-j\frac{d}{d\phi}ln\left(\left|\frac{h}{g}(\phi)\right|\right) + \frac{d}{d\phi}\left(\theta(\phi)\right)\right\}\Bigg|_{\phi=\phi_o}$$

$$D = -\frac{d}{d\phi}\theta(\phi)\Bigg|_{\phi=\phi_0} \tag{2.40a,b}$$

and thus the return group delay evaluated on the imaginary axis is proportional to the derivative of the phase of the reflectance. Note that the imaginary part of (2.40a) is zero at a transmission zero. The expression for the delay given above (2.36) can also be represented as

$$D = \frac{1}{2}\left(\frac{g'}{g} - \frac{h'}{h} + \left(\frac{g'}{g} - \frac{h'}{h}\right)_*\right) \tag{2.41}$$

However, the above evaluated at a transmission zero, when $ff_* = 0$, yields

$$\left(\frac{g'}{g} - \frac{h'}{h}\right)_* = \frac{g'}{g} - \frac{h'}{h} \tag{2.42}$$

as can be shown by the differentiation of the analytic continuation of the Feldtkeller equation (2.21). Thus, the expression for the delay can be simplified to

$$D = \left(\frac{g'}{g} - \frac{h'}{h}\right)\Bigg|_{\psi=j\phi_o} \tag{2.43}$$

where g' refers to the differentiation of g by ψ. The following Theorem shows that D evaluated at a transmission zero as given above is real and positive for a complex lossless and reciprocal two-port.

<u>Theorem 2.2:</u>

The return group delay D given by (2.43) is both real and strictly positive when evaluated at a transmission zero, and can be expressed as

$$D = \left(\frac{g'}{g} - \frac{h'}{h}\right)\Bigg|_{\psi=j\phi_o} \tag{2.44a}$$

Proof:

Consider the delay function (2.44a) evaluated at a transmission zero. From (2.41-42) above, the delay is real. To show that it is positive, we first show that the sign of the delay is equal to the sign of the derivative of the immittance at a real part zero. To this end, consider the definition of the reflectance referenced to a constant positive immittance of the same type as $Z(\psi)$ as given by

$$\frac{h}{g} = \frac{Z(\psi) - Z_0^*}{Z(\psi) + Z_0}, \quad Z_0 = R_0 + jX_0, \quad R_0 > 0 \tag{2.44b}$$

After the differentiation of the left-most equation of the above with respect to ψ and some rearrangement, the following is derived:

$$\frac{g'}{g} - \frac{h'}{h} = \frac{2\,\mathrm{Re}\{Z_0\}}{|Z_0|^2 - Z^2 - Z\left(Z_0 - Z_0^*\right)} \frac{dZ}{d\psi} \tag{2.44c}$$

However, at a real part zero of the immittance $Z = jX$ (which is always true for a lossless function), the above becomes

$$D = \frac{g'}{g} - \frac{h'}{h} = \frac{2\,\mathrm{Re}\{Z_0\}}{|Z_0|^2 + X^2 + 2\,\mathrm{Im}\{Z_0\}X} \frac{dZ}{d\psi} \tag{2.44d}$$

The denominator can be expressed as

$$|Z_0|^2 + X^2 + 2\,\mathrm{Im}\{Z_0\}X = R_0^2 + (X + X_0)^2 \tag{2.44e}$$

and thus is always positive. Furthermore, $\mathrm{Re}\{Z_0\} = R_0 > 0$ by assumption, and thus the sign of the delay is equal to the sign of the derivative of the immittance. At a real part zero, the derivative of the immittance is real and positive as mentioned in Section 2.3, and thus the delay is real and positive.

2.5 Reflection-Free Port of A Complex Lossless Two-Port

In many applications it is useful to have the freedom of inducing the reflection-free property at one of the ports of a complex lossless two-port. A port is reflection-free if the reflected wave for the port is independent of the corresponding incident wave when evaluated at $\psi = 1$ (that is, the corresponding diagonal element of the scattering matrix is zero at $\psi = 1$). Inducing the reflection-free property requires the absorption of a constant two-port into the original dynamic section, thereby changing the canonic polynomials so

that either h or $h*$ has a zero at $\psi = 1$, for port 1 or port 2, respectively. An example of this process is shown in the following figure, where port 2 is made reflection-free.

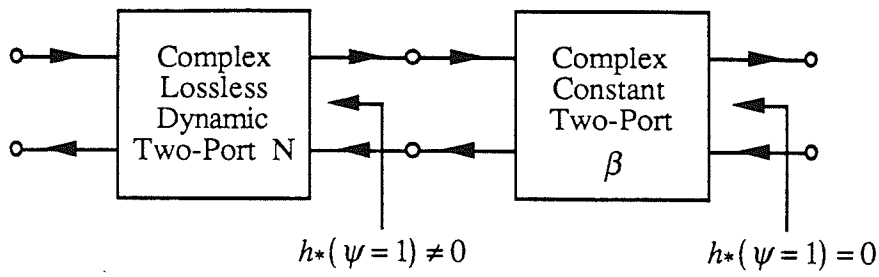

Figure 2.1: Reflection-free two-port.

There is a great deal of freedom in choosing the canonic polynomials of the constant section. Two free real parameters are required, and thus a possible choice for the polynomials are given below as a function of a complex scalar constant β ,

$$f = 1$$

$$h = \frac{-\beta^*}{\sqrt{1 - \beta\beta^*}}$$

$$g = \frac{1}{\sqrt{1 - \beta\beta^*}}$$

$$\sigma = 1 \qquad (2.45a,b,c,d)$$

Note that $f = 1$, which removes the third degree of freedom commonly found in a complex constant section (see Section 2.6.3). There is a total of three distinct choices for the scalar polynomials since the value of unity can be assigned to one of the other polynomials, namely h or g. However, no advantage is found with a different definition for the constant section than the one given above. The analog section corresponding to the above when β is complex is given in the following figure,

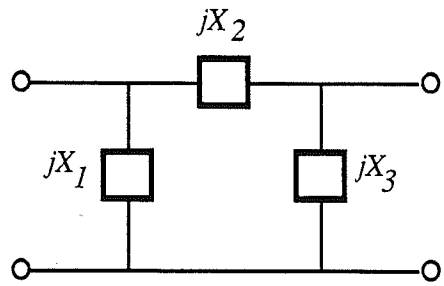

Figure 2.2: Complex constant two-port.

where the values of the imaginary resistors are given by

$$X_1 = \frac{\mathrm{Im}\{\beta\}}{1 - \sqrt{1 - \beta\beta^*} + \mathrm{Re}\{\beta\}}$$

$$X_2 = \frac{\mathrm{Im}\{\beta\}}{\sqrt{1 - \beta\beta^*}}$$

$$X_3 = \frac{\mathrm{Im}\{\beta\}}{1 - \sqrt{1 - \beta\beta^*} - \mathrm{Re}\{\beta\}} \qquad (2.46a,b,c)$$

When β is real, the above polynomials (2.45) describe a real transformer with a turns ratio of

$$n = \sqrt{\frac{1 - \beta}{1 + \beta}} \qquad (2.47)$$

The development for inducing the reflection-free property for port two will be given in the following. A similar argument can be given for port one, however, this will not be required in this thesis and thus will not be presented.

Consider a general complex, dynamic two-port with a transfer matrix

$$\mathbf{T} = \frac{1}{f}\begin{bmatrix} \sigma g_* & h \\ \sigma h_* & g \end{bmatrix} \qquad (2.48)$$

The section can be made reflection-free for the port two by inserting a constant section with polynomials as given in (2.45) on the right, as shown in Figure 2.2, giving the following

overall transfer matrix for the new section,

$$\mathbf{T} = \frac{1}{\sqrt{1 - \beta\beta^*}\, f}\begin{bmatrix} \sigma g_* - \beta h & h - \beta^* \sigma g_* \\ \sigma h_* - \beta g & g - \beta^* \sigma h_* \end{bmatrix} \tag{2.49}$$

From the scattering matrix (2.20), it is clear that inducing port two reflection-free requires $h_*|_{\psi=1} = 0$. From the general form of the transfer matrix of the reflection-free two-port (2.49), the relation $h_*|_{\psi=1} = 0$ clearly implies

$$\beta = \left.\frac{\sigma h_*}{g}\right|_{\psi=1} \tag{2.50}$$

and since g is hurwitz by assumption, $|\beta| < 1$. The new reflection-free polynomials are given by

$$f_{RF} = f$$

$$h_{RF} = \frac{1}{\sqrt{1 - \beta\beta^*}}\left(h - \beta^* \sigma g_*\right)$$

$$g_{RF} = \frac{1}{\sqrt{1 - \beta\beta^*}}\left(g - \beta^* \sigma h_*\right)$$

$$\sigma_{RF} = \sigma \tag{2.51a,b,c,d}$$

Notice that both the f polynomial and the σ value for the section do not change.

2.6 Complex Elementary Sections

As will be shown in Chapter III, a complex lossless two-port network of any order can be composed exclusively of complex first-order and zeroth-order sections. The following will present all of the complex sections needed for the synthesis of a real or complex network of arbitrary finite order. First, the complex reciprocal first-order sections realizing a transmission zero at infinity or at the origin will be given. Second, the complex reciprocal first-order sections realizing a finite imaginary axis zero will be presented. Third, the complex non-reciprocal first-order sections realizing a transmission zero anywhere in the finite ψ plane will be given, where the real axis is a special case. Finally, the complex zeroth-order sections, otherwise known as the complex constant sections, will be presented. The elementary sections are given in table form, with each table containing a

Parameters section, a *V-I domain Matrix* description, and the *Canonic Polynomials* for the section. Note that if the appropriate imaginary resistors are assigned values of either zero or infinity, all of the complex sections reduce to real sections.

The *Parameters* section contains the analog domain symbol for the section showing the actual lumped-elements required for the definition of the section and the defining equations. For the reciprocal first-order sections, the reflectance and the delay evaluated at the transmission zero are given in terms of the section element values, and the element values are given in terms of the delay, the reflectance, and, where appropriate, the value of the transmission zero. The defining equations given in the two domains, that is, the V-I and the wave domain, demonstrates that each first-order section can be adequately represented in either domain with a canonic number of parameters (namely three parameters for reciprocal sections and four parameters for non-reciprocal sections). For non-reciprocal sections the delay is not needed and thus will not be supplied.

The *V-I domain Matrix* description gives either the open-circuit impedance matrix, the short-circuit admittance matrix, or the chain matrix, with the order showing the preference for the presentation.

The *Canonic Polynomials* section gives the defining polynomials both in terms of the V-I lumped element values, and also the reflectance, the transmission zero if appropriate, and for reciprocal sections the delay. The β value defined from (2.50) and the resulting canonic polynomials defined by (2.51) are given for port two reflection-free.

2.6.1 Complex First-Order Reciprocal Sections

In the following, the complex first-order reciprocal sections will be presented. The reflectance evaluated at the transmission zero for a section is unimodular.

2.6.1.1 Sections that Realize a Transmission Zero at Infinity

The following two tables define the CA1_∞ and the CB1_∞ sections which realize a transmission zero at infinity.

CA1_∞ Section: Transmission zero at infinity		
Parameters	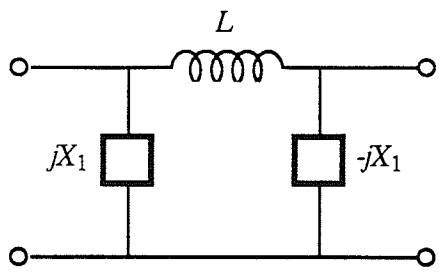	$L = \frac{\cos\theta + 1}{d}$ $X_1 = \frac{1 + \cos\theta}{\sin\theta}$ $\rho(\psi = \infty) = \frac{X_1 + j}{X_1 - j} = e^{j\theta}$ $d(\psi = \infty) = \frac{2X_1^2}{(X_1^2 + 1)L} > 0$
Z Matrix	$Z = \begin{bmatrix} \frac{(X_1 + jL\psi)X_1}{L\psi} & \frac{X_1^2}{L\psi} \\ \frac{X_1^2}{L\psi} & \frac{(X_1 - jL\psi)X_1}{L\psi} \end{bmatrix}$	
Canonic Polynomials	Original	Port 2 Reflection-free
	$f = 1$ $h = \frac{1}{2}\frac{(X_1 + j)^2 L\psi}{X_1^2} = \frac{e^{j\theta}\psi}{d}$ $g = \frac{1}{2}\frac{(X_1^2 + 1)L\psi}{X_1^2} + 1 = \frac{\psi}{d} + 1$ $\sigma = 1$	$\beta = \frac{-e^{j\theta}}{d + 1}$ $f_{RF} = 1$ $h_{RF} = \frac{(\psi + 1)e^{j\theta}}{\sqrt{(d + 2)d}}$ $g_{RF} = \frac{\psi + d + 1}{\sqrt{(d + 2)d}}$ $\sigma_{RF} = 1$

Table 2.1: The CA1_∞ section that realizes a transmission zero at infinity.

CB1_∞ Section: Transmission zero at infinity		
Parameters	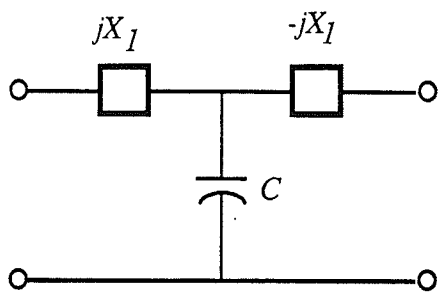	$C = \frac{1-\cos\theta}{d}$ $X_1 = \frac{1+\cos\theta}{\sin\theta}$ $\rho(\psi=\infty) = \frac{X_1+j}{X_1-j} = e^{j\theta}$ $d(\psi=\infty) = \frac{2}{(X_1^2+1)C} > 0$
Z Matrix	$\mathbf{Z} = \begin{bmatrix} \frac{jCX_1\psi+1}{C\psi} & \frac{1}{C\psi} \\ \frac{1}{C\psi} & \frac{-jCX_1\psi+1}{C\psi} \end{bmatrix}$	
Canonic Polynomials	Original	Port 2 Reflection-free
	$f=1$ $h = \frac{1}{2}(X_1+j)^2 C\psi = \frac{e^{j\theta}\psi}{d}$ $g = \frac{1}{2}(X_1^2+1)C\psi + 1 = \frac{\psi}{d} + 1$ $\sigma = 1$	$\beta = \frac{-e^{j\theta}}{d+1}$ $f_{RF} = 1$ $h_{RF} = \frac{(\psi+1)e^{j\theta}}{\sqrt{(d+2)d}}$ $g_{RF} = \frac{\psi+d+1}{\sqrt{(d+2)d}}$ $\sigma_{RF} = 1$

Table 2.2: The CB1_∞ section that realizes a transmission zero at infinity.

2.6.1.2 Sections that Realize a Transmission Zero at the Origin

The following two tables define the CC1_0 and the CD1_0 sections which realize a transmission zero at the origin.

CC1_0 Section: Transmission zero at the origin		
Parameters	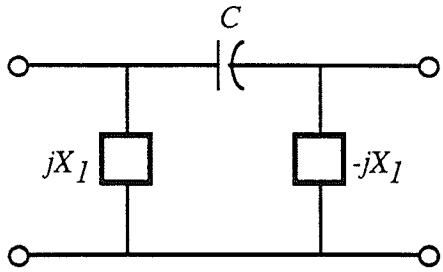	$C = \frac{d}{\cos\theta + 1}$ $X_1 = \frac{1+\cos\theta}{\sin\theta}$ $\rho(\psi=0) = \frac{X_1 + j}{X_1 - j} = e^{j\theta}$ $d(\psi=0) = \frac{2CX_1^2}{X_1^2+1} > 0$
Z Matrix	$\mathbf{Z} = \begin{bmatrix} (CX_1\psi + j)X_1 & CX_1^2\psi \\ CX_1^2\psi & (CX_1\psi - j)X_1 \end{bmatrix}$	
Canonic Polynomials	Original	Port 2 Reflection-free
	$f = \psi$ $h = \frac{1}{2}\frac{(X_1+j)^2}{CX_1^2} = \frac{e^{j\theta}}{d}$ $g = \psi + \frac{1}{2}\frac{X_1^2+1}{CX_1^2} = \psi + \frac{1}{d}$ $\sigma = -1$	$\beta = \frac{-e^{j\theta}}{d+1}$ $f_{RF} = \psi$ $h_{RF} = \frac{(\psi+1)e^{j\theta}}{\sqrt{d+2}\sqrt{d}}$ $g_{RF} = \frac{(d+1)\psi + 1}{\sqrt{d+2}\sqrt{d}}$ $\sigma_{RF} = -1$

Table 2.3: The CC1_0 section that realizes a transmission zero at the origin.

CD1_0 Section: Transmission zero at the origin		
Parameters	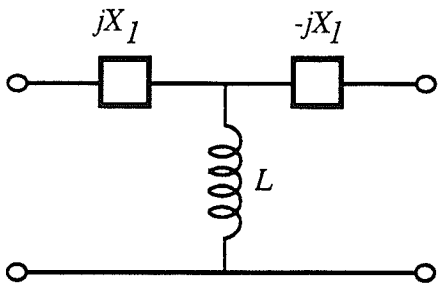	$L = \frac{d}{1-\cos\theta}$ $X_1 = \frac{1+\cos\theta}{\sin\theta}$ $\rho(\psi=0) = \frac{X_1+j}{X_1-j} = e^{j\theta}$ $d(\psi=0) = \frac{2L}{X_1^2+1} > 0$
Z Matrix	$Z = \begin{bmatrix} jX_1 + L\psi & L\psi \\ L\psi & -jX_1 + L\psi \end{bmatrix}$	
Canonic Polynomials	Original	Port 2 Reflection-free
	$f = \psi$ $h = \frac{(X_1+j)^2}{2L} = \frac{e^{j\theta}}{d}$ $g = \psi + \frac{1}{2}\frac{X_1^2+1}{L} = \psi + \frac{1}{d}$ $\sigma = -1$	$\beta = \frac{-e^{j\theta}}{d+1}$ $f_{RF} = \psi$ $h_{RF} = \frac{(\psi+1)e^{j\theta}}{\sqrt{d+2}\sqrt{d}}$ $g_{RF} = \frac{(d+1)\psi+1}{\sqrt{d+2}\sqrt{d}}$ $\sigma_{RF} = -1$

Table 2.4: The CD1_0 section that realizes a transmission zero at the origin.

2.6.1.3 Sections that Realize a Transmission Zero On the Finite $j\phi$ Axis

The following four tables define the CA1_$j\phi$, CB1_$j\phi$, CC1_$j\phi$, and the CD1_$j\phi$ sections which realize a finite transmission zero anywhere on the imaginary axis, except at the origin or at infinity.

CA1_$j\phi$ Section: Transmission zero at $j\phi_0$	
Parameters	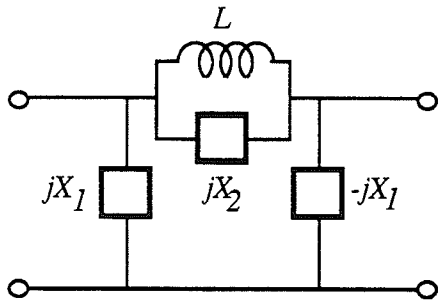 $L=\frac{\cos\theta+1}{d\phi_0^{\,2}}$ $\quad \phi_0=\frac{-X_2}{L}$ $X_1=\frac{1+\cos\theta}{\sin\theta}$ $\quad X_2=-L\phi_0$ $\rho(j\phi_0)=\frac{X_1+j}{X_1-j}=e^{j\theta}$ $d(j\phi_0)=2\frac{LX_1^{\,2}}{(X_1^{\,2}+1)X_2^{\,2}}>0$
Z Matrix	$Z=\begin{bmatrix} \frac{[X_2X_1+j(X_2-X_1)L\psi]X_1}{LX_2\psi} & \frac{(X_2-jL\psi)X_1^{\,2}}{LX_2\psi} \\ \frac{(X_2-jL\psi)X_1^{\,2}}{LX_2\psi} & \frac{[X_2X_1-j(X_2+X_1)L\psi]X_1}{LX_2\psi} \end{bmatrix}$

Canonic Polynomials	Original	Port 2 Reflection-free
	$f=\psi+\frac{jX_2}{L}=\psi-j\phi_0$ $h=\frac{1}{2}\frac{j(X_1+j)^2X_2\psi}{X_1^2}=\frac{-je^{j\theta}\psi}{d\phi_0}$ $g=\frac{1}{2}\frac{[j(X_1^{\,2}+1)X_2+2X_1^{\,2}]\psi}{X_1^{\,2}}+\frac{jX_2}{L}$ $=\frac{(d\phi_0-j)\psi}{d\phi_0}-j\phi_0$ $\sigma=1$	$X=d\phi_0^{\,2}+1+jd\phi_0$ $\beta=\frac{e^{-j\theta}}{X}$ $f_{RF}=\psi-j\phi_0$ $h_{RF}=\frac{-j\phi_0(\psi+1)\sqrt{X}e^{j\theta}}{\sqrt{XX^*-1}\sqrt{X^*}}$ $g_{RF}=\frac{-j\phi_0\sqrt{X}[(jd\phi_0+1+d)\psi+X^*]}{\sqrt{XX^*-1}\sqrt{X^*}}$ $\sigma_{RF}=1$

Table 2.5: The CA1_$j\phi$ section that realizes a finite non-zero transmission zero.

CB1_$j\phi$ Section: Transmission zero at $j\phi_0$		
Parameters	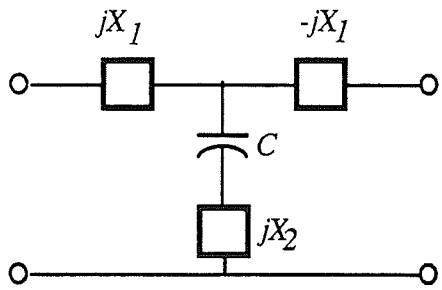	$C = \dfrac{1-\cos\theta}{d\phi_0^{\,2}}$ $\quad \phi_0 = \dfrac{1}{CX_2}$ $X_1 = \dfrac{1+\cos\theta}{\sin\theta}$ $\quad X_2 = \dfrac{1}{C\phi_0}$ $\rho(j\phi_0) = \dfrac{X_1+j}{X_1-j} = e^{j\theta}$ $d(j\phi_0) = 2\dfrac{CX_2^{\,2}}{X_1^{\,2}+1} > 0$
Z Matrix	$Z = \begin{bmatrix} \dfrac{j(X_2+X_1)C\psi+1}{C\psi} & \dfrac{jCX_2\psi+1}{C\psi} \\ \dfrac{jCX_2\psi+1}{C\psi} & \dfrac{j(X_2-X_1)C\psi+1}{C\psi} \end{bmatrix}$	
Canonic Polynomials	Original	Port 2 Reflection-free
	$f = \psi - \dfrac{j}{CX_2} = \psi - j\phi_0$ $h = \frac{1}{2}\dfrac{-j(X_1+j)^2\psi}{X_2} = \dfrac{-je^{j\theta}\psi}{d\phi_0}$ $g = \frac{1}{2}\dfrac{\left(2X_2 - jX_1^{\,2} - j\right)\psi}{X_2} - \dfrac{j}{CX_2}$ $= \dfrac{\left(d\phi_0 - j\right)\psi}{d\phi_0} - j\phi_0$ $\sigma = 1$	$X = d\phi_0^{\,2} + 1 + jd\phi_0$ $\beta = \dfrac{e^{-j\theta}}{X}$ $f_{RF} = \psi - j\phi_0$ $h_{RF} = \dfrac{-j\phi_0(\psi+1)\sqrt{X}e^{j\theta}}{\sqrt{XX^*-1}\sqrt{X^*}}$ $g_{RF} = \dfrac{-j\phi_0\sqrt{X}\left[\left(jd\phi_0+1+d\right)\psi + X^*\right]}{\sqrt{XX^*-1}\sqrt{X^*}}$ $\sigma_{RF} = 1$

Table 2.6: The CB1_$j\phi$ section that realizes a finite non-zero transmission zero.

CC1_$j\phi$ Section: Transmission zero at $j\phi_0$		
Parameters	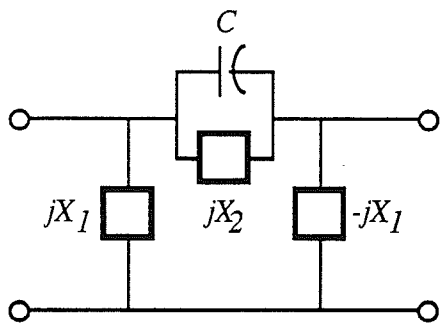	$C=\dfrac{d}{\cos\theta+1}$ $\quad \phi_0=\dfrac{1}{CX_2}$ $X_1=\dfrac{1+\cos\theta}{\sin\theta}$ $\quad X_2=\dfrac{1}{C\phi_0}$ $\rho(j\phi_0)=\dfrac{X_1+j}{X_1-j}=e^{j\theta}$ $d(j\phi_0)=2\dfrac{CX_1^2}{X_1^2+1}>0$
Z Matrix	$Z=\begin{bmatrix} \dfrac{[j(X_2-X_1)+CX_2X_1\psi]X_1}{X_2} & \dfrac{j(jCX_2\psi+1)X_1^2}{X_2} \\ \dfrac{j(jCX_2\psi+1)X_1^2}{X_2} & \dfrac{[-j(X_2+X_1)+CX_2X_1\psi]X_1}{X_2} \end{bmatrix}$	
Canonic Polynomials	Original	Port 2 Reflection-free
	$f=\psi-\dfrac{j}{CX_2}=\psi-j\phi_0$ $h=\dfrac{1}{2}\dfrac{X_1^2-1}{CX_1^2}+\dfrac{j}{CX_1}=\dfrac{e^{j\theta}}{d}$ $g=\psi+\dfrac{1}{2}\dfrac{X_1^2+1}{CX_1^2}-\dfrac{j}{CX_2}$ $=\psi+\dfrac{1}{d}-j\phi_0$ $\sigma=-1$	$X=d+1+jd\phi_0$ $\beta=\dfrac{-e^{j\theta}}{X^*}$ $f_{RF}=\psi-j\phi_0$ $h_{RF}=\dfrac{(\psi+1)\sqrt{X^*}e^{j\theta}}{\sqrt{XX^*-1}\sqrt{X}}$ $g_{RF}=\dfrac{\left(X\psi+d\phi_0^2+1-jd\phi_0\right)\sqrt{X^*}}{\sqrt{XX^*-1}\sqrt{X}}$ $\sigma_{RF}=-1$

Table 2.7: The CC1_$j\phi$ section that realizes a finite non-zero transmission zero.

CD1_$j\phi$ Section: Transmission zero at $j\phi_0$		
Parameters	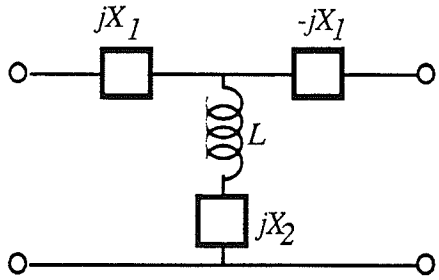	$L=\dfrac{d}{1-\cos\theta}$ $\quad \phi_0=\dfrac{-X_2}{L}$ $X_1=\dfrac{1+\cos\theta}{\sin\theta}$ $\quad X_2=-L\phi_0$ $\rho(j\phi_0)=\dfrac{X_1+j}{X_1-j}=e^{j\theta}$ $d(j\phi_0)=2\dfrac{L}{X_1^2+1}>0$
Z Matrix	$Z=\begin{bmatrix} j(X_2+X_1)+L\psi & jX_2+L\psi \\ jX_2+L\psi & j(X_2-X_1)+L\psi \end{bmatrix}$	
Canonic Polynomials	Original	Port 2 Reflection-free
	$f=\psi+\dfrac{jX_2}{L}=\psi-j\phi_0$ $h=\dfrac{1}{2}\dfrac{X_1^2-1}{L}+\dfrac{jX_1}{L}=\dfrac{e^{j\theta}}{d}$ $g=\psi+\dfrac{1}{2}\dfrac{X_1^2+1}{L}+\dfrac{jX_2}{L}$ $=\psi+\dfrac{1}{d}-j\phi_0$ $\sigma=-1$	$X=d+1+jd\phi_0$ $\beta=\dfrac{-e^{j\theta}}{X^*}$ $f_{RF}=\psi-j\phi_0$ $h_{RF}=\dfrac{(\psi+1)\sqrt{X^*}e^{j\theta}}{\sqrt{XX^*-1}\sqrt{X}}$ $g_{RF}=\dfrac{\left(X\psi+d\phi_0^2+1-jd\phi_0\right)\sqrt{X^*}}{\sqrt{XX^*-1}\sqrt{X}}$ $\sigma_{RF}=-1$

Table 2.8: The CD1_$j\phi$ section that realizes a finite non-zero transmission zero.

2.6.2 Complex First-Order Non-Reciprocal Sections

In the following, the complex first-order non-reciprocal sections will be presented. The reflectance evaluated at the transmission zero for a section is not unimodular. A restriction on the location of the real part of the transmission zero $(-\phi_r)$ implied by passivity is given by

$$\begin{aligned} \eta>1 &\Leftrightarrow (-\phi_r)<0 \\ \eta<1 &\Leftrightarrow (-\phi_r)>0 \end{aligned} \tag{2.52}$$

where η is the magnitude of the reflectance evaluated at the transmission zero.

2.6.2.1 Sections that Realize a Transmission Zero Anywhere in ψ Plane

The following two tables define the CE1 and CF1 sections which realize a finite transmission zero anywhere in the ψ plane.

CE1 Section: Transmission zero at $-\phi_r - j\phi_i$	
Parameters	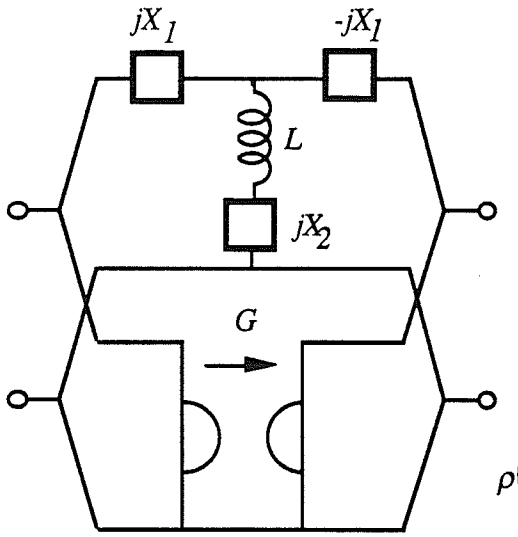 $G = \dfrac{-\eta^2+1}{2\eta\cos\theta+\eta^2+1}$ $\quad \phi_r = \dfrac{-X_1^2 G}{L}$ $X_1 = \dfrac{1}{2}\dfrac{2\eta\cos\theta+\eta^2+1}{\eta\sin\theta}$ $\quad \phi_i = \dfrac{X_2}{L}$ $X_2 = \dfrac{1}{4}\dfrac{(\eta^2-1)(2\eta\cos\theta+\eta^2+1)\phi_i}{\phi_r\eta^2\sin^2\theta}$ $L = \dfrac{1}{4}\dfrac{(\eta^2-1)(2\eta\cos\theta+\eta^2+1)}{\phi_r\eta^2\sin^2\theta}$ $\rho(-\phi_r - j\phi_i) = \dfrac{(-G^2+1)X_1^2 - 1 + 2jX_1}{(G+1)^2X_1^2+1} = \eta e^{j\theta}$
Z Matrix	$Z = \dfrac{1}{X_1^2G^2+1}\begin{bmatrix} j(X_2+X_1)+L\psi & jX_2+X_1^2G+L\psi \\ jX_2-X_1^2G+L\psi & j(X_2-X_1)+L\psi \end{bmatrix}$

Canonic Polynomials	Original	Port 2 Reflection-free
	$f = \psi - \dfrac{X_1^2G}{L} + \dfrac{jX_2}{L} = \psi + \phi_r + j\phi_i$ $h = \dfrac{\frac{1}{2}(-G^2+1)X_1^2 - 1}{L} + \dfrac{jX_1}{L}$ $h = 2\dfrac{\phi_r\eta e^{j\theta}}{\eta^2-1}$ $g = \psi + \dfrac{\frac{1}{2}(G^2+1)X_1^2+1}{L} + \dfrac{jX_2}{L}$ $= \psi + \dfrac{(\eta^2+1)\phi_r}{\eta^2-1} + j\phi_i$ $\sigma = -1$	$\beta = -2\dfrac{e^{-j\theta}\phi_r\eta}{-j\phi_i+\phi_r-1+(j\phi_i+\phi_r+1)\eta^2}$ $f_{RF} = \psi + \phi_r + j\phi_i$ $h_{RF} = 2\dfrac{(\psi+1)e^{j\theta}\phi_r\eta}{[j\phi_i+\phi_r+(-j\phi_i+\phi_r+1)\eta^2-1]\sqrt{-\beta\beta^*+1}}$ $g_{RF} = \dfrac{\lambda+[j\phi_i+\phi_r+(-j\phi_i+\phi_r+1)\eta^2-1]\psi}{[j\phi_i+\phi_r+(-j\phi_i+\phi_r+1)\eta^2-1]\sqrt{-\beta\beta^*+1}}$ $\lambda = -\phi_i^2 - j\phi_i - \phi_r^2 + \phi_r + (\phi_i^2 + j\phi_i + \phi_r^2 + \phi_r)\eta^2$ $\sigma_{RF} = -1$

Table 2.9: The CE1 section that realizes a transmission zero anywhere on the ψ plane.

CF1 Section: Transmission zero at $-\phi_r - j\phi_i$

Parameters

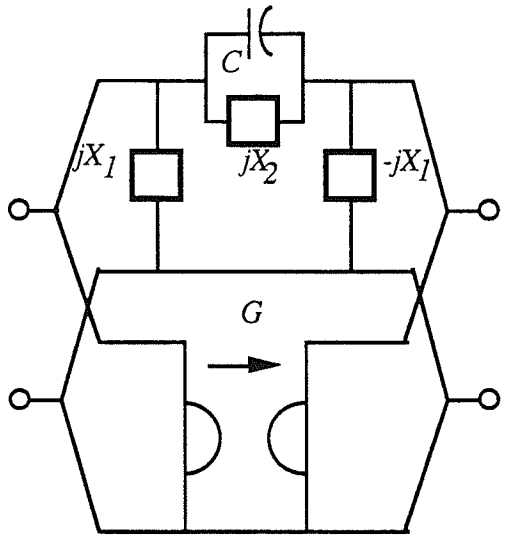

$$G = \frac{-\eta^2 + 1}{2\eta\cos\theta + \eta^2 + 1} \qquad \phi_r = \frac{-G}{C}$$

$$X_1 = \frac{1}{2}\frac{2\eta\cos\theta + \eta^2 + 1}{\eta\sin\theta} \qquad \phi_i = \frac{-1}{CX_2}$$

$$X_2 = \frac{\left(2\eta\cos\theta + \eta^2 + 1\right)\phi_r}{\left(-\eta^2 + 1\right)\phi_i}$$

$$C = \frac{\eta^2 - 1}{\left(2\eta\cos\theta + \eta^2 + 1\right)\phi_r}$$

$$\rho\left(-\phi_r - j\phi_i\right) = \frac{\left(-G^2 + 1\right)X_1{}^2 - 1 + 2jX_1}{(G+1)^2 X_1{}^2 + 1} = \eta e^{j\theta}$$

Z Matrix

$$Z = \frac{1}{G^2 X_1{}^2 + 1}\begin{bmatrix} \dfrac{[j(X_2 - X_1) + CX_2X_1\psi]X_1}{X_2} & \dfrac{(GX_2 + CX_2\psi - j)X_1{}^2}{X_2} \\ \dfrac{(-GX_2 + CX_2\psi - j)X_1{}^2}{X_2} & \dfrac{[-j(X_2 + X_1) + CX_2X_1\psi]X_1}{X_2} \end{bmatrix}$$

Canonic Polynomials

Original	Port 2 Reflection-free
$f = \psi - \frac{G}{C} - \frac{j}{CX_2} = \psi + \phi_r + j\phi_i$	$\beta = -2\frac{e^{-j\theta}\phi_r\eta}{-j\phi_i + \phi_r - 1 + \left(j\phi_i + \phi_r + 1\right)\eta^2}$
$h = \frac{1}{2}\frac{\left(-G^2 + 1\right)X_1{}^2 - 1}{CX_1{}^2} + \frac{j}{CX_1}$	$f_{RF} = \psi + \phi_r + j\phi_i$
$h = 2\frac{\phi_r\eta e^{j\theta}}{\eta^2 - 1}$	$h_{RF} = 2\frac{(\psi + 1)e^{j\theta}\phi_r\eta}{\left[j\phi_i + \phi_r + \left(-j\phi_i + \phi_r + 1\right)\eta^2 - 1\right]\sqrt{-\beta\beta^* + 1}}$
$g = \psi + \frac{1}{2}\frac{\left(G^2 + 1\right)X_1{}^2 + 1}{CX_1{}^2} - \frac{j}{CX_2}$	$g_{RF} = \frac{\lambda + \left[j\phi_i + \phi_r + \left(-j\phi_i + \phi_r + 1\right)\eta^2 - 1\right]\psi}{\left[j\phi_i + \phi_r + \left(-j\phi_i + \phi_r + 1\right)\eta^2 - 1\right]\sqrt{-\beta\beta^* + 1}}$
$= \psi + \frac{\left(\eta^2 + 1\right)\phi_r}{\eta^2 - 1} + j\phi_i$	$\lambda = -\phi_i{}^2 - j\phi_i - \phi_r{}^2 + \phi_r + \left(\phi_i{}^2 + j\phi_i + \phi_r{}^2 + \phi_r\right)\eta^2$
$\sigma = -1$	$\sigma_{RF} = -1$

Table 2.10: The CF1 section that realizes a transmission zero anywhere on the ψ plane.

2.6.2.2 Sections that Realize a Transmission Zero on the Real Axis

The following two tables define the CG1 and CH1 sections which realize a finite transmission zero anywhere on the finite real axis, except at the origin.

CG1 Section: Transmission zero at $-\phi_r$	
Parameters	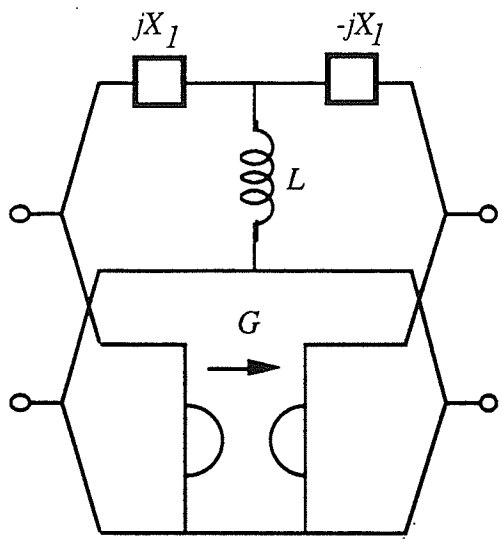 $G=\dfrac{-\eta^2+1}{2\eta\cos\theta+\eta^2+1}$ $X_1=\dfrac{1}{2}\dfrac{2\eta\cos\theta+\eta^2+1}{\eta\sin\theta}$ $L=\dfrac{1}{4}\dfrac{(\eta^2-1)(2\eta\cos\theta+\eta^2+1)}{\phi_r(\eta\sin\theta)^2}$ $\phi_r=\dfrac{-GX_1^2}{L}$ $\rho(-\phi_r)=\dfrac{(-G^2+1)X_1^2-1+2jX_1}{(G+1)^2X_1^2+1}=\eta e^{j\theta}$
Z Matrix	$Z=\dfrac{1}{G^2X_1^2+1}\begin{bmatrix} jX_1+L\psi & GX_1^2+L\psi \\ -GX_1^2+L\psi & -jX_1+L\psi \end{bmatrix}$

Canonic Polynomials	Original	Port 2 Reflection-free
	$f=\psi-\dfrac{GX_1^2}{L}=\psi+\phi_r$ $h=\dfrac{1}{2}\dfrac{(-G^2+1)X_1^2-1+2jX_1}{L}$ $h=2\dfrac{\phi_r\eta e^{j\theta}}{\eta^2-1}$ $g=\psi+\dfrac{1}{2}\dfrac{(G^2+1)X_1^2+1}{L}$ $=\psi+\dfrac{(\eta^2+1)\phi_r}{\eta^2-1}$ $\sigma=-1$	$\beta=-2\dfrac{\phi_r\eta e^{-j\theta}}{(\eta^2+1)\phi_r+\eta^2-1}$ $f_{RF}=\psi+\phi_r$ $h_{RF}=2\dfrac{(\psi+1)\phi_r\eta e^{j\theta}}{\sqrt{-\beta\beta^*+1}\left[(\eta^2+1)\phi_r+\eta^2-1\right]}$ $g_{RF}=\dfrac{\left[(\eta^2-1)\phi_r+\eta^2+1\right]+\left[(\eta^2+1)\phi_r+\eta^2-1\right]\psi}{\sqrt{-\beta\beta^*+1}\left[(\eta^2+1)\phi_r+\eta^2-1\right]}$ $\sigma_{RF}=-1$

Table 2.11: The CG1 section that realizes a transmission zero on the finite real axis.

CH1 Section: Transmission zero at $-\phi_r$

Parameters

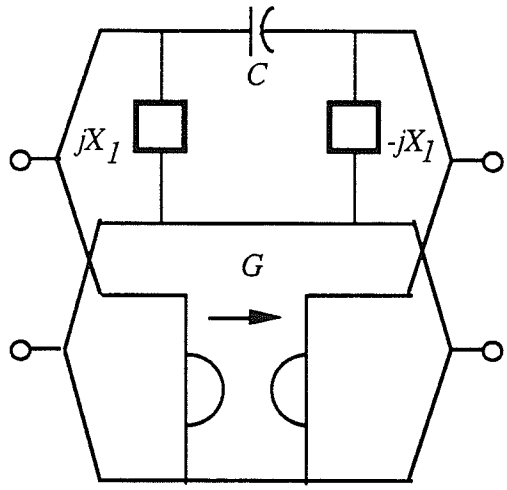

$$G = \frac{-\eta^2 + 1}{2\eta\cos\theta + \eta^2 + 1}$$

$$X_1 = \frac{1}{2}\frac{2\eta\cos\theta + \eta^2 + 1}{\eta\sin\theta}$$

$$C = \frac{\eta^2 - 1}{(2\eta\cos\theta + \eta^2 + 1)\phi_r}$$

$$\phi_r = \frac{-G}{C}$$

$$\rho(-\phi_r) = \frac{(-G^2 + 1)X_1^2 - 1 + 2jX_1}{(G+1)^2 X_1^2 + 1} = \eta e^{j\theta}$$

Z Matrix

$$\mathbf{Z} = \frac{1}{G^2 X_1^2 + 1}\begin{bmatrix} (CX_1\psi + j)X_1 & (G + C\psi)X_1^2 \\ (-G + C\psi)X_1^2 & (CX_1\psi - j)X_1 \end{bmatrix}$$

Canonic Polynomials

Original	Port 2 Reflection-free
$f = \psi - \frac{G}{C} = \psi + \phi_r$	$\beta = -2\frac{\phi_r \eta e^{-j\theta}}{(\eta^2+1)\phi_r + \eta^2 - 1}$
$h = \frac{(-G^2+1)X_1^2 - 1 + 2jX_1}{2CX_1^2}$	$f_{RF} = \psi + \phi_r$
$h = 2\frac{\phi_r \eta e^{j\theta}}{\eta^2 - 1}$	$h_{RF} = 2\frac{(\psi+1)\phi_r \eta e^{j\theta}}{\sqrt{-\beta\beta^* + 1}\left[(\eta^2+1)\phi_r + \eta^2 - 1\right]}$
$g = \psi + \frac{1}{2}\frac{(G^2+1)X_1^2 + 1}{CX_1^2}$	$g_{RF} = \frac{\left[(\eta^2-1)\phi_r + \eta^2 + 1\right] + \left[(\eta^2+1)\phi_r + \eta^2 - 1\right]\psi}{\sqrt{-\beta\beta^* + 1}\left[(\eta^2+1)\phi_r + \eta^2 - 1\right]}$
$= \psi + \frac{(\eta^2+1)\phi_r}{\eta^2 - 1}$	$\sigma_{RF} = -1$
$\sigma = -1$	

Table 2.12: The CH1 section that realizes a transmission zero on the finite real axis.

2.6.3 Complex Constant Sections

A constant section, also known as a zeroth-order section, is usually used to either induce the reflection-free property at a port, or as the last section in a realization. The most general constant section contains three real parameters. This is evident from the inspection of the canonic polynomials representing the section. They appear to be represented by four real parameters since two out of six degrees of freedom are removed from the polynomials (they can be scaled by the value of either polynomial setting one polynomial to unity). However, from the Feldtkeller equation (2.21), one parameter is dependent upon the others giving a total of three real parameters. The general zeroth-order sections are given in Tables 2.13 and 2.14 as a π and T connection of imaginary resistors.

Note that under certain conditions the π or T connection can be replaced with a section containing two imaginary resistors and a real ideal transformer. If $X_2 \neq -X_3$, then the T connection is equivalent to the following:

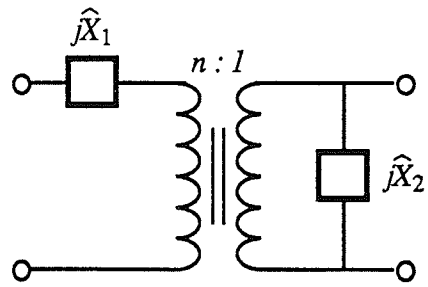

Figure 2.3: Equivalent of the T connection of imaginary resistors with $X_2 \neq -X_3$.

where the values are given by

$$n = \frac{X_2}{X_2 + X_3}$$
$$\hat{X}_1 = X_1 + nX_3$$
$$\hat{X}_2 = \frac{X_2}{n} \tag{2.53}$$

If $X_1 \neq -X_2$, then the T connection is also equivalent to the following Figure:

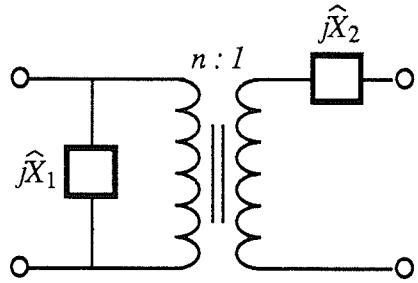

Figure 2.4: Equivalent of the T connection of imaginary resistors with $X_1 \neq -X_2$.

where the values are given by

$$n = \frac{X_1 + X_2}{X_2}$$
$$\hat{X}_1 = nX_2$$
$$\hat{X}_2 = X_3 + \frac{X_1}{n} \tag{2.54}$$

Note that if $X_1 = -X_2 = X_3$, the T connection is equivalent to a complex gyrator as defined by (2.3) with an imaginary gyration admittance.

C0_π Section: Constant Section	
Parameters	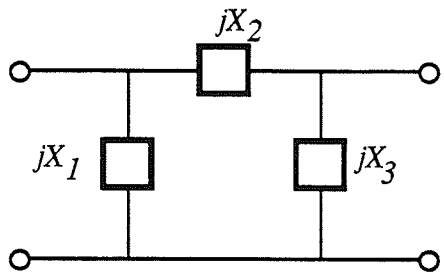 $X_1 = \frac{\mathrm{Im}\{g\} + \mathrm{Im}\{h\}}{\mathrm{Re}\{g\} - \mathrm{Re}\{h\} - 1}$ $X_2 = \mathrm{Im}\{g\} + \mathrm{Im}\{h\}$ $X_3 = \frac{\mathrm{Im}\{g\} + \mathrm{Im}\{h\}}{\mathrm{Re}\{g\} + \mathrm{Re}\{h\} - 1}$
Z Matrix	$Z = \frac{1}{X_3 + X_2 + X_1}\begin{bmatrix} j(X_3 + X_2)X_1 & jX_3X_1 \\ jX_3X_1 & j(X_2 + X_1)X_3 \end{bmatrix}$
Canonic Polynomials	$f = 1$ $h = \frac{1}{2}\frac{-X_3X_2 + X_2X_1}{X_3X_1} + \frac{1}{2}j\left[X_2 + \frac{X_3 + X_2 + X_1}{X_3X_1}\right]$ $g = \frac{1}{2}\frac{X_3X_2 + X_2X_1}{X_3X_1} + 1 + \frac{1}{2}j\left[X_2 + \frac{-(X_3 + X_2 + X_1)}{X_3X_1}\right]$ $\sigma = 1$

Table 2.13: C0_π constant section.

C0_T Section: Constant Section	
Parameters	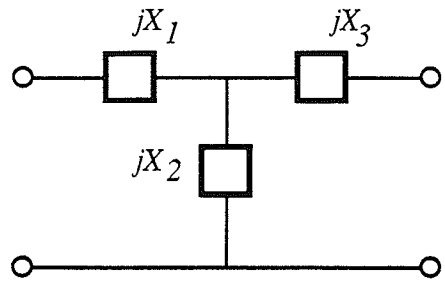 $X_1 = \frac{j[\mathrm{Re}\{g\} + \mathrm{Re}\{h\} - 1]}{-\mathrm{Im}\{g\} + \mathrm{Im}\{h\}}$ $X_2 = \frac{j}{-\mathrm{Im}\{g\} + \mathrm{Im}\{h\}}$ $X_3 = \frac{j[\mathrm{Re}\{g\} - \mathrm{Re}\{h\} - 1]}{-\mathrm{Im}\{g\} + \mathrm{Im}\{h\}}$
Z Matrix	$\mathbf{Z} = \begin{bmatrix} j(X_2 + X_1) & jX_2 \\ jX_2 & j(X_3 + X_2) \end{bmatrix}$
Canonic Polynomials	$f = 1$ $h = \frac{1}{2}\frac{-X_3 + X_1}{X_2} + \frac{1}{2}\frac{j[X_3X_2 + X_3X_1 + X_2X_1 + 1]}{X_2}$ $g = \frac{1}{2}\frac{X_3 + X_1}{X_2} + 1 + \frac{1}{2}\frac{j[X_3X_2 + X_3X_1 + X_2X_1 - 1]}{X_2}$ $\sigma = -1$

Table 2.14: C0_T constant section.

Two special forms of the constant section with two free parameters are given in Tables 2.15 and 2.16, and are labelled the C0_1 and C0_2 sections, respectively. The C0_1 section contains a series imaginary resistor and a real transformer, and the C0_2 section contains a shunt imaginary resistor and a real transformer. Note the form of the canonic polynomials, where the imaginary parts of the h and g polynomials are equal for the C0_1 section, and are the additive inverse of each other for the C0_2 section. Thus, neither of the sections are appropriate for inducing the reflection-free property using the definitions of the polynomials given in (2.45).

The complex transformer is given in Table 2.17. The real transformer is a special case and is found by replacing n^* with n in the definitions.

C0_1 Section: Constant Section with real transformer	
Parameters	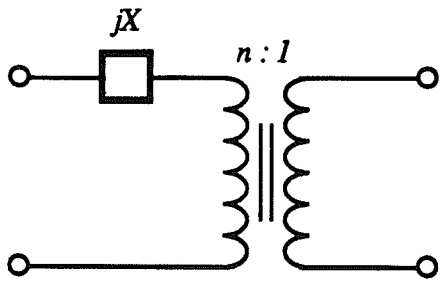 $n=\sqrt{[\mathrm{Re}\{h\}]^2+1}+\mathrm{Re}\{h\}>0$ $X=2n[\mathrm{Im}\{h\}]$ $n=\sqrt{[\mathrm{Re}\{g\}]^2-1}+\mathrm{Re}\{g\}>0$ $X=2n[\mathrm{Im}\{g\}]$
Y Matrix	**Canonic Polynomials**
$Y=\begin{bmatrix} \frac{-j}{X} & \frac{nj}{X} \\ \frac{nj}{X} & \frac{-n^2 j}{X} \end{bmatrix}$	$f=1$ $h=\frac{1}{2}\frac{n^2-1}{n}+\frac{1}{2}\frac{jX}{n}$ $g=\frac{1}{2}\frac{n^2+1}{n}+\frac{1}{2}\frac{jX}{n}$ $\sigma=1$

Table 2.15: Series imaginary resistor and real transformer C0_1 constant section.

C0_2 Section: Constant Section with real transformer	
Parameters	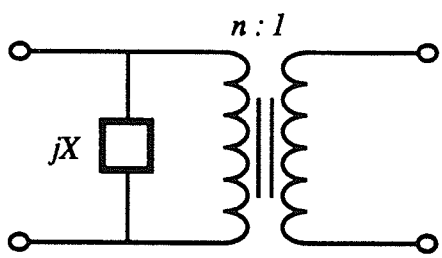 $n=\sqrt{[\mathrm{Re}\{h\}]^2+1}+\mathrm{Re}\{h\}>0$ $X=\frac{1}{2}\frac{n}{\mathrm{Im}\{h\}}$ $n=\sqrt{[\mathrm{Re}\{g\}]^2-1}+\mathrm{Re}\{g\}>0$ $X=\frac{1}{2}\frac{n}{\mathrm{Im}\{g\}}$
Z Matrix	**Canonic Polynomials**
$Z=\begin{bmatrix} jX & \frac{jX}{n} \\ \frac{jX}{n} & \frac{jX}{n^2} \end{bmatrix}$	$f=1$ $h=\frac{1}{2}\frac{n^2-1}{n}+\frac{1}{2}\frac{nj}{X}$ $g=\frac{1}{2}\frac{n^2+1}{n}-\frac{1}{2}\frac{nj}{X}$ $\sigma=1$

Table 2.16: Shunt imaginary resistor and real transformer C0_2 constant section.

T0 Section: Complex transformer	
Parameters	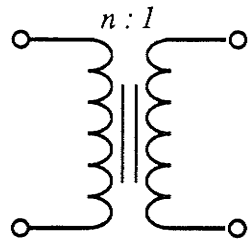 $n = \frac{1}{g-h}$ $n^* = g + h$
Chain Matrix	Canonic Polynomials
$K = \begin{bmatrix} n^* & 0 \\ 0 & n \end{bmatrix}$	$f = 1$ $h = \frac{1}{2}\frac{nn^* - 1}{n}$ $g = \frac{1}{2}\frac{nn^* + 1}{n}$ $\sigma = \frac{n^*}{n}$

Table 2.17: Complex transformer T0 section.

2.7 Real elementary Sections

The real elementary sections are given in [16], however they are presented here for completeness since they may be required for the synthesis given in Chapter III. Note that the canonic polynomials representing the sections will be given in a different form and also the port two reflection-free polynomials will be supplied. Also, the F1 non-reciprocal section containing an inductor was not defined earlier in [16] and is given in Table 2.23.

2.7.1 First Order Reciprocal Real Sections

The first-order real sections that realize a transmission zero at the origin or at infinity are given in the following Tables 2.18-21.

A1 Section: Transmission zero at infinity		
Parameters	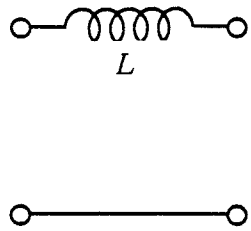 $L = 2\frac{1}{d}$ $\rho(\psi=\infty) = 1$ $d(\psi=\infty) = \frac{2}{L} > 0$	$Y = \begin{bmatrix} \frac{1}{\psi L} & \frac{1}{\psi L} \\ \frac{1}{\psi L} & \frac{1}{\psi L} \end{bmatrix}$
Canonic Polynomials	Original	Port 2 Reflection-free
	$f = 1$ $h = \frac{1}{2}L\psi = \frac{\psi}{d}$ $g = \frac{1}{2}L\psi + 1 = \frac{\psi}{d} + 1$ $\sigma = 1$	$f_{RF} = 1$ $h_{RF} = \frac{\psi + 1}{\sqrt{(d+2)d}}$ $g_{RF} = \frac{\psi + d + 1}{\sqrt{(d+2)d}}$ $\sigma_{RF} = 1$ $\beta = \frac{-1}{d+1}$

Table 2.18: Real A1 section that realizes a transmission zero at infinity.

B1 Section: Transmission zero at infinity		
Parameters	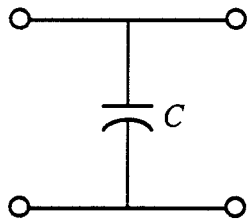 $C = 2\frac{1}{d}$ $\rho(\psi=\infty) = -1$ $d(\psi=\infty) = \frac{2}{C} > 0$	$Z = \begin{bmatrix} \frac{1}{\psi C} & \frac{1}{\psi C} \\ \frac{1}{\psi C} & \frac{1}{\psi C} \end{bmatrix}$
Canonic Polynomials	Original	Port 2 Reflection-free
	$f = 1$ $h = -\frac{1}{2}C\psi = \frac{-\psi}{d}$ $g = \frac{1}{2}L\psi + 1 = \frac{\psi}{d} + 1$ $\sigma = 1$	$f_{RF} = 1$ $h_{RF} = \frac{-(\psi + 1)}{\sqrt{(d+2)\,d}}$ $g_{RF} = \frac{\psi + d + 1}{\sqrt{(d+2)d}}$ $\sigma_{RF} = 1$ $\beta = \frac{1}{d+1}$

Table 2.19: Real B1 section that realizes a transmission zero at infinity.

C1 Section: Transmission zero at the origin		
Parameters	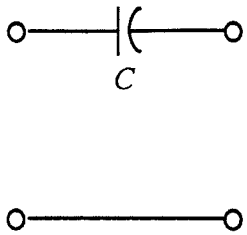 $C = \frac{1}{2}d$ $\rho(\psi = 0) = 1$ $d(\psi = 0) = 2C > 0$	$Y = \begin{bmatrix} C\psi & -C\psi \\ -C\psi & C\psi \end{bmatrix}$
Canonic Polynomials	Original	Port 2 Reflection-free
	$f = \psi$ $h = \frac{1}{2}\frac{1}{C} = \frac{1}{d}$ $g = \psi + \frac{1}{2}\frac{1}{C} = \psi + \frac{1}{d}$ $\sigma = -1$	$f_{RF} = \psi$ $h_{RF} = \frac{\psi + 1}{\sqrt{(d+2)d}}$ $g_{RF} = \frac{(d+1)\psi + 1}{\sqrt{(d+2)d}}$ $\sigma_{RF} = -1$ $\beta = \frac{-1}{d+1}$

Table 2.20: Real C1 section that realizes a transmission zero at the origin.

D1 Section: Transmission zero at the origin		
Parameters	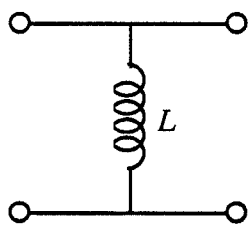 $L = \frac{1}{2}d$ $\rho(\psi = 0) = -1$ $d(\psi = 0) = 2L > 0$	$Z = \begin{bmatrix} L\psi & L\psi \\ L\psi & L\psi \end{bmatrix}$
Canonic Polynomials	Original	Port 2 Reflection-free
	$f = \psi$ $h = -\frac{1}{2}\frac{1}{L} = \frac{-1}{d}$ $g = \psi + \frac{1}{2}\frac{1}{L} = \psi + \frac{1}{d}$ $\sigma = -1$	$f_{RF} = \psi$ $h_{RF} = \frac{-(\psi + 1)}{\sqrt{(d+2)d}}$ $g_{RF} = \frac{(d+1)\psi + 1}{\sqrt{(d+2)d}}$ $\sigma_{RF} = -1$ $\beta = \frac{1}{d+1}$

Table 2.21: Real D1 section that realizes a transmission zero at the origin.

2.7.2 First Order Non-Reciprocal Real Sections

The two first-order non-reciprocal sections that realize a transmission zero on the real axis are given in the following two tables. The E1 section contains a capacitor while the F1 section contains an inductor.

E1 Section: Real transmission zero at $(-\phi_r)$		
Parameters	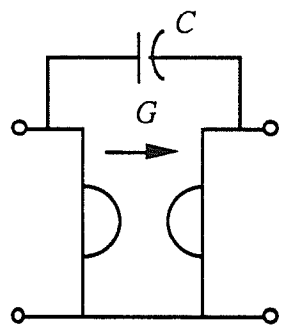	$G = \frac{-\rho+1}{\rho+1}$ $C = \frac{-G}{\phi_r}$ $\quad \phi_r = \frac{-G}{C}$ $\rho(\psi = -\phi_r) = \rho$
Z Matrix	$Z = \begin{bmatrix} \frac{C\psi}{G^2} & \frac{G+C\psi}{G^2} \\ \frac{-G+C\psi}{G^2} & \frac{C\psi}{G^2} \end{bmatrix}$	
Canonic Polynomials	Original	Port 2 Reflection-free
	$f = \psi - \frac{G}{C} = \psi + \phi_r$ $h = \frac{1}{2}\frac{-G^2+1}{C} = 2\frac{\rho\phi_r}{\rho^2-1}$ $g = \psi + \frac{1}{2}\frac{G^2+1}{C}$ $= \psi + \frac{(\rho^2+1)\phi_r}{\rho^2-1}$ $\sigma = -1$	$\beta = -2\frac{\rho\phi_r}{\phi_r - 1 + (\phi_r+1)\rho^2}$ $f_{RF} = \psi + \phi_r$ $h_{RF} = 2\frac{(\psi+1)\rho\phi_r}{\sqrt{-\beta^2+1}\left[\phi_r - 1 + (\phi_r+1)\rho^2\right]}$ $g_{RF} = \frac{\left[(\rho^2-1)\phi_r + \rho^2 + 1\right]\phi_r + \left[\phi_r - 1 + (\phi_r+1)\rho^2\right]\psi}{\sqrt{-\beta^2+1}\left[\phi_r - 1 + (\phi_r+1)\rho^2\right]}$ $\sigma_{RF} = -1$

Table 2.22: Real E1 section that realizes a transmission zero on the real axis.

F1 Section: Real transmission zero at $(-\phi_r)$		
Parameters	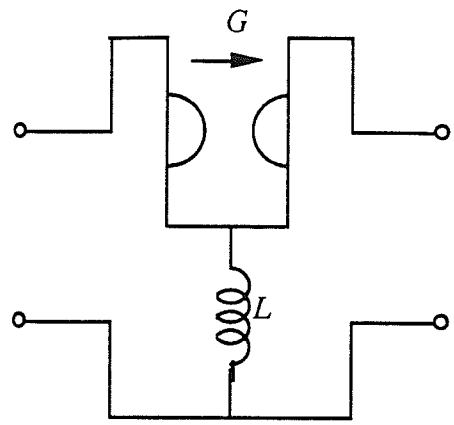	$G = \frac{-\rho+1}{\rho+1}$ $L = \frac{\rho+1}{(\rho-1)\phi_r}$ $\rho(\psi = -\phi_r) = \rho$ $\phi_r = \frac{-1}{GL}$
Z Matrix	$Z = \begin{bmatrix} L\psi & \frac{1}{G} + L\psi \\ -\frac{1}{G} + L\psi & L\psi \end{bmatrix}$	
Canonic Polynomials	Original	Port 2 Reflection-free
	$f = \psi - \frac{1}{GL} = \psi + \phi_r$ $h = \frac{1}{2}\frac{-G^2+1}{G^2L} = 2\frac{\rho\phi_r}{\rho^2-1}$ $g = \psi + \frac{1}{2}\frac{G^2+1}{G^2L}$ $= \psi + \frac{(\rho^2+1)\phi_r}{\rho^2-1}$ $\sigma = -1$	$\beta = -2\frac{\rho\phi_r}{\phi_r - 1 + (\phi_r+1)\rho^2}$ $f_{RF} = \psi + \phi_r$ $h_{RF} = 2\frac{(\psi+1)\rho\phi_r}{\sqrt{-\beta^2+1}\left[\phi_r - 1 + (\phi_r+1)\rho^2\right]}$ $g_{RF} = \frac{\left[(\rho^2-1)\phi_r + \rho^2 + 1\right]\phi_r + \left[\phi_r - 1 + (\phi_r+1)\rho^2\right]\psi}{\sqrt{-\beta^2+1}\left[\phi_r - 1 + (\phi_r+1)\rho^2\right]}$ $\sigma_{RF} = -1$

Table 2.23: Real F1 section that realizes a transmission zero on the real axis.

2.7.3 Second-Order Reciprocal Real Sections

The following three tables give the A2, B2 and Brune second-order sections. The A2 and B2 sections realize two complex conjugate transmission zeros on the $j\phi$ axis when the reflectance is plus or minus one. The Brune section is more general since it also realizes two complex conjugate transmission zeros on the $j\phi$ axis, but the reflectance can be any unimodular constant. The port 2 reflection free polynomials are not given for the Brune section since they are very complicated and are not necessary.

A2 Section: Two transmission zeros at $\pm j\phi_0$		
Parameters	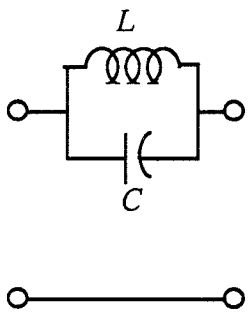	$L = 4\frac{1}{d\phi_0^2}$ $\quad \phi_0^2 = \frac{1}{CL}$ $C = \frac{1}{4}d$ $\rho\left(\psi^2 = -\phi_0^2\right) = 1$ $d\left(\psi^2 = -\phi_0^2\right) = 4C > 0$
Y Matrix	$Y = \begin{bmatrix} \frac{1+\psi^2 LC}{L\psi} & -\frac{1+\psi^2 LC}{L\psi} \\ -\frac{1+\psi^2 LC}{L\psi} & \frac{1+\psi^2 LC}{L\psi} \end{bmatrix}$	
Canonic Polynomials	Original	Port 2 Reflection-free
	$f = \psi^2 + \frac{1}{CL} = \psi^2 + \phi_0^2$ $h = \frac{1}{2C}\frac{\psi}{} = 2\frac{\psi}{d}$ $g = \psi^2 + \frac{1}{2C}\frac{\psi}{} + \frac{1}{CL}$ $= \psi + 2\frac{\psi}{d} + \phi_0^2$ $\sigma = 1$	$\beta = -2\frac{1}{d\phi_0^2 + d + 2}$ $f_{RF} = \psi^2 + \phi_0^2$ $h_{RF} = 2\frac{(\psi+1)\left(\phi_0^2 + \psi\right)}{\sqrt{\left(\phi_0^2+1\right)d+4}\sqrt{\left(\phi_0^2+1\right)d}}$ $g_{RF} = \frac{\left(d\phi_0^2+d+2\right)\left(\psi^2+\phi_0^2\right) + 2\left(\phi_0^2+1\right)\psi}{\sqrt{\left(\phi_0^2+1\right)d+4}\sqrt{\left(\phi_0^2+1\right)d}}$ $\sigma_{RF} = 1$

Table 2.24: Real A2 section that realizes complex conjugate transmission zeros on $j\phi$ axis.

B2 Section: Two transmission zeros at $\pm j\phi_0$		
Parameters	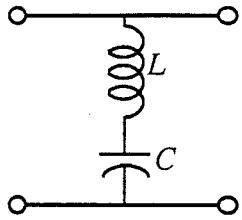	$L = \frac{1}{4}d$ $C = 4\frac{1}{d\phi_0^2}$ $\rho\left(\psi^2 = -\phi_0^2\right) = -1$ $d\left(\psi^2 = -\phi_0^2\right) = 4L > 0$ $\phi_0^2 = \frac{1}{CL}$
Z Matrix	$Z = \begin{bmatrix} \frac{1+\psi^2 LC}{\psi C} & \frac{1+\psi^2 LC}{\psi C} \\ \frac{1+\psi^2 LC}{\psi C} & \frac{1+\psi^2 LC}{\psi C} \end{bmatrix}$	
Canonic Polynomials	Original	Port 2 Reflection-free
	$f = \psi^2 + \frac{1}{CL} = \psi^2 + \phi_0^2$ $h = -\frac{1}{2}\frac{\psi}{L} = -2\frac{\psi}{d}$ $g = \psi^2 + \frac{1}{2}\frac{\psi}{L} + \frac{1}{CL}$ $= \psi + 2\frac{\psi}{d} + \phi_0^2$ $\sigma = 1$	$\beta = 2\frac{1}{d\phi_0^2 + d + 2}$ $f_{RF} = \psi^2 + \phi_0^2$ $h_{RF} = -2\frac{(\psi+1)\left(\phi_0^2 + \psi\right)}{\sqrt{\left(\phi_0^2+1\right)d+4}\sqrt{\left(\phi_0^2+1\right)d}}$ $g_{RF} = \frac{\left(d\phi_0^2+d+2\right)\left(\psi^2+\phi_0^2\right) + 2\left(\phi_0^2+1\right)\psi}{\sqrt{\left(\phi_0^2+1\right)d+4}\sqrt{\left(\phi_0^2+1\right)d}}$ $\sigma_{RF} = 1$

Table 2.25: Real B2 section that realizes complex conjugate transmission zeros on $j\phi$ axis.

Brune Section: Two transmission zeros at $\pm j\phi_0$

Parameters

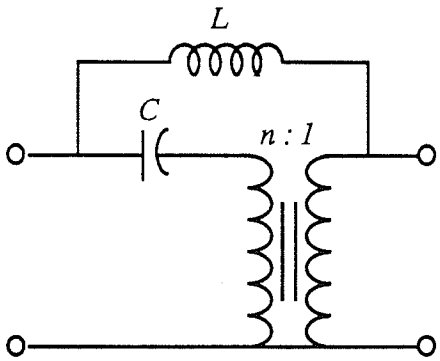

$$L = 2\frac{\cos(\theta)+1}{(d\phi_0+\sin(\theta))\phi_0} \qquad C = \frac{1}{2}\frac{d\phi_0-\sin(\theta)}{(\cos(\theta)+1)\phi_0}$$

$$n = \frac{d\phi_0+\sin(\theta)}{d\phi_0-\sin(\theta)} \qquad \phi_0^{\,2} = \frac{1}{nCL}$$

$$\rho\left(\psi^2 = -\phi_0^{\,2}\right) = \frac{\sqrt{\frac{nL}{C}}+j(n-1)}{\sqrt{\frac{nL}{C}}-j(n-1)} = e^{j\theta}$$

$$d\left(\psi^2 = -\phi_0^{\,2}\right) = 2\frac{(n+1)nCL}{(n-1)^2C+nL} > 0$$

Z Matrix

$$\mathbf{Z} = \begin{bmatrix} \dfrac{n^2CL\psi^2+1}{(n-1)^2C\psi} & \dfrac{nCL\psi^2+1}{(n-1)^2C\psi} \\ \dfrac{nCL\psi^2+1}{(n-1)^2C\psi} & \dfrac{CL\psi^2+1}{(n-1)^2C\psi} \end{bmatrix}$$

Canonic Polynomials

$$f = \psi^2 + \frac{1}{nCL} = \psi^2 + \phi_0^{\,2}$$

$$h = \frac{1}{2}\frac{(n^2-1)\psi^2}{n} + \frac{1}{2}\frac{\left[-(n-1)^2C+L\right]\psi}{nCL} = \frac{\left[d\phi_0\cos(\theta)-\sin(\theta)+\sin(\theta)d\psi\right]\psi\phi_0}{d^2\phi_0^{\,2}-\sin^2(\theta)}$$

$$g = \frac{1}{2}\frac{(n^2+1)\psi^2}{n} + \frac{1}{2}\frac{\left[(n-1)\}^2C+L\right]\psi}{nCL} + \frac{1}{nCL}$$

$$= \frac{\left[d^2\phi_0^2+\sin^2\theta\right]\psi^2}{d^2\phi_0^2-\sin^2\theta} + 2\frac{\left[d\phi_0 - \cos\theta\ \sin\theta\right]\phi_0\psi}{d^2\phi_0^2-\sin^2\theta} + \phi_0^2$$

$$\sigma = 1$$

Table 2.26: Real Brune section that realizes complex conjugate transmission zeros on the $j\phi$ axis.

2.8 Equivalences Between the Brune Section and the Complex Sections

The Brune section given in the preceding table is a general second-order section that realizes two complex conjugate transmission zeros on the $j\phi$ axis. Consider the realization of the two complex conjugate transmission zeros using any of the four first-order complex sections CA1_$j\phi$, CB1_$j\phi$, CC1_$j\phi$, or CD1_$j\phi$. Clearly, if the two zeros are realized using consecutive complex sections of the same type, then within at most a constant section the two complex sections grouped together must be equivalent to the respective Brune section on a two-port basis.

Let the Brune section as given in Table 2.26 be described by the lumped-element parameters L, C and n. The equivalence between each of the four complex first-order sections mentioned in the preceding paragraph and the Brune section are given in the following four tables, where for each table the equivalence from both perspectives are supplied. Thus a Brune section can be replaced with two complex first-order sections and vice-versa.

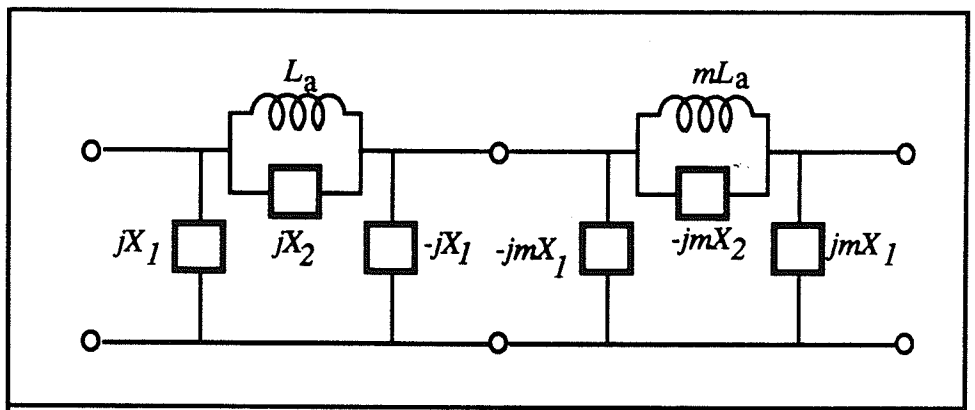

Complex Sections	Brune
$L_a = \frac{nL}{n+1}$	$L = \frac{2X_1L_a}{X_1 - X_2}$
$X_1 = \frac{1}{1-n}\sqrt{\frac{nL}{C}}$	$C = \frac{(X_1 + X_2)\,L_a}{2X_1X_2^2}$
$X_2 = \frac{1}{1+n}\sqrt{\frac{nL}{C}}$	$n = \frac{X_1 - X_2}{X_1 + X_2}$
$m = \frac{X_1 + X_2}{X_1 - X_2} = \frac{1}{n}$	

Table 2.27: Equivalence between the Brune section and two CA1_$j\phi$ complex sections.

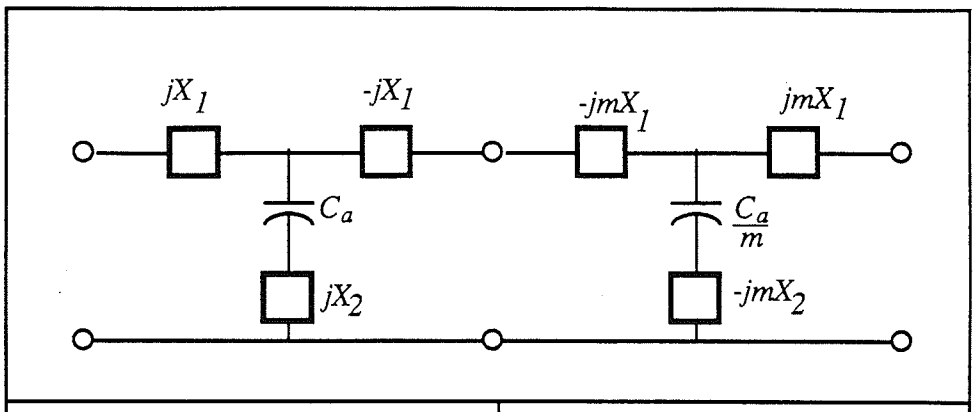

Complex Sections	Brune
$C_a = \frac{(n-1)^2 C}{n+1}$ $X_1 = \frac{1}{n-1}\sqrt{\frac{nL}{C}}$ $X_2 = \frac{(n+1)}{(n-1)^2}\sqrt{\frac{nL}{C}}$ $m = \frac{X_2 - X_1}{X_2 + X_1} = \frac{1}{n}$	$L = \frac{2X_1^2 X_2 C_a}{X_1 + X_2}$ $C = \frac{(X_2 - X_1)\, X_2 C_a}{2X_1^2}$ $n = \frac{X_2 + X_1}{X_2 - X_1}$

Table 2.28: Equivalence between the Brune section and two CB1_$j\phi$ complex sections.

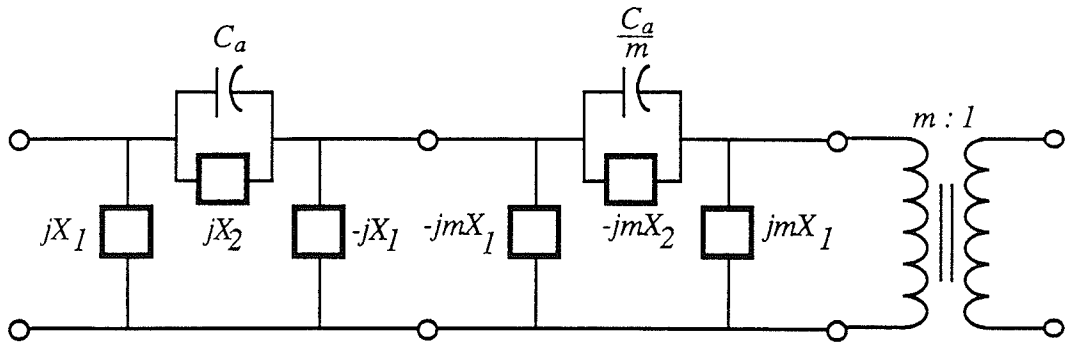

Complex Sections	Brune
$C_a = (n+1)\,C$	$L = \dfrac{2X_1X_2^2C_a}{X_1+X_2}$
$X_1 = \dfrac{1}{n-1}\sqrt{\dfrac{nL}{C}}$	$C = \dfrac{(X_1 - X_2)\,C_a}{2X_1}$
$X_2 = \dfrac{1}{(n+1)}\sqrt{\dfrac{nL}{C}}$	$n = \dfrac{X_1+X_2}{X_1-X_2}$
$m = \dfrac{X_1+X_2}{X_1-X_2} = n$	

Table 2.29: Equivalence between the Brune section and two CC1_$j\phi$ complex sections.

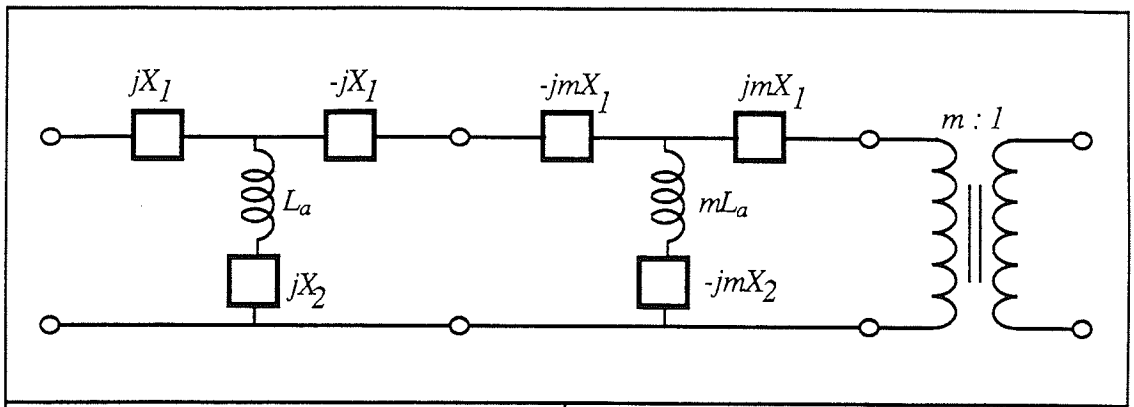

Complex Sections	Brune
$L_a = \frac{(n+1)\,nL}{(n-1)^2}$ $X_1 = \frac{1}{1-n}\sqrt{\frac{nL}{C}}$ $X_2 = \frac{(n+1)}{(n-1)^2}\sqrt{\frac{nL}{C}}$ $m = \frac{X_2 - X_1}{X_2 + X_1} = n$	$L = \frac{2X_1^2 L_a}{(X_2 - X_1)\,X_2}$ $C = \frac{(X_1 + X_2)\,L_a}{2X_1^2 X_2}$ $n = \frac{X_2 - X_1}{X_2 + X_1}$

Table 2.30: Equivalence between the Brune section and two CD1_$j\phi$ complex sections.

2.9 Equivalences Between the Complex Sections

Each first order complex section is equivalent to another section, that is, each section can be replaced with an equivalent section without affecting the operation of the network. This is because one section is the dual of the equivalent section. This can also be seen from Tables 2.1-12 giving the canonic polynomials representing the sections defined as a function of the reflectance, transmission zero, and for reciprocal sections the delay. From the tables, the following sections are equivalent: CA1_∞ and CB1_∞, CC1_0 and CD1_0, CA1_$j\phi$ and CB1_$j\phi$, CC1_$j\phi$ and CD1_$j\phi$, CE1 and CF1, and finally CG1 and CH1. The equivalences are given for the reciprocal sections in the following Tables 2.31-34.

CA1_∞	CB1_∞
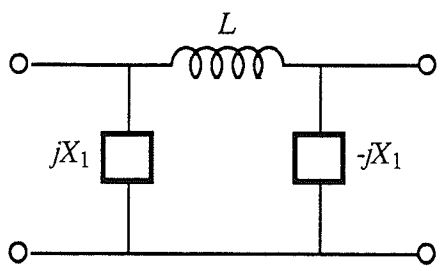	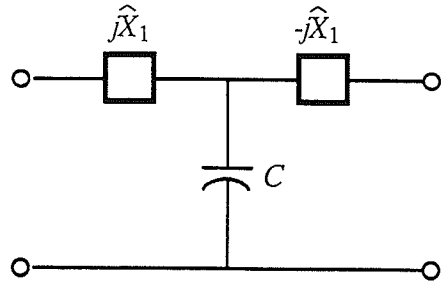
$L = C\,\hat{X}_1^2$ $X_1 = \hat{X}_1$	$C = \dfrac{L}{X_1^2}$ $\hat{X}_1 = X_1$

Table 2.31: Equivalence between the CA1_∞ and the CB1_∞ complex sections.

CC1_0	CD1_0
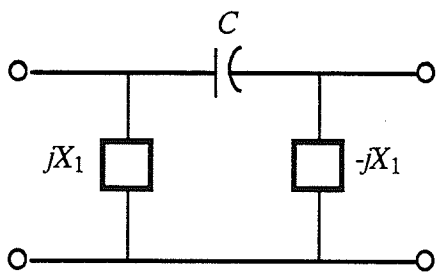	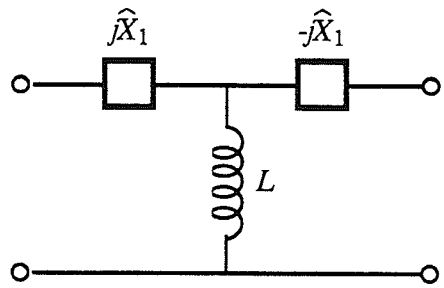
$C = \dfrac{L}{\hat{X}_1^2}$ $X_1 = \hat{X}_1$	$L = C\,X_1^2$ $\hat{X}_1 = X_1$

Table 2.32: Equivalence between the CC1_0 and the CD1_0 complex sections.

CA1_$j\phi$	CB1_$j\phi$
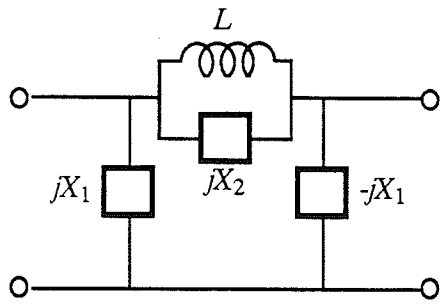	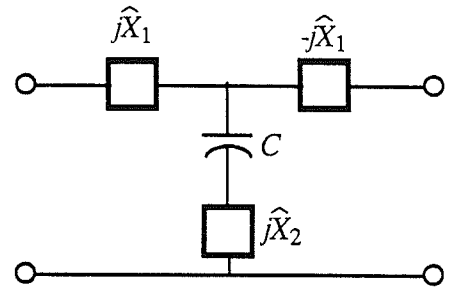
$L = C\,\hat{X}_1^2$ $X_1 = \hat{X}_1$ $X_2 = \frac{-\hat{X}_1^2}{\hat{X}_2}$	$C = \frac{L}{X_1^2}$ $\hat{X}_1 = X_1$ $\hat{X}_2 = \frac{-X_1^2}{X_2}$

Table 2.33: Equivalence between the CA1_$j\phi$ and the CB1_$j\phi$ complex sections.

CC1_$j\phi$	CD1_$j\phi$
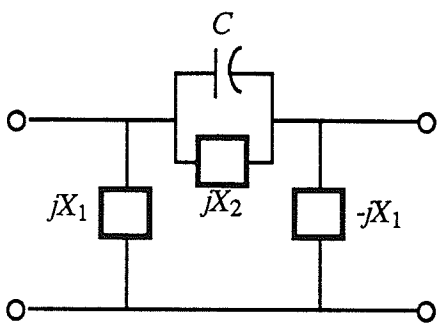	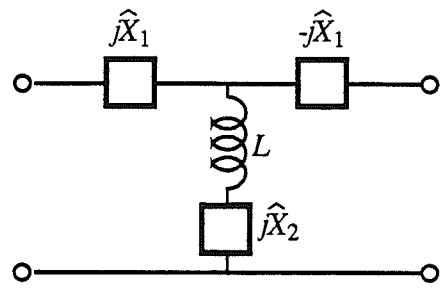
$C = \frac{L}{\hat{X}_1^2}$ $X_1 = \hat{X}_1$ $X_2 = \frac{-\hat{X}_1^2}{\hat{X}_2}$	$L = C\,X_1^2$ $\hat{X}_1 = X_1$ $\hat{X}_2 = \frac{-X_1^2}{X_2}$

Table 2.34: Equivalence between the CC1_$j\phi$ and the CD1_$j\phi$ complex sections.

Chapter III

Synthesis of Complex Lossless Two-Ports

The synthesis of real doubly-terminated lossless two-ports has a rich history. The basic problem is to realize a lossless two-port as shown below

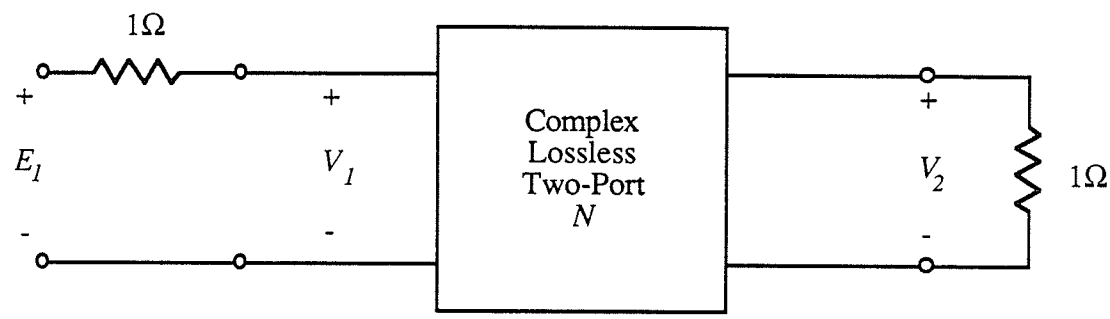

Figure 3.1: Doubly-terminated complex network.

where the resistive terminations are assumed to be normalized to a value of unity.

A first attempt to realize a lossless two-port involved the realization of either the open-circuit impedance matrix or the V-I chain matrix. Since these matrices contain more than the canonic number of polynomials needed to represent the network, an alternate approach has recently been adopted [55,59,60,61].

In this method, the synthesis is carried out in the scattering wave domain through the factorization of the scattering transfer matrix. Information about the network parameters (that is, the impedance or admittance parameters) are not required and the synthesis of the network is based on three polynomials that are derived from the required steady-state transfer function. The polynomials will be designated by f, h, and g, and satisfy the properties given in Section 2.4. Thus, the network is represented by the canonic number of polynomials and since the synthesis is based entirely on these polynomials, a greater accuracy can be obtained over the earlier approach since implicit relationships between matrix elements do not need to be maintained.

The accepted approach to the implementation of the factorization method applied to the synthesis of networks involves extensive zero-finding and polynomial manipulation routines [55,59,60,61]. This method can derive networks with high accuracy, however

the algorithm strongly dependents upon how the zero-finding routine converges and how the tolerances are matched to the problem to be solved. For accurate solutions, the amount of computational time required can be considerable.

In this work, the synthesis algorithm suggested by Jarmasz [16] will be extended to the complex domain to allow the realization of general real or complex lossless two-ports. The new algorithm is based on polynomial *evaluations* only and does not require either the zero-finding routines or the polynomial manipulations. Thus the computer implementation is several orders of magnitude faster than the earlier method with comparable accuracy. Each elementary section is represented by a set of canonic parameters, namely, the transmission zero, the reflectance and for reciprocal sections the delay. Greater freedom in the realization process will be found since complex networks composed exclusively of either inductors or capacitors as the dynamic elements are possible.

It should be noted that all synthesis algorithms assume that the given f, h, and g polynomials satisfy the conditions given in Section 2.4, that is, the polynomials represent a stable and realizable lossless two-port network.

In the real case, the number of realizations of the transmittance that are possible from the given canonic polynomials is finite. However, for complex networks the number of realizations is infinite, although the number of unique structures is finite. This is a result of the added degree of freedom that can be found by scaling the h polynomial by a unimodular multiplier (which will not effect the transmittance of the network).

3.1 Extraction of An Elementary Section via Factorization of the Scattering Transfer Matrix

All synthesis algorithms are based on the removal of a low-order section from a network, leaving a remaining network with a lower order than the original. The low-order sections referred to in this thesis are the real and complex elementary lossless sections given in Chapter II. The class of synthesis algorithms are basically distinguished by the way in which the low-order network is extracted and similarly by the way in which the remaining network is represented. The scattering matrix factorization (also called decomposition) synthesis algorithm will be briefly outlined in the following.

A lossless two-port network N can be presented by the canonic polynomials given in the form of a transfer matrix as

$$T = \frac{1}{f}\begin{bmatrix} \sigma g_* & h \\ \sigma h_* & g \end{bmatrix} \tag{3.1}$$

An elementary lossless section denoted by N_a can be extracted from the above transfer matrix leaving a remaining network denoted by N_R as shown below.

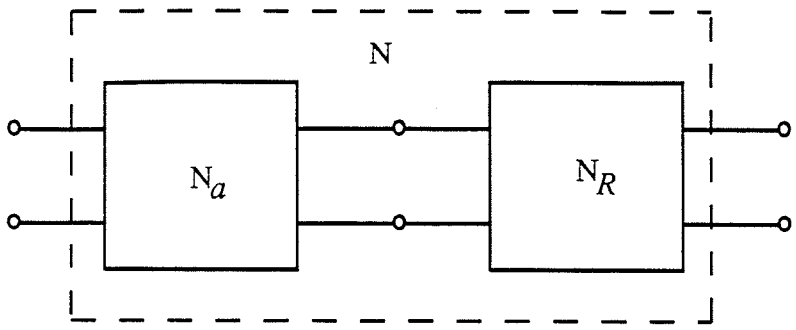

Figure 3.2: Extraction of an elementary section.

This process is equivalent to factoring the scattering transfer matrix as follows:

$$\frac{1}{f}\begin{bmatrix} \sigma g_* & h \\ \sigma h_* & g \end{bmatrix} = \frac{1}{f_a f_R}\begin{bmatrix} \sigma_a g_{a*} & h_a \\ \sigma_a h_{a*} & g_a \end{bmatrix}\begin{bmatrix} \sigma_R g_{R*} & h_R \\ \sigma_R h_{R*} & g_R \end{bmatrix} \tag{3.2}$$

The sum of the orders of N_a and N_R are assumed to equal the order of N. From the above, the following relations must hold,

$$\begin{aligned} f &= f_a f_R \\ h &= h_a g_R + \sigma_a g_{a*} h_R \\ g &= g_a g_R + \sigma_a h_{a*} h_R \\ \sigma &= \sigma_a \sigma_R \end{aligned} \tag{3.3a,b,c,d}$$

Solving for the polynomials of the remaining network N_R, the following are derived:

$$f_R = \frac{f}{f_a}$$

$$h_R = \frac{g_a h - h_a g}{\sigma_a f_a f_{a*}}$$

$$g_R = \frac{g_{a*} g - h_{a*} h}{f_a f_{a*}}$$

$$\sigma_R = \frac{\sigma}{\sigma_a} \tag{3.4a,b,c,d}$$

The section N_a realizes at least one of the transmission zeros of N and thus (3.4a) is a polynomial. In order for h_R and g_R to represent polynomials, the polynomial $f_a f_{a*}$ must divide into the numerators of (3.4b,c), or in other words, the numerators must contain the

zeros of $f_a f_{a*}$.

A solution for (3.4b,c) was shown to exist by Fettweis [59,60] and formulated in terms of the solution of a linear set of equations. This inherently requires the coefficient form in the representation of the canonic polynomials, which introduces inaccuracies in higher order systems. A more accurate solution using the product form of the polynomials which requires the use of zero-finding routines is given for the real case in [61] and for the complex case in [55]. Both methods require polynomial manipulations.

Jarmasz [16] formulated the synthesis problem in a different manner by recognizing that if the canonic polynomials of a network are evaluated at a transmission zero, the section that realizes the transmission zero is effectively decoupled from the network. This observation allows the development of the efficient synthesis algorithm given in [16]. In the following, the algorithm due to Jarmasz will be extended to include the synthesis of complex lossless two-ports.

3.2 Canonic Representation of Elementary Complex Sections

A canonic number of parameters, which are easily calculated, is needed to represent the complex elementary sections. Reciprocal and non-reciprocal sections require three and four real parameters, respectively. To this end, consider the flow diagram for the networks N_a and N_R as given in the following figure where the network N_a is assumed to represent a complex elementary section.

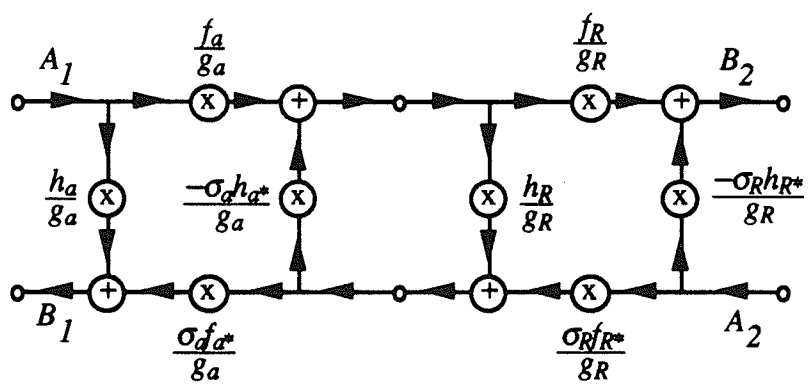

Figure 3.3: Flow diagram of the N_a and N_R networks.

For the synthesis process assume that the signal from port two does not contribute to B_1 (that is $A_2 = 0$). Evaluating the canonic polynomials of the network at the transmission zero ψ_a of the section N_a, we have $f_a(\psi_a) = 0$, which decouples the left-most part of N_a from the remaining network (since $A_2 = 0$) as shown in the following figure:

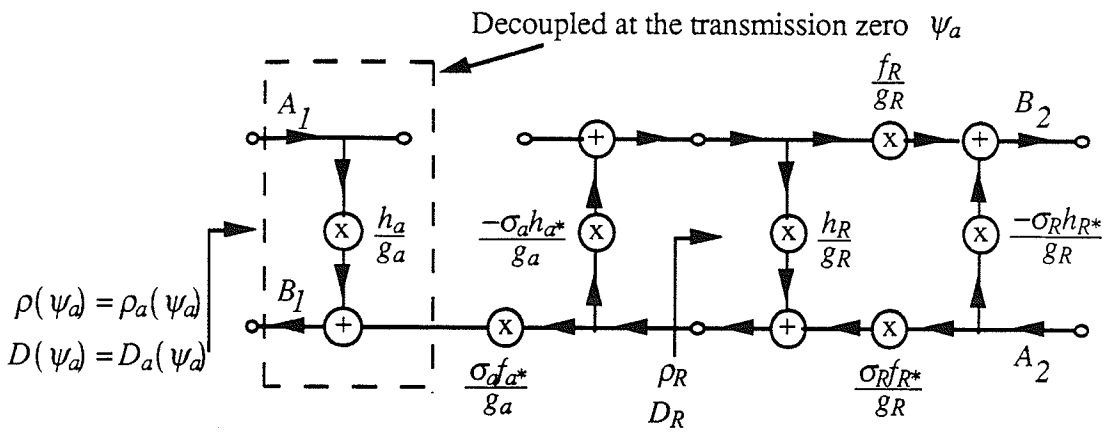

Figure 3.4: Flow diagram of the N_a and N_R networks evaluated at ψ_a.

Note that for reciprocal sections $f_{a*}(\psi_a) = 0$ and thus the left-most section is then decoupled regardless of the remainder of the network. In either case, it is clear from the above figure that from the viewpoint of port one, the only element that contributes to B_1 is the ratio of the h and g polynomials for the first section. This is by definition the reflectance ρ, and therefore

$$\rho(\psi_a) = \frac{B_1}{A_1}(\psi_a) = \frac{h_a}{g_a}(\psi_a) = \rho_a(\psi_a) \tag{3.5}$$

and thus the reflectance of the first section ρ_a is equal to the overall reflectance ρ when evaluated at the transmission zero ψ_a,

$$\rho(\psi_a) = \rho_a(\psi_a) \tag{3.6}$$

Two parameters associated with the first elementary section are now known, namely the location of the transmission zero (which is supplied in the original f polynomial) and the reflectance evaluated at the transmission zero. For non-reciprocal sections, both parameters are general complex numbers and thus the two parameters are all that is needed to completely characterize the section.

However, for reciprocal sections, both parameters are real numbers, they are namely the imaginary part of the transmission zero and the angle of the reflectance (since the reflectance is unimodular). Thus for reciprocal sections, one more real parameter is needed. Intuitively, the extra parameter should only be a function of the ratio of the h and g polynomials for the section. This is because the only known quantity, from Figure 3.4, is the reflectance of the section. Another way of stating this is that a degree of freedom might be lost if the f polynomial of the section is used, since it will go to zero at the

transmission zero. Although many possibilities may exist, a convenient choice for the extra parameter is the return group delay (known here after as the delay D) given in Chapter II and as suggested in [16]. The delay is real and positive when evaluated at the transmission zero as shown in Theorem 2.2, and only a function of the ratio of the h and g polynomials of the section as shown by the definition (2.36), repeated below:

$$D = -\,\mathrm{Ev}\left\{\frac{d}{d\psi}\,ln\left(\frac{h(\psi)}{g(\psi)}\right)\right\}\Bigg|_{\psi = j\phi_o} \tag{3.7}$$

Thus from the above observations and from (3.5-6), it is clear that

$$D_a(j\phi_a) = -\,\mathrm{Ev}\left\{\frac{d}{d\psi}\,ln\left(\frac{h_a(j\phi_a)}{g_a(j\phi_a)}\right)\right\} = -\,\mathrm{Ev}\left\{\frac{d}{d\psi}\,ln\left(\frac{h(j\phi_a)}{g(j\phi_a)}\right)\right\} = D\,(j\phi_a) \tag{3.8}$$

and thus the delay of the first elementary reciprocal section is equal to the delay of the overall network when evaluated at the transmission zero of the section.

The reflectance, and for reciprocal sections the delay are given in the Tables of the elementary sections in Chapter II. For reciprocal sections the reflectance is unimodular and the delay is positive as shown by the tables. Similarly, for non-reciprocal sections the reflectance is not unimodular and the delay is not needed. In either case, it is clear from the tables that an elementary section can be represented by the transmission zero, the reflectance and for reciprocal sections the delay of the section. These will be defined as the canonic parameters.

Thus, it is clear from the tables given in Chapter II, a complex first-order section, or a real second-order section (where appropriate), can be chosen. Therefore the canonic polynomials of the first elementary section are known.

3.3 Recomputation for the Remaining Network

The canonic parameters completely represent an elementary complex section. The above discussion focussed on the first section of a network, where the first section was assumed to be identified and completely defined. In order to represent the remaining sections, a more in depth formulation is required as given in the following.

The canonic parameters for the sections realizing the remaining transmission zeros of a network can be calculated in the same manner as used for the first section. Consider the parameters for the second elementary complex section, which would represent the parameters of the first section of N_R from Figure 3.4. This can be thought of as realizing N_R as two sections, N_b and N_r, where N_b is assumed to be the elementary complex section (the same procedure as before) and N_r is whatever remains. Assume that the transmission zeros of N_a and N_b are not equal. The parameters of N_b as calculated from the original f,

h and g polynomials do not represent the actual section, rather they represent a combination of the reflectance and where appropriate the delay of both the first and second sections, N_a and N_b. Thus to find the actual canonic parameters for the second section, the first section must be *extracted* from the network.

The canonic polynomials for the second section are given as a function of the first section and the original canonic polynomials from equations (3.4). From the above discussion, it is appropriate to relabel section N_R as N_b in (3.4). Clearly, (3.4) gives a general relationship which can be evaluated at any appropriate location.

In order to calculate the parameters for N_b, the evaluation of the h and g polynomials for the second section must be passed through the first section, giving a new set of evaluations for the h and g polynomials as shown below,

$$h_b(\psi_b) = \frac{g_a(\psi_b)h(\psi_b) - h_a(\psi_b)g(\psi_b)}{\sigma_a f_a(\psi_b) f_{a*}(\psi_b)}$$

$$g_b(\psi_b) = \frac{g_{a*}(\psi_b)g(\psi_b) - h_{a*}(\psi_b)h(\psi_b)}{f_a(\psi_b) f_{a*}(\psi_b)} \tag{3.9a,b}$$

where the polynomials f_a, h_a, and g_a for N_a are known. The calculated complex numbers $h_b(\psi_b)$ and $g_b(\psi_b)$ now represent the actual polynomials evaluated at the transmission zero for the section. Thus the reflectance as given by

$$\rho_b(\psi_b) = \frac{h_b}{g_b}(\psi_b) = \frac{g_a(\psi_b)h(\psi_b) - h_a(\psi_b)g(\psi_b)}{\sigma_a\left(g_{a*}(\psi_b)g(\psi_b) - h_{a*}(\psi_b)h(\psi_b)\right)} \tag{3.10}$$

is known. Note that the reflectance can be expressed in terms of the original reflectance calculated for N_b as given by

$$\rho_b(\psi_b) = \frac{g_a(\psi_b)\rho(\psi_b) - h_a(\psi_b)}{\sigma_a\left(g_{a*}(\psi_b) - h_{a*}(\psi_b)\rho(\psi_b)\right)} \tag{3.11}$$

The same observations will apply to the delay of the section N_b and will not be repeated. Consider a reciprocal section, the delay is given from (3.7) and (3.9) as

$$D_b = \frac{d}{d\psi} ln\left(\frac{g_b(\psi)}{h_b(\psi)}\right) = \frac{d}{d\psi} ln\left(\sigma_a \frac{g(\psi)}{h(\psi)} \frac{\left(g_{a*}(\psi) - h_{a*}(\psi)\frac{h(\psi)}{g(\psi)}\right)}{g_a(\psi) - h_a(\psi)\frac{g(\psi)}{h(\psi)}}\right) \tag{3.12}$$

where it is understood that after all algebraic manipulations have been completed, all

polynomials will be evaluated at ψ_b. Simplifying the above gives the following:

$$D_b = \frac{d}{d\psi}\left[ln(\sigma_a) + ln\left(\frac{g(\psi)}{h(\psi)}\right) + ln\left(g_{a*}(\psi) - h_{a*}(\psi)\frac{h(\psi)}{g(\psi)}\right) - ln\left(g_d(\psi) - h_d(\psi)\frac{g(\psi)}{h(\psi)}\right)\right] \tag{3.13a}$$

$$D_b = \frac{d}{d\psi}ln\left(\frac{g(\psi)}{h(\psi)}\right) + \frac{d}{d\psi}ln\left(g_{a*}(\psi) - h_{a*}(\psi)\frac{h(\psi)}{g(\psi)}\right) - \frac{d}{d\psi}ln\left(g_d(\psi) - h_d(\psi)\frac{g(\psi)}{h(\psi)}\right) \tag{3.13b}$$

$$D_b = D + \frac{\frac{d}{d\psi}g_{a*}(\psi) - \frac{d}{d\psi}(h_{a*}(\psi))\frac{h(\psi)}{g(\psi)} - \frac{d}{d\psi}\left(\frac{h(\psi)}{g(\psi)}\right)h_{a*}(\psi)}{g_{a*}(\psi) - h_{a*}(\psi)\frac{h(\psi)}{g(\psi)}} + \frac{-\frac{d}{d\psi}g_d(\psi) + \frac{d}{d\psi}(h_d(\psi))\frac{g(\psi)}{h(\psi)} + \frac{d}{d\psi}\left(\frac{g(\psi)}{h(\psi)}\right)h_d(\psi)}{g_d(\psi) - h_d(\psi)\frac{g(\psi)}{h(\psi)}} \tag{3.13c}$$

After multiplying the numerator and denominator of the second term by g/h and the third term by h/g, and then recognizing the definition of the delay, we get

$$D_b = D + \frac{\frac{d}{d\psi}(h_d(\psi)) + D\, h_d(\psi) - \frac{d}{d\psi}(g_d(\psi))\frac{h(\psi)}{g(\psi)}}{g_d(\psi)\frac{h(\psi)}{g(\psi)} - h_d(\psi)} + \frac{-\frac{d}{d\psi}(h_{a*}(\psi)) + D\, h_{a*}(\psi) + \frac{d}{d\psi}(g_{a*}(\psi))\frac{g(\psi)}{h(\psi)}}{g_{a*}(\psi)\frac{g(\psi)}{h(\psi)} - h_{a*}(\psi)} \tag{3.14}$$

Apply the property

$$\frac{d}{d\psi}(h_*(\psi)) = -\left[\frac{d}{d\psi}(h(\psi))\right]_* \tag{3.15}$$

we derive

$$D_b = D + \frac{\frac{d}{d\psi}(h_d(\psi)) + D\, h_d(\psi) - \frac{d}{d\psi}(g_d(\psi))\frac{h(\psi)}{g(\psi)}}{g_d(\psi)\frac{h(\psi)}{g(\psi)} - h_d(\psi)} + \frac{\left[\frac{d}{d\psi}(h_d(\psi))\right]_* + D\, h_{a*}(\psi) - \left[\frac{d}{d\psi}(g_{a*}(\psi))\right]_*\frac{g(\psi)}{h(\psi)}}{g_{a*}(\psi)\frac{g(\psi)}{h(\psi)} - h_{a*}(\psi)} \tag{3.16}$$

Finally, after recognizing that at a transmission zero of a reciprocal section,

$$\frac{g(\psi)}{h(\psi)} = \left[\frac{h(\psi)}{g(\psi)}\right]_* \tag{3.17}$$

the following is derived:

$$D_b = D + \frac{\frac{d}{d\psi}(h_a(\psi)) + D\, h_a(\psi) - \frac{d}{d\psi}(g_a(\psi))\frac{h(\psi)}{g(\psi)}}{g_a(\psi)\frac{h(\psi)}{g(\psi)} - h_a(\psi)} + \frac{\left[\frac{d}{d\psi}(h_a(\psi))\right]_* + D\, h_{a*}(\psi) - \left[\frac{d}{d\psi}(g_a(\psi))\right]_* \left[\frac{h(\psi)}{g(\psi)}\right]_*}{g_{a*}(\psi)\left[\frac{h(\psi)}{g(\psi)}\right]_* - h_{a*}(\psi)} \tag{3.18}$$

Define the function

$$\Delta(\psi) = \frac{\frac{d}{d\psi}(h_a(\psi)) + D\, h_a(\psi) - \frac{d}{d\psi}(g_a(\psi))\frac{h(\psi)}{g(\psi)}}{g_a(\psi)\frac{h(\psi)}{g(\psi)} - h_a(\psi)} \tag{3.19}$$

which is found in (3.18). Thus, the delay can be expressed as

$$D_b(\psi_b) = D(\psi_b) + \Delta(\psi_b) + \Delta_*(\psi_b) \tag{3.20}$$

by recognizing that $D_* = D$ since D is real. This is an expression giving the actual delay of the second elementary section and is a generalization of the expression given in [16].

Thus the reflectance and the delay of the second elementary complex section are known. Therefore, after choosing the appropriate section, all information pertaining to the second section is completely known. The canonic parameters of the first and second section can now be used to derive the third section, and so on. This synthesis process will be generalized in a later section.

3.4 Calculation of the Reflectance and the Delay

The observations made above, namely equations (3.10, 20), assumed that all of the transmission zeros were distinct. However, the general case should provide for multiple transmission zeros, that is, the case of more than one transmission zero at the same location. A simple example of this is an allpole filter that contain all of the transmission zeros at infinity. For this case the canonic parameters for all multiple transmission zero sections will be the same, and thus another method of calculating the reflectance and the

delay is needed.

The method used for the multiple transmission zero case was given by Jarmasz [16] which followed suggestions by Martens [57]. In this method, the polynomial evaluations at the transmission zero are not used explicitly. Rather, the polynomials are sampled at N sample points around a circle of nonzero radius centered at the transmission zero. The resulting set of values will be known as the sample characterization.

The actual values of the polynomials can be found by recognizing that the Taylor series expansion of the polynomial about the transmission zero has the same form as the discrete Fourier transform generalized to a nonzero radius. Consider the Taylor series expansion of the h and g polynomials of order N about the transmission zero of section k, where

$$1 \leq k \leq N \tag{3.21}$$

as given by

$$h(\psi) = \sum_{i=0}^{N-1} a_i (\psi - \psi_k)^i$$

$$g(\psi) = \sum_{i=0}^{N-1} b_i (\psi - \psi_k)^i \tag{3.22a,b}$$

where the complex a_i and b_i are the Taylor series coefficients [52], and N is given by

$$N = \deg\{g\} + 1 \tag{3.23}$$

Evaluate the above (3.22) at N equally spaced intervals of the circle of radius r centered at the transmission zero ψ_k as given by

$$\psi = \psi_k + r\, e^{j\frac{2\pi}{N}n}, \quad n = 0\ (1)\ (N\text{-}1) \tag{3.24}$$

and as shown in Figure 3.5,

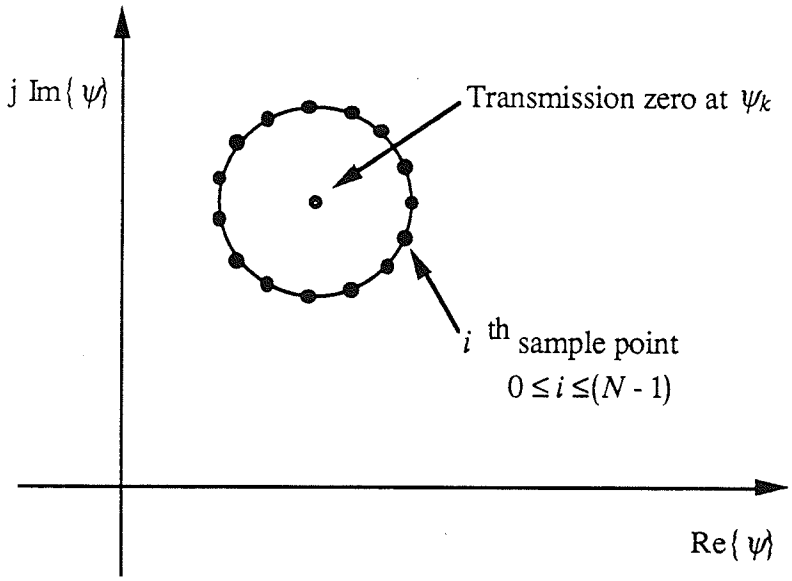

Figure 3.5: Sample points for the sample characterization.

in order to derive

$$h[n, k] = \sum_{i=0}^{N-1} a_i(k) r^i e^{j\frac{2\pi}{N}ni}$$

$$g[n, k] = \sum_{i=0}^{N-1} b_i(k) r^i e^{j\frac{2\pi}{N}ni} \qquad (3.25a,b)$$

where $h[n, k]$ and $g[n, k]$ represent the N sample points on the circle for section k, which is defined as the *sample characterization.* The above equations have the form of the DFT of the discrete sequences a_i and b_i generalized to radius r. Thus, one can view the Taylor series coefficients a_i and b_i as discrete-time sequences with the corresponding DFT of $h[n, k]$ and $g[n, k]$, that is, the following represent DFT pairs:

$$a_i(k) \leftrightarrow h[n, k]$$
$$b_i(k) \leftrightarrow g[n, k] \qquad (3.26a,b)$$

The sample characterization given by (3.25) can be conveniently calculated by simply sampling the h and g polynomials at the points (3.24) as given below

$$h[n, k] = h\left(\psi_k + r\, e^{j\frac{2\pi}{N}n}\right)$$

$$g[n, k] = g\left(\psi_k + r\, e^{j\frac{2\pi}{N}n}\right) \tag{3.27a,b}$$

Note that for a transmission zero at infinity, first apply the mapping

$$\psi \rightarrow \frac{1}{\psi} \tag{3.27c}$$

to the h and g polynomials, and after rationalizing the numerator and denominator, let $\psi \rightarrow 0$. This mapping also changes the sign of σ for all first-order sections.

The radius r is chosen to be less than the shortest Euclidean distance between distinct transmission zeros, and as suggested in [16], 0.2 of this distance works well in practise.

As mentioned earlier, the quantities needed for the evaluation of the canonic parameters are both the h and g polynomials and their derivatives evaluated at the transmission zero of the section. By using the Taylor series expansion (3.22) and the observation regarding the DFT pairs (3.26), the quantities are easily evaluated from the definition of the DFT as

$$h(\psi_k) = a_0 = \frac{1}{N}\sum_{n=0}^{N-1} h[n, k]$$

$$g(\psi_k) = b_0 = \frac{1}{N}\sum_{n=0}^{N-1} g[n, k] \tag{3.28a,b}$$

and

$$\left[\frac{d}{d\psi}h(\psi)\right]\Bigg|_{\psi=\psi_k} = a_1 = \frac{1}{rN}\sum_{n=0}^{N-1} h[n, k]\, e^{-j\frac{2\pi}{N}n}$$

$$\left[\frac{d}{d\psi}g(\psi)\right]\Bigg|_{\psi=\psi_k} = b_1 = \frac{1}{rN}\sum_{n=0}^{N-1} g[n, k]\, e^{-j\frac{2\pi}{N}n} \tag{3.29a,b}$$

Note that the higher order derivatives can be calculated in the same way, but for this application, only the zeroth and first derivatives are needed. Using (3.28-29), the reflectance and delay are calculated as

$$\rho(\psi_k) = \frac{h(\psi_k)}{g(\psi_k)}$$

$$D(\psi_k) = \frac{\left[\frac{d}{d\psi} g(\psi)\right]\Big|_{\psi=\psi_k}}{g(\psi_k)} - \frac{\left[\frac{d}{d\psi} h(\psi)\right]\Big|_{\psi=\psi_k}}{h(\psi_k)} \tag{3.30a,b}$$

The recomputation formulae for section N_b given earlier (3.9) can be expressed in terms of the sample characterization as

$$h_b[n, b] = \frac{g_a[n, b]h[n, b] - h_a[n, b]g[n, b]}{\sigma_a f_a[n, b] f_{a*}[n, b]}$$

$$g_b[n, b] = \frac{g_{a*}[n, b]g[n, b] - h_{a*}[n, b]h[n, b]}{f_a[n, b] f_{a*}[n, b]}$$

$$0 \le n \le (N - 1) \tag{3.31a,b,c}$$

where

$$f_a[n, b] = f_a\left(\psi_b + r\, e^{j\frac{2\pi}{N}n}\right)$$

$$h_a[n, b] = h_a\left(\psi_b + r\, e^{j\frac{2\pi}{N}n}\right)$$

$$g_a[n, b] = g_a\left(\psi_b + r\, e^{j\frac{2\pi}{N}n}\right) \tag{3.32a,b,c}$$

This simply maps the original sample characterization for the section into the actual characterization for the section. Equations (3.28-30) can then be used to calculate the canonic parameters. Note that all f polynomials must be monic as given in the tables of Chapter II.

3.5 Complex Synthesis Algorithm

The algorithm for the synthesis of complex lossless two-ports follows from the discussion given above. The f, h, and g polynomials for a network are assumed to be known, where the order of the zeros of the f polynomial represents the desired order of the elementary sections realizing the finite transmission zeros. If they exist, transmission zeros at infinity can be realized at any appropriate location. The procedure for the synthesis of the network is equivalent to the realization of the transmission zeros given by ψ_k, where $1 \le k \le N$.

Although the sample characterization is not required for all cases, the synthesis algorithm will be presented in terms of the sample characterization for simplicity. That is, the sample characterization can realize either the distinct or the multiple transmission zero

case, and thus the algorithm presented will be the most general.

For the kth transmission zero, ψ_k, calculate the sample characterization as given in (3.27a,b), that is calculate the $h_k[n, k]$ and the $g_k[n, k]$ complex numbers from the original polynomials for $1 \leq k \leq N$. Then calculate the canonic parameters for the first section ($k = 1$) and identify the section from the tables in Chapter II, including the section's canonic polynomials. Now *extract* the first section by mapping the sample characterization using (3.33) for $2 \leq k \leq N$. Repeat this process by extracting section l and recomputing for the remaining sections as shown below for $(l + 1) \leq k \leq N$ inclusively.

$$h_k[n, k] = \frac{g_l[n, k]h_k[n, k] - h_l[n, k]g_k[n, k]}{\sigma_l f_l[n, k]f_{l*}[n, k]}$$

$$g_k[n, k] = \frac{g_{l*}[n, k]g_k[n, k] - h_{l*}[n, k]h_k[n, k]}{f_l[n, k]f_{l*}[n, k]} \qquad (3.33a,b,c)$$

The complex numbers $h_k[n, k]$ and $g_k[n, k]$ on the right of the above equations are recomputed and reassigned on the left. Note that the $f_l[n, k]$, the $h_l[n, k]$ and the $g_l[n, k]$ terms represent new polynomial evaluations of the known polynomials for section l, and all of the polynomial evaluations for a section occur at the same frequency as given by (3.24). The kth elementary complex section can be identified from the canonic parameters given from the sets $h_k[n, k]$ and $g_k[n, k]$ and (3.30), and thus all relevant information about the kth section is known. Continue this process until l equals N when the synthesis is complete.

Fettweis has shown [59-60] that the extraction of a lossless elementary section is possible as long as the given canonic polynomials satisfy the conditions given in Section 2.4. Namely, the scattering matrix representing the network must be unitary on the imaginary axis and the g canonic polynomial must be strictly Hurwitz. Now it is possible to determine the canonic polynomials given in (3.4) that represent a lossless sub-network of order $N - m$, where m is the order of the extracted section. Furthermore, the canonic polynomials can be represented in terms of the canonic parameters and vice versa as given in the Tables characterizing the elementary sections found in Chapter II. Thus, from the preceding observations, it is clear that an elementary section can be extracted from a network using the synthesis algorithm, thereby reducing the order of the remaining sub-network by the order of the extracted section. Note that the extraction did not involve the manipulation of intermediate polynomials. Also, the relative magnitude of the reflectance (either unimodular, greater than one, or less than one in magnitude) is invariant and the delay for reciprocal sections is positive for each elementary section since the section is realizable.

From the tables of Chapter II, there is some freedom in the choice for a complex section; that is, a section with either an inductor or a capacitor as the dynamic element is possible for a given set of canonic parameters. Also, freedom is found in the case of complex conjugate transmission zeros, since they can be realized as either two first-order complex sections or a real second-order section. Note that if two first-order complex sections are chosen the sections are not required to follow one another in the cascade and they can be placed anywhere within the network.

Thus a particular set of canonic parameters does not necessarily specify a unique section. Moreover, the canonic parameters for the sections are derived from the polynomials of the network and are thus independent of the exact sections used (except for the finite transmission zero case, unless either sections {CA1_jw, CB1_jw} or {CC1_jw, CD1_jw} are used exclusively). This leads to the result that the canonic parameters completely specify a network and are equally as important as the lumped element values of a network. In fact, the parameters are *equivalent* to the lumped element values as shown by the relationships given in the tables. The equivalences in Tables 2.31-34 show the relationships between the sections.

The synthesis algorithm is based entirely on polynomial *evaluations*, and thus routines for zero-finding and polynomials manipulations are not needed. The sample characterization approach requires more evaluations than the method of evaluating the polynomials at the transmission zero, however, the added computational time is not significant. Furthermore, the sample characterization method can handle the synthesis of both the multiple and the distinct transmission zero cases, and thus only one computer program is needed for general network synthesis.

3.6 Extraction of the Last (Constant Complex) Section

After the last dynamic elementary section is extracted, a final complex constant section (or a real section as a special case) must be realized in order for the synthesized network to satisfy the original canonic polynomials and for the load resistive termination to equal unity in Figure 3.1. This is performed by extracting the last dynamic section and recomputing the sample characterization. Label the resulting constant section (N+1).

The sample characterization and the canonic parameters, including the transmission zero, are known for the last dynamic section. Thus recompute the sample characterization using

$$h_{N+1}[n] = \frac{g_N[n, N]h_{N+1}[n, N] - h_N[n, N]g_{N+1}[n, N]}{\sigma_N f_N[n, N]f_{N*}[n, N]}$$

$$g_{N+1}[n] = \frac{g_{N*}[n, N]g_{N+1}[n, N] - h_{N*}[n, N]h_{N+1}[n, N]}{f_N[n, N]f_{N*}[n, N]} \qquad (3.34a,b)$$

which extracts the last dynamic section leaving a constant section. The sample characterizations $h_{N+1}[n, N]$ and $g_{N+1}[n, N]$ represent the characterizations from the extraction of the preceding section. The complex sets $h_{N+1}[n]$ and $g_{N+1}[n]$ represent the constant h and g polynomials for the last section, which are given by

$$h_{N+1} = \frac{1}{N} \sum_{n=0}^{N-1} h_{N+1}[n]$$

$$g_{N+1} = \frac{1}{N} \sum_{n=0}^{N-1} g_{N+1}[n] \qquad (3.35a,b)$$

The f_{N+1} polynomial is equal to unity since by assumption all f polynomials are monic. The σ_{N+1} value is arbitrary since the σ value for the overall network is usually arbitrary. Thus from the constant f_{N+1}, h_{N+1} and g_{N+1} polynomials for the section and Tables 2.13-17, the last constant section can be determined.

Note that the last section will be a real ideal transformer for a real network as well as for many complex networks realizing real canonic polynomials. However, the latter is not always the case, particularly when at least one complex section is made reflection-free or when the original h polynomial is scaled by a complex unimodular constant.

3.7 Recomputation Using a Constant Complex Section

In the synthesis of electrical networks, it is desirable to have the freedom of inducing a particular property in a section. The three most common properties that are induced are port one reflection-free, port two reflection free and a pass-through at a certain frequency. All of the elementary sections listed in the tables of Chapter II behave as a pass-through at a certain frequency as given by the definition of the section. However, the reflection-free property must be explicitly induced in an elementary section.

From the discussion in Section 2.5, a general constant complex section is needed to make a port reflection-free. After inserting the appropriate complex section at the desired port, the set of the sample characterization for the remaining sections (all dynamic sections to the right of the current section) in the network must be recomputed. The recomputation formulae given in (3.33) can be used where the f_l, h_l, and g_l polynomials are replaced with the constant polynomials that represent the inserted constant section. Thus the recomputation process in this case requires no polynomial evaluations, since it involves only complex number operations. This process can be viewed as extracting a constant section from the network in the same way that a dynamic section is extracted, as discussed

in an earlier Section.

Note that the above only discussed the case for a reflection-free port. However, a complex constant section can be inserted anywhere in the network in order to induce a desirable property. The same steps would be followed for the recomputation for the remaining network.

The insertion of a constant complex section is a form of scaling, that is, changing the parameter *values* of the elementary sections. Thus, inserting the constant section will not alter the *structure* of the network. For example, consider a network that is first realized without inducing any properties in the sections, and then realized a second time inducing reflection-free ports. The dynamic elementary sections for both cases can always be chosen to be the same, albeit with different parameter values. Note that these observations only apply to the dynamic sections. For example, the last constant section obtained from the realization may change.

3.8 Design Examples

Few examples of complex analog networks exist in the literature, and no examples exist of either realizations of frequency shifted networks or realizations of networks with the phase of the h polynomial scaled by an arbitrary real constant. In order to give examples of complex analog networks and to support the observations made in this thesis, Appendix A contains the following five examples of classical filters: Elliptic filters of orders 4, 5, 8, 14, and a Chebyshev filter of order 5. All filters are of the lowpass type except the 14th order Elliptic which is of the bandpass type.

All examples were generated using the synthesis algorithm outlined above with a program written by the author in the PASCAL computer language. The program requires: the canonic polynomials of the network in factored form, the imaginary axis shift, the h polynomial phase shift and type of complex section desired (when a choice between sections is appropriate).

Note that the example that required the most computer time was the 14th order Elliptic filter realized with complex sections and reflection-free ports. However, the solution to this example required under a minute to calculate on a Macintosh II computer with a clock speed of 16 MHz. In order to put this in perspective, the 8th order Elliptic filter realized using the method of Cascade Synthesis (factoring the transfer matrix) [55] without reflection-free ports required over four hours on the same computer for the same accuracy as the example presented.

It should be noted that the synthesis algorithm implemented is very sensitive to the accuracy of the given polynomials. However, this usually will not create a problem since the transmittance gain can be found to a high degree of accuracy from a given set of poles and zeros. It then remains to find an h polynomial that accurately fits the analytic continuation of the Feldtkeller equation (2.21). This can be easily done using a zero-

finding routine. However, this process is independent of the algorithm since it deals with the polynomial description of the network.

In all examples both the canonic parameters and the lumped element values are given in order to provide an indication of the relative magnitudes of the values. This again demonstrates that either type of description can characterize a network. All of the transmission zeros were realized in the order given in the tables in the Appendix, and if they exist, transmission zeros at infinity were realized last (although this need not be the case since the transmission zeros can be realized in any order).

The following general observations can be made about the dynamic sections from the examples. It is possible to realize the given real canonic polynomials with real sections. Complex sections are needed if the polynomials are shifted along the imaginary axis or if the phase of the h polynomial is changed by an arbitrary constant not equal to 0° or 180°. From the 4th order Elliptic and the 5th order Chebyshev examples, equivalent realizations are possible using the same type of first-order complex section regardless of either, the filter order, or the change of phase of the h polynomial if finite transmission zeros exist. Also, from the 5th and 8th order Elliptic examples, realizations are possible using the same type of first-order complex section with the polynomial shift along the imaginary axis. It is possible to realize a network using either of the four first-order complex reciprocal sections exclusively as shown by the 5th order Elliptic example, and thus realizations containing only inductors or capacitors as the dynamic elements are possible. Non-reciprocal sections can be realized as shown by Tables A.71-72. Finally, any section, whether real or complex, can be made reflection-free as shown by all of the examples.

The following observations can be made about the constant sections for networks with finite transmission zeros. The last constant section will be a complex constant section if any of the following is true, the network is realized with reflection-free complex sections, the polynomials of an odd order filter are shifted along the imaginary axis, or the phase of the h polynomial is changed by an arbitrary constant not equal to 0° or 180°. The real sections of a real network can be made reflection-free using real transformers, while the complex sections will require a constant complex section whether the network polynomials are real or not.

For all-pole filters, the same observations apply except that the last section will be a real ideal transformer for the change of phase of the h polynomial.

The accuracy of the synthesis algorithm can be tested by comparing the canonic parameters for the very narrow band 14th order Elliptic bandpass filter to those found in [16]. This filter represents a very difficult case since a high degree of accuracy is needed in the realization because it has a relative bandwidth of only 0.025% and the finite transmission zeros are indistinguishable to three significant digits. From the comparison of the parameters from Table A.74, it is clear that the two sets of parameters agree to at least 5 significant digits. The discrepancy may be due to the use of the sample characterization in

the derivation of the example. A comparison for the complex case is not possible, however, a realization using the CB1_jw section throughout gave a final ideal transformer value of 0.83179907921888, which is in agreement with [16] to six significant digits, and thus the complex realization is considered acceptable.

The complex analog networks derived will be used as the reference networks for the wave-digital filters presented in the following chapters. Either the lumped element values or the canonic parameters can be used to represent the sections. The freedom to choose either set of parameters allows for two efficient and equivalent methods of realizing complex digital filters, as outlined in Chapter V.

Chapter IV

Introduction to Complex Wave Digital Networks

The arguments given in the Introduction suggest that the one-real approach to the realization of complex reference networks is too restrictive and it will therefore be abandoned for the following more general theory of CWD filters that allows constant complex reference impedances.

It is known that the wave digital realization of a network maps an analog network to its equivalent digital network in a one-to-one correspondence [6]. Also, if a digital filter structure is found which possesses the desirable properties of low sensitivity and zero-input and forced-response stability, then it is necessarily equivalent to a wave digital filter [18]. Thus the generalization of wave digital filters to the complex plane should have these properties. The following new definitions realize this objective.

4.1 Definition of the Complex Voltage and Power Wave Variables

A new generalization of WD networks is found with the following new definition of the incident and reflected voltage waves, A and B, in terms of the steady-state voltage V and the current I where ψ is a frequency variable (discussed below) defined as follows:

$$\begin{aligned} A(\psi) &= V(\psi) + Z\,I(\psi) \\ B(\psi) &= V(\psi) - Z^*\,I(\psi) \\ Z &= R + jX \end{aligned} \qquad (4.1a,b,c)$$

The impedance Z, henceforth known as the port reference impedance, is an arbitrary complex constant containing a positive resistance R and a constant reactance X. The above equations simply map an analog voltage-current network to an analog wave network (in terms of the steady-state variables). Note that the conjugate sign in equation (4.1b) which defines the reflected wave is necessary for the power equation to reduce to a simple form (and thus for a stability theory similar to the real case to exist) as shown in the next section. This mapping is most easily visualized in terms of a complex one-port network as shown below.

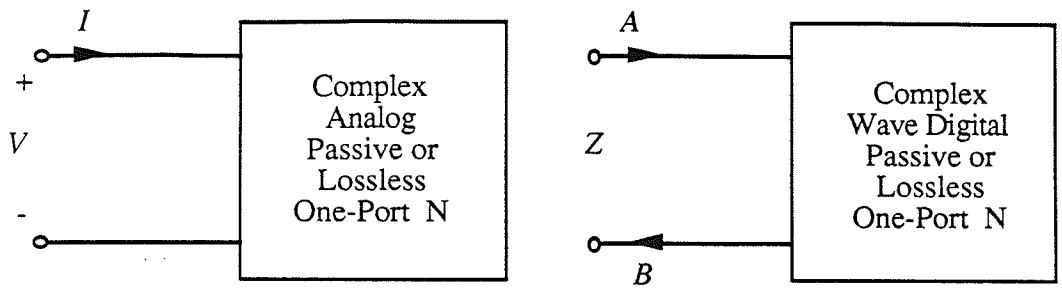

Figure 4.1: Complex one-ports in the analog and CWD domains.

The network is then transformed to the discrete (digital) domain with the familiar bilinear transformation

$$\psi = \frac{z-1}{z+1} \quad \Leftrightarrow \quad z = \frac{1+\psi}{1-\psi} \tag{4.2a,b}$$

The complex frequency variable ψ is used to map rational functions in the digital domain to rational functions in the ψ domain and is related to the frequency variable $z = e^{sT}$, by

$$\psi = \tanh\left(\frac{sT}{2}\right) = \frac{z-1}{z+1} = \frac{1-z^{-1}}{1+z^{-1}} \tag{4.3}$$

where T is the sampling period. If $s = \sigma + j\omega$ and $\psi = \phi_r + j\phi$, the above becomes

$$\phi_r + j\phi = \frac{e^{\sigma}e^{j\omega} - 1}{e^{\sigma}e^{j\omega} + 1} \tag{4.4}$$

Thus the (real) frequency variables in both domains are related by

$$\phi = \tan\left(\frac{\omega T}{2}\right) \tag{4.5}$$

which maps the Nyquist range $-\pi < \omega T < \pi$, in a one-to-one correspondence, onto the Laplacian range $-\infty < \phi < \infty$. Substituting the bilinear transformation (4.2a) into the voltage wave variables (4.1) gives

$$\begin{aligned} A\left(z^{-1}\right) &= V\left(z^{-1}\right) + Z\,I\left(z^{-1}\right) \\ B\left(z^{-1}\right) &= V\left(z^{-1}\right) - Z^{*}\,I\left(z^{-1}\right) \end{aligned} \tag{4.6a,b}$$

and hence a wave analog complex network is transformed to a wave discrete complex network henceforth known as the complex wave digital (CWD) domain.

The return group delay given for analog filters by (2.43) can be expressed as a function of the discrete variable z^{-1} as given by

$$D(z^{-1}) = \frac{\frac{d}{dz^{-1}} g(z^{-1})}{g(z^{-1})} - \frac{\frac{d}{dz^{-1}} h(z^{-1})}{h(z^{-1})} \tag{4.7}$$

and is related to the delay given in the analog domain by the following:

$$D(z^{-1}) = \frac{-2\left(D(\psi)\big|_{\psi = \frac{1-z^{-1}}{1+z^{-1}}}\right)}{(1+z^{-1})^2} \tag{4.8}$$

As suggested in [16], a more appropriate choice for the function in terms of z^{-1} is given by

$$\delta(z^{-1}) = -z^{-1} D(z^{-1})$$

$$\delta(z^{-1}) = \frac{2z^{-1}\left(D(\psi)\big|_{\psi = \frac{1-z^{-1}}{1+z^{-1}}}\right)}{(1+z^{-1})^2} \tag{4.9}$$

which is a function of $D(z^{-1}) \Leftrightarrow D(\psi)$. On the unit circle $z^{-1} = e^{-j\omega T}$, the above becomes

$$\delta(e^{-j\omega T}) = \frac{D(j\phi)\big|_{\phi = \tan\left(\frac{\omega T}{2}\right)}}{2\left(\cos\left(\frac{\omega T}{2}\right)\right)^2} \tag{4.10}$$

The above definitions (4.1) lead to the recognized form of the reflection coefficient for complex impedances [40]

$$\rho = \frac{\hat{Z}(\psi) - Z^*}{\hat{Z}(\psi) + Z} \tag{4.11}$$

where $\hat{Z}(\psi)$ is the complex driving-point impedance of the one-port. The voltage and current given by the inverse transformation are

$$V = \frac{Z^*A + ZB}{Z + Z^*}$$

$$I = \frac{A - B}{Z + Z^*} \tag{4.12a,b}$$

Now consider a complex n-port N which can be characterized using a variety of matrices (eg. scattering, transfer, etc.) and shown below.

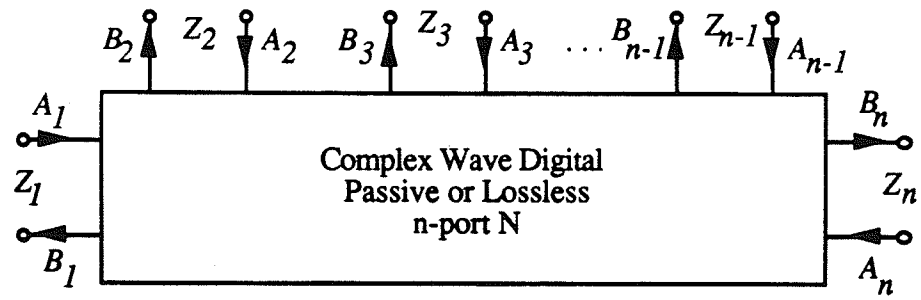

Figure 4.2: CWD n-port.

Fettweis [6] has extended the work of Belevitch [40] to give a canonical representation of the network in the form of a complex scattering matrix **S**, which relates the column vector **A** of incident voltage waves A_i to the column vector **B** of reflected voltage waves B_i, $i = 1(1)n$ by **B** = **SA**.

For a general complex n-port network with impedance matrix $\hat{\mathbf{Z}}$ and port references Z_i, $i = 1(1)n$, the scattering matrix is given by

$$\mathbf{S} = (\hat{\mathbf{Z}} - \mathbf{Z}^*)(\hat{\mathbf{Z}} + \mathbf{Z})^{-1} \tag{4.13}$$

which can also be rewritten as

$$\mathbf{S} = \mathbf{I}_n - 2\mathbf{R}(\hat{\mathbf{Z}} + \mathbf{Z})^{-1} \tag{4.14}$$

where **Z** is a strictly diagonal port reference impedance matrix with the corresponding port references on the diagonal, and **R** is the real part of **Z**. The voltage wave variables given in matrix form are given by

$$\begin{aligned} \mathbf{A} &= \mathbf{V} + \mathbf{ZI} \\ \mathbf{B} &= \mathbf{V} - \mathbf{Z}^*\mathbf{I} \end{aligned} \tag{4.15a,b}$$

and the inverse transformation is given by

$$\begin{aligned} \mathbf{V} &= \frac{1}{2}\tilde{\mathbf{G}}\,(\mathbf{Z}^*\mathbf{A} + \mathbf{ZB}) \\ \mathbf{I} &= \frac{1}{2}\tilde{\mathbf{G}}\,(\mathbf{A} - \mathbf{B}) \end{aligned} \tag{4.16a,b}$$

where $\widetilde{\mathbf{G}}$ is a real diagonal matrix containing the inverses of the real parts of the port references, and is in general not equal to the real part of the port admittance matrix as shown by

$$\begin{aligned} \mathbf{Z} &= \mathbf{R} + j\mathbf{X} \\ \widetilde{\mathbf{G}} &= \mathbf{R}^{-1} \end{aligned} \tag{4.17a,b}$$

where the inverse always exists because of the choice of the diagonal resistance matrix.

Intimately coupled with the definitions of voltage-waves are the so-called incident $\widehat{\mathbf{A}}$ and reflected $\widehat{\mathbf{B}}$ power waves [6] as redefined for the complex case in matrix form by

$$\begin{aligned} \widehat{\mathbf{A}} &= \frac{1}{2}\widetilde{\mathbf{G}}^{1/2}(\mathbf{V} + \mathbf{Z}\mathbf{I}) \\ \widehat{\mathbf{B}} &= \frac{1}{2}\widetilde{\mathbf{G}}^{1/2}(\mathbf{V} - \mathbf{Z}^{*}\mathbf{I}) \end{aligned} \tag{4.18a,b}$$

where $\widetilde{\mathbf{G}}^{1/2}$ is the positive definite square root of $\widetilde{\mathbf{G}}$.

4.2 Definition of Power

Using this characterization, the definition of the power (also called pseudo-power) of an n-port in terms of the more commonly used voltage waves is given by

$$P = \mathbf{A}^{*\mathrm{T}}(\widetilde{\mathbf{G}} - \mathbf{S}^{*\mathrm{T}}\widetilde{\mathbf{G}}\mathbf{S})\mathbf{A}$$

$$P = \sum_{i=1}^{n} (|A_i|^2 - |B_i|^2)\widetilde{G}_i \tag{4.19a,b}$$

where the asterisk symbol denotes conjugation of all the elements within the matrix when evaluated along the $\psi = j\phi$ axis. These expressions are derived using the fact that the quadratic form of a Hermitian matrix is purely real as shown in the following derivation.

The definition of the apparent power in the analog domain is given by

$$U = \mathbf{I}^{*\mathrm{T}}\mathbf{V} \tag{4.20}$$

where U is a complex scalar, and $\mathbf{V}$ and $\mathbf{I}$ are voltage and current column matrices of the same order, respectively. Substituting the definitions for the current and voltage in terms of the voltage wave variables as given in (4.16) leads to

$$U = \frac{1}{4}\left(\mathbf{A}^{*T} - \mathbf{B}^{*T}\right)\widetilde{\mathbf{G}}^2\left(\mathbf{Z}^*\mathbf{A} + \mathbf{Z}\mathbf{B}\right) \tag{4.21}$$

since

$$\widetilde{\mathbf{G}}^{*T} = \widetilde{\mathbf{G}} \tag{4.22}$$

Rewriting the above and ignoring the scalar multiplier, we get

$$U = \mathbf{A}^{*T}\widetilde{\mathbf{G}}^2\mathbf{Z}^*\mathbf{A} - \mathbf{B}^{*T}\widetilde{\mathbf{G}}^2\mathbf{Z}\mathbf{B} + \mathbf{A}^{*T}\widetilde{\mathbf{G}}^2\mathbf{Z}\mathbf{B} - \mathbf{B}^{*T}\widetilde{\mathbf{G}}^2\mathbf{Z}^*\mathbf{A} \tag{4.23}$$

and after substituting the relation relating the incident and reflected signals $\mathbf{B} = \mathbf{S}\mathbf{A}$, the above simplifies to

$$U = \mathbf{A}^{*T}\left(\widetilde{\mathbf{G}}^2\mathbf{Z}^* - \mathbf{S}^{*T}\widetilde{\mathbf{G}}^2\mathbf{Z}\mathbf{S} + \widetilde{\mathbf{G}}^2\mathbf{Z}\mathbf{S} - \mathbf{S}^{*T}\widetilde{\mathbf{G}}^2\mathbf{Z}^*\right)\mathbf{A} \tag{4.24}$$

By definition, the power P is the real part of the apparent power U,

$$P = Re\{U\} = Re\left\{\mathbf{A}^{*T}\left(\widetilde{\mathbf{G}}^2\mathbf{Z}^* - \mathbf{S}^{*T}\widetilde{\mathbf{G}}^2\mathbf{Z}\mathbf{S} + \widetilde{\mathbf{G}}^2\mathbf{Z}\mathbf{S} - \mathbf{S}^{*T}\widetilde{\mathbf{G}}^2\mathbf{Z}^*\right)\mathbf{A}\right\} \tag{4.25}$$

We can identify the Hermitian $\mathbf{H}$ and the anti-Hermitian $\mathbf{H}^A$ matrix components of the inner-most bracketed term as

$$\mathbf{H} = \left(\mathbf{Z} + \mathbf{Z}^*\right)\widetilde{\mathbf{G}}^2 - \mathbf{S}^{*T}\left(\mathbf{Z} + \mathbf{Z}^*\right)\widetilde{\mathbf{G}}^2\mathbf{S}$$

$$\mathbf{H}^A = \left(\mathbf{Z}^* - \mathbf{Z}\right)\widetilde{\mathbf{G}}^2 + \mathbf{S}^{*T}\left(\mathbf{Z}^* - \mathbf{Z}\right)\widetilde{\mathbf{G}}^2\mathbf{S} + 2\widetilde{\mathbf{G}}^2\mathbf{Z}\mathbf{S} - 2\mathbf{S}^{*T}\widetilde{\mathbf{G}}^2\mathbf{Z}^* \tag{4.26a,b}$$

where we have used the fact that diagonal matrices commute under multiplication. Thus the real power is given by

$$P = Re\left\{\mathbf{A}^{*T}\left(\mathbf{H} + \mathbf{H}^A\right)\mathbf{A}\right\} = Re\left\{\mathbf{A}^{*T}\left(\mathbf{H}\right)\mathbf{A}\right\} + Re\left\{\mathbf{A}^{*T}\left(\mathbf{H}^A\right)\mathbf{A}\right\} \tag{4.27}$$

However, the quadratic form of a Hermitian matrix is purely real and the quadratic form of an anti-Hermitian matrix is purely imaginary, and thus the power is given by

$$P = \mathbf{A}^{*T}\left\{\left(\mathbf{Z} + \mathbf{Z}^*\right)\widetilde{\mathbf{G}}^2 - \mathbf{S}^{*T}\left(\mathbf{Z} + \mathbf{Z}^*\right)\widetilde{\mathbf{G}}^2\mathbf{S}\right\}\mathbf{A} \tag{4.28}$$

The above can be written in a simpler form by identifying $\left(\mathbf{Z} + \mathbf{Z}^*\right)$ as twice the resistance

matrix **R**, giving (again ignore any constants)

$$P = \mathbf{A}^{*T}(\widetilde{\mathbf{G}} - \mathbf{S}^{*T}\widetilde{\mathbf{G}}\mathbf{S})\,\mathbf{A} \tag{4.29}$$

as given in (4.19a).

The conditions for passivity ($P \geq 0$) and losslessness ($P = 0$) (also called pseudo-passivity and pseudo-losslessness) from the above equations are given by

$$\widetilde{\mathbf{G}} - \mathbf{S}^{*T}\,\widetilde{\mathbf{G}}\,\mathbf{S} \;\geq\; 0 \tag{4.30}$$

(non-negative definite) and

$$\widetilde{\mathbf{G}} = \mathbf{S}^{*T}\,\widetilde{\mathbf{G}}\,\mathbf{S} \tag{4.31}$$

respectively, when evaluated along the $\psi = j\phi$ axis.

The last equation shown above can be used to define the power wave (normalized) form of the complex scattering matrix. Assuming that **S** characterizes a lossless network, the normalized form of the scattering matrix, namely $\widehat{\mathbf{S}}$, is unitary (the complex form of orthogonal) and is given by

$$\widehat{\mathbf{S}} = \widetilde{\mathbf{G}}^{1/2}\,\mathbf{S}\,\widetilde{\mathbf{G}}^{-1/2} \tag{4.32}$$

This corresponds to simple scaling in the signal paths, that is, real scaling transformers at the ports of the scattering matrix. This effectively sets the *real parts* of the port references to *unity*, while the imaginary parts are not constrained.

4.3 Two-Port Scattering Matrix

For a lossless two-port, the scattering matrix **S** can be represented by

$$\mathbf{S} = \frac{1}{g}\begin{bmatrix} h & \sigma\frac{R_1}{R_2}f_* \\ f & -\sigma h_* \end{bmatrix} \tag{4.33}$$

where R_1 and R_2 are the real parts of the port references, and f, h, and g are known as the canonic polynomials and are functions of either ψ or z. The lower asterisk operator $*$ is the para-conjugate defined by

$$f_*(\psi) = f^*(-\psi^*) \quad \Leftrightarrow \quad f_*(z^{-1}) = z^{-n} f^*(z^*) \tag{4.34a,b}$$

where n is equal to the degree of the g polynomial. If the network is reciprocal, the complex constant σ is given by

$$\sigma = \frac{f}{f_*} \frac{R_2}{R_1} \tag{4.35}$$

The polynomial g has all of its zeros strictly in the left-half plane (ie. it is Hurwitz). For lossless two-port networks the following relation holds

$$gg_* = \frac{R_1}{R_2} ff_* + hh_* \tag{4.36}$$

which is known as the analytic continuation of the Feldtkeller equation. For normalized networks, simply let

$$R_1 = R_2 \tag{4.37}$$

in the above equations (4.33,35-36), and thus the complex constant σ becomes unimodular.

For a complex two-port characterized by an open-circuit impedance matrix

$$\mathbf{Z} = \begin{bmatrix} z_{11} & z_{12} \\ z_{21} & z_{22} \end{bmatrix} \tag{4.38}$$

with port references

$$\begin{aligned} Z_1 &= R_1 + jX_1 \\ Z_2 &= R_2 + jX_2 \end{aligned} \tag{4.39a,b}$$

the scattering matrix can be written as

$$\mathbf{S} = \frac{1}{-Z_1 Z_2 - Z_1 z_{22} - Z_2 z_{11} - \Delta_z} \begin{bmatrix} (Z_2 + z_{22}) Z_1^* - Z_2 z_{11} - \Delta_z & -2R_1 z_{12} \\ -2R_2 z_{21} & (Z_1 + z_{11}) Z_2^* - Z_1 z_{22} - \Delta_z \end{bmatrix}$$

$$\Delta_z = z_{11} z_{22} - z_{12} z_{21} \tag{4.40a,b}$$

Similarly, if the complex two-port is represented by a short-circuit admittance matrix

$$\mathbf{Y}=\begin{bmatrix} y_{11} & y_{12} \\ y_{21} & y_{22} \end{bmatrix} \tag{4.41}$$

with the port references as given above, the scattering matrix can be written as

$$\mathbf{S}=\frac{1}{-y_{22}Z_2-y_{11}Z_1-1-\Delta_y Z_1 Z_2}\begin{bmatrix} -y_{22}Z_2+y_{11}Z_1^*-1+\Delta_y Z_1^* Z_2 & 2R_1 y_{12} \\ 2R_2 y_{21} & -y_{11}Z_1+y_{22}Z_2^*-1+\Delta_y Z_1 Z_2^* \end{bmatrix}$$

$$\Delta_y = y_{11}y_{22} - y_{12}y_{21} \tag{4.42a,b}$$

and through the inverse transformation, the open-circuit impedance matrix is given by

$$\mathbf{Z}=\frac{1}{(g-g_*\sigma)-(h-h_*\sigma)}\begin{bmatrix} (Z_1 h+Z_1^* h_*\sigma)+(Z_1^* g+Z_1 g_*\sigma) & 2R_1 f_*\sigma \\ 2R_1 f & (Z_2^* g+Z_2 g_*\sigma)-(Z_2^* h+Z_2 h_*\sigma) \end{bmatrix} \tag{4.43}$$

Note that the condition for reciprocity [37] remains unchanged as

$$\mathbf{S}^T\widetilde{\mathbf{G}} = \widetilde{\mathbf{G}}\mathbf{S} \tag{4.44}$$

where **S** is now complex.

4.4 Impedances Mapped to the CWD Domain

Using the transformations from the voltage-current to the CWD domain, as given by (4.12), simple combinations of impedances can be mapped into the corresponding (equivalent) CWD element. For dynamic one-port impedances, the corresponding CWD element is an allpass section. Only constant two-port elements will be considered in this section, namely the complex transformer and the imaginary resistor in series and parallel combinations.

4.4.1 One-port Impedances

The one-port dynamic and constant elements found in complex reference networks are the voltage source, the resistor, the imaginary resistor, the inductor and the capacitor. When each element is mapped to a CWD one-port, the port reference is chosen in order to simplify the resulting reflectance and to guarantee computability of the resulting section. The port reference is the complex conjugate of the driving-point impedance of the one-port evaluated at $\Psi = 1$ (forcing the reflectance at $\Psi = 1$ to be zero).

	Imaginary Resistor	Imaginary Resistor	Resistor series I.R.	Resistive source & I.R.
Analog Ψ-domain	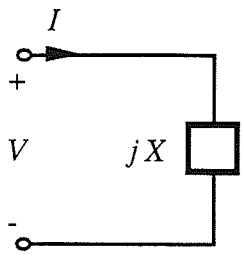	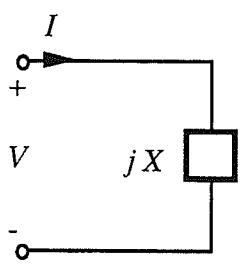	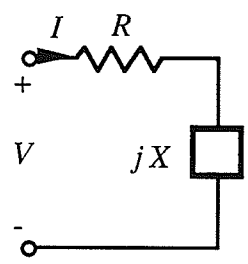	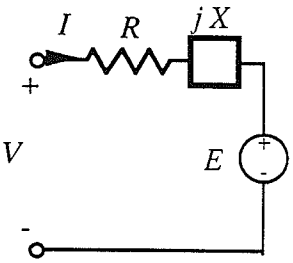
	$V = jXI$	$V = jXI$ $X = \frac{R_1}{\tan\left(\frac{1}{2}\theta\right)} - X_1 \quad \theta \neq 0$	$V = (R + jX)I$	$V = E + (R + jX)I$
CWD domain (voltage-wave)	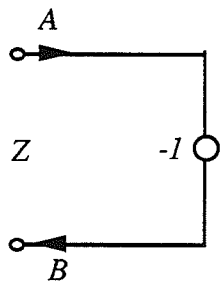	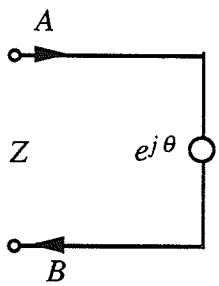	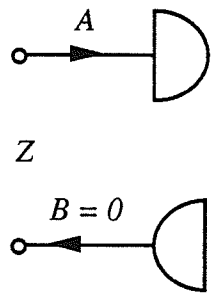	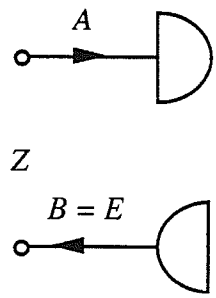
	$Z = R_1 - jX$ $B = -A$	$Z = R_1 + jX_1$ $B = e^{j\theta}A$	$Z = R - jX$ $B = 0$	$Z = R - jX$ $B = E$

Table 4.1: Source and non-dynamic one-ports in the analog and CWD domains.

Table 4.1 shows the equivalence between the common non-dynamic one-ports in both domains. The imaginary resistor can be viewed in two different ways, depending upon the domain in which the equivalence is desired, which is related to the choice of the reference impedance. The first view point is shown in the first column, where we require the equivalence of the analog imaginary resistor. Here the reflectance is a simple inversion and the real part of the port reference is arbitrary. The second view point as given in the second column adds an extra degree of freedom (found in the general reference impedance Z) which is needed when we desire the equivalence of the CWD imaginary resistor in the form of a unimodular multiplier (in other words, finding the equivalent of a CWD unimodular multiplier when viewed as a one-port).

The third column of Table 4.1 shows a simple complex termination, which corresponds to a wave sink and zero input. A more general form of this is shown in the fourth column with the inclusion of an ideal voltage source. In this case, the CWD one-port equivalent is

a wave sink and an input equal to the value of the voltage source.

The one-port inductor and capacitor equivalences are given in Tables 4.2-3, respectively.

	Inductor	Inductor series I.R.	Inductor parallel I.R.
Analog ψ-domain	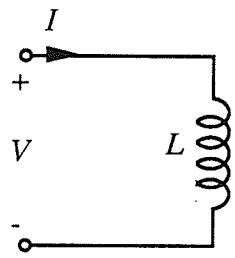	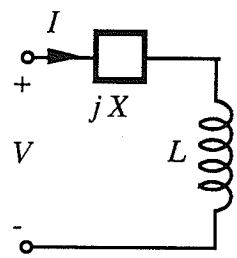	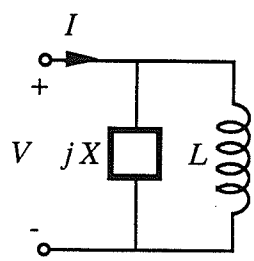
	$V = L\psi I$	$V = (L\psi + jX)I$	$V = \frac{jXL\psi}{L\psi + jX} I$
CWD domain (voltage-wave)	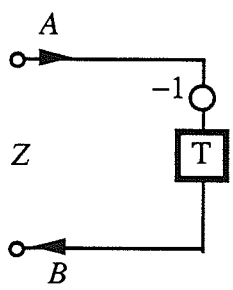	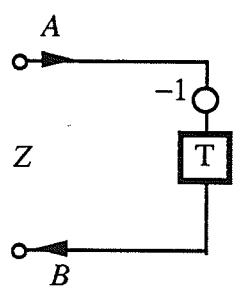	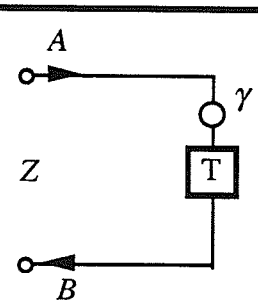
	$Z = L$ $B = -z^{-1}A$	$Z = L - jX$ $B = -z^{-1}A$	$Z = \frac{-jXL}{L - jX}$ $B = \gamma z^{-1} A$ $\gamma = \frac{L - jX}{L + jX}$

Table 4.2: Inductive one-ports in the analog and CWD domains.

Notice that a unimodular multiplier in series with a delay is needed only for the section with the inductor in parallel with the imaginary resistor. In all other cases, only a simple inversion is needed (no computations are required and no quantizations are necessary).

	Capacitor	Capacitor series I.R.	Capacitor parallel I.R.
Analog ψ-domain	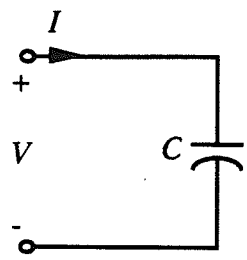	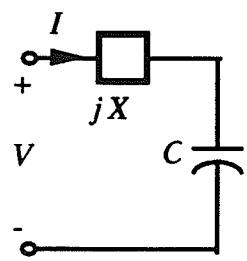	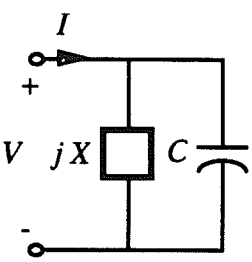
	$V=\frac{I}{C\psi}$	$V=\left(\frac{1}{C\psi}+jX\right)I$	$V=\frac{jX}{1+jXC\psi}I$
CWD domain (voltage-wave)	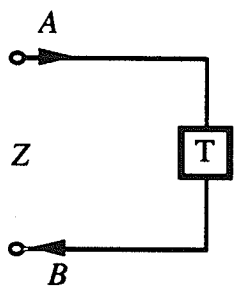	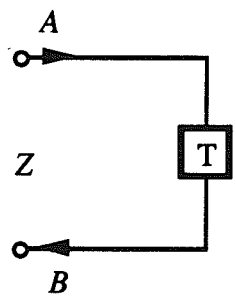	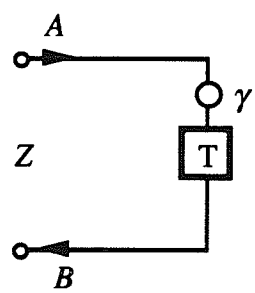
	$Z=\frac{1}{C}$ $B=z^{-1}A$	$Z=\frac{1}{C}-jX$ $B=z^{-1}A$	$Z=\frac{-jX}{1-jXC}$ $B=\gamma z^{-1}A$ $\gamma=-\left(\frac{1-jXC}{1+jXC}\right)$

Table 4.3: Capacitive one-ports in the analog and CWD domains.

For this case, a unimodular multiplier in series with a delay is needed only for the section with the capacitor in parallel with the imaginary resistor. Again, in all other cases, only a simple inversion is needed (no computations are required and no quantizations are necessary).

4.4.2 Non-Dynamic Two-Ports

The only new complex non-dynamic two-port sections are the complex transformer [40] and the series and parallel connections of the imaginary resistor. Table 4.4 gives the correspondence between these sections in the analog and CWD domains.

	Complex Transformer	Series Imaginary Resistor	Parallel Imaginary Resistor
Analog Ψ-domain	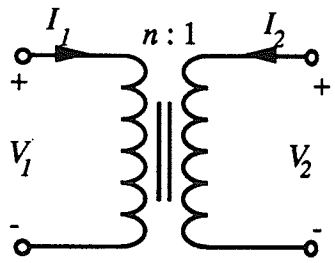	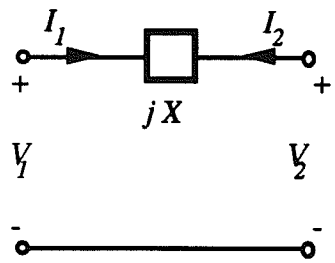	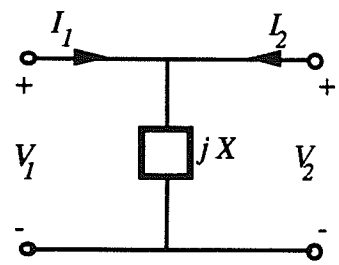
	$V_1 = n^* V_2$ $I_2 = -n I_1$	$V_1 - V_2 = jX I_1$ $I_1 = -I_2$	$V_1 = jX(I_1 + I_2)$ $V_1 = V_2$
CWD domain (voltage-wave)	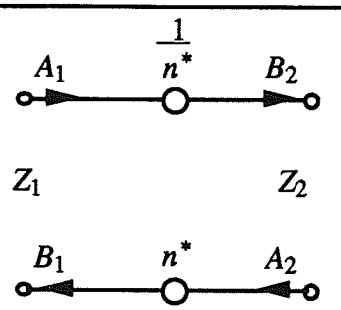	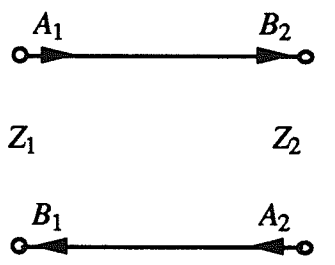	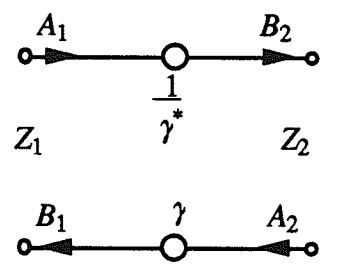
	$Z_1 = R_1 + jX_1$ $Z_2 = \frac{R_1 - jX_1}{nn^*} = \frac{Z_1^*}{nn^*}$	$Z_1 = R_1 + jX_1$ $Z_2 = R_1 - j(X + X_1)$ $Z_2 = Z_1^* - jX$	$Z_1 = R_1 + jX_1$ $Z_2 = \frac{-jX Z_1^*}{Z_1^* - jX} = \frac{Z_1^*}{\gamma}$ $\gamma = \frac{Z_1^* - jX}{-jX}$

Table 4.4: Non-dynamic two-ports in the analog and CWD domains.

In each case, the second port impedance was chosen to simplify the scattering matrix of the section and to guarantee computability of the resulting section. For the complex transformer, the second port reference is a real scalar multiple of the first. Thus a complex transformer cannot be used for an arbitrary change of reference impedance as in the real case. That is, only the magnitude of the reference impedance can be changed with a complex transformer, not the real and imaginary parts independently. Note that with a unimodular turns-ratio the second port reference is the complex conjugate of the first, and thus this section does not have an effect upon the port impedance. With the two-port series imaginary resistor, the second port reference is the sum of the complex conjugates of the first port reference and the imaginary resistor value. Similarly, with the two-port parallel

imaginary resistor, the second port reference is the parallel combination of the complex conjugates of the first port reference and the imaginary resistor value. Thus we can see the domination (or carry-over) of the familiar characteristics of the analog domain.

The scattering matrix of the complex transformer is in the familiar form of scaling (a pair of inverse multipliers). For the series imaginary resistor, the scattering matrix has a particularly simple form where the signal quantities are passed through the section unmodified. However, for the parallel imaginary resistor, the scattering matrix is in a hybrid form of scaling, that is, one multiplier is the complex conjugate inverse of the other. This can be thought of as a constant change of phase. Obviously, of the two configurations for the imaginary resistor, the series form is preferred when a choice is available since it does not involve computations.

It should be noted that the scattering matrices for the series and parallel connections of the imaginary resistor cannot be derived by using series and parallel complex three-port adaptors, respectively, since a delay-free loop would result.

The reference impedance for port two was explicitly chosen in the expressions given in Table 4.4, however, this may be undesirable in some situations. It is possible to have independent port references for ports one and two. However, care must be taken in the placement of the resulting section in a digital network because the sections will not contain a reflection-free port.

The general expressions for the series imaginary resistor, the parallel imaginary resistor and the complex transformer as a function of both port references are given by, respectively:

$$\begin{bmatrix} B_1 \\ B_2 \end{bmatrix} = \frac{1}{Z_1 + Z_2 + jX} \begin{bmatrix} -Z_1^* + Z_2 + jX & 2R_1 \\ 2R_2 & Z_1 - Z_2^* + jX \end{bmatrix} \begin{bmatrix} A_1 \\ A_2 \end{bmatrix}$$

$$\begin{bmatrix} B_1 \\ B_2 \end{bmatrix} = \frac{1}{Z_1 Z_2 + jX\,(Z_1 + Z_2)} \begin{bmatrix} -Z_1^* Z_2 + jX\left(-Z_1^* + Z_2\right) & 2jX\,R_1 \\ 2jX\,R_2 & -Z_1 Z_2^* + jX\left(Z_1 - Z_2^*\right) \end{bmatrix} \begin{bmatrix} A_1 \\ A_2 \end{bmatrix}$$

$$\begin{bmatrix} B_1 \\ B_2 \end{bmatrix} = \frac{1}{Z_1 + nn^* Z_2} \begin{bmatrix} -Z_1^* + nn^* Z_2 & 2n^*\,R_1 \\ 2n\,R_2 & Z_1 - nn^* Z_2^* \end{bmatrix} \begin{bmatrix} A_1 \\ A_2 \end{bmatrix} \qquad (4.45a,b,c)$$

The scattering matrices can be expressed in normalized form using (4.32) and are given below for the series imaginary resistor, the parallel imaginary resistor and the complex transformer, respectively:

$$\begin{bmatrix} \hat{B}_1 \\ \hat{B}_2 \end{bmatrix} = \frac{1}{Z_1 + Z_2 + jX} \begin{bmatrix} -Z_1^* + Z_2 + jX & 2\sqrt{R_1 R_2} \\ 2\sqrt{R_1 R_2} & Z_1 - Z_2^* + jX \end{bmatrix} \begin{bmatrix} \hat{A}_1 \\ \hat{A}_2 \end{bmatrix}$$

$$\begin{bmatrix} \hat{B}_1 \\ \hat{B}_2 \end{bmatrix} = \frac{1}{Z_1 Z_2 + jX\,(Z_1 + Z_2)} \begin{bmatrix} -Z_1^* Z_2 + jX\left(-Z_1^* + Z_2\right) & 2jX\sqrt{R_1 R_2} \\ 2jX\sqrt{R_1 R_2} & -Z_1 Z_2^* + jX\left(Z_1 - Z_2^*\right) \end{bmatrix} \begin{bmatrix} \hat{A}_1 \\ \hat{A}_2 \end{bmatrix}$$

$$\begin{bmatrix} \hat{B}_1 \\ \hat{B}_2 \end{bmatrix} = \frac{1}{Z_1 + nn^* Z_2} \begin{bmatrix} -Z_1^* + nn^* Z_2 & 2n^*\sqrt{R_1 R_2} \\ 2n\sqrt{R_1 R_2} & Z_1 - nn^* Z_2^* \end{bmatrix} \begin{bmatrix} \hat{A}_1 \\ \hat{A}_2 \end{bmatrix}$$

(4.46a,b,c)

4.5 Interconnection of Ports

A CWD network is composed of at least one and usually many building blocks connected together in such a way that the resulting network has the same characteristics as an analog reference network. However, before the blocks can be connected together, they must be compatible for connection, that is, the port references for the ports to be connected must be related. The conditions that must be satisfied for compatibility of ports numbered 1 and 2 are given in both domains as

$$\begin{aligned} V_1 &= V_2 \\ I_1 &= -I_2 \\ B_1 &= A_2 \\ B_2 &= A_1 \end{aligned} \qquad (4.47\text{a-d})$$

After the substitution of these conditions into the definitions of the voltage-wave variables (4.6), the following compatibility condition is derived relating the port references for the two ports:

$$Z_1 = Z_2^* \qquad (4.48)$$

Thus the port references must be the complex conjugate of each other in order to be compatible for connection (this forces zero reflectance at the port connection).

4.6 CWDF Adaptors

It was noted in a preceding section that the wave-digital transformation maps an analog network to a digital network and the digital network inherits the same characteristics as the reference analog network. As an example, consider a ladder network composed of interconnections of one-ports containing dynamic elements. The digital network inherits the properties because each dynamic element is treated as a one-port, which is easily transformed to a CWD element using Tables 4.2-4.3. Similarly, the interconnection of the elements (both series and parallel) is mapped to the CWD domain as either a series or parallel adaptor (usually with three ports). That is, the physical connection of analog elements is transformed to series and parallel adaptors using the definition of the wave variables and Kirchhoff's Laws. In general, an adaptor could have any number of ports (but at least two); however, WD networks are primarily composed of two-port and three-port series and parallel adaptors.

In order for the resulting CWD network to be computable, all three-port adaptors in a network except one will have to contain a reflection-free port. Furthermore, the reflection-free port must be connected to another CWD building block and chosen to eliminate any delay-free loops that may otherwise exist [6]. A reflection-free port has the corresponding reflected wave independent of the incident wave, and thus the corresponding diagonal element of the scattering matrix is zero. Ordinarily, the chosen reflection-free port is not unique, however, in the following the last port of the adaptor will arbitrarily be made reflection-free with the understanding that other combinations exist.

All of the adaptors derived are lossless and reciprocal under infinite-precision conditions and they can be made passive under finite-arithmetic conditions (after they have been quantized). With a real adaptor after quantization, the port reference resistances corresponding to the quantized form of the adaptor can be found. This leads to losslessness under quantized conditions. However, this relationship does not hold for complex adaptors unless the adaptor reduces to the form of the real adaptor, when at most the real parts of the quantized port reference impedances will be identifiable.

In the following, all definitions and derivations reduce to the known theory of real wave digital filters if all quantities are restricted to be real as required for the generalization.

4.6.1 General *n*-port Complex Series Adaptor

The series adaptor is used to represent an analog series connection of one-ports in the CWD domain. This involves mapping the Kirchhoff Laws and the conditions for a series connection through the given transformation (4.6).

4.6.1.1 Definition of the Complex Series Adaptor

The complex series adaptor must represent a series connection of ports in the analog domain with complex port references. This condition is given by

$$\begin{aligned} V_1 + V_2 + V_3 + \ldots + V_n &= 0 \\ I_1 = I_2 = I_3 = \ldots &= I_n \end{aligned} \qquad (4.49a,b)$$

Assume that the port reference impedances are given by

$$Z_\upsilon = R_\upsilon + jX_\upsilon\,, \quad R_\upsilon > 0, \quad \upsilon = 1(1)n \qquad (4.50a,b)$$

From the definition of the wave quantities (4.6), we know that for ports $\upsilon = 1(1)n$

$$\begin{aligned} A_\upsilon &= V_\upsilon + Z_\upsilon I_\upsilon \\ B_\upsilon &= V_\upsilon - Z_\upsilon^* I_\upsilon \end{aligned} \qquad (4.51a,b)$$

Solving for V_υ from (4.51a) above and substituting with appropriate subscripts into (4.49a), we get

$$A_1 - Z_1 I_1 + A_2 - Z_2 I_2 + A_3 - Z_3 I_3 + \ldots + A_n - Z_n I_n = 0 \qquad (4.52)$$

However, all I_υ, $\upsilon = 1(1)n$ are equal, and thus the above becomes

$$A_1 + A_2 + A_3 + \ldots + A_n - (Z_1 + Z_2 + Z_3 + \ldots + Z_n)\, I_\upsilon = 0 \qquad (4.53)$$

Solving for I_υ from (4.51b) and substituting into the above

$$2\,R_\upsilon (A_1 + A_2 + A_3 + \ldots + A_n) - (Z_1 + Z_2 + Z_3 + \ldots + Z_n)(A_\upsilon - B_\upsilon) = 0 \qquad (4.54)$$

and solving for B_υ,

$$B_\upsilon = A_\upsilon - \frac{2\,R_\upsilon (A_1 + A_2 + A_3 + \ldots + A_n)}{Z_1 + Z_2 + Z_3 + \ldots + Z_n}\,, \quad \upsilon = 1(1)n \qquad (4.55)$$

Define the complex scalar quantity known as the port coefficient

$$\beta_\upsilon = \frac{2\,R_\upsilon}{Z_1 + Z_2 + Z_3 + \ldots + Z_n} \qquad (4.56)$$

and finally

$$B_\upsilon = A_\upsilon - \beta_\upsilon (A_1 + A_2 + A_3 + \ldots + A_n), \quad \upsilon = 1(1)n \tag{4.57}$$

Define the sum of the port reference impedances as

$$Z_{tot} = \sum_{i=1}^{n} Z_i \tag{4.58}$$

then

$$\beta_1 + \beta_2 + \beta_3 + \ldots + \beta_n = 1 + \frac{Z_{tot}^*}{Z_{tot}} \tag{4.59}$$

From the above and (4.56) it is easily shown that the magnitude of the coefficient is bounded above

$$|\beta_\upsilon| \leq 2 \tag{4.60}$$

although usually this bound is pessimistic. The complex scattering matrix for the general n-port series adaptor is given by

$$\begin{bmatrix} B_1 \\ B_2 \\ B_3 \\ \vdots \\ B_n \end{bmatrix} = \begin{bmatrix} 1-\beta_1 & -\beta_1 & -\beta_1 & \cdots & -\beta_1 \\ -\beta_2 & 1-\beta_2 & -\beta_2 & \cdots & -\beta_2 \\ -\beta_3 & -\beta_3 & 1-\beta_3 & \cdots & -\beta_3 \\ \vdots & \vdots & \vdots & \ddots & \vdots \\ -\beta_n & -\beta_n & -\beta_n & \cdots & 1-\beta_n \end{bmatrix} \begin{bmatrix} A_1 \\ A_2 \\ A_3 \\ \vdots \\ A_n \end{bmatrix} \tag{4.61}$$

The adaptor cannot be factored in such a way that a real n-port series adaptor can be identified using real or complex diagonal scaling matrices, unless one port is reflection-free. An attempt at this operation would generate a matrix with all but the diagonal elements equal to the corresponding real series adaptor without a reflection-free port. Unfortunately, the diagonal elements of the scattering matrix cannot be independently scaled using diagonal scaling matrices.

4.6.1.2 Dependent Coefficient

From equation (4.59) above, it is clear that one of the port coefficients β_υ is dependent upon the remaining coefficients, and furthermore this dependency encompasses all of the ports. Let the dependent coefficient be the nth coefficient. Solving for β_n and substituting into (4.55) we derive

$$B_\upsilon = A_\upsilon - \beta_\upsilon (A_1 + A_2 + A_3 + \ldots + A_n) \ , \quad \upsilon = 1(1)\, n - 1$$

$$B_n = -\left[B_1 + B_2 + B_3 + \ldots + B_{n-1} + \left(\frac{Z_{tot}^*}{Z_{tot}}\right)(A_1 + A_2 + A_3 + \ldots + A_n)\right] \tag{4.62a,b}$$

It is clear from (4.56) that the number of real independent parameters that characterize the series adaptor is n, and they are given by

$$\frac{R_\upsilon}{R_1}, \quad 2 \le \upsilon \le n, \text{ and } \frac{1}{R_1}\sum_{i=1}^{n} X_i \tag{4.63}$$

which is one more than the real case. Clearly, the adaptor coefficients can be determined from these parameters. However, only the real parts of the actual port references can be found, whereas only the sum of the imaginary parts of the references is known.

4.6.1.3 Reflection-free Port

The nth port can arbitrarily be made reflection-free by setting $S_{nn} = 0$ in the scattering matrix. This adds another constraint which allows the removal of another coefficient, namely

$$\beta_n = 1 \tag{4.64}$$

Substituting this into (4.56) we get

$$Z_1 + Z_2 + Z_3 + \ldots + Z_{n-1} = Z_n^* \tag{4.65}$$

or, in terms of the port resistances and port constant reactances

$$R_n = R_1 + R_2 + R_3 + \ldots + R_{n-1}$$

$$0 = X_1 + X_2 + X_3 + \ldots + X_n \tag{4.66a,b}$$

Thus the sum of the port impedances is purely *real*, and from the definition of the coefficients β_υ from (4.56), it is clear that with a reflection-free port with general complex port impedances *all of the coefficients are purely real* (thus the scattering matrix is purely real). It is now clear that this case reduces to the definitions of the real series adaptor with a reflection-free port and the generalization to the complex plane requires no extra computations over the real case. Also, for every port we have an extra degree of freedom (that is, an extra parameter) in the imaginary part of the port impedance which can be used to simplify the form of other CWD elements.

In this case the values of the coefficients have a particularly simple form. It is clear that

$$\sum_{i=1}^{n} Z_i = 2\,R_n \tag{4.67}$$

which, when substituted into (4.56) leads to the following condition

$$\beta_\upsilon = \frac{R_\upsilon}{R_n}\ , \qquad \upsilon = 1(1)n$$

$$\beta_\upsilon = \frac{R_\upsilon}{(R_1 + R_2 + \ldots + R_{n-1})}\ , \qquad \upsilon = 1(1)n \tag{4.68a,b}$$

and thus there are only (n-2) real parameters. Again, given the parameters, the real parts of the port references can be found. However, no information is given for the imaginary parts of the port references. The condition on the nth coefficient (4.65) leads to the following relation

$$\beta_1 + \beta_2 + \beta_3 + \ldots + \beta_{n-1} = \frac{Z^*_{tot}}{Z_{tot}} \tag{4.69}$$

Using the same argument as the earlier case, one coefficient is dependent upon the others and it can be removed. The $(n\text{-}1)^{\text{th}}$ coefficient can be arbitrarily chosen as dependent, and the following equations are derived,

$$\begin{aligned} B_\upsilon &= A_\upsilon + \beta_\upsilon (B_n - A_n)\ , \qquad \upsilon = 1(1)\,n-2 \\ B_{n-1} &= -(A_n + B_1 + B_2 + B_3 + \ldots + B_{n-2}) \\ B_n &= -(A_1 + A_2 + A_3 + \ldots + A_{n-1}) \end{aligned} \tag{4.70a,b,c}$$

4.6.1.4 Symbols of the General *n*-port Complex Series Adaptor

The symbols used for both the dependent port case and the reflection-free case are shown below, where the second figure has a bar associated with the reflected wave of port *n* showing that it is reflection free.

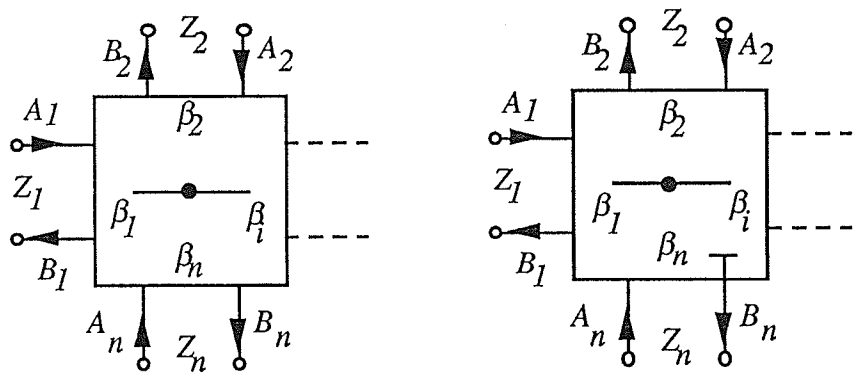

Figure 4.3: Symbols used for the *n*-port complex series adaptor.

4.6.1.5 Complex three-port Series Adaptor

The complex three-port series adaptor deserves special attention because of its usefulness in CWD networks. With the complexity of the form of (4.62), the non-reflection-free case is presented without a dependent coefficient with the following scattering matrix

$$\begin{bmatrix} B_1 \\ B_2 \\ B_3 \end{bmatrix} = \begin{bmatrix} 1-\beta_1 & -\beta_1 & -\beta_1 \\ -\beta_2 & 1-\beta_2 & -\beta_2 \\ -\beta_3 & -\beta_3 & 1-\beta_3 \end{bmatrix} \begin{bmatrix} A_1 \\ A_2 \\ A_3 \end{bmatrix} \tag{4.71}$$

where the complex coefficients are given by

$$\beta_\upsilon = \frac{2\,R_\upsilon}{Z_1 + Z_2 + Z_3}\ , \quad \upsilon = 1(1)\,3 \tag{4.72}$$

From the earlier observations, the adaptor is a function of three real parameters. Again, note that this adaptor cannot be factored in such a way that a real three-port series adaptor can be identified using real or complex diagonal scaling matrices. A wave-flow diagram is given in the following figure.

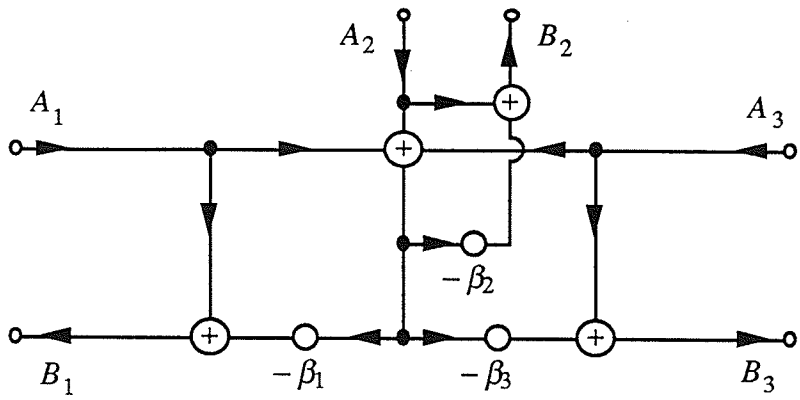

Figure 4.4: Wave-flow diagram of the complex three-port series adaptor without a RF port.

The reflection-free case with port three reflection-free and a dependent coefficient 2 has the following scattering matrix,

$$\begin{bmatrix} B_1 \\ B_2 \\ B_3 \end{bmatrix} = \begin{bmatrix} 1 - \beta_1 & -\beta_1 & -\beta_1 \\ \beta_1 - 1 & \beta_1 & \beta_1 - 1 \\ -1 & -1 & 0 \end{bmatrix} \begin{bmatrix} A_1 \\ A_2 \\ A_3 \end{bmatrix} \tag{4.73}$$

where the real coefficient is given by

$$\beta_1 = \frac{R_1}{R_1 + R_2} \tag{4.74}$$

From the earlier observations, this is exactly the definition of the real three -port series adaptor with port three reflection-free. Clearly, in this case only one real quantization is required in the binary implementation of this adaptor, and similarly the adaptor is a function of one real parameter. The wave-flow diagram is given in the following figure.

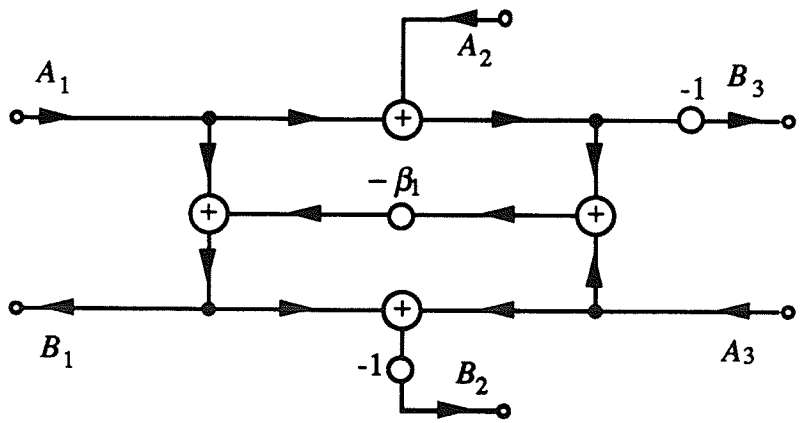

Figure 4.5: Wave-flow diagram of the complex three-port series adaptor with a RF port.

The port impedances are related by

$$Z_1 + Z_2 = Z_3^* \tag{4.75}$$

The scattering matrix given as a function of the port references is given by

$$\begin{bmatrix} B_1 \\ B_2 \\ B_3 \end{bmatrix} = \begin{bmatrix} \frac{R_2}{R_1+R_2} & \frac{-R_1}{R_1+R_2} & \frac{-R_1}{R_1+R_2} \\ \frac{-R_2}{R_1+R_2} & \frac{R_1}{R_1+R_2} & \frac{-R_2}{R_1+R_2} \\ -1 & -1 & 0 \end{bmatrix} \begin{bmatrix} A_1 \\ A_2 \\ A_3 \end{bmatrix} \tag{4.76}$$

which can be expressed in normalized form using (4.32) as given by

$$\begin{bmatrix} \hat{B}_1 \\ \hat{B}_2 \\ \hat{B}_3 \end{bmatrix} = \begin{bmatrix} \frac{R_2}{R_1+R_2} & \frac{-\sqrt{R_1R_2}}{R_1+R_2} & \frac{-\sqrt{R_1}}{\sqrt{R_1+R_2}} \\ \frac{-\sqrt{R_1R_2}}{R_1+R_2} & \frac{R_1}{R_1+R_2} & \frac{-\sqrt{R_2}}{\sqrt{R_1+R_2}} \\ \frac{-\sqrt{R_1}}{\sqrt{R_1+R_2}} & \frac{-\sqrt{R_2}}{\sqrt{R_1+R_2}} & 0 \end{bmatrix} \begin{bmatrix} \hat{A}_1 \\ \hat{A}_2 \\ \hat{A}_3 \end{bmatrix} \tag{4.77}$$

The symbols used are shown below, where the second figure has a bar associated with the reflected wave of port three showing that it is reflection free.

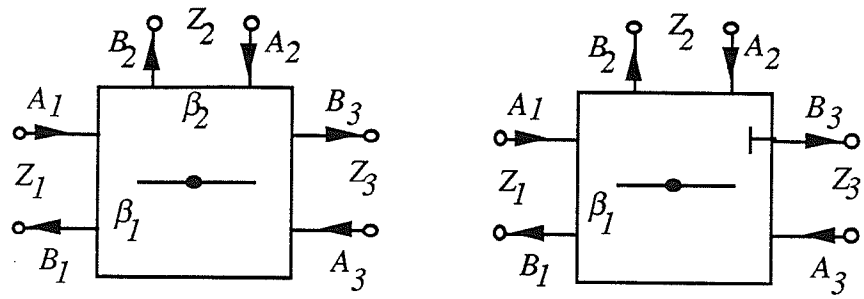

Figure 4.6: Symbols used for the three-port series adaptors.

4.6.2 General *n*-port Complex Parallel Adaptor

The parallel adaptor is used to represent an analog parallel connection of one-ports in the CWD domain. This involves mapping the Kirchhoff Laws and the conditions for a parallel connection through the given transformation.

4.6.2.1 Definition of the Complex Parallel Adaptor

The complex parallel adaptor must represent a parallel connection of ports in the analog domain with complex port references. This condition is given by

$$\begin{aligned} V_1 = V_2 = V_3 = \ldots = V_n \\ I_1 + I_2 + I_3 + \ldots + I_n = 0 \end{aligned} \tag{4.78a,b}$$

Assume that the port reference impedances are given by

$$Z_\upsilon = R_\upsilon + jX_\upsilon\,, \quad R_\upsilon > 0, \quad \upsilon = 1(1)n \tag{4.79a,b}$$

and define the port admittances as

$$Y_\upsilon = \frac{1}{Z_\upsilon} = G_\upsilon + jQ_\upsilon\ , \quad \upsilon = 1(1)n \tag{4.80}$$

From the definition of the wave quantities (4.6), we know that for ports $\upsilon = 1(1)n$,

$$\begin{aligned} A_\upsilon &= V_\upsilon + Z_\upsilon I_\upsilon \\ B_\upsilon &= V_\upsilon - Z_\upsilon^* I_\upsilon \end{aligned} \tag{4.81a,b}$$

Solving for I_υ from (4.81a) and substituting into the condition for a parallel connection (4.80b), we get

$$(A_1 - V_1)\, Y_1 + (A_2 - V_2)\, Y_2 + (A_3 - V_3)\, Y_3 + \ldots + (A_n - V_n)\, Y_n = 0 \qquad (4.82)$$

However, all of the port voltages are equal, thus

$$(A_1 - V_\upsilon)\, Y_1 + (A_2 - V_\upsilon)\, Y_2 + (A_3 - V_\upsilon)\, Y_3 + \ldots + (A_n - V_\upsilon)\, Y_n = 0 \qquad (4.83)$$

Substituting the definition of the port voltage in terms of the incident and reflected waves of the port, namely

$$V_\upsilon = \frac{Z_\upsilon^* A_\upsilon - Z_\upsilon B_\upsilon}{2\, R_\upsilon} \qquad (4.84)$$

into (4.83) and solving for the reflected wave we get

$$B_\upsilon = \left(\frac{2\, R_\upsilon (Y_1 A_1 + Y_2 A_2 + Y_3 A_3 + \ldots + Y_n A_n)}{Z_\upsilon (Y_1 + Y_2 + Y_3 + \ldots + Y_n)}\right) - \frac{Z_\upsilon^*}{Z_\upsilon} A_\upsilon \;, \quad \upsilon = 1(1)n \qquad (4.85)$$

Define the complex scalar quantity α_υ^m as the mth coefficient associated with port υ by

$$\alpha_\upsilon^m = \frac{2R_\upsilon\, Y_m}{Z_\upsilon (Y_1 + Y_2 + Y_3 + \ldots + Y_n)} \qquad (4.86)$$

and define the unimodular constant $\widehat{\alpha}_\upsilon$ as

$$\widehat{\alpha}_\upsilon = \frac{Z_\upsilon^*}{Z_\upsilon}, \quad |\widehat{\alpha}_\upsilon| = 1 \qquad (4.87)$$

giving the new form of B_υ as

$$B_\upsilon = \alpha_\upsilon^1 A_1 + \alpha_\upsilon^2 A_2 + \alpha_\upsilon^3 A_3 + \ldots + \alpha_\upsilon^n A_n - \widehat{\alpha}_\upsilon A_\upsilon \;, \quad \upsilon = 1(1)n \qquad (4.88)$$

Other choices for the definition of the coefficients are possible, however, the choice presented here gives a more uniform scattering matrix and the coefficients collapse in a natural way to the definitions of the real parallel adaptor if the port references are purely real. Note that the sum of the coefficients over the port υ is

$$\alpha_\upsilon^1 + \alpha_\upsilon^2 + \alpha_\upsilon^3 + \ldots + \alpha_\upsilon^n = \frac{2R_\upsilon}{Z_\upsilon} \qquad (4.89)$$

and thus the magnitude of each coefficient is bounded above by

$$|\alpha_\upsilon^m| \leq 2 \tag{4.90}$$

although usually this bound is pessimistic. The complex scattering matrix for the general n-port parallel adaptor is given by

$$\begin{bmatrix} B_1 \\ B_2 \\ B_3 \\ \vdots \\ B_n \end{bmatrix} = \begin{bmatrix} \alpha_1^1 - \hat{\alpha}_1 & \alpha_1^2 & \alpha_1^3 & \cdots & \alpha_1^n \\ \alpha_2^1 & \alpha_2^2 - \hat{\alpha}_2 & \alpha_2^3 & \cdots & \alpha_2^n \\ \alpha_3^1 & \alpha_3^2 & \alpha_3^3 - \hat{\alpha}_3 & \cdots & \alpha_3^n \\ \vdots & \vdots & \vdots & \ddots & \vdots \\ \alpha_n^1 & \alpha_n^2 & \alpha_n^3 & \cdots & \alpha_n^n - \hat{\alpha}_n \end{bmatrix} \begin{bmatrix} A_1 \\ A_2 \\ A_3 \\ \vdots \\ A_n \end{bmatrix} \tag{4.91}$$

Similar to the comments for the series adaptor, the parallel adaptor cannot be factored in such a way that a real n-port parallel adaptor can be identified using real or complex diagonal scaling matrices, unless one port is reflection-free. Again, an attempt at this operation would generate a matrix with all but the diagonal elements equal to the corresponding real parallel adaptor without a reflection-free port. As mentioned earlier, the diagonal elements of the scattering matrix cannot be independently scaled using diagonal scaling matrices.

4.6.2.2 Dependent Coefficient

Similar to the series adaptor case, from equation (4.89) above, it is clear that one of the coefficients α_υ^m is dependent upon the remaining coefficients for a particular port υ, and obviously this dependency is not constant over all ports. Let the dependent coefficient for port υ be the υth coefficient. Solving for α_υ^υ and substituting into (4.88) we derive

$$B_1 = A_1 - \sum_{i=2}^{n} \alpha_1^i (A_1 - A_i)$$

$$B_\upsilon = A_\upsilon - \sum_{i=1}^{\upsilon-1} \alpha_\upsilon^i (A_\upsilon - A_i) - \sum_{i=\upsilon+1}^{n} \alpha_\upsilon^i (A_\upsilon - A_i), \quad \upsilon = 2(1)\, n-1$$

$$B_n = A_n - \sum_{i=1}^{n-1} \alpha_n^i (A_n - A_i) \tag{4.92a,b,c}$$

4.6.2.3 Reflection-free Port

The nth port can arbitrarily be made reflection-free by setting $S_{nn} = 0$ in the scattering matrix (4.91). This adds a constraint on α_n^n, namely

$$\alpha_n^n = \hat{\alpha}_n = \frac{Z_n^*}{Z_n} \tag{4.93}$$

Substituting this expression into the definition of α_υ^m, we get

$$Y_1 + Y_2 + Y_3 + \ldots + Y_{n-1} = Y_n^* \tag{4.94}$$

which is similar to the expression found for the series adaptor (the only difference is that the above expression uses admittances while the earlier expression used impedances). Equation (4.94) can be rewritten in terms of the port conductances and susceptances as

$$\begin{aligned} G_n &= G_1 + G_2 + G_3 + \ldots + G_{n-1} \\ 0 &= Q_1 + Q_2 + Q_3 + \ldots + Q_n \end{aligned} \tag{4.95a,b}$$

From the definition of the coefficients α_υ^m and the condition given above (4.94), it is clear that the reflection-free property does not lead to a real scattering matrix for the parallel adaptor.

With the added constraint given by (4.93), a new condition on the sum of the coefficients for port n is derived as follows

$$\alpha_n^1 + \alpha_n^2 + \alpha_n^3 + \ldots + \alpha_n^{n-1} = 1 \tag{4.96}$$

Similar to the earlier case, a coefficient associated with port n is dependent upon the others, and thus it can be removed. Let coefficient (n-1) be the dependent coefficient of port n, and for the other ports υ, let the υth coefficient be dependent. The following equations are derived

$$B_1 = A_1 - \sum_{i=2}^{n} \alpha_1^i (A_1 - A_i)$$

$$B_\upsilon = A_\upsilon - \sum_{i=1}^{\upsilon-1} \alpha_\upsilon^i (A_\upsilon - A_i) - \sum_{i=\upsilon+1}^{n} \alpha_\upsilon^i (A_\upsilon - A_i) \ , \quad \upsilon = 2(1)\, n-2$$

$$B_{n-1} = (1 - \alpha_{n-1}^{n})\, A_{n-1} + \alpha_{n-1}^{n}\, A_n - \sum_{i=1}^{n-2} \alpha_{n-1}^{i} (A_{n-1} - A_i)$$

$$B_n = A_{n-1} - \sum_{i=1}^{n-2} \alpha_n^i (A_{n-1} - A_i) \qquad (4.97a,b,c,d)$$

4.6.2.4 Symbols of the General *n*-port Complex Parallel Adaptor

The symbols used for both the dependent port case and the reflection-free case are shown below, where the second figure has a bar associated with the reflected wave of port *n* showing that it is reflection free.

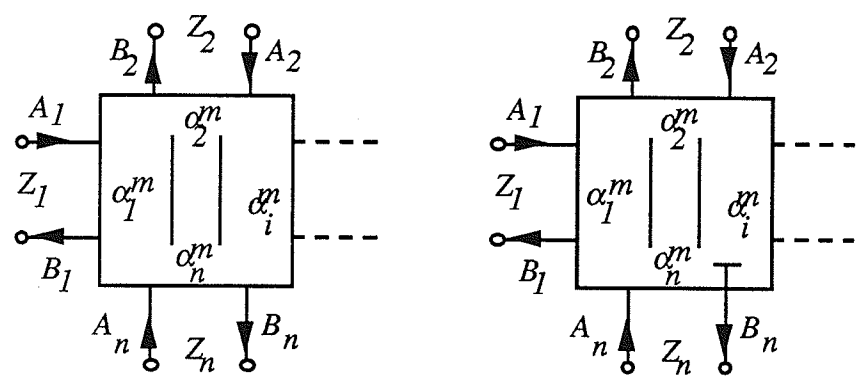

Figure 4.7: Symbols used for the *n*-port complex parallel adaptor.

4.6.2.5 Complex three-port Parallel Adaptor

The complex three-port parallel adaptor deserves special attention for the same reason as the three-port series adaptor. With the complexity of the form of (4.91), the non-reflection-free case is presented (for completeness) without a dependent coefficient with the following scattering matrix.

$$\begin{bmatrix} B_1 \\ B_2 \\ B_3 \end{bmatrix} = \begin{bmatrix} \alpha_1^1 - \hat{\alpha}_1 & \alpha_1^2 & \alpha_1^3 \\ \alpha_2^1 & \alpha_2^2 - \hat{\alpha}_2 & \alpha_2^3 \\ \alpha_3^1 & \alpha_3^2 & \alpha_3^3 - \hat{\alpha}_3 \end{bmatrix} \begin{bmatrix} A_1 \\ A_2 \\ A_3 \end{bmatrix} \qquad (4.98)$$

Again, note that this adaptor cannot be factored in such a way that a real three-port parallel

adaptor can be identified using real or complex diagonal scaling matrices.

One would question whether simplifications may occur in the scattering matrix which would allow fewer independent quantizations when the definitions of the coefficients are inserted. To investigate this, consider a different (but equivalent) form of the scattering matrix with a new definition of the coefficients. Let the coefficients be redefined by

$$\alpha_\upsilon = \frac{2\,Y_\upsilon}{(Y_1 + Y_2 + Y_3 + \ldots + Y_n)}\ , \quad \upsilon = 1(1)n \tag{4.99}$$

which associates one coefficient per port. Now the sum of the coefficients over all the ports is exactly two, and one coefficient is dependent. Let this coefficient be the third, after substituting this constraint, the scattering matrix becomes

$$\begin{bmatrix} B_1 \\ B_2 \\ B_3 \end{bmatrix} = \begin{bmatrix} \frac{R_1\alpha_1 - Z_1^*}{Z_1} & \frac{R_1\alpha_2}{Z_1} & \frac{R_1(2 - \alpha_1 - \alpha_2)}{Z_1} \\ \frac{R_2\alpha_1}{Z_2} & \frac{R_2\alpha_2 - Z_2^*}{Z_2} & \frac{R_2(2 - \alpha_1 - \alpha_2)}{Z_2} \\ \frac{R_3\alpha_1}{Z_3} & \frac{R_3\alpha_2}{Z_3} & 1 - \frac{R_3(\alpha_1 + \alpha_2)}{Z_3} \end{bmatrix} \begin{bmatrix} A_1 \\ A_2 \\ A_3 \end{bmatrix} \tag{4.100}$$

The matrix appears to be not only a function of two independent coefficients α_υ, but also three independent ratios

$$\frac{R_\upsilon}{Z_\upsilon}\ , \quad \upsilon = 1(1)\,3 \tag{4.101}$$

Clearly, no simplifications occur leading to fewer independent quantizations. A wave-flow diagram is given in the following figure.

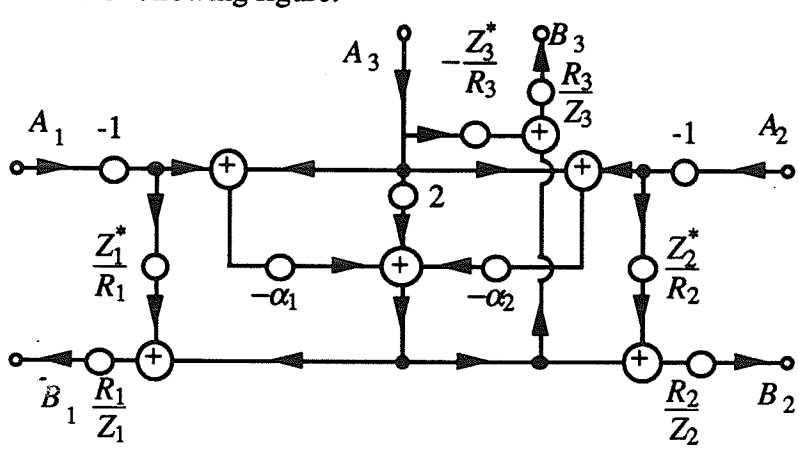

Figure 4.8: Wave-flow diagram of the complex three-port parallel adaptor without a RF port.

The scattering matrix of the complex three-port parallel adaptor with port three reflection-free and with the alternate definition of the coefficients as given by (4.100) is given below

$$\begin{bmatrix} B_1 \\ B_2 \\ B_3 \end{bmatrix} = \begin{bmatrix} \frac{R_1\alpha_1}{Z_1} - \frac{Z_1^*}{Z_1} & \frac{R_1}{Z_1}\left(\frac{Z_3}{R_3} - \alpha_1\right) & \frac{R_1 Z_3^*}{Z_1 R_3} \\ \frac{R_2\alpha_1}{Z_2} & \frac{R_2}{Z_2}\left(\frac{Z_3}{R_3} - \alpha_1\right) - \frac{Z_2^*}{Z_2} & \frac{R_2 Z_3^*}{Z_2 R_3} \\ \frac{R_3\alpha_1}{Z_3} & 1 - \frac{R_3\alpha_1}{Z_3} & 0 \end{bmatrix} \begin{bmatrix} A_1 \\ A_2 \\ A_3 \end{bmatrix} \tag{4.102}$$

where the port admittances are related by

$$Y_1 + Y_2 = Y_3^* \tag{4.103}$$

Again, to investigate whether simplifications occur when the scattering matrix is given in a more elemental form, consider the following equivalent representation of the above scattering matrix,

$$\begin{bmatrix} B_1 \\ B_2 \\ B_3 \end{bmatrix} = \begin{bmatrix} \frac{-G_2}{G_1 + G_2}\frac{Y_1}{Y_1^*} & \frac{G_1}{G_1 + G_2}\frac{Y_2}{Y_1^*} & \frac{G_1}{G_1 + G_2}\frac{\left(Y_1^* + Y_2^*\right)}{Y_1^*} \\ \frac{G_2}{G_1 + G_2}\frac{Y_1}{Y_2^*} & \frac{-G_1}{G_1 + G_2}\frac{Y_2}{Y_2^*} & \frac{G_2}{G_1 + G_2}\frac{\left(Y_1^* + Y_2^*\right)}{Y_2^*} \\ \frac{Y_1}{Y_1 + Y_2} & \frac{Y_2}{Y_1 + Y_2} & 0 \end{bmatrix} \begin{bmatrix} A_1 \\ A_2 \\ A_3 \end{bmatrix} \tag{4.104}$$

where

$$G_\upsilon = Re\{Y_\upsilon\} \ , \ \upsilon = 1(1)\,3 \tag{4.105}$$

The scattering matrix can be factored as shown below

$$\begin{bmatrix} B_1 \\ B_2 \\ B_3 \end{bmatrix} = \begin{bmatrix} \frac{1}{Y_1^*} & 0 & 0 \\ 0 & \frac{1}{Y_2^*} & 0 \\ 0 & 0 & \frac{1}{Y_3^*} \end{bmatrix} \begin{bmatrix} \frac{-G_2}{G_1+G_2} & \frac{G_1}{G_1+G_2} & \frac{G_1}{G_1+G_2} \\ \frac{G_2}{G_1+G_2} & \frac{-G_1}{G_1+G_2} & \frac{G_2}{G_1+G_2} \\ 1 & 1 & 0 \end{bmatrix} \begin{bmatrix} Y_1 & 0 & 0 \\ 0 & Y_2 & 0 \\ 0 & 0 & Y_3 \end{bmatrix} \begin{bmatrix} A_1 \\ A_2 \\ A_3 \end{bmatrix} \tag{4.106}$$

where again Y_3 is given by (4.103). The outer most matrices on the right side of (4.106) correspond to simple inverse conjugate multipliers in the signal paths at the ports, which appear to be very similar to the CWD form of a parallel connected imaginary resistor as given in the last column of Table 4.4. However, the sections represented by these matrices do not correspond to the parallel connected imaginary resistor in general, since the value of the imaginary resistor must remain real. Notice that the inner most matrix is only a function of G_1 and G_2, and appears to have the same general form as the reflection-free series adaptor. The inner most matrix can be further factored to give

$$\begin{bmatrix} B_1 \\ B_2 \\ B_3 \end{bmatrix} = \begin{bmatrix} \frac{G_1}{Y_1^*} & 0 & 0 \\ 0 & \frac{G_2}{Y_2^*} & 0 \\ 0 & 0 & \frac{G_3}{Y_3^*} \end{bmatrix} \begin{bmatrix} \frac{-G_2}{G_1+G_2} & \frac{G_2}{G_1+G_2} & 1 \\ \frac{G_1}{G_1+G_2} & \frac{-G_1}{G_1+G_2} & 1 \\ \frac{G_1}{G_1+G_2} & \frac{G_2}{G_1+G_2} & 0 \end{bmatrix} \begin{bmatrix} \frac{Y_1}{G_1} & 0 & 0 \\ 0 & \frac{Y_2}{G_2} & 0 \\ 0 & 0 & \frac{Y_3}{G_3} \end{bmatrix} \begin{bmatrix} A_1 \\ A_2 \\ A_3 \end{bmatrix} \tag{4.107}$$

The additional factors that were removed correspond to real ideal transformers located at the ports. The inner most matrix is the definition of the real three-port parallel adaptor with a reflection-free port, and thus it can be concluded that the complex three-port parallel adaptor is equivalent to a real three-port parallel adaptor (with a reflection-free port) with inverse conjugate multipliers in the signal paths. The above scattering matrix can be expressed as a function of the real parameter α_1 defined by

$$\alpha_1 = \frac{G_1}{G_1 + G_2} \tag{4.108}$$

as given by

$$\begin{bmatrix} B_1 \\ B_2 \\ B_3 \end{bmatrix} = \begin{bmatrix} \frac{G_1}{Y_1^*} & 0 & 0 \\ 0 & \frac{G_2}{Y_2^*} & 0 \\ 0 & 0 & \frac{G_3}{Y_3^*} \end{bmatrix} \begin{bmatrix} \alpha_1 - 1 & 1-\alpha_1 & 1 \\ \alpha_1 & -\alpha_1 & 1 \\ \alpha_1 & 1-\alpha_1 & 0 \end{bmatrix} \begin{bmatrix} \frac{Y_1}{G_1} & 0 & 0 \\ 0 & \frac{Y_2}{G_2} & 0 \\ 0 & 0 & \frac{Y_3}{G_3} \end{bmatrix} \begin{bmatrix} A_1 \\ A_2 \\ A_3 \end{bmatrix} \tag{4.109}$$

The wave-flow diagram is given in the following figure.

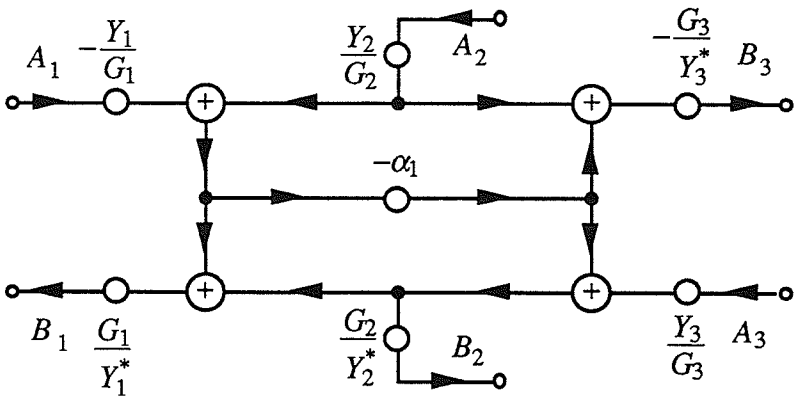

Figure 4.9: Wave-flow diagram of the complex three-port parallel adaptor with a RF port.

From (4.104), it is clear that the complex three-port parallel adaptor with a reflection-free port is a function of three real parameters, namely

$$\left\{ \frac{G_2}{G_1}, \frac{Q_1}{G_1}, \frac{Q_2}{G_2} \right\} \tag{4.110}$$

where again the G_i are given by (4.105) and correspond to the real parts of the port admittances. Note that the ratio Q_3/G_3 can be expressed as a function of the ratios given in (4.110) using (4.103) as shown below.

$$\frac{Q_3}{G_3} = \left(\frac{\frac{G_2}{G_1}}{1 + \frac{G_2}{G_1}} \right) \left(\frac{Q_2}{G_2} + \frac{\frac{Q_1}{G_1}}{\frac{G_2}{G_1}} \right) \tag{4.111}$$

The symbols used are shown in Figure 4.10, where the second figure has a bar associated with the reflected wave of port three showing that it is reflection free.

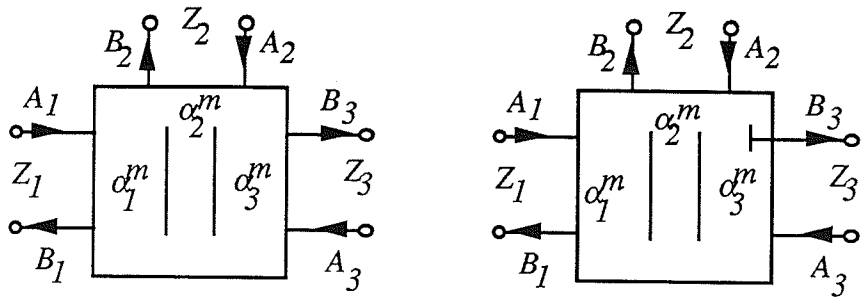

Figure 4.10: Symbols used for the three-port parallel adaptors.

4.6.3 Equivalence Between the Reflection-free three-port Adaptors

The complex series three-port adaptor with a reflection-free port has the same scattering matrix as the real case (4.73-76), and the complex parallel three-port adaptor with a reflection-free port can be decomposed into a real parallel adaptor with inverse-conjugate multipliers in the signal paths at the ports (4.107-109). These observations leads to an equivalence between the complex series and parallel adaptors with a reflection-free port since a real three-port adaptor of one type can always be replaced with the other type[6].

Consider the scattering matrix of the complex parallel three-port adaptor with port three reflection-free as given in (4.109) and shown below

$$\mathbf{S}_p = \begin{bmatrix} \frac{G_1}{Y_1^*} & 0 & 0 \\ 0 & \frac{G_2}{Y_2^*} & 0 \\ 0 & 0 & \frac{G_3}{Y_3^*} \end{bmatrix} \begin{bmatrix} \alpha_1 - 1 & 1 - \alpha_1 & 1 \\ \alpha_1 & -\alpha_1 & 1 \\ \alpha_1 & 1 - \alpha_1 & 0 \end{bmatrix} \begin{bmatrix} \frac{Y_1}{G_1} & 0 & 0 \\ 0 & \frac{Y_2}{G_2} & 0 \\ 0 & 0 & \frac{Y_3}{G_3} \end{bmatrix} \tag{4.112}$$

The matrix can be factored as shown below,

$$\mathbf{S}_p = \begin{bmatrix} \frac{-\alpha_1 G_1}{Y_1^*} & 0 & 0 \\ 0 & \frac{-(1-\alpha_1)G_2}{Y_2^*} & 0 \\ 0 & 0 & \frac{-G_3}{Y_3^*} \end{bmatrix} \begin{bmatrix} 1-\alpha_1 & -\alpha_1 & -\alpha_1 \\ \alpha_1-1 & \alpha_1 & \alpha_1-1 \\ -1 & -1 & 0 \end{bmatrix} \begin{bmatrix} \frac{Y_1}{\alpha_1 G_1} & 0 & 0 \\ 0 & \frac{Y_2}{(1-\alpha_1)G_2} & 0 \\ 0 & 0 & \frac{Y_3}{G_3} \end{bmatrix} \tag{4.113}$$

The inner most matrix is the definition of the series adaptor with port three reflection-free as a function of the parameter α_1. Since this scattering matrix is exactly the scattering matrix of the complex series adaptor, the following equivalence is given

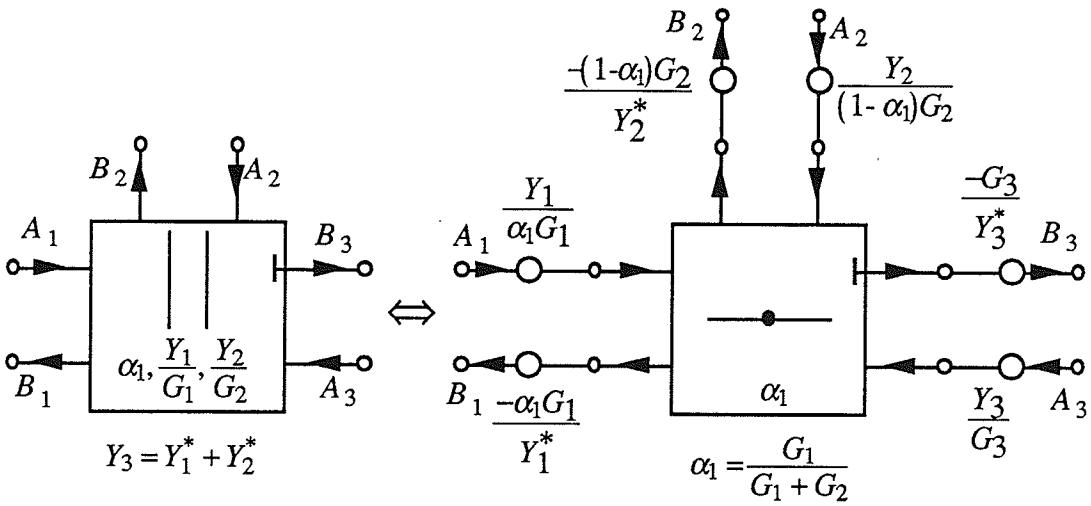

Figure 4.11: Equivalence between the complex parallel and series 3-port adaptors.

Similarly, the complex three-port series adaptor with port three reflection-free has the following scattering matrix

$$\mathbf{S}_s = \begin{bmatrix} 1-\beta_1 & -\beta_1 & -\beta_1 \\ \beta_1 - 1 & \beta_1 & \beta_1 - 1 \\ -1 & -1 & 0 \end{bmatrix} \tag{4.114}$$

The above matrix can be expressed in terms of the scattering matrix of the complex parallel adaptor as given below:

$$\mathbf{S}_s = \begin{bmatrix} \frac{-Y_1^*}{\beta_1 G_1} & 0 & 0 \\ 0 & \frac{-Y_2^*}{(1-\beta_1)G_2} & 0 \\ 0 & 0 & \frac{-Y_3^*}{G_3} \end{bmatrix} \begin{bmatrix} \textit{Complex Parallel Adaptor} \\ \textit{Scattering matrix} \\ \textit{function of } \beta_1, \frac{Y_1}{G_1}, \frac{Y_2}{G_2} \end{bmatrix} \begin{bmatrix} \frac{\beta_1 G_1}{Y_1} & 0 & 0 \\ 0 & \frac{(1-\beta_1)G_2}{Y_2} & 0 \\ 0 & 0 & \frac{G_3}{Y_3} \end{bmatrix} \tag{4.115}$$

as shown in the following figure,

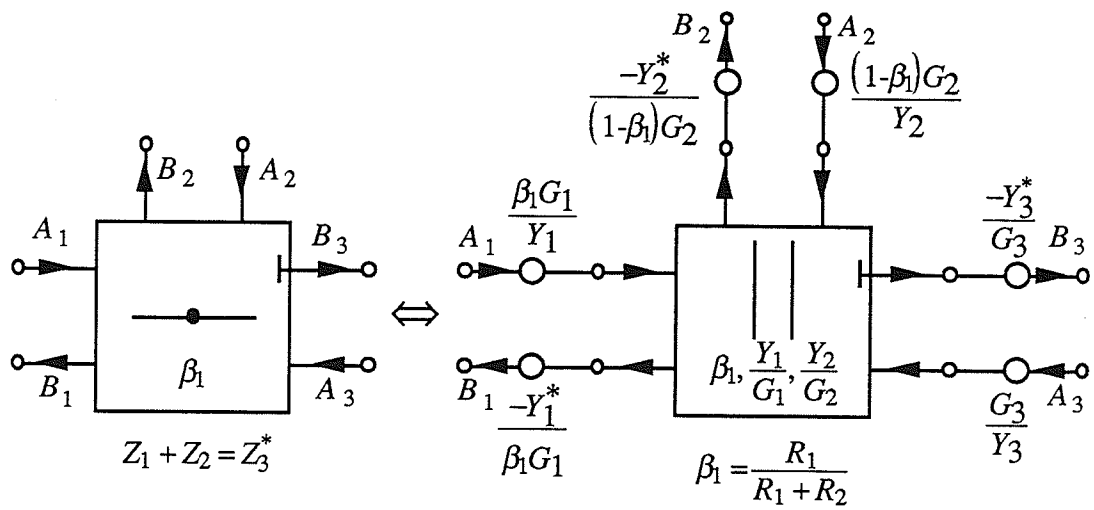

Figure 4.12: Equivalence between the complex series and parallel three-port adaptors.

4.6.4 Complex Two-port Adaptor

The two-port adaptor can either be defined as a series or parallel adaptor. However, from the convention set by Fettweis [6], it will be defined from the parallel adaptor. The complex two-port adaptor simply adapts the reference impedance seen from a port and has the following symbol as a function of one complex scalar parameter α.

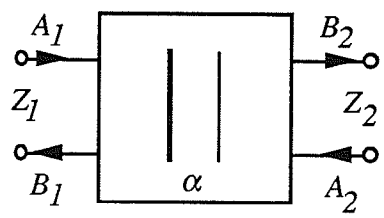

Figure 4.13: Symbol of the complex two-port adaptor.

The heavy bar identifies port one with the definition of α in (4.118). The adaptor represents a simple connection in the analog domain, and thus the conditions that must be satisfied are given by

$$\begin{aligned} V_1 &= V_2 \\ I_1 &= -I_2 \\ Z_1 &= R_1 + jX_1 \\ Z_2 &= R_2 + jX_2 \end{aligned} \tag{4.116a-d}$$

where Z_1 and Z_2 are the port references for ports one and two, respectively. When the above equations are mapped to the voltage-CWD domain, the following scattering matrix results:

$$\begin{bmatrix} B_1 \\ B_2 \end{bmatrix} = \begin{bmatrix} -\left(\dfrac{Z_1^* - Z_2}{Z_1 + Z_2}\right) & \dfrac{2R_1}{Z_1 + Z_2} \\ \dfrac{2R_2}{Z_1 + Z_2} & \dfrac{Z_1 - Z_2^*}{Z_1 + Z_2} \end{bmatrix} \begin{bmatrix} A_1 \\ A_2 \end{bmatrix} \tag{4.117}$$

Define the complex coefficient of the two-port adaptor as

$$\alpha = \frac{Z_1 - Z_2^*}{Z_1 + Z_2} \tag{4.118}$$

which is a function of two real parameters, namely

$$\left\{\frac{R_1}{R_2}, \frac{(X_1 + X_2)}{R_2}\right\} \tag{4.119}$$

After substituting the definition of the complex parameter into (4.117), the scattering matrix becomes

$$\begin{bmatrix} B_1 \\ B_2 \end{bmatrix} = \begin{bmatrix} -\alpha^*\left(\dfrac{1-\alpha}{1-\alpha^*}\right) & \dfrac{1-\alpha\alpha^*}{1-\alpha^*} \\ 1-\alpha & \alpha \end{bmatrix} \begin{bmatrix} A_1 \\ A_2 \end{bmatrix} \tag{4.120}$$

which is a function of one complex parameter (as expected since it must be a function of two real parameters from (4.119)). The diagonal terms are bounded in magnitude by one and the off-diagonal terms are bounded by two, which is expected for voltage-wave reflectances and transmittances. Also, the complex two-port adaptor is lossless under infinite-precision conditions as expected. The wave-flow diagram is shown in the following figure:

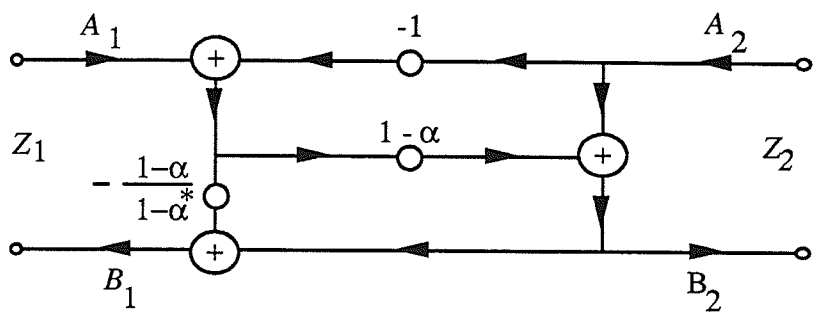

Figure 4.14: Wave flow diagram of the complex two-port adaptor.

which is similar in form to the real case except an inversion is replaced by an unimodular multiplier.

The scattering matrix (4.120) can be factored by expressing the constant complex parameter in polar form

$$\alpha = \beta\, e^{j\theta} \tag{4.121}$$

where $|\beta| \le 1$ (the equality holds only when the real part of one port reference is zero, which is ordinarily not allowed), as given by

$$S = \begin{bmatrix} \dfrac{(1-\beta)}{1-\alpha^*} & 0 \\ 0 & 1 \end{bmatrix} \begin{bmatrix} e^{-j\theta/2} & 0 \\ 0 & e^{j\theta/2} \end{bmatrix} \begin{bmatrix} -\beta & 1+\beta \\ 1-\beta & \beta \end{bmatrix} \begin{bmatrix} e^{-j\theta/2} & 0 \\ 0 & e^{j\theta/2} \end{bmatrix} \begin{bmatrix} \dfrac{1-\alpha}{1-\beta} & 0 \\ 0 & 1 \end{bmatrix} \tag{4.122}$$

The inner-most matrix is the definition of the real two-port adaptor as a function of the real parameter β, which corresponds to the magnitude of the complex two-port parameter. The outer most matrices correspond to mutually inverse conjugate multipliers in the signal paths (similar to the parallel connected imaginary resistor), and is represented by the following signal flow diagram:

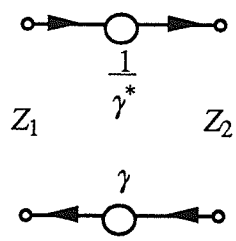

Figure 4.15: Signal flow diagram of mutually inverse conjugate multipliers.

The analog equivalent of the above section is given by one of the following constant sections, depending upon which port of the above is considered independent.

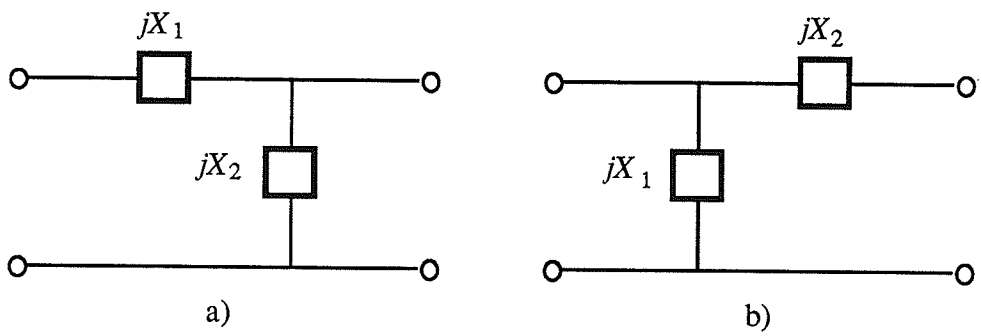

Figure 4.16: Analog equivalent of inverse conjugate multipliers:
a) given in terms of port two, b) given in terms of port one.

The imaginary resistor values for Figure 4.16a) are given by

$$X_1 = \frac{j\left[(\gamma - 1)Z_1 + \left(\gamma^* - 1\right)Z_1{}^*\right]}{\gamma - \gamma^*}$$

$$X_2 = 2\frac{jR_1}{\gamma - \gamma^*} \qquad (4.123a,b)$$

with the port impedance of the second port

$$Z_2 = 2\frac{(\gamma - 1)R_1}{(\gamma - \gamma^*)\,\gamma}$$

$$R_2 = \frac{R_1}{\gamma\gamma^*} \tag{4.124a,b}$$

where R_1 (R_2) is the real part of Z_1 (Z_2). Similarly, the imaginary resistor values for Figure 4.16b) are given by

$$X_1 = 2\frac{jR_2\gamma\gamma^*}{\gamma - \gamma^*}$$

$$X_2 = -\frac{j\left[(\gamma^* - 1)Z_2\gamma + (\gamma - 1)Z_2{}^*\gamma^*\right]}{\gamma - \gamma^*} \tag{4.125a,b}$$

with the port impedance of the first port

$$Z_1 = 2\frac{(1 - \gamma^*)R_2\gamma\gamma^*}{\gamma - \gamma^*}$$

$$R_1 = R_2\gamma\gamma^* \tag{4.126a,b}$$

In both cases, the real parts of the port impedances are related by a real constant.

The remaining matrices of (4.122), which are identical and are given by

$$\begin{bmatrix} e^{-j\theta/2} & 0 \\ 0 & e^{j\theta/2} \end{bmatrix} \tag{4.127}$$

are a special case of the above Figure 4.15 and correspond to sections as shown in the following figure:

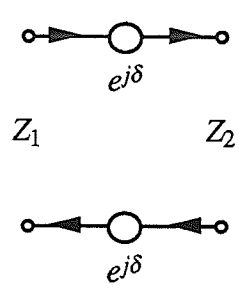

Figure 4.17: Complex section with unimodular multipliers.

where $\delta = -\theta/2$ and $\delta = \theta/2$ for the sections on the left and on the right of the real two-port adaptor, respectively. In this case, the values of the imaginary resistors from Figure 4.16a) simplify to

$$X_1 = \frac{[\cos(\delta) - 1]R_1 - \sin(\delta)\,\mathrm{Im}\{Z_1\}}{\sin(\delta)}$$

$$X_2 = \frac{R_1}{\sin(\delta)} \tag{4.128a,b}$$

with the port reference

$$Z_2 = \frac{R_1}{\cos\left(\frac{\delta}{2}\right)} e^{\frac{-j\delta}{2}} = R_1 - j\,R_1 \tan\left(\frac{\delta}{2}\right)$$

$$R_2 = R_1 \tag{4.129a,b}$$

Similarly for Figure 4.16b), simply exchange the numerals 1 and 2 in the above expressions for the imaginary resistors and the port impedances.

Note that for the section with unimodular multipliers shown in Figure 4.17, the real parts of the port impedances of both ports are equal; that is, the section does not change the real part of the port impedances. This is consistent with the theory of normalized sections since the scattering matrix is unitary (see Section 4.2). Also note that the imaginary part of one port impedance as given in the above equation (4.129a) is independent of the imaginary part of the other port impedance. This independence can be removed by inserting a third imaginary resistor in series in order to form a T-connection, with the value equal to the imaginary part of the appropriate port impedance.

A section with one of the unimodular multipliers equal to unity in Figure 4.17 can be considered to be equal to the section in Figure 4.17 cascaded with a complex transformer with a unimodular turns ratio. In this case, since a transformer with a unimodular turns ratio does not effect the port impedance, the resulting section contains the same external port references. The complex transformer can be shifted through the network using flowgraph transformations if this becomes desirable.

The factorization of the complex two-port adaptor as given in (4.122) into the sections mentioned above is shown in the figure below:

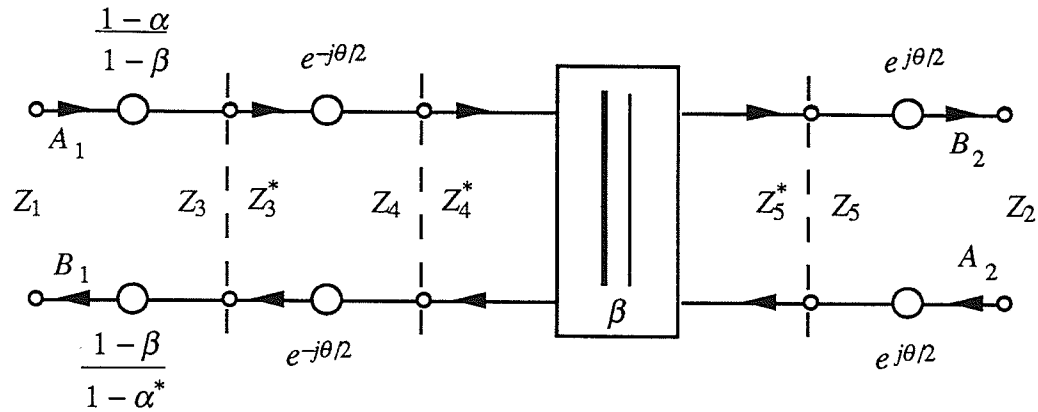

Figure 4.18: Equivalent of a complex two-port adaptor in terms of a real adaptor.

where the inner two-port adaptor is real and the dashed lines represent port interconnections. Using equations (4.124a-126a), the port impedances Z_3, Z_4 and Z_5 can be determined as a function of α from (4.118) and β, θ from (4.121). The value of the real parameter β of the real two-port adaptor is given by the following ratio:

$$\beta = \frac{\mathrm{Re}\{Z_4\} - \mathrm{Re}\{Z_5\}}{\mathrm{Re}\{Z_4\} + \mathrm{Re}\{Z_5\}} \tag{4.130}$$

This can be derived by identifying Z_4 and Z_5, and by recognizing that $\beta^2 = \alpha\alpha^*$ from (4.121) and the ratio of the off-diagonal terms of the scattering matrix (4.120) gives,

$$\frac{R_1}{R_2} = \frac{(1-\alpha\alpha^*)}{(1-\alpha)(1-\alpha^*)} \tag{4.131}$$

Note that the real parameter β as given above (4.130) is consistent with the theory of real WD filters. The analog domain equivalent of the real two-port adaptor with the complex port impedances Z_4 and Z_5 is a series connected imaginary resistor with a value of

$$X_1 = \frac{1}{2}\frac{-(Z_2Z_1 - Z_2^*Z_1^*) - (Z_1Z_2^* - Z_2Z_1^*)\beta}{j(\beta+1)R_2} \tag{4.132}$$

Thus the analog equivalent of the network given in Figure 4.18 consists of a ladder connection of seven imaginary resistors (four from the two sections to the left and two from the section on the right of the real two-port adaptor, and one from the real two-port adaptor itself). However, the values of the imaginary resistors are related in such a way

that the section reduces to a short circuit between the two ports. This is expected since the analog equivalent of the section in Figure 4.13 is originally defined from a simple connection as defined by equations (4.116a,b).

The power-wave (or normalized) form of the scattering matrix, as defined by equation (4.32), is given by

$$\begin{bmatrix} \hat{B}_1 \\ \hat{B}_2 \end{bmatrix} = \begin{bmatrix} -\alpha^*\left(\frac{1-\alpha}{1-\alpha^*}\right) & \sqrt{\left(\frac{1-\alpha}{1-\alpha^*}\right)\left(1-\alpha\alpha^*\right)} \\ \sqrt{\left(\frac{1-\alpha}{1-\alpha^*}\right)\left(1-\alpha\alpha^*\right)} & \alpha \end{bmatrix} \begin{bmatrix} \hat{A}_1 \\ \hat{A}_2 \end{bmatrix} \tag{4.133}$$

The above given in terms of the port references is given by

$$\begin{bmatrix} \hat{B}_1 \\ \hat{B}_2 \end{bmatrix} = \begin{bmatrix} -\left(\frac{Z_1^* - Z_2}{Z_1 + Z_2}\right) & \frac{2\sqrt{R_1 R_2}}{Z_1 + Z_2} \\ \frac{2\sqrt{R_1 R_2}}{Z_1 + Z_2} & \frac{Z_1 - Z_2^*}{Z_1 + Z_2} \end{bmatrix} \begin{bmatrix} \hat{A}_1 \\ \hat{A}_2 \end{bmatrix} \tag{4.134}$$

Since the magnitude of α is bounded above by one, let

$$\alpha = \left(\cos\beta\right) e^{j\theta} \tag{4.135}$$

and define

$$e^{j2\gamma} = \frac{1 - \alpha}{1 - \alpha^*} \tag{4.136}$$

Substituting the above two equations into the normalized form of the scattering matrix, we derive the following more elegant form

$$\begin{bmatrix} \hat{B}_1 \\ \hat{B}_2 \end{bmatrix} = \begin{bmatrix} -\left(\cos\beta\right) e^{j(2\gamma - \theta)} & \left(\sin\beta\right) e^{j\gamma} \\ \left(\sin\beta\right) e^{j\gamma} & \left(\cos\beta\right) e^{j\theta} \end{bmatrix} \begin{bmatrix} \hat{A}_1 \\ \hat{A}_2 \end{bmatrix} \tag{4.137}$$

Again, this scattering matrix can be factored as

$$S = \begin{bmatrix} e^{j\gamma} & 0 \\ 0 & 1 \end{bmatrix} \begin{bmatrix} e^{-j\theta/2} & 0 \\ 0 & e^{j\theta/2} \end{bmatrix} \begin{bmatrix} -\cos\beta & \sin\beta \\ \sin\beta & \cos\beta \end{bmatrix} \begin{bmatrix} e^{-j\theta/2} & 0 \\ 0 & e^{j\theta/2} \end{bmatrix} \begin{bmatrix} e^{j\gamma} & 0 \\ 0 & 1 \end{bmatrix} \tag{4.138}$$

Notice that the inner most matrix is the definition of the normalized real two-port adaptor

given in [16]. The same comments apply to the other matrices as in the earlier case since they correspond to three sections, each with equal unimodular multipliers in the signal paths.

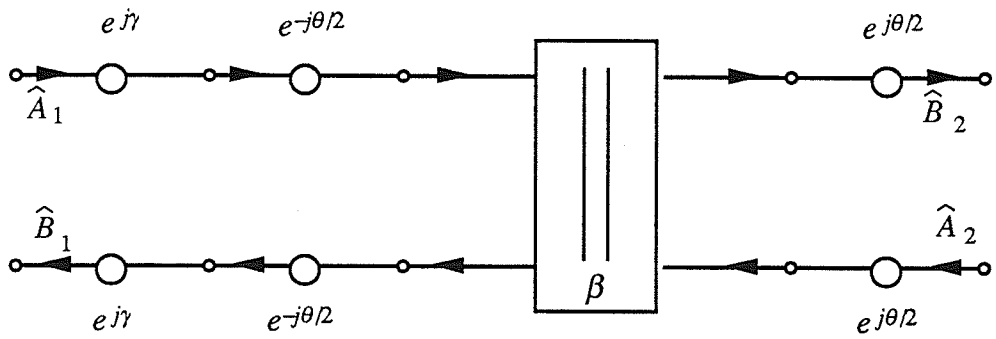

Figure 4.19: A complex normalized two-port adaptor in terms of a real adaptor.

4.6.5 Equivalence Between the Complex Two-port Adaptor and Complex Transformer

Consider the normalized form of the CWD complex transformer with general port references given by (4.46c) and the complex two-port adaptor given by (4.134). The scattering matrix for the transformer is written as

$$S = \frac{1}{Z_1 + nn^* Z_2}\begin{bmatrix} -Z_1^* + nn^* Z_2 & 2n^*\sqrt{R_1R_2} \\ 2n\sqrt{R_1R_2} & Z_1 - nn^* Z_2^* \end{bmatrix} \tag{4.139}$$

which can be expressed as

$$S = \frac{2n\sqrt{R_1R_2}}{Z_1 + nn^* Z_2}\begin{bmatrix} \dfrac{-Z_1^* + nn^* Z_2}{2n\sqrt{R_1R_2}} & \dfrac{n^*}{n} \\ 1 & \dfrac{Z_1 - nn^* Z_2^*}{2n\sqrt{R_1R_2}} \end{bmatrix} \tag{4.140}$$

or as

$$S = \frac{2n\sqrt{R_1R_2}}{Z_1 + nn^* Z_2}\begin{bmatrix} \dfrac{-Z_1^* + nn^* Z_2}{2n\sqrt{R_1R_2}} & 1 \\ 1 & \dfrac{Z_1 - nn^* Z_2^*}{2n^*\sqrt{R_1R_2}} \end{bmatrix}\begin{bmatrix} 1 & 0 \\ 0 & \dfrac{n^*}{n} \end{bmatrix} \tag{4.141}$$

By setting $n = 1$ in either of the above scattering matrices, the definition of the complex two-port adaptor is found as given by (4.134), with the complex parameter given in

(4.118). Note that if unnormalized matrices are used, the same conclusions can be drawn.

Another case of interest is found by placing the following constraint on the port references in the above scattering matrix (4.141)

$$Z_1 = Z_2^* \tag{4.142}$$

which is the matching condition for port references discussed in Section 4.5. Substitute (4.142) into (4.141) in order to derive

$$S = \frac{2nR_1}{Z_1 + nn^* Z_1^*} \begin{bmatrix} \dfrac{-Z_1^* + nn^* Z_1^*}{2nR_1} & 1 \\ 1 & \dfrac{Z_1 - nn^* Z_1}{2n^* R_1} \end{bmatrix} \begin{bmatrix} 1 & 0 \\ 0 & \dfrac{n^*}{n} \end{bmatrix} \tag{4.143}$$

Note that if unnormalized matrices were used, the above matrix would also have been generated. Consider equating the left-most scattering matrix

$$S_c = \frac{2nR_1}{Z_1 + nn^* Z_1^*} \begin{bmatrix} \dfrac{Z_1^* \left(nn^* - 1\right)}{2nR_1} & 1 \\ 1 & \dfrac{Z_1 \left(1 - nn^*\right)}{2n^* R_1} \end{bmatrix} \tag{4.144}$$

to the normalized two-port adaptor scattering matrix given by

$$S_2 = \begin{bmatrix} -\left(\cos\beta\right) e^{j(2\gamma - \theta)} & \left(\sin\beta\right) e^{j\gamma} \\ \left(\sin\beta\right) e^{j\gamma} & \left(\cos\beta\right) e^{j\theta} \end{bmatrix} = \left(\sin\beta\right) e^{j\gamma} \begin{bmatrix} -\left(\dfrac{\cos\beta}{\sin\beta}\right) e^{-j\theta} e^{j\gamma} & 1 \\ 1 & \left(\dfrac{\cos\beta}{\sin\beta}\right) e^{j\theta} e^{-j\gamma} \end{bmatrix} \tag{4.145}$$

in order to derive the following equations,

$$\frac{Z_1^* \left(1 - nn^*\right)}{2nR_1} = \frac{\cos\beta}{\sin\beta} e^{-j\theta} e^{j\gamma}$$

$$\frac{Z_1 + nn^* Z_1^*}{2nR_1} = \frac{e^{-j\gamma}}{\sin\beta} \tag{4.146a,b}$$

Solve for n from the two above equations as

$$n = \frac{(\sin\beta)\, e^{j\gamma}}{1 + (\cos\beta)\, e^{-j\theta} e^{j2\gamma}} \tag{4.147}$$

which gives a relation between the complex turns ratio and the complex two-port adaptor parameter. The above can be simplified by recognizing that

$$\begin{aligned} (\sin\beta)\, e^{j\gamma} &= \sqrt{1 - \alpha\alpha^*}\, \sqrt{\frac{1-\alpha}{1-\alpha^*}} \\ (\cos\beta)\, e^{-j\theta} e^{j2\gamma} &= \alpha^* \frac{1-\alpha}{1-\alpha^*} \end{aligned} \tag{4.148a,b}$$

in order to derive

$$n = \sqrt{\frac{(1-\alpha)(1-\alpha^*)}{(1-\alpha\alpha^*)}} \tag{4.149}$$

and thus the complex turns ratio corresponding to a normalized complex two-port adaptor is purely real. Note that the remaining section in (4.143) represents a straight pass-through connection since the turns ratio is real.

Note that the complex two-port adaptor can also be derived from either the series $(X = 0)$ or parallel $(X = \infty)$ connected imaginary resistor as given in (4.45a,b) for the unnormalized case and (4.46a,b) for the normalized case, respectively. The values of the imaginary resistor in each case correspond to a pass through connection in the analog domain, which again shows the carry-over of properties between the CWD and analog domains.

4.6.6 Complex Two-port and Three-port Adaptor Equivalences

Two normalized real two-port adaptors can be used in an elegant combination in order to realize either the series or parallel real three-port adaptor. The same equivalents used in the real case can also be used for both the complex reflection-free series and the complex parallel three-port adaptors, since each adaptor can be expressed in terms of the corresponding real adaptor. The two equivalents will be given using the normalized forms of the respective scattering matrices.

Consider the section composed of two normalized complex two-port adaptors as shown in the figure below:

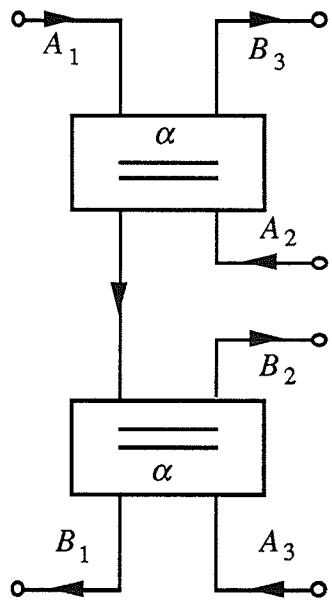

Figure 4.20: Section composed of complex two-port adaptors.

where α is the parameter of the normalized complex two-port adaptor. The scattering matrix with the ports labelled as above is given by

$$\mathbf{S} = \begin{bmatrix} \dfrac{(-\alpha+1)(-\alpha\alpha^*+1)}{-\alpha^*+1} & \dfrac{\sqrt{-\alpha+1}\sqrt{-\alpha\alpha^*+1}\,\alpha}{\sqrt{-\alpha^*+1}} & \dfrac{(\alpha-1)\alpha^*}{-\alpha^*+1} \\ \dfrac{\sqrt{-\alpha+1}\sqrt{-\alpha\alpha^*+1}\,\alpha}{\sqrt{-\alpha^*+1}} & \alpha^2 & \dfrac{\sqrt{-\alpha+1}\sqrt{-\alpha\alpha^*+1}}{\sqrt{-\alpha^*+1}} \\ \dfrac{(\alpha-1)\alpha^*}{-\alpha^*+1} & \dfrac{\sqrt{-\alpha+1}\sqrt{-\alpha\alpha^*+1}}{\sqrt{-\alpha^*+1}} & 0 \end{bmatrix} \tag{4.150}$$

However, if the parameter α is real, then the scattering matrix is also real and reduces to the following form

$$\mathbf{S} = \begin{bmatrix} -\alpha^2+1 & \sqrt{-\alpha^2+1}\,\alpha & -\alpha \\ \sqrt{-\alpha^2+1}\,\alpha & \alpha^2 & \sqrt{-\alpha^2+1} \\ -\alpha & \sqrt{-\alpha^2+1} & 0 \end{bmatrix} \tag{4.151}$$

The normalized form of the scattering matrix for the series adaptor is given by (4.77), and

is repeated below.

$$\hat{\mathbf{S}} = \begin{bmatrix} \frac{R_2}{R_1+R_2} & \frac{-\sqrt{R_1R_2}}{R_1+R_2} & \frac{-\sqrt{R_1}}{\sqrt{R_1+R_2}} \\ \frac{-\sqrt{R_1R_2}}{R_1+R_2} & \frac{R_1}{R_1+R_2} & \frac{-\sqrt{R_2}}{\sqrt{R_1+R_2}} \\ \frac{-\sqrt{R_1}}{\sqrt{R_1+R_2}} & \frac{-\sqrt{R_2}}{\sqrt{R_1+R_2}} & 0 \end{bmatrix} \tag{4.152}$$

It is clear that the above two scattering matrices (4.151-152) are equal if

$$\alpha = \frac{\sqrt{R_1}}{\sqrt{R_1+R_2}} = \sqrt{\beta_1} \tag{4.153}$$

where β_1 is the real parameter of the series adaptor given in (4.74). The above (4.153) gives the equivalence for the complex three-port series adaptor with port three reflection-free and the section in Figure 4.20 as shown in the following figure:

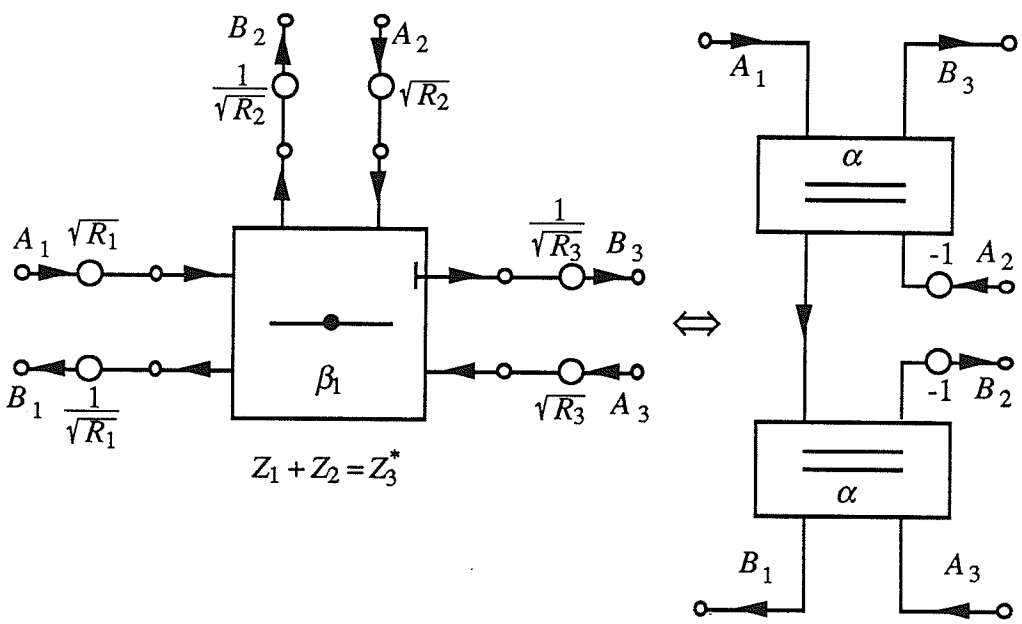

Figure 4.21: Equivalent form of the complex series three-port adaptor.

Similarly, using the equivalence between the series and parallel adaptors given in Figure 4.11 and in equation (4.112), the following is derived:

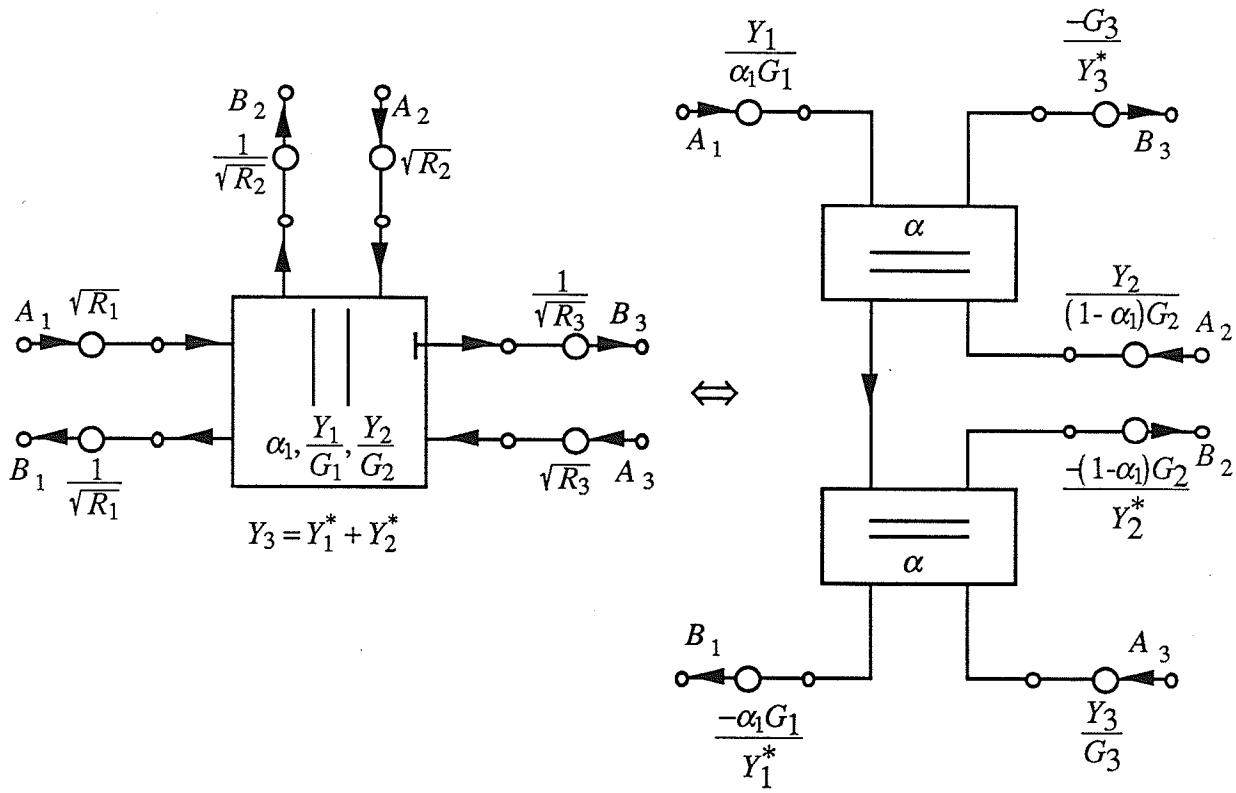

Figure 4.22: Equivalent form of the complex parallel three-port adaptor.

which gives the equivalence for the complex three-port parallel adaptor. The complex two-port adaptor parameter is given by

$$\alpha = \sqrt{\alpha_1} \tag{4.154}$$

The above two equivalences suggest that the general structure of Figure 4.20 can be used instead of either of the series or the parallel three-port adaptors in a network. This observation will be used in the following chapter in order to derive the CWD realizations of the complex canonic sections given in the tables in Chapter II.

4.7 Robustness of Complex Wave Digital Filters

A discrete filter behaves ideally if all signal levels are calculated with high precision without the existence of overflows or underflows. In this case the floating-point representation of the signals is ordinarily used. However, during the recursive operation of a digital filter, the actual signal levels within the structure deviate from the ideal signal levels. This is a result of representing the actual signals with a finite number of bits, which lead to underflow and overflow quantization errors. The *robustness* [69] of a digital filter

is a measure of how well the digital filter behaves as compared to the ideal filter (within the constraints imposed by finite arithmetic). Another way of stating this is that the deviation between the actual and digital signals within the operation of a robust filter should be small. Thus the property of robustness encompasses not only the zero-input and forced-response stability of a filter, but also other desirable properties. The stability of a complex wave digital filter was presented in [53] and will be briefly summarized in the following Section.

4.7.1 Stability of Complex Wave Digital Filters

The stability of a digital network under zero-input, forced response and looped conditions is critical for the usefulness of the filter. It has been shown that under infinite precision conditions, when all values are calculated using floating-point values and no underflow or overflow errors can occur in the linear system, the wave digital filter can be designed to be stable for all bounded input signals. However, in a digital system values are represented with a finite number of digits and usually in binary. Thus, all signals and results of additions or multiplications are quantized and the system is no longer linear. This process creates underflow errors, which are errors in signals due to the inability to represent an infinite number of digits, and overflow errors, which develop because the magnitude of the largest number that can be represented is bounded (usually by one or two). Underflow errors create relatively small deviations in the signals of the network, whereas overflow errors create large deviations from the nominal values of the signals and thus should be avoided if possible.

The discussion of the stability of a complex WD network follows from the generalization of the concepts used in the real domain. These include the definitions of the norms operating on complex sequences associated with an n-port digital network. However, the existence of the generalization of the stability argument is based on the definition of the steady-state power of the complex digital system as given by

$$P = \mathbf{A}^{*\mathrm{T}}\left(\widetilde{\mathbf{G}} - \mathbf{S}^{*\mathrm{T}}\widetilde{\mathbf{G}}\mathbf{S}\right)\mathbf{A} \tag{4.155}$$

which is the same expression suggested by Fettweis given in [26].

This definition leads to the conditions on the (non-linear) complex operators acting on the signals in order to guarantee both the zero-input and the forced-response stability of the digital system. A condition for stability is that the complex overflow operator ζ and the complex underflow operator δ must be contractive, as given by

$$\|\zeta\| \leq 1$$

$$\|\delta\| \leq 1 \tag{4.156a,b}$$

The notation in the above refers to the norm of the operator, expressed as

$$\|\zeta\| = \sup_{x \neq 0}\left(\frac{|\zeta(x)|}{|x|}\right)$$

$$\|\delta\| = \sup_{x \neq 0}\left(\frac{|\delta(x)|}{|x|}\right) \tag{4.157a,b}$$

where $|x|$ is the magnitude of the complex number x. The arguments of both operators are the real and imaginary parts of the complex input signal. Thus, in the real domain, the operators are viewed as being two-dimensional in nature; whereas in the complex domain, the operators are clearly one-dimensional. The two-dimensional view is the most useful one to adopt where the real and imaginary parts of the operators can be considered independently, that is (for either operator),

$$\begin{aligned} y &= \zeta(x) \\ \zeta(x) &= \zeta_r(x_r) + j\zeta_i(x_i) \\ y_r &= \zeta_r(x_r) \\ y_i &= \zeta_i(x_i) \end{aligned} \tag{4.158a,b,c,d}$$

where $\{x,y\} \varepsilon \mathbb{C}$, $\{x_r, x_i, y_r, y_i\} \varepsilon \mathbb{R}$, and ζ_r and ζ_i are the equivalent real operators of the complex operator $\zeta(x)$.

Viewing the operators as non-linear one-ports connected in series with complex circulators at the output of the state ports, the above immediately implies that the one-ports must be passive. Thus as long as the non-linear complex one-ports are passive it is guaranteed that no zero-input parasitic oscillations can exist [53].

Conditions similar to those in [43] are given for forced response stability. They extend to the complex case by letting the overflow truncation function, as shown below for the equivalent real and imaginary operators, ζ_r and ζ_i, of the complex operator ζ (the real and imaginary functions can be chosen the same), lie within the shaded area,

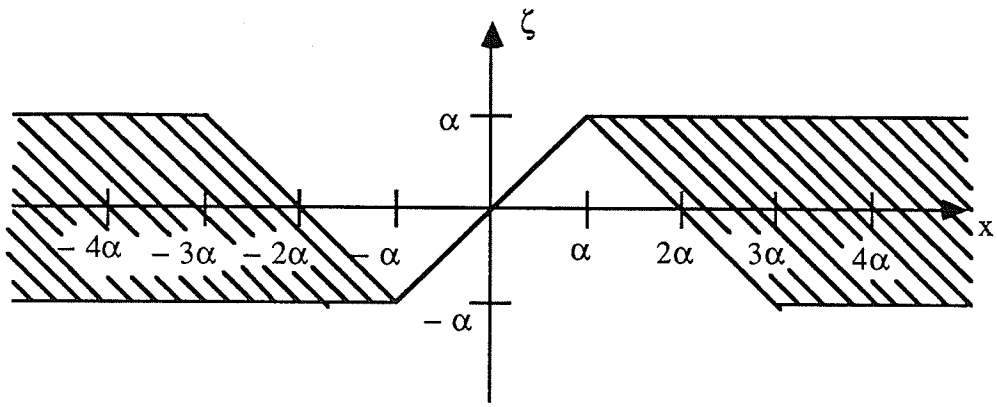

Figure 4.23: Real or imaginary equivalent of the overflow truncation function.

where α is the maximum allowable signal amplitude. This gives incremental passivity as extended to complex networks as discussed in [53]. Notice that the overflow truncation function satisfies the restriction on the magnitude of the norm of the operator as given in (4.156).

The overflow function cannot have a slope greater than plus or minus one, ie. the continuous curve cannot have a slope exceeding $\pm 45^{o}$. Various forms of the overflow error function have been found as summarized in [67] that meet this constraint. They include the saturation function, as shown in Figure 4.24

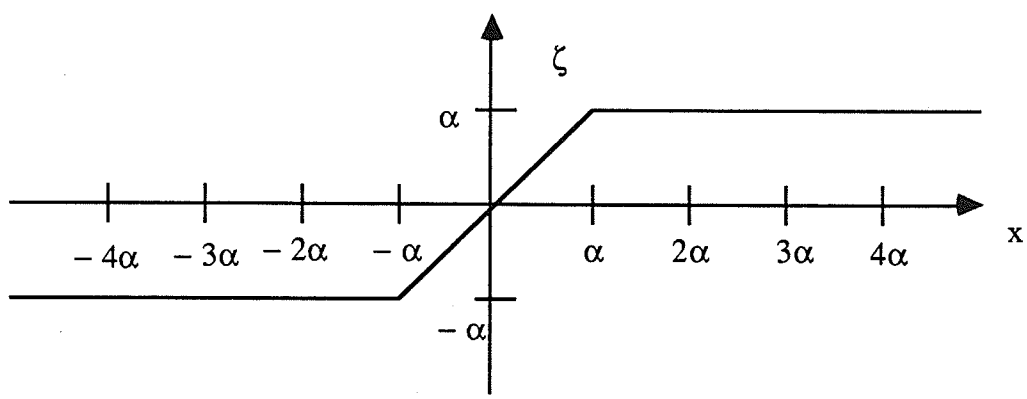

Figure 4.24: Saturation overflow function.

and the triangle function as shown in Figure 4.25.

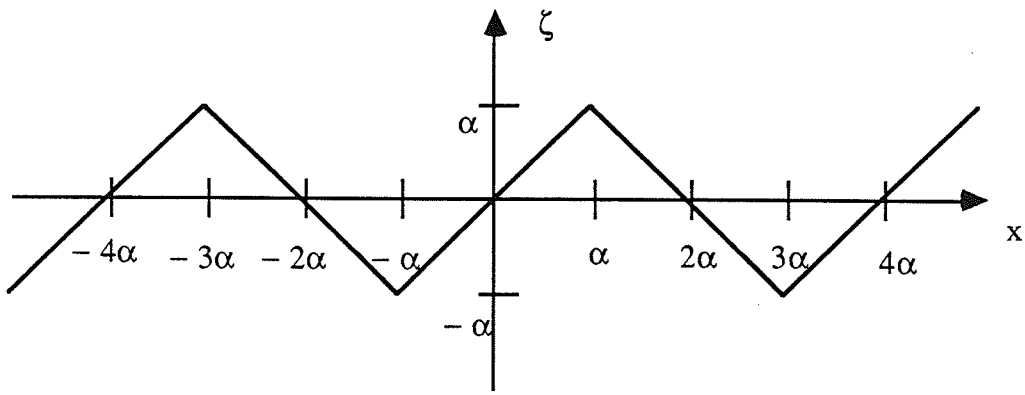

Figure 4.25: Triangle overflow function.

Both of the above functions give incremental passivity, and thus forced response stability. Notice that the triangle overflow function has a greater signal deviation error than the saturation function.

4.7.2 Robustness

It is impossible to measure precisely the robustness of either an actual digital filter, or more generally a digital filter structure, because of the many variables involved. However, as suggested in [69], a list of desirable properties can be compiled, such as the stability and sensitivity behavior of the filter under consideration. If a particular filter satisfies all of the desirable properties, then the filter will be called *robust.*

A brief review of the properties found in [69] will be summarized in the following. For robustness, we require:

a) No zero input parasitic oscillations can exist. It is essential for overflow oscillations, however, it is tolerable for underflow oscillations if the amplitudes are small.
b) For non-zero input the superimposed parasitic oscillations should be small.
c) The dynamic range should be as high as possible.
d) Forced-response stability should be guaranteed.
e) Attractivity should be maintained, that is, small changes in the initial conditions should not cause lasting changes in the output signal (ignoring the granular response from underflow errors).
f) For any fixed initial conditions, small changes in the input signal should cause only small changes in the output signal.
g) There should be no chaotic behavior (again, ignoring the granular response from underflow errors).
h) The saturation behavior should be as good as possible under the constraint of

binary (fixed wordlength) operations. This implies that the behavior should be approximately linear for small signal levels, with a monotonous transition towards saturation at higher signal levels.

i) The above properties must be able to be satisfied not only for the quantized coefficients, but also for a finite neighborhood of the quantized values.

j) All operations that must be performed on the signals must be sufficiently simple so that their actual application in digital hardware is feasible.

The generalization of real wave digital filters to the complex domain found in this thesis inherits the robustness of its real counterpart. This is mainly due to the carry-over of the critical stability argument [53] used in the real case. Namely, passivity and incremental passivity, which guarantee zero-input and forced-response stability, respectively, also guarantee properties *a*, *b*, and *d* to *f*. Property *c* is associated with the low sensitivity of WD filters. The overflow and underflow operators discussed earlier that give passivity and incremental passivity satisfy properties *g*, *h*, and *j*. Finally, property *i* is associated with low sensitivity.

Thus a well-designed CWD filter can be considered robust as defined above.

Chapter V

Cascade and Ladder Realizations Using Complex Wave Digital Networks

The theory presented in the preceding chapters allows the realization of general complex reference networks without alteration (that is, without making them one-real), as can be proved by construction. Since all of the familiar WD elements have now been successfully derived, the first condition for the generalization to be of practical use, as given in Chapter I, has been achieved. A stability theory guaranteeing zero-input and forced-response stability has been derived [53] and follows from the definition of the steady-state power

$$P = \mathbf{A}^{*\mathrm{T}}\left(\widetilde{\mathbf{G}} - \mathbf{S}^{*\mathrm{T}}\widetilde{\mathbf{G}}\mathbf{S}\right)\mathbf{A} \tag{5.1}$$

The resulting networks can contain any of the CWD elements thus far discussed. Other elements not discussed such as the n-port circulator, the unit element, and the so-called lattice adaptor can easily be generalized for CWD networks and thus will not be presented here.

Complex networks arise from four main sources. The first source is from the method of frequency shifting discussed in Chapter II, where a real network is frequency shifted by applying the following transformation on the frequency variable:

$$\psi \rightarrow \psi - j\phi_0 \tag{5.2}$$

The second source arises from changing the phase of the h polynomial by an arbitrary real constant. The third arises from the realization of a real transfer function using the new first-order elementary sections presented in Chapter II. Finally, the fourth arises from a direct approximation with a complex transfer function.

All of the first-order elementary complex sections realize a transmission zero independently of any other transmission zero (as opposed to grouping the transmission zeros in complex conjugate pairs). Four of the sections can realize a transmission zero anywhere on the $\psi = j\phi$ axis. Although one form of these sections has been quoted in the literature [40], the significance of the sections, namely that any of the four sections is the most general first-order reciprocal section, may have been somewhat overlooked. The

other sections realize transmission zeros at the origin, at infinity, on the real axis, or anywhere on the finite plane (excluding the preceding cases). A section can be viewed as equivalent to another section when viewed as a two-port (one section contains an inductor while the other contains a capacitor as the dynamic element). That is, it is always possible to use one section in place of the other.

A complex network consisting of the complex canonic sections given in the tables of Chapter II can be realized using one of two different viewpoints. The first inherently requires the use of three-port series and parallel adaptors since dynamic elements are realized as one-ports, while the second requires the development of a more general first-order section that will be viewed as a dynamic two-port. The method using three-port adaptors involves the element-by-element transformation of a reciprocal network, while the other method transforms each reciprocal or non-reciprocal canonic section of a network. The method using the three-port adaptors allows both canonic and non-canonic networks in a form of cascade synthesis known as the ladder configuration. However, the dynamic first-order section method is inherently canonic in nature. This method will be referred to as the Cascade Realization method.

In the following, complex quantities will be assumed throughout.

5.1 Ladder Realization Using three-port Adaptors

In the following, a brief review will be given of the WD realization method using three-port adaptors as well as scaling and quantization considerations for CWD networks. This method realizes a network by transforming the elements and the interconnection of elements that compose the network to the CWD domain. Each element is considered to be a one-port except those non-dynamic elements that are defined as a two-port (for example, the complex transformer). Examples of this realization method will be given in Section 5.2.

5.1.1 CWD Realization of Complex Reference Networks

A complex analog (reference) network in a ladder configuration composed of RLCX elements can be realized using the CWD elements given in the preceding Chapter. The realization is equivalent to a direct mapping of the analog elements in a one-to-one relationship to the corresponding CWD elements. Each analog one-port is mapped to a CWD one-port, and each connection of analog n-ports is mapped to a discrete (or algorithmic) representation of the connection in the form of either a parallel or series complex adaptor. By convention, a dynamic two-port is realized using a dynamic one-port connected to a three-port adaptor, while a constant two-port is realized using a constant CWD two-port. During the realization process, the port impedances of all one-ports and two-ports are given by Tables 4.1-4.4, including the port impedances of all input (external)

ports.

These conditions alone cannot uniquely define a CWD network. However, from the realizability condition discussed in Section 4.6, no delay-free directed loops can exist which imposes a further constraint on the CWD network. This constraint requires all but one of the three-port adaptors to contain a reflection-free port, and this port must be connected (through a simple directed path) to the port of another three-port adaptor. Thus using equations (4.69,4.97) defining the port impedances of the reflection-free ports, all of the port impedances of the CWD network are defined.

The choice of location of the one three-port adaptor that does not contain a reflection-free port is arbitrary. However, it is usually chosen to be the central adaptor in order to minimize the path length needed to compute the value of all of the signal nodes in the operation of the filter in real-time.

A CWD network derived from a complex reference network through cascade (ladder) synthesis is inherently viewed as a two-port. Normally, the input is associated with port one and the output with port two. The input of port two and the output of port one is normally ignored (though they need not be) when realizing doubly-terminated reference filters, thus giving a one-input, one-output network realizing a transmittance.

This process can be easily visualized with an example. Consider the following doubly-terminated[1] analog domain network

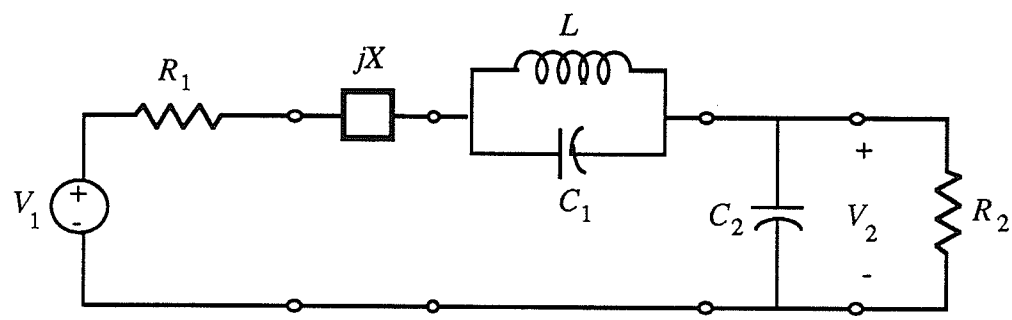

Figure 5.1: Example of a complex analog network.

which contains three dynamic elements and one constant element (ignoring the port resistors). This can be viewed as two dynamic two-ports (each requiring at least one three-port adaptor) and a constant two-port. The above network has the following CWD equivalent,

[1] Doubly-terminated networks are commonly used because of their excellent sensitivity properties [40].

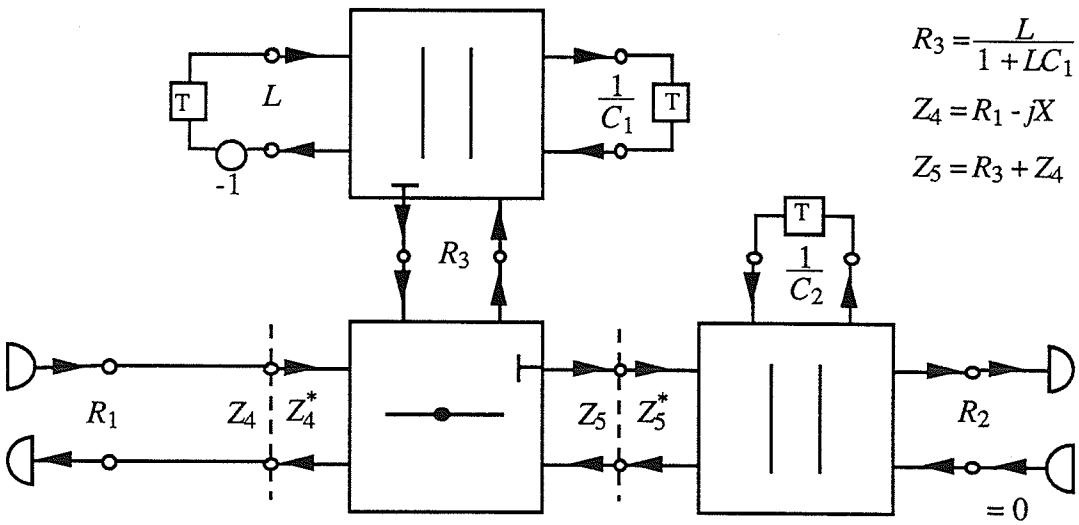

Figure 5.2: CWD equivalent of Figure 5.1.

where the series adaptor was made reflection-free and "T" represents a delay. The equivalence of the above network is clear when considering Tables 4.1-4.4 along with the definitions of the complex adaptors. From the relevant port impedances as given in the diagram, all of the parameters of the adaptors are defined. Notice that although complex port impedances are found throughout the structure, only the right-most parallel adaptor contains complex parameters. However, the existence of the complex port impedances allows the CWD equivalent of a complex network to be computable, and thus this example demonstrates the significance of Theorem 1.1.

Of course, other combinations of complex analog elements can occur. Two of the general first-degree reciprocal sections, which can be made equivalent when considered as a two-port and as discussed in Section 2.6.1.3, have the following CWD equivalents.

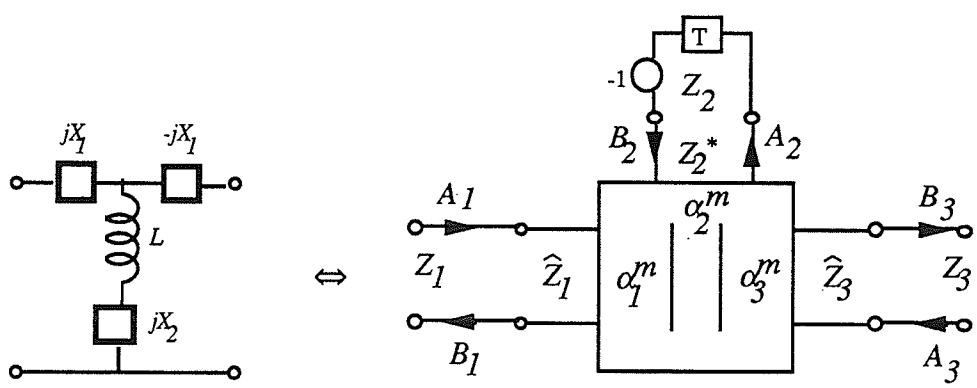

Figure 5.3: CWD equivalent of the parallel inductor first-order complex section.

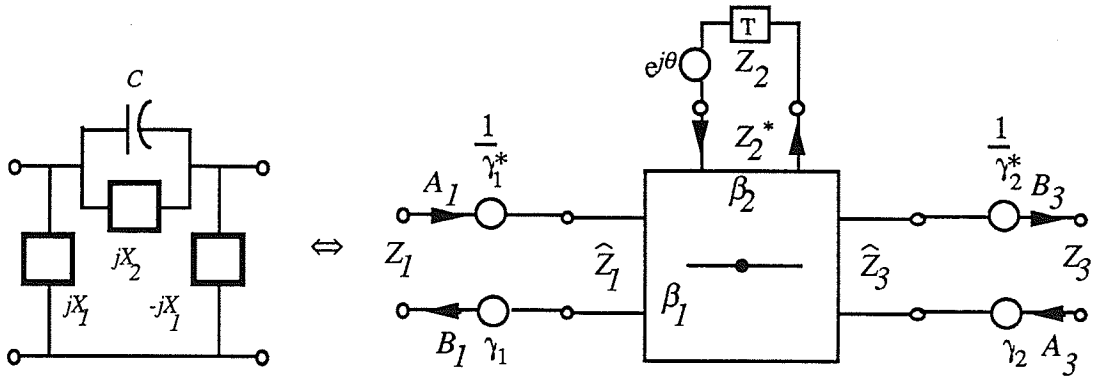

Figure 5.4: CWD equivalent of the series capacitor first-order complex section.

In each case the values of Z_1 and Z_3 are arbitrary, whereas the values of $\hat{Z}_1$, $\hat{Z}_3$, and Z_2 are given by Tables 4.2-4.4.

From the above two examples it is clear that CWD networks may or may not contain external multipliers, that is, multipliers external to the adaptor blocks. The external multipliers arise from the constant two-ports as given in Table 4.4 and any unimodular multipliers that are defined by dynamic one-ports.

In order to simplify the quantization process as discussed in Section 5.1.3, one has the option of absorbing all external multipliers into the associated scattering matrix. In some cases this process forces the elements of the scattering matrices associated with CWD blocks to have a magnitude in the range that would lead to a favorable dynamic range. However, as shown in the examples in Section 5.2, this process may lead to a less favorable implementation in some cases, and thus the realizations with and without external multipliers should be investigated.

5.1.2 Scaling the CWD Networks

During the operation of a CWD filter in real-time, the values of signals at many of the nodes[2] may frequently approach or exceed the bounds on the largest and smallest number that can be represented. Since this limits the dynamic range [6] of the filter, which also increases the noise [6], the CWD filter must be *scaled* before it is implemented. The way in which a filter is scaled depends upon the constraint that the designer wishes to place on the filter. The two most popular constraints for scaling are the normalized form and the L_2-norm at the states of the network [6,9-11]. Scaling is ordinarily performed on the three-port adaptor matrices (a constant two-port such as those given in Table 4.4 cannot be scaled).

[2] A node refers to a location that contains a signal value.

5.1.2.1 Normalized Scaling

This scaling condition imposes the constraint that the L_∞-norm at the states within the network must be less than or equal to one for a unit impulse input. This decreases the probability of overflow at the states. However, since the flow graph of a CWD filter is proper [73], this will also inherently decrease the probability of overflow at the internal nodes of the blocks. This scaling condition is associated with normalized or power wave digital filters. From equation (4.32) relating the scattering matrices of a voltage and a power wave network, and repeated below,

$$\hat{\mathbf{S}} = \tilde{\mathbf{G}}^{1/2}\,\mathbf{S}\,\tilde{\mathbf{G}}^{-1/2} \tag{5.3}$$

it is clear that simple real scaling transformers can be used on each three-port adaptor in order to realize the normalized form scaled network and the value of the turns ratio of each transformer is defined by the square-root of the associated port conductance ($\tilde{G} = R^{-1}$). This method associates three real scaling transformers with each three-port.

5.1.2.2 L_2-Norm Scaling

The scaling constraint of L_2-norm scaling sets the L_2-norm at each state equal to unity for a unit impulse input. This can be achieved with one real scaling transformer for every state. The scaling transformer is placed in the main signal path and is calculated by numerically finding the L_2 norm at the state before scaling, then selecting the transformer value to set this norm to unity. The L_2-norm is numerically computed using the impulse response in the discrete domain.

5.1.3 Quantization of A CWD Network

As mentioned in an earlier section, the implementation of a digital filter in digital hardware inherently requires the filter to be in a form that is compatible with the hardware. In other words, the digital filter must first be *quantized*, that is, represented in binary form as an integer divided by an integer power of two. The two constraints on this process are the following: the resulting filter must remain passive (as given by equation(4.26)), and satisfy the frequency specifications. A non-linear optimization method has been developed by the author which quantizes the scattering matrices associated with the blocks of a CWD network, and is described in [76].

In order to maintain passivity, magnitude truncation is used when quantizing each value. Thus, each element of the scattering matrix is quantized using magnitude truncation.

Real external multipliers that are found in inverse pairs, such as the real ideal transformer, are quantized to a power of two, and therefore both of the multipliers are quantized at once (the inverse of a power of two value is another power of two value). Note that with complex inverse multipliers this method cannot be used, and four independent real quantizations will be needed with magnitude truncation (the multipliers represent passive and not lossless sections after quantization). In the same way single complex multipliers, such as unimodular multipliers, require two independent quantizations with the same conclusions.

Note that after a network has been expressed in binary form the resulting frequency response may contain a frequency independent shift. This is a result of the fact that CWD networks cannot be made lossless under binary conditions, and thus only passivity can be guaranteed. However, a frequency independent shift is not significant since it represents a constant shift for all frequencies. If it becomes necessary, a multiplier can be inserted at the output node in order to remove the shift. If the network realizes a transmittance and operates as a single-input, single-output filter, then the multiplier inserted corresponds to an ideal transformer.

5.2 Design Examples Using three-port Complex Adaptors

A computer program written for the Macintosh computer in the PASCAL computer language has been developed by the author that derives a scaled and quantized CWD filter from a lumped RLCX reference filter. The attenuation responses of the CWD and nominal filters are generated over the digital frequency range $-\pi < \omega T \leq \pi$. However, the responses are presented as a function of the normalized frequency which ranges from -0.5 to +0.5. The following presents several design examples that show the validity of the theory developed.

5.2.1 Non-canonic CWD Realization of Frequency Shifted Filters

The realization of a real reference filter in the form of an LCX ladder with finite transmission zeros and without coupled coils is necessarily non-canonic. A filter with complex elements can be derived from such a filter by frequency shifting as given in (5.1) above. The CWD network realizing the complex filter will have the same *form* as the corresponding real WD filter realizing the unshifted network with the only difference being the use of complex adaptors instead of real adaptors and the inclusion of unimodular multipliers.

Consider an 8th order Elliptic filter in a non-canonic realization that has been shifted by 1.1 r/s in order to generate a complex filter. The attenuation responses of both the nominal and the CWD filter are shown in the following plots.

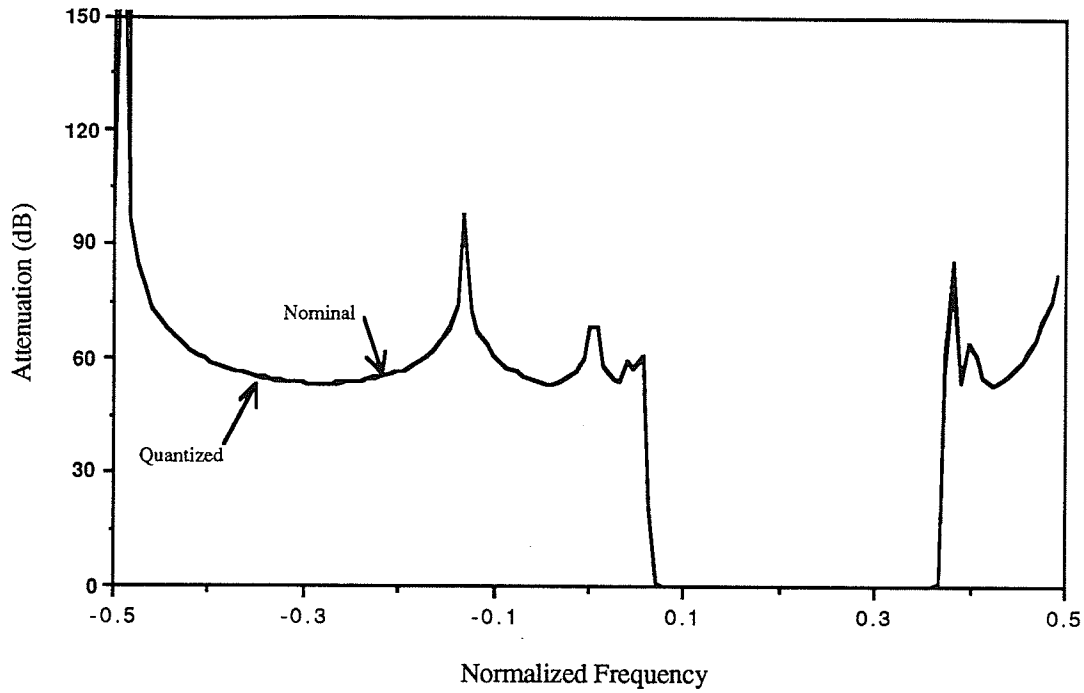

Figure 5.5: Stopband attenuation of the 8th order Elliptic filter.

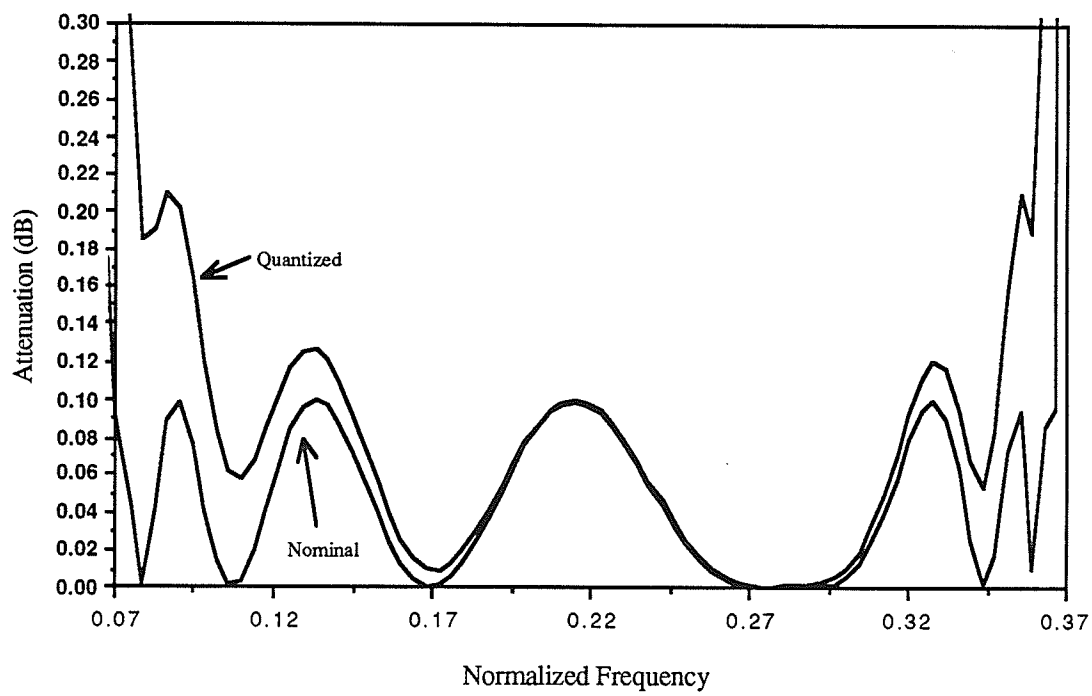

Figure 5.6: Passband attenuation of the 8th order Elliptic filter.

The CWD filter was scaled for the L_∞-norm and quantized using 11 bits. The nominal and quantized attenuation plots are virtually identical in the stopband which is a result of the large number of bits used. The passband shows a small deviation, which is expected from the property of low passband sensitivity. The deviation at the corners is a characteristic of a passive (rather than lossless) WD network.

5.2.2 Canonic CWD Realization of Complex Filters

It is now clear that reference filters with a real transfer function can be implemented using CWD networks (for example, the sections given in the equivalences in Figures 5.3 and 5.4). A CWD network may contain only series (with a series capacitor or inductor) or parallel (with a parallel inductor or capacitor) complex adaptors.

Consider the 4th order Elliptic example given in Appendix A of a complex filter realization of the real transfer function. The following two sections will present the CWD filter equivalents of both the inductor-section (CD1_$j\phi$) and the capacitor-section (CC1_$j\phi$) realizations. For all realizations power wave scaling will be used.

5.2.2.1 Realization Using Complex Parallel Adaptors Exclusively

The 4th order Elliptic filter is realized with the CD1_$j\phi$ section exclusively. The only CWD elements needed with this method of realization are the complex parallel three-port adaptor, the delay, the ideal transformer and the wave source and sink (any simple inversions are ignored).

This example is first realized from the definition of the CWD network without alteration (Figures 5.7 and 5.8). A second realization is derived by absorbing all external multipliers into the associated scattering matrices (Figures 5.9 and 5.10). Both realization are quantized to the same specifications with a 1.5 dB passband ripple. The attenuation responses of both the nominal and the CWD quantized filters are shown in the following four plots.

The first realization with external multipliers as shown in Figures 5.7 and 5.8 required 10 bits for the quantization for a 1.5dB ripple in the passband. The quantized passband and stopband responses are indistinguishable from the nominal response as a result of the large number of bits required to meet the frequency specifications. The second realization without external multipliers as shown in Figures 5.9 and 5.10 required 12 bits for the quantization. The necessity for the two extra bits over the previous case is mainly the result of absorbing the final ideal transformer into the last scattering matrix. However, although two extra bits are used, the quantized passband and stopband responses do not compare favorably with the earlier case. Thus the first realization method is preferred.

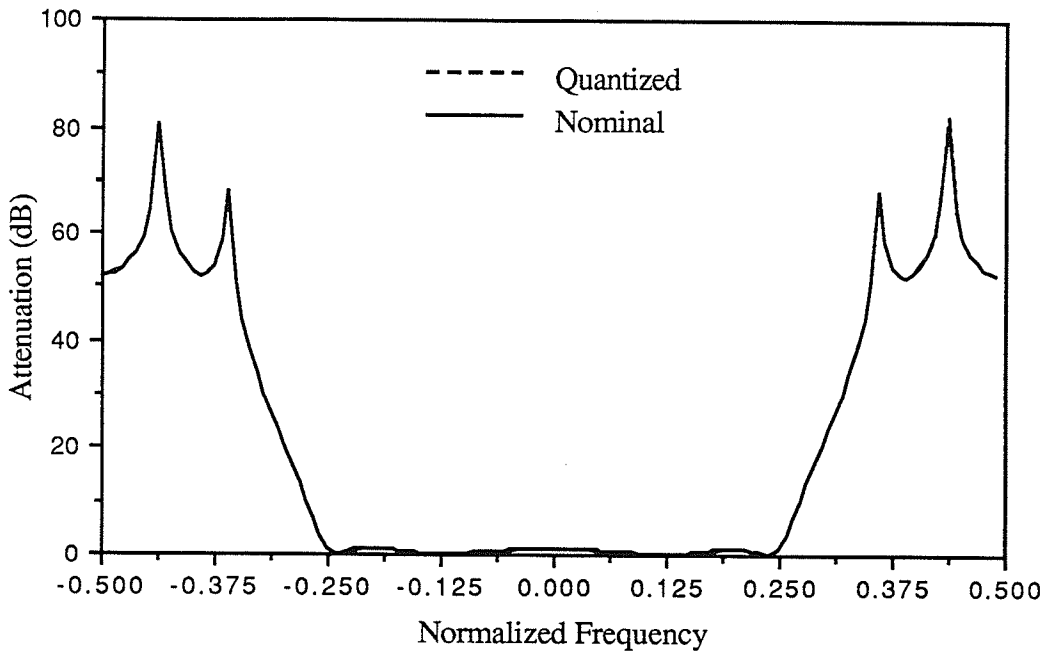

Figure 5.7: Stopband of the 4th order Elliptic filter with external multipliers.

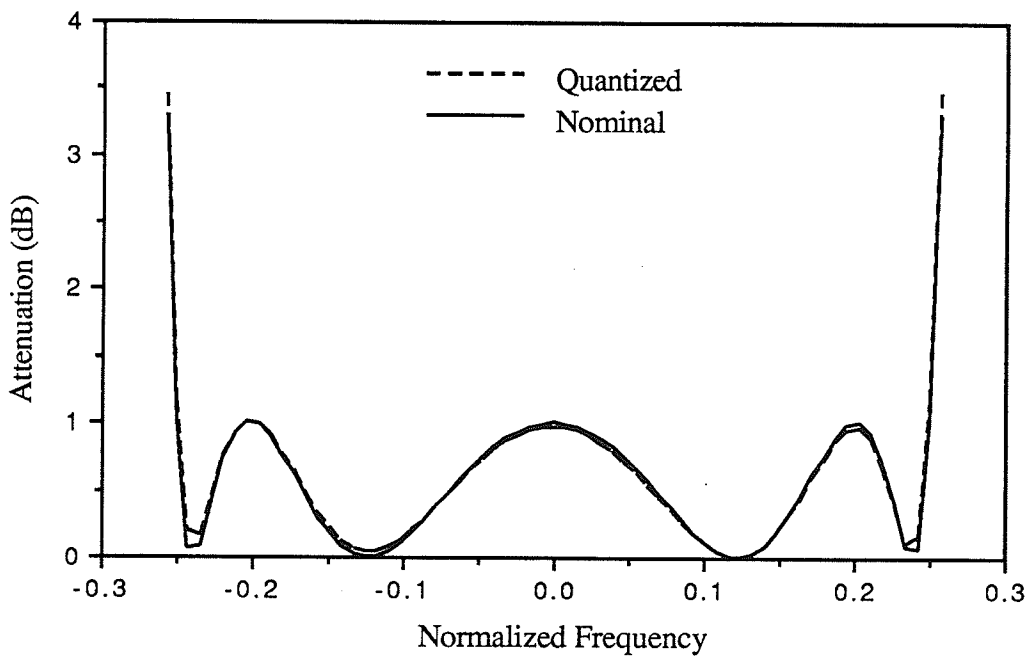

Figure 5.8: Passband of the 4th order Elliptic filter with external multipliers.

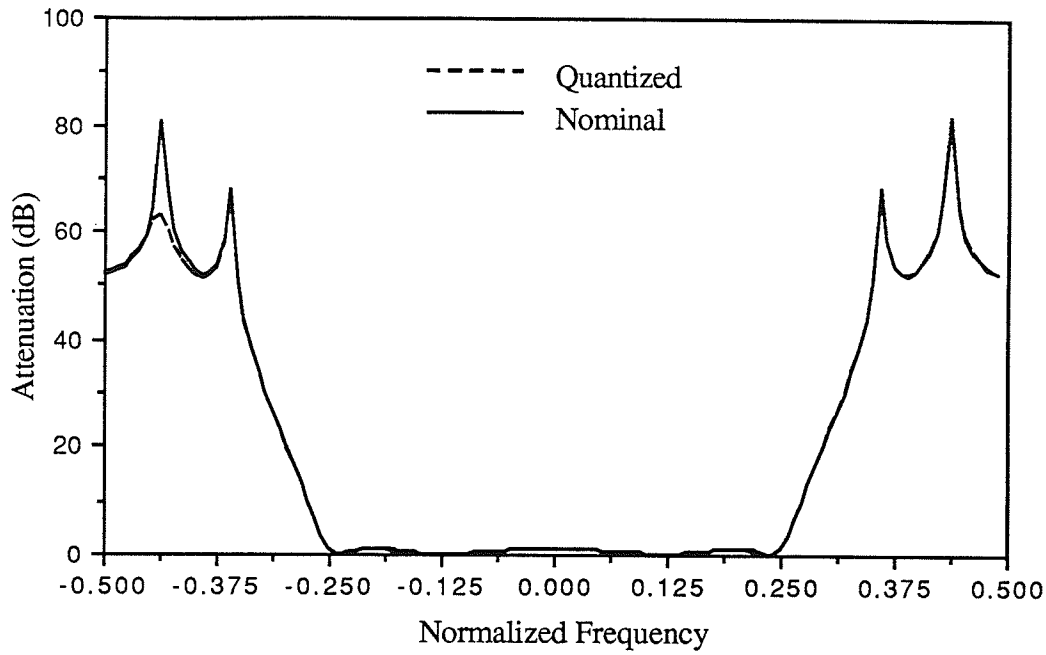

Figure 5.9: Stopband of the 4th order Elliptic filter without external multipliers.

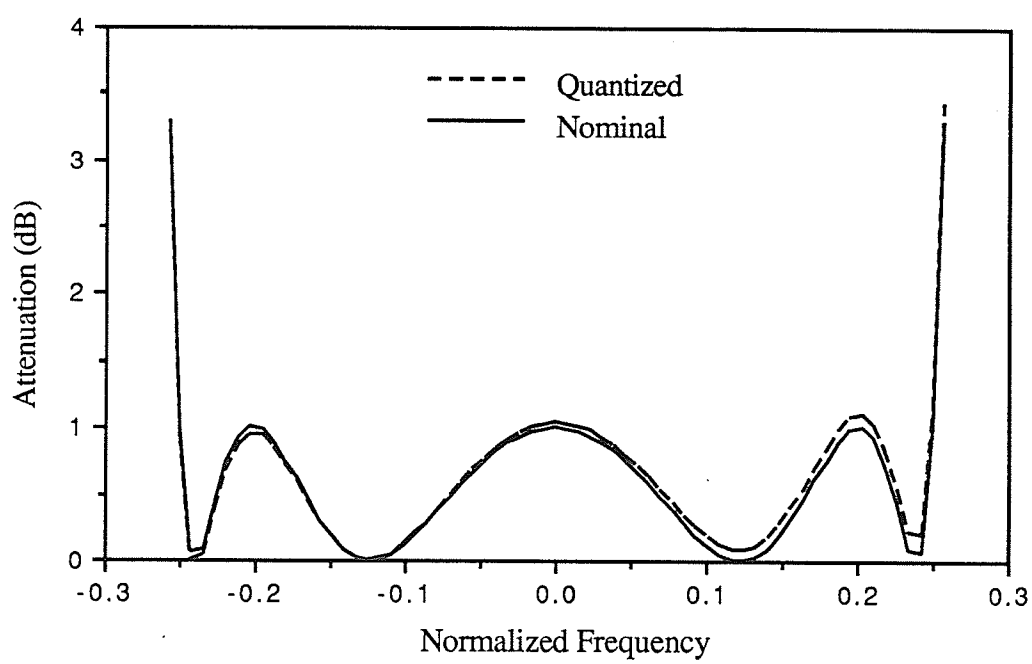

Figure 5.10: Passband of the 4th order Elliptic filter without external multipliers.

5.2.2.2 Realization Using Complex Series Adaptors Exclusively

The 4th order Elliptic filter is realized with the CC1_$j\phi$ section exclusively. The only CWD elements needed with this method of realization are the CWD equivalents of the parallel combination of the imaginary resistor, as well as the unimodular multiplier connected to the complex three-port series adaptor.

As with the earlier example, this example is realized with and without external multipliers in order to derive two networks. The differences between the two implementations is more significant in this case than the earlier example since external complex multipliers exist from the equivalents of the parallel connected imaginary resistors.

Both quantized realizations required 7 bits in order to meet the same frequency specifications as the earlier example of a 1.5 dB passband ripple (compared with 10 bits with external multipliers and 12 bits without external multipliers for the earlier example). However, from the attenuation plots given in the following four figures, the quantized responses for both realizations show several differences.

The response of the quantized realization with external multipliers as shown in Figures 5.11 and 5.12 is similar to the nominal response. However, the stopband did not achieve the same attenuation. The passband response performed better than the nominal near zero frequency, with the response deteriorating near the edges of the passband.

The response of the quantized realization without external multipliers as shown in Figures 5.13 and 5.14 compares poorly to the realization with external multipliers. The stopband greatly deviates from the nominal and the desired attenuation is not reached. Also, the passband is very poor since the ripple width is larger than any of the earlier examples, and the response is irregular and it is not symmetric about the origin.

Clearly, although the same number of bits are required for both realizations in order to meet the frequency specifications, the implementation with the external multipliers quantized separately has a superior response in both the stopband and the passband. Thus, again in this case, the realization with external multipliers is preferred.

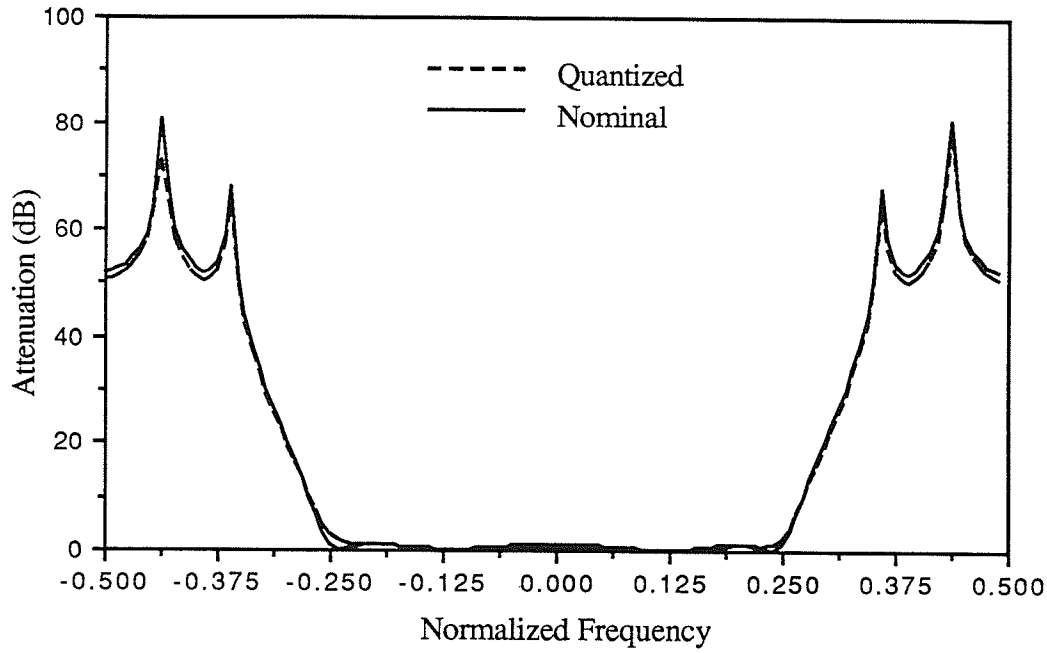

Figure 5.11: Stopband of the 4th order Elliptic filter with external multipliers.

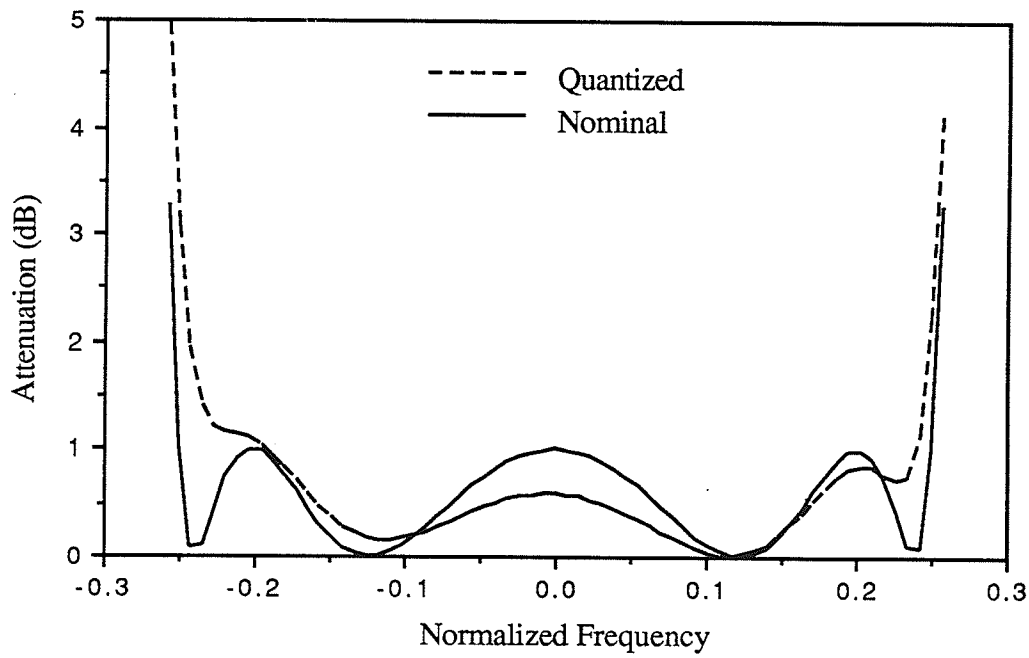

Figure 5.12: Passband of the 4th order Elliptic filter with external multipliers.

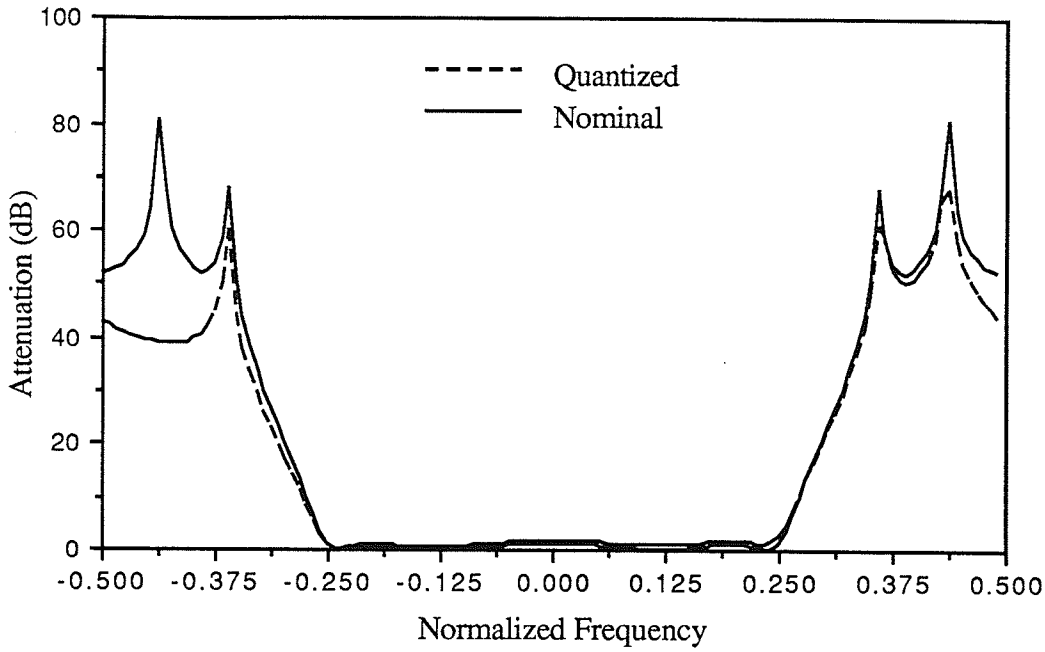

Figure 5.13: Stopband of the 4th order Elliptic filter without external multipliers.

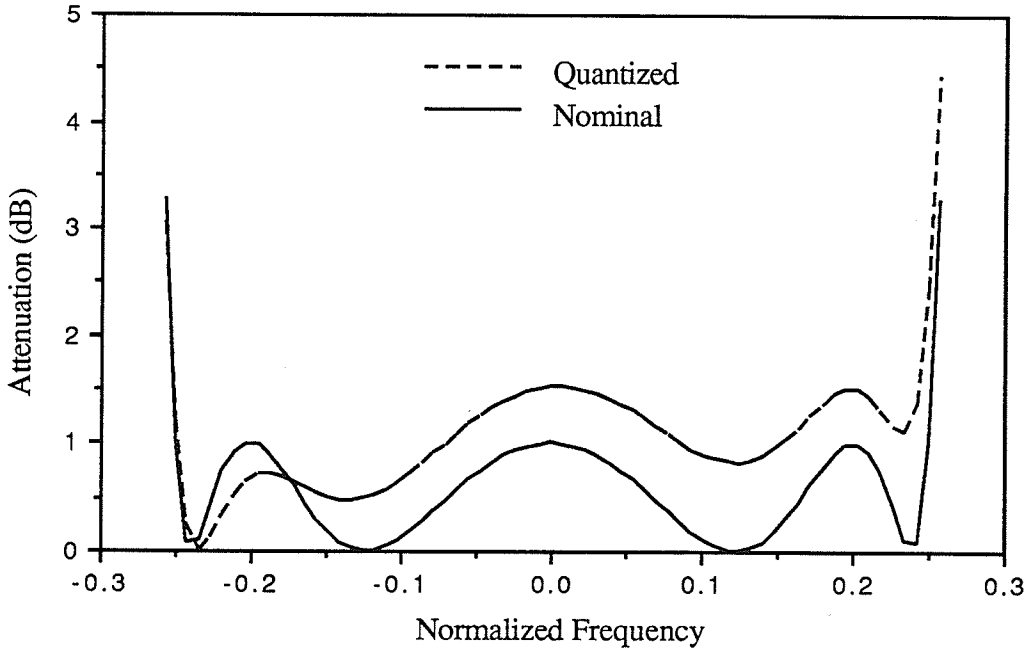

Figure 5.14: Passband of the 4th order Elliptic filter without external multipliers.

5.2.2.3 Comments On the Two Equivalent Realizations

The two techniques presented in the earlier sections shows that it is possible to realize the same reference filter using a CWD network containing either series or parallel three-port complex adaptors exclusively. From either a quantization or scaling point of view using the schemes outlined in Sections 5.1.2 and 5.1.3, both networks are equivalent in so far as they realize the same canonic polynomials.

The major difference between the networks is found by recalling the differences between the three-port series and parallel complex adaptors. The series three-port adaptor is significantly simpler in form than the parallel adaptor, particularly with a reflection-free port. The network with series adaptors is equivalent, on a block basis, to the network with parallel adaptors with specific complex multipliers removed from the parallel adaptor scattering matrix as shown in Figure 4.11. However, from the two previous examples, the quantized form of both networks that realize the same reference filter show differences with respect to both the number of bits needed for a set of frequency specifications.

5.2.2.4 Elliptic Example of order 5

Consider as another example the 5th order Elliptic filter given in Appendix A. Since the filter order is odd a real canonic section appears as the last dynamic section. The filter realizations containing the CC1_$j\phi$ and CD1_$j\phi$ sections were quantized to satisfy the same frequency specifications and 9 bits were required for both cases. The nominal and quantized stopband attenuation plots are identical as a result of the large number of bits used. The nominal and quantized passband attenuation plots are shown in Figure 5.15 given below.

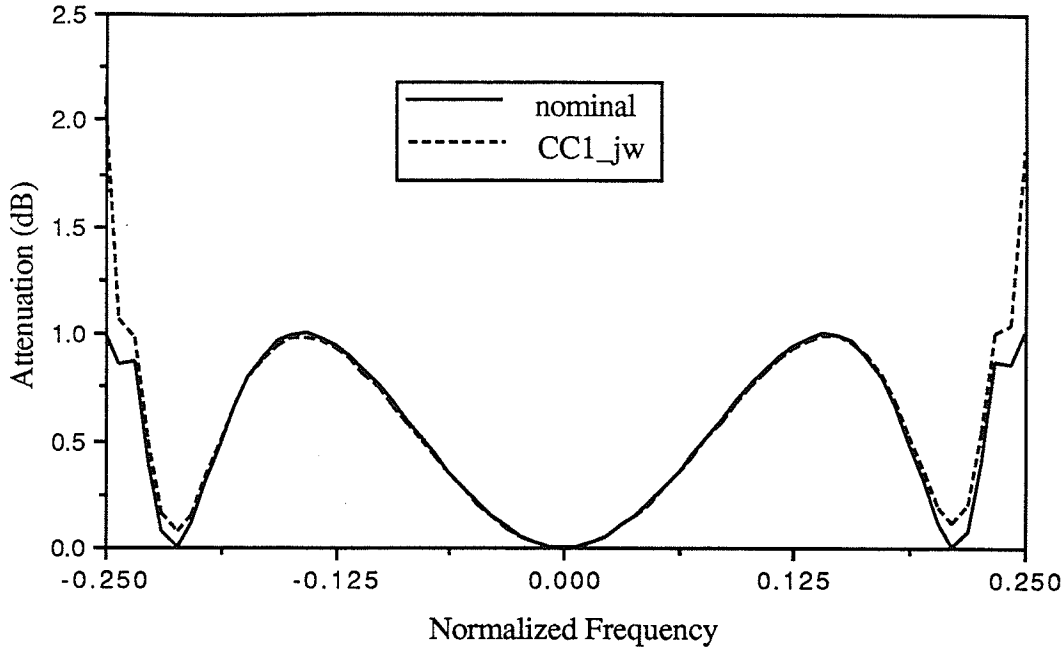

Figure 5.15: Passband of the quantized 5th order Elliptic filter.

Both realizations were quantized in the same manner as the 4th order Elliptic example, however, the phenomenon observed with that example is not apparent in this case. This may be the result of the existence of the last real dynamic section. This section may act in a similar manner for both realizations thereby desensitizing the quantized realizations with respect to the type of adaptor used.

In order to investigate the effect of the number of bits used in the quantization for this example, realizations were generated using 4, 5, 6, 7, and 8 bits for the realization using the series adaptor. The stopband attenuation plot of the nominal and 4 bit quantized realization is shown in Figure 5.16. Clearly the desired attenuation is not reached. The stopband attenuation plots of the remaining realizations converge to the nominal response as more bits are used and thus they will not be presented.

The passband attenuation plots for the five quantized realizations are shown in Figure 5.17. Clearly, the realization with 4 bits has the greatest deviation. The case with 8 bits is similar to the case given above in Figure 5.15 using 9 bits. Notice that with this example the operation of quantization caused the greatest deviations at the edges of the passband (a frequency independent shift is not significant since it can be removed with a scalar multiplier at the output port).

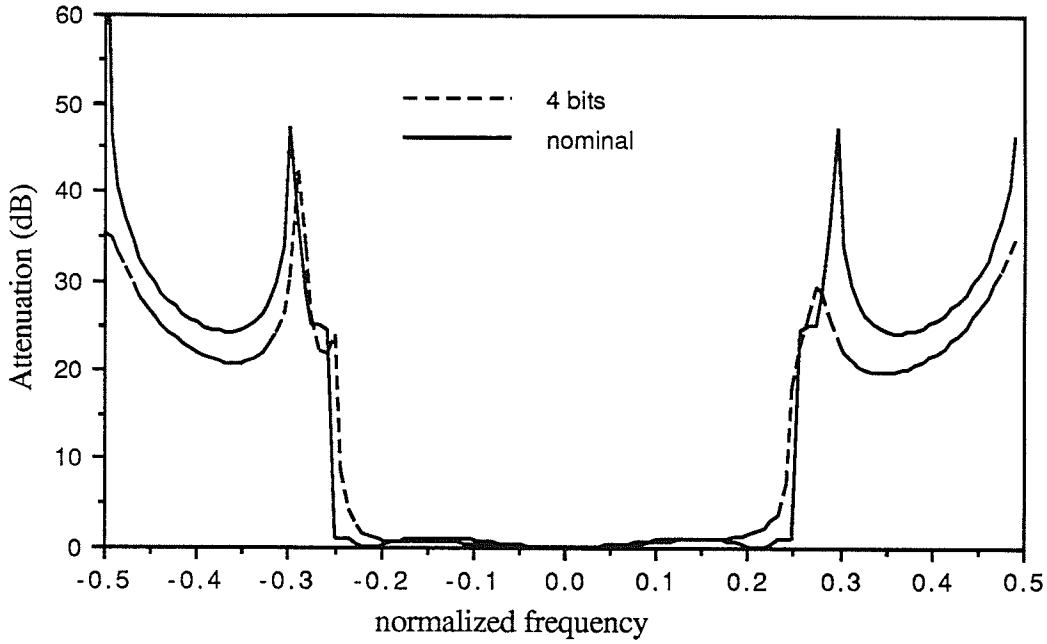

Figure 5.16: Stopband of the quantized 5th order Elliptic filter.

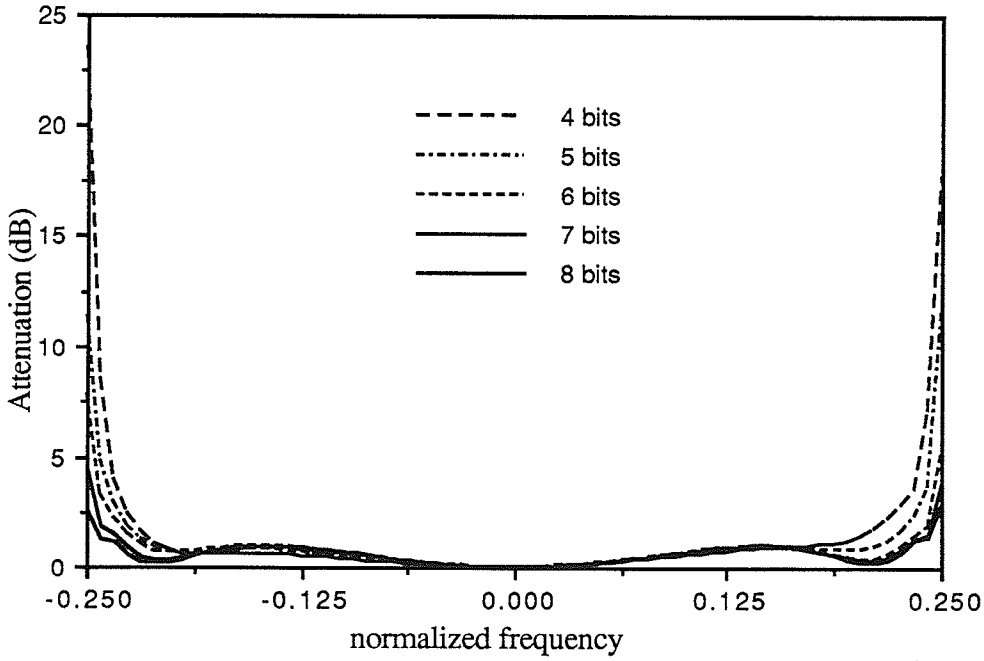

Figure 5.17: Passband of the quantized 5th order Elliptic filter.

5.3 Cascade Realization of Complex Networks

It is known that an elegant combination of real two-port adaptors can be used to replace either the series or the parallel real three-port adaptor (Section 4.6.6). Thus real first-order sections realized using the real three-port adaptors can be replaced with the equivalent realization using only real two-port adaptors. This observation was given a theoretical foundation in [16] by transforming an analog four-port to the WD domain. With the correct terminations, the real canonic elementary sections can be realized in this manner.

The reflection-free versions of the complex three-port adaptors can be made equivalent to the corresponding real adaptors with simple multipliers in the signal paths. This observation along with the comments given in the preceding paragraph suggest that a general complex first-order section exists which is composed of complex two-port adaptors in a configuration similar to the real case. The following will give the derivation of this section, which hereafter will be known as the *canonic cascade section.* Note that the normalized complex two-port adaptor will be used exclusively throughout since it is already scaled for power waves.

5.3.1 Derivation of the Canonic Cascade Section

A general first-order complex section exists that can realize a transmission zero anywhere in the complex plane. Thus, it must represent the first-order complex canonic sections given in Chapter II mapped to the CWD domain. Also, it must reduce to the real first-order sections given in [16] if all quantities are restricted to be real.

The derivation of the section is based on a generalization of the section given in the real case with two additional degrees of freedom. These additional parameters are found in the arguments of two unimodular multipliers introduced in order to supply the canonic number of parameters required by a first-order section. Although the form of the section is not unique, it will be chosen in order to parallel the real case wherever possible. To this end, consider the canonic cascade section given in the figure shown below.

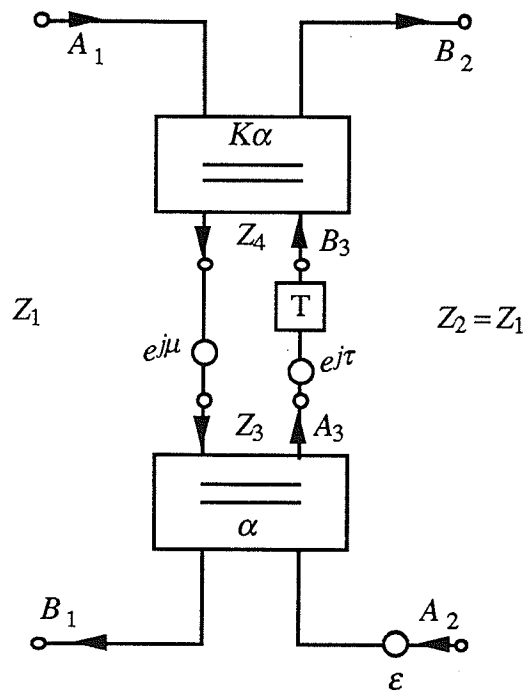

Figure 5.18: General canonic cascade section.

The figure shows that the canonic cascade section contains two complex normalized two-port adaptors and two unimodular multipliers. It will be found from the canonic polynomials representing this section, as given by (5.5), that it has port two reflection-free. Note that the multiplier ε can take on the values

$$\varepsilon = \pm 1 \tag{5.4}$$

and usually has a value of +1 (and thus can usually be ignored). The parameter ε will be used to change the sign of σ if necessary. The two complex normalized two-port adaptors are functions of the real parameter K and the complex parameter α. The real parameter K will be referred to as the *gain* of the second adaptor with respect to the first. For reciprocal sections the gain will be unity, while for non-reciprocal sections the gain can be any real value (including zero). The canonic polynomials of this section (ignoring ε) are given by

$$f = z^{-1} \frac{K\alpha^*}{\alpha e^{j(\tau+\mu)}}$$

$$h = \frac{\sqrt{-\alpha+1}\sqrt{-K\alpha^*+1}\sqrt{-\alpha\alpha^*+1}\sqrt{-K^2\alpha\alpha^*+1}\,e^{-j\tau}}{\sqrt{-\alpha^*+1}\sqrt{-K\alpha+1}\,\alpha}$$

$$g = \frac{1}{e^{j(\tau+\mu)}\alpha}\frac{-K\alpha^*+1}{-K\alpha+1} - K\alpha\frac{-K\alpha^*+1}{-K\alpha+1}z^{-1}$$

$$\sigma = -\frac{(-\alpha+1)(-K\alpha^*+1)\alpha^* e^{-j(\tau+\mu)}}{(-\alpha^*+1)(-K\alpha+1)\alpha} \qquad (5.5a,b,c,d)$$

It is clear that the f polynomial contains a zero anywhere on the z^{-1} plane with the appropriate choice of the parameters found in Figure 5.18, since the magnitude of the zero is given by the constant K and the phase is dependent upon the free parameters τ and μ. Since the central two-port in the form given above represents an unrecognizable CWD element as it is composed of a delay and two unimodular multipliers, Figure 5.18 is given in an equivalent form as shown below.

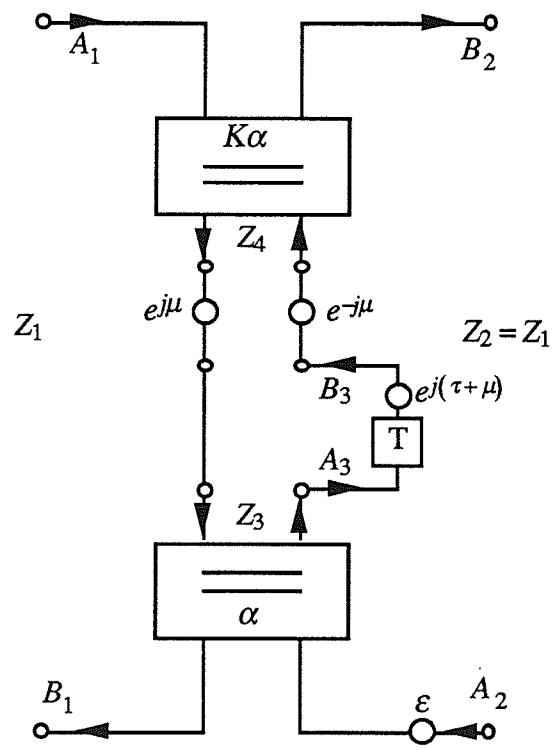

Figure 5.19: Equivalent form of the general canonic cascade section.

Notice that the internal connections located between the two-port adaptors represent a complex ideal transformer and a dynamic one-port.

The port impedance of port two is equal to that of port one (since the node weights [18]

for ports one and two are equal) and the port impedances of the inner ports are given by

$$Z_3 = \frac{(-\alpha^* + 1)Z_1{}^* + (\alpha - 1)Z_1\alpha^*}{-\alpha\alpha^* + 1}$$

$$Z_4 = \frac{(-K\alpha^* + 1)Z_1{}^* + (K\alpha - 1)Z_1 K\alpha^*}{-K^2\alpha\alpha^* + 1} \qquad (5.6a,b)$$

Consider the special case of a transmission zero on the unity circle (that is, the $j\phi$-axis on the reference frequency domain) which represents a reciprocal section. The section in this case reduces to the form shown in the following figure:

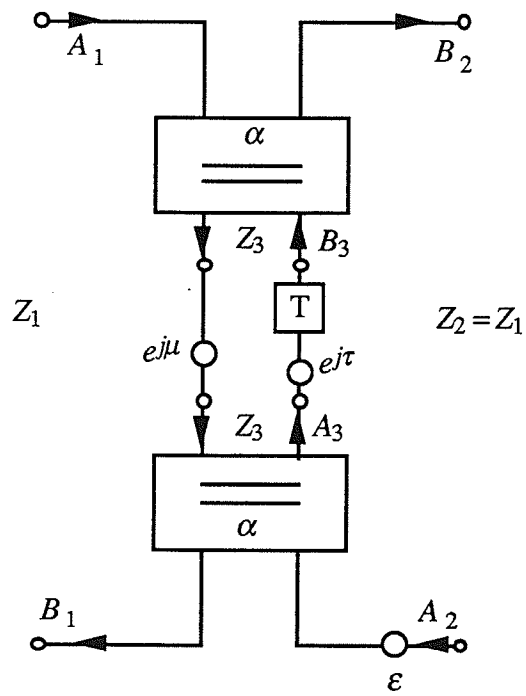

Figure 5.20: Reciprocal canonic cascade section.

with the following canonic polynomials

$$f = z^{-1}\frac{\alpha^*}{\alpha e^{j(\tau+\mu)}}$$

$$h = \frac{(-\alpha\alpha^* + 1)e^{-j\tau}}{\alpha}$$

$$g = \frac{1}{e^{j(\tau+\mu)}\alpha}\frac{-\alpha^* + 1}{-\alpha + 1} - \alpha\frac{-\alpha^* + 1}{-\alpha + 1}z^{-1}$$

$$\sigma = -\frac{\alpha^* e^{-j(\tau+\mu)}}{\alpha} \tag{5.7a,b,c,d}$$

and the port impedance given by

$$Z_3 = \frac{(-\alpha^* + 1)Z_1{}^* + (\alpha - 1)Z_1\alpha^*}{-\alpha\alpha^* + 1} \tag{5.8}$$

By using the general form of the canonic polynomials representing either the non-reciprocal (5.5) or the reciprocal (5.7) form of the canonic cascade section, all of the canonic sections given in the tables in Chapter II can be mapped to the CWD domain. This is achieved by first transforming all port two reflection-free polynomials for the first-order sections to the z^{-1} domain by using the bilinear transformation (4.2a). Then the resulting polynomials are equated to the polynomials representing the canonic cascade section (5.5,5.7) in order to derive the values of the real and complex constant parameters given in Figures 5.18 and 5.20. Note that the derivation for the real sections are given in [16] and thus will not be repeated here.

5.3.2 Canonic First-Order Complex Sections Mapped to the CWD Domain

The following presents the solutions for the canonic cascade section parameters in tabular form. Since every complex first-order section is equivalent to the dual of the section, the tables give the parameters that represent both sections. Each table contains the analog symbol for each of the two equivalent sections, the z^{-1} domain polynomials for the sections, and the constant parameters. Note that the parameters α and $K\alpha$ are treated as independent quantities for the special case in Table 5.8. All quantities are expressed in terms of the analog domain canonic parameters, namely, the location of the analog transmission zero (ϕ_0 for reciprocal sections and $(-\phi_r - j\phi_i)$ for non-reciprocal sections), the reflectance evaluated at the transmission zero $\eta e^{j\theta}$, and for reciprocal sections the analog delay d. The quantities are also given in terms of the discrete transmission zero $\zeta e^{j\nu}$ (for reciprocal sections $\zeta = 1$ and $\nu = \omega_0 T$), the reflectance evaluated at the transmission zero $\eta e^{j\theta}$, and for reciprocal sections the discrete delay δ. Note that the synthesis algorithm presented in Chapter III can be extended to the z^{-1} domain using the discrete canonic parameters and polynomials. The real first-order and second-order reciprocal and non-reciprocal sections are given in [16].

Note that the parameters given in the tables represent the mapping of the complex first-order sections given in Chapter II to the CWD domain. This contrasts with the realization method outlined in Section 5.1, where instead of mapping an entire dynamic section (requiring the canonic cascade section), the individual elements are mapped to the CWD domain (requiring three-port adaptors with dynamic one-ports and constant two-ports). Also, the number of real parameters required to represent each section is the canonic number, namely three and four parameters for reciprocal and non-reciprocal sections, respectively.

CA1_∞ and CB1_∞ Sections		
Analog Symbols	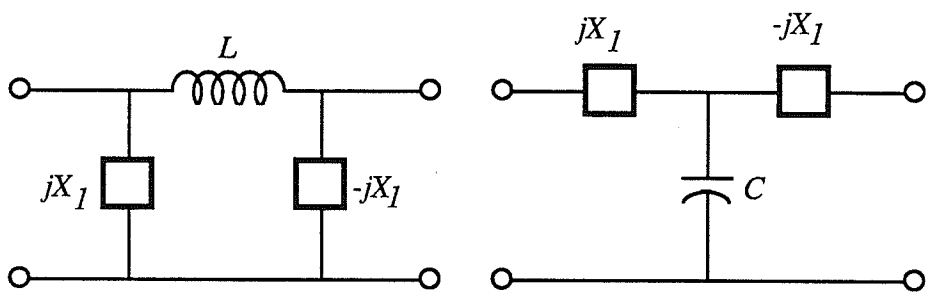	
	Function of Analog Parameters	Function of Discrete Parameters
Discrete Canonic Polynomials	$d = 2\delta$ $f_{RF} = z^{-1} + 1$ $h_{RF} = 2\frac{e^{j\theta}}{\sqrt{d+2}\sqrt{d}}$ $g_{RF} = \frac{\sqrt{d+2}}{\sqrt{d}} + \frac{\sqrt{d}z^{-1}}{\sqrt{d+2}}$ $\sigma_{RF} = 1$	$\delta = \frac{1}{2}d$ $f_{RF} = z^{-1} + 1$ $h_{RF} = \frac{e^{j\theta}}{\sqrt{\delta+1}\sqrt{\delta}}$ $g_{RF} = \frac{\sqrt{\delta+1}}{\sqrt{\delta}} + \frac{\sqrt{\delta}z^{-1}}{\sqrt{\delta+1}}$ $\sigma_{RF} = 1$
CWD Parameters	$K = 1$ $\alpha = -\frac{\sqrt{d}}{\sqrt{d+2}}$ $e^{j\mu} = e^{j\theta}$ $e^{j\tau} = -e^{-j\theta}$ $\varepsilon = 1$	$K = 1$ $\alpha = -\frac{\sqrt{\delta}}{\sqrt{\delta+1}}$ $e^{j\mu} = e^{j\theta}$ $e^{j\tau} = -e^{-j\theta}$ $\varepsilon = 1$

Table 5.1: CWD equivalent of the CA1_∞ and the CB1_∞ sections.

CC1_0 and CD1_0 Sections		
Analog Symbols	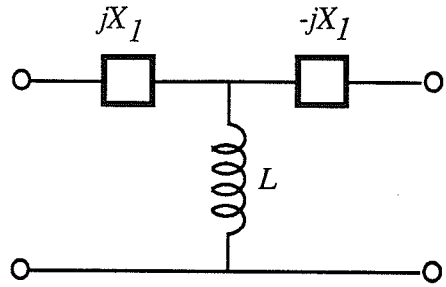	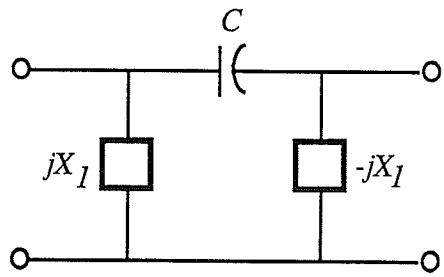
	Function of Analog Parameters	Function of Discrete Parameters
Discrete Canonic Polynomials	$d = 2\delta$ $f_{RF} = z^{-1} - 1$ $h_{RF} = -\frac{2e^{j\theta}}{\sqrt{d+2}\sqrt{d}}$ $g_{RF} = -\frac{\sqrt{d+2}}{\sqrt{d}} + \frac{\sqrt{d}z^{-1}}{\sqrt{d+2}}$ $\sigma_{RF} = -1$	$\delta = \frac{1}{2}d$ $f_{RF} = z^{-1} - 1$ $h_{RF} = -\frac{e^{i\theta}}{\sqrt{\delta+1}\sqrt{\delta}}$ $g_{RF} = -\frac{\sqrt{\delta+1}}{\sqrt{\delta}} + \frac{\sqrt{\delta}z^{-1}}{\sqrt{\delta+1}}$ $\sigma_{RF} = -1$
CWD Parameters	$K = 1$ $\alpha = -\frac{\sqrt{d}}{\sqrt{d+2}}$ $e^{j\mu} = e^{j\theta}$ $e^{j\tau} = e^{-j\theta}$ $\varepsilon = 1$	$K = 1$ $\alpha = -\frac{\sqrt{\delta}}{\sqrt{\delta+1}}$ $e^{j\mu} = e^{j\theta}$ $e^{j\tau} = e^{-j\theta}$ $\varepsilon = 1$

Table 5.2: CWD equivalent of the CC1_0 and the CD1_0 sections.

CA1_$j\phi_0$ and CB1_$j\phi_0$ Sections		
Analog Symbols	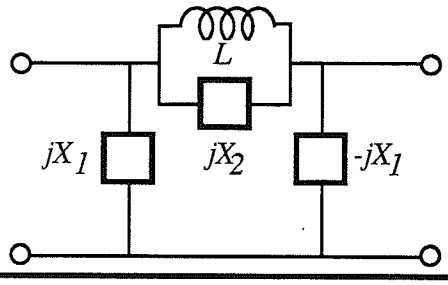	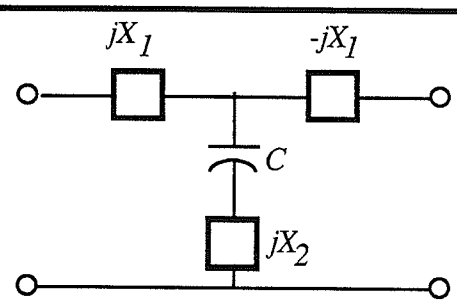
	Function of Analog Parameters	Function of Discrete Parameters
Discrete Canonic Polynomials	$\xi = \frac{\sqrt{d\phi_0^2 + d + 2}}{\sqrt{d}(1 + j\phi_0)}$ $\quad e^{j\Delta} = \frac{\sqrt{d\phi_0^2 + 1 + jd\phi_0}}{\sqrt{d\phi_0^2 + 1 - jd\phi_0}}$ $f_{RF} = z^{-1} - \frac{1 - j\phi_0}{1 + j\phi_0}$ $h_{RF} = 2\frac{je^{j(\theta+\Delta)}}{d\xi(1 + j\phi_0)^2}$ $g_{RF} = je^{j\Delta}\left[\xi - \frac{z^{-1}}{\xi}\right]$ $\sigma_{RF} = \frac{1 - j\phi_0}{1 + j\phi_0}$	$e^{j\omega_0 T} = \frac{1 + j\phi_0}{1 - j\phi_0}$ $\quad \delta = 2\frac{de^{-j\omega_0 T}}{(1 + e^{-j\omega_0 T})^2}$ $e^{j\Delta} = \sqrt{\frac{1 + (1 - e^{-j\omega_0 T})\delta}{1 + (1 - e^{j\omega_0 T})\delta}}$ $f_{RF} = z^{-1} - e^{-j\omega_0 T}$ $h_{RF} = -\frac{je^{j[\theta + \Delta - \frac{1}{2}\omega_0 T]}}{\sqrt{\delta + 1}\sqrt{\delta}}$ $g_{RF} = 2j\left[\frac{\sqrt{\delta + 1}}{\sqrt{\delta}} - \frac{\sqrt{\delta}e^{j\omega_0 T}z^{-1}}{\sqrt{\delta + 1}}\right]e^{j[\Delta - \frac{1}{2}\omega_0 T]}$ $\sigma_{RF} = e^{-j\omega_0 T}$
CWD Parameters	$e^{j\lambda} = \frac{\sqrt{d\phi_0^2 + d + 2} + j(1 + j\phi_0)\sqrt{d}\,e^{j\Delta}}{\sqrt{d\phi_0^2 + d + 2} - j(1 - j\phi_0)\sqrt{d}\,e^{-j\Delta}}$ $K = 1$ $\alpha = \frac{je^{j(-\lambda+\Delta)}}{\xi}$ $e^{j\mu} = e^{j(\lambda+\theta)}$ $e^{j\tau} = -e^{j(\lambda-\theta-2\Delta)}$ $\varepsilon = -1$	$e^{j\lambda} = -\frac{[\sqrt{\delta}e^{j\Delta} + j\sqrt{\delta + 1}\,e^{(-\frac{1}{2}j\omega_0 T)}]e^{j\omega_0 T}}{\sqrt{\delta}e^{-j\Delta} - j\sqrt{\delta + 1}\,e^{(\frac{1}{2}j\omega_0 T)}}$ $K = 1$ $\alpha = -j\frac{\sqrt{\delta}}{\sqrt{\delta + 1}}e^{j[\frac{1}{2}\omega_0 T - \lambda + \Delta]}$ $e^{j\mu} = e^{j(\lambda+\theta)}$ $e^{j\tau} = -e^{j(\lambda-\theta-2\Delta)}$ $\varepsilon = -1$

Table 5.3: CWD equivalent of the CA1_$j\phi$ and the CB1_$j\phi$ sections.

CC1_$j\phi_0$ and CD1_$j\phi_0$ Sections		
Analog Symbols	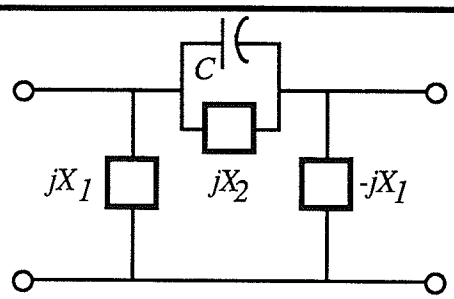	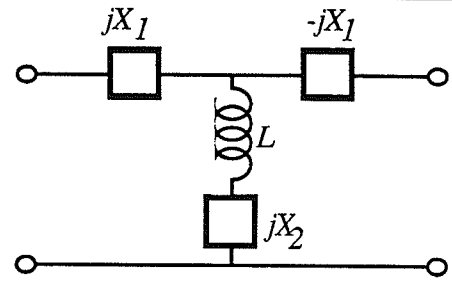
	Function of Analog Parameters	Function of Discrete Parameters
Discrete Canonic Polynomials	$\xi = \frac{\sqrt{d\phi_0^2 + d + 2}}{\sqrt{d}(1 + j\phi_0)}$ $\quad e^{j\Delta} = \frac{\sqrt{d + 1 - jd\phi_0}}{\sqrt{d + 1 + jd\phi_0}}$ $f_{RF} = z^{-1} - \frac{1 - j\phi_0}{1 + j\phi_0}$ $h_{RF} = -2\frac{j\phi_0 e^{j(\theta+\Delta)}}{d\xi(1 + j\phi_0)^2}$ $g_{RF} = \left[\frac{z^{-1}}{\xi} - \xi\right] e^{j\Delta}$ $\sigma_{RF} = -\frac{1 - j\phi_0}{1 + j\phi_0}$	$e^{j\omega_0 T} = \frac{1 + j\phi_0}{1 - j\phi_0}$ $\quad \delta = 2\frac{de^{-j\omega_0 T}}{(1 + e^{-j\omega_0 T})^2}$ $e^{j\Delta} = \sqrt{\frac{1 + (1 + e^{-j\omega_0 T})\delta}{1 + (1 + e^{j\omega_0 T})\delta}}$ $f_{RF} = z^{-1} - e^{-j\omega_0 T}$ $h_{RF} = -\left(\frac{1 - e^{-j\omega_0 T}}{1 + e^{-j\omega_0 T}}\right)\frac{e^{j\left[\theta + \Delta - \frac{1}{2}\omega_0 T\right]}}{\sqrt{\delta + 1}\sqrt{\delta}}$ $g_{RF} = \left[-\frac{\sqrt{\delta + 1}}{\sqrt{\delta}} + \frac{\sqrt{\delta} e^{j\omega_0 T} z^{-1}}{\sqrt{\delta + 1}}\right] e^{j\left[\Delta - \frac{1}{2}\omega_0 T\right]}$ $\sigma_{RF} = -e^{-j\omega_0 T}$
CWD Parameters	$e^{j\lambda} = \frac{\sqrt{d\phi_0^2 + d + 2} - (1 + j\phi_0)\sqrt{d}\, e^{j\Delta}}{\sqrt{d\phi_0^2 + d + 2} - (1 - j\phi_0)\sqrt{d}\, e^{-j\Delta}}$ $K = 1$ $\alpha = -\frac{1}{\xi} e^{j(-\lambda + \Delta)}$ $e^{j\mu} = e^{j(\lambda + \theta)}$ $e^{j\tau} = e^{j(\lambda - \theta - 2\Delta)}$ $\varepsilon = 1$	$e^{j\lambda} = \frac{\left[\sqrt{\delta + 1}\, e^{-\frac{1}{2}j\omega_0 T} - \sqrt{\delta} e^{j\Delta}\right] e^{j\omega_0 T}}{\sqrt{\delta + 1}\, e^{\frac{1}{2}j\omega_0 T} - \sqrt{\delta} e^{-j\Delta}}$ $K = 1$ $\alpha = -\frac{\sqrt{\delta}}{\sqrt{\delta + 1}} e^{j\left[\Delta - \lambda + \frac{1}{2}\omega_0 T\right]}$ $e^{j\mu} = e^{j(\lambda + \theta)}$ $e^{j\tau} = e^{j(\lambda - \theta - 2\Delta)}$ $\varepsilon = 1$

Table 5.4: CWD equivalent of the CC1_$j\phi$ and the CD1_$j\phi$ sections.

CE1 and CF1 Sections

Analog Symbol

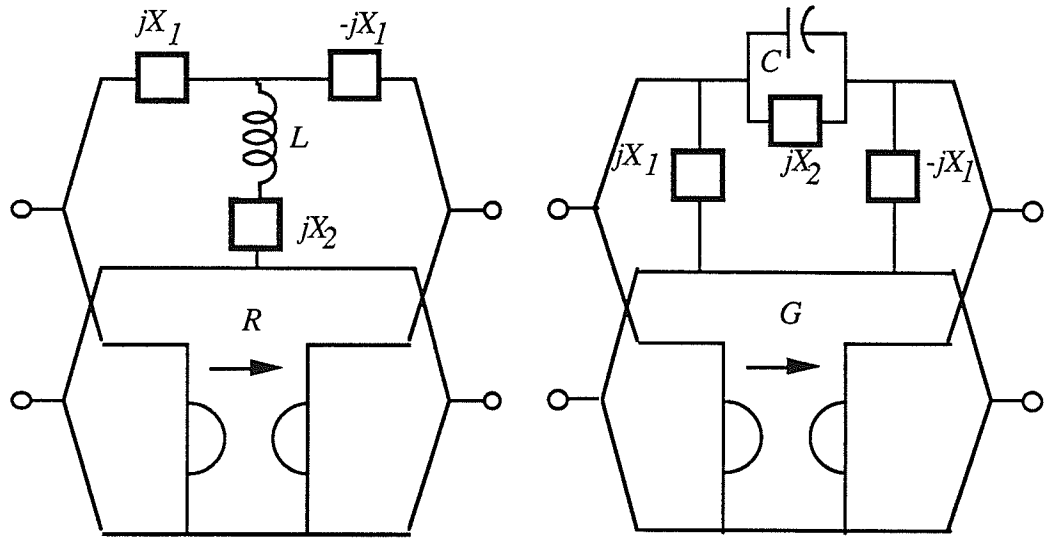

CWD Domain — Canonic Polynomials

$$\zeta e^{j\nu} = \frac{1+\phi_r + j\phi_i}{1-\phi_r - j\phi_i} \qquad \beta = \frac{1}{2}\frac{(1-\phi_r - j\phi_i)(\zeta^2-1)\eta e^{-j\theta}}{1-\eta^2\zeta e^{j(\nu-\kappa)}}$$

$$f_{RF} = z^{-1} - \zeta e^{j\nu}$$

$$h_{RF} = \frac{\Gamma(\zeta^2-1)\eta e^{j(\theta+\kappa)}}{1-\eta^2} \qquad e^{j\kappa} = \frac{1-\phi_r + j\phi_i}{1-\phi_r - j\phi_i} \qquad \Pi = \frac{1-\eta^2}{1-\zeta^2\eta^2}$$

$$g_{RF} = \Gamma e^{j\kappa}\left[\zeta e^{-j\nu} z^{-1} - \frac{1}{\Pi}\right] \qquad \Gamma = \frac{\left[\Pi(1-\eta^2\zeta e^{j(\nu-\kappa)})(1-\eta^2\zeta e^{j(-\nu+\kappa)})\right]^{1/2}}{1-\eta^2\zeta e^{j(-\nu+\kappa)}}$$

$$\sigma_{RF} = -e^{j\kappa}$$

CWD Domain — CWD Parameters

$$e^{j\Lambda} = \frac{\left[(1-\eta^2\zeta e^{j(-\nu+\kappa)})\Gamma + \eta^2\right]\zeta - e^{j(\nu-\kappa)}}{\left[(1-\eta^2\zeta e^{j(-\nu+\kappa)})\Gamma + \eta^2\right]\zeta - e^{j(-\nu+\kappa)}}\left[\frac{1-\Pi\zeta + (1-\zeta)e^{j(-\nu+\kappa)}\Gamma}{1-\Pi\zeta + (1-\zeta)e^{j(\nu-\kappa)}\Gamma^*}\right]^{1/2}$$

$$K = \zeta \qquad e^{j\mu} = \frac{\alpha^*}{\alpha}e^{-j(\tau+\nu)} \qquad \alpha\alpha^\dagger = \Pi$$

$$\alpha = \frac{\Pi\zeta - \Gamma e^{j(-\nu+\kappa)}}{1-\Gamma\zeta e^{j(-\nu+\kappa)}} \qquad e^{j\tau} = e^{j(-\theta+\Lambda-\nu)} \qquad \varepsilon = 1$$

Table 5.5: CWD equivalent of the CE1 and the CF1 sections.

CG1 and CH1 Sections		
Analog Symbol	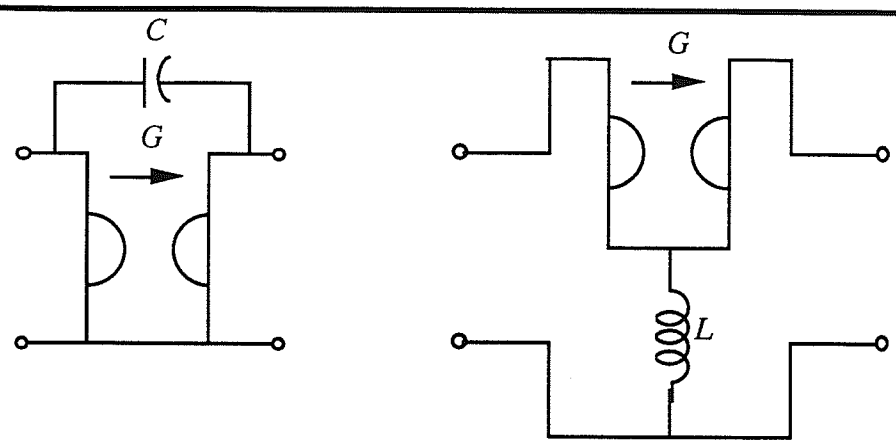	
	Canonic Polynomials	CWD Parameters
CWD Domain	$\beta = -2\dfrac{r\eta e^{-j\theta}}{(\eta^2+1)r+\eta^2-1}$ $f_{RF} = z^{-1} - K$ $h_{RF} = 4\dfrac{r\eta e^{j\theta}}{(1-\eta)^2\left[(1-\eta^2)(1-K^2\eta^2)\right]^{1/2}}$ $g_{RF} = \dfrac{-(1-K^2\eta^2)+(1-\eta^2)Kz^{-1}}{\left[(1-\eta^2)(1-K^2\eta^2)\right]^{1/2}}$ $\sigma_{RF} = -1$	$K = \dfrac{1+r}{1-r}$ $\alpha = \dfrac{-(1-\eta^2)}{\left[(1-\eta^2)(1-K^2\eta^2)\right]^{1/2}}$ $e^{j\mu} = e^{j\theta}$ $e^{j\tau} = e^{-j\theta}$ $\varepsilon = 1$

Table 5.6: CWD equivalent of the CG1 and the CH1 sections.

Special case: Transmission zero at $r = -1$		
	Canonic Polynomials	CWD Parameters
CWD Domain	$\beta = -\eta e^{-j\theta}$ $f_{RF} = z^{-1}$ $h_{RF} = -\dfrac{\eta e^{j\theta}}{\sqrt{-\eta^2+1}}$ $g_{RF} = -\dfrac{1}{\sqrt{-\eta^2+1}}$ $\sigma_{RF} = -1$	$K = 0$ $\alpha = -\sqrt{-\eta^2+1}$ $e^{j\mu} = e^{j\theta}$ $e^{j\tau} = e^{-j\theta}$ $\varepsilon = 1$

Table 5.7: Special case of the CG1 and the CH1 sections with $r = -1$.

Special case: Transmission zero at $r = 1$		
	Canonic Polynomials	CWD Parameters
CWD Domain	$\beta = -\dfrac{e^{-j\theta}}{\eta}$ $f_{RF} = 1$ $h_{RF} = \dfrac{e^{j\theta}}{\eta\sqrt{1-1/\eta^2}}$ $h_{RF} = \dfrac{1}{\sqrt{1-1/\eta^2}}$ $\sigma_{RF} = -1$	$\alpha = 0$ $K\alpha = -\sqrt{1-1/\eta^2}$ $e^{j\mu} = e^{j\theta}$ $e^{j\tau} = e^{-j\theta}$ $\varepsilon = 1$

Table 5.8: Special case of the CG1 and the CH1 sections with $r = 1$.

5.3.3 Complex Zero-Order (Constant) Complex Sections

The following will present the CWD equivalences of the zeroth-order (constant) complex sections as given in Tables 2.13-17. A constant section in a CWD network as discussed in Section 5.3 normally only appears as the last section in the network. All of the CWD constant sections have the form shown in Figure 5.21, that is, inverse conjugate multipliers in the signal paths.

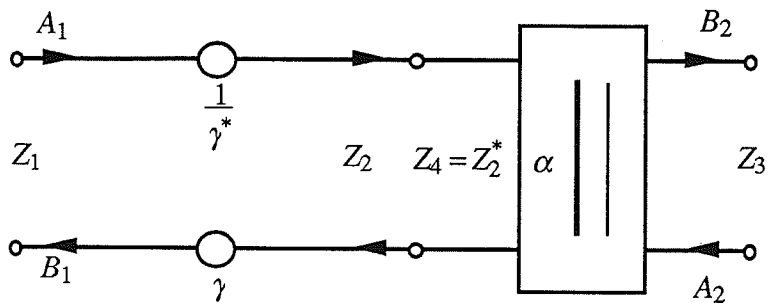

Figure 5.21: General form of a complex constant section.

For each section, the value of the multiplier and the reference impedance of port two in terms of port one will be given. Note that in general a complex two-port adaptor will be required between ports three and two in order to adapt the port reference to satisfy the port interconnection criterion (4.48) in a CWD network.

C0_π Section	
Analog Symbol	CWD Parameters
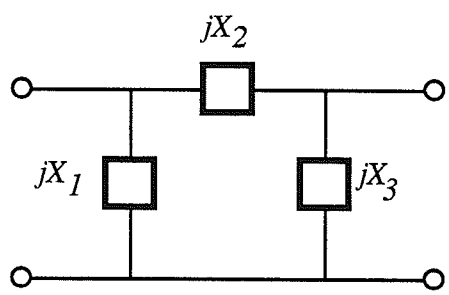	$\gamma = \frac{-j(X_3+X_2)X_1 + (X_3+X_2+X_1)\,Z_1^*}{-jX_3X_1}$ $Z_2 = \frac{X_3X_2X_1 + j(X_2+X_1)X_3Z_1^*}{j(X_3+X_2)X_1 - (X_3+X_2+X_1)\,Z_1^*}$

Table 5.9: CWD equivalent of the C0_π section.

C0_T Section	
Analog Symbol	CWD Parameters
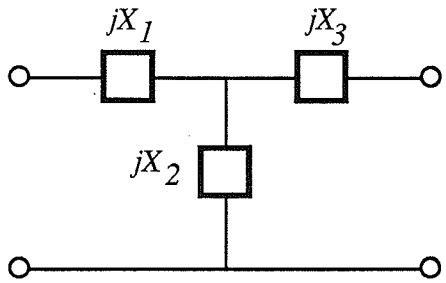	$\gamma = \frac{-j(X_2 + X_1) + Z_1^*}{-jX_2}$ $Z_2 = \frac{X_3X_2 + X_3X_1 + X_2X_1 + j(X_3 + X_2)Z_1^*}{j(X_2 + X_1) - Z_1^*}$

Table 5.10: CWD equivalent of the C0_T section.

C0_1 Section	
Analog Symbol	CWD Parameters
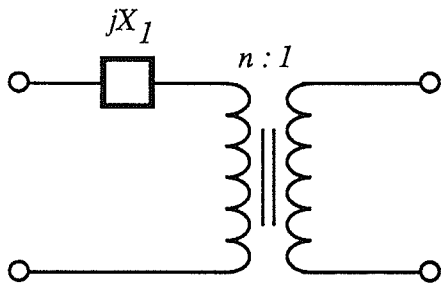	$\gamma = n$ $Z_2 = \frac{Z_1^* - jX}{n^2}$

Table 5.11: CWD equivalent of the C0_1 section.

C0_2 Section	
Analog Symbol	CWD Parameters
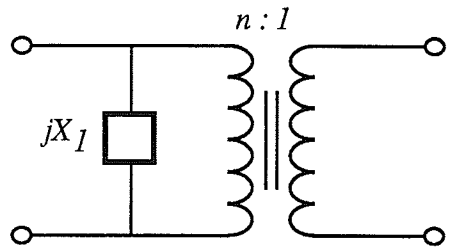	$\gamma = \frac{n\left(X + jZ_1^*\right)}{X}$ $Z_2 = \frac{XZ_1^*}{n^2\left(X + jZ_1^*\right)}$

Table 5.12: CWD equivalent of the C0_2 section.

T0 Section	
Analog Symbol	CWD Parameters
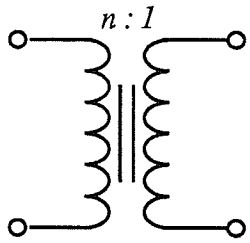	$\gamma = n^*$ $Z_2 = \frac{Z_1^*}{nn^*}$

Table 5.13: CWD equivalent of the T0 section.

5.3.4 CWD Ladder Realization

As mentioned in Chapter III, an elementary section is described by the section type, and the analog (discrete) domain canonic parameters as given by the location of the transmission zero ψ_0 (ω_0), the reflectance evaluated at the transmission zero $\eta e^{j\theta}$, and for reciprocal sections the delay evaluated at the transmission zero D (δ). The canonic parameters are assumed to have been calculated using the synthesis algorithm given in Chapter III.

The ordering of the sections is given by the order of the transmission zeros, and since

each section is determined by the canonic parameters mentioned in the preceding paragraph, the network is completely known. The discrete CWD ladder network is realized by interconnecting the transformed sections as given in Tables 5.1-5.8 while imposing the constraint of the port interconnection criterion.

The port reference of the left-most port is assumed to be normalized to unity. Since both ports of all dynamic two-ports contain the same port reference impedance as shown in Figures 5.18-20, the external port references of all dynamic sections will thus be equal to unity. The dynamic sub-network of the CWD ladder network is realized by simply interconnecting the canonic sections defined in the above tables as a function of the analog domain canonic parameters.

The last section, which is the section farthest to the right, is normally a constant section. The form of the last section is given in Figure 5.21, with the port reference of port two given in Tables 5.9-5.13. Notice that in general the impedance of port two is not unity. However, the value of the load resistance is assumed to be normalized to unity as shown in Figure 3.1. Thus, in order to connect the last section, a complex two-port adaptor is inserted at port two of Figure 5.21 in order to complete the CWD network.

5.3.5 Canonic Cascade Section Using Real two-port Adaptors

The canonic cascade section as given in Figure 5.18 can be decomposed into a section containing normalized real two-port adaptors and unimodular multipliers. The equivalence shown in Figure 4.19 along with the properties of linear networks can be used in order to derive the equivalent of the canonic cascade section as shown in Figure 5.22, where the real normalized two-port adaptor angles are given by

$$\begin{aligned} \alpha &= (\cos\beta_1)\, e^{j\gamma} \\ \cos\beta_1 &= |\alpha| \\ \cos\beta_2 &= |K\alpha| \end{aligned} \tag{5.9a,b,c}$$

and the unimodular constants are given by

$$\begin{aligned} e^{j\Gamma_1} &= \sqrt{\frac{1-K\alpha}{1-K\alpha^*}} \\ e^{j\Gamma_2} &= \sqrt{\frac{1-\alpha}{1-\alpha^*}} \end{aligned} \tag{5.10a,b,c}$$

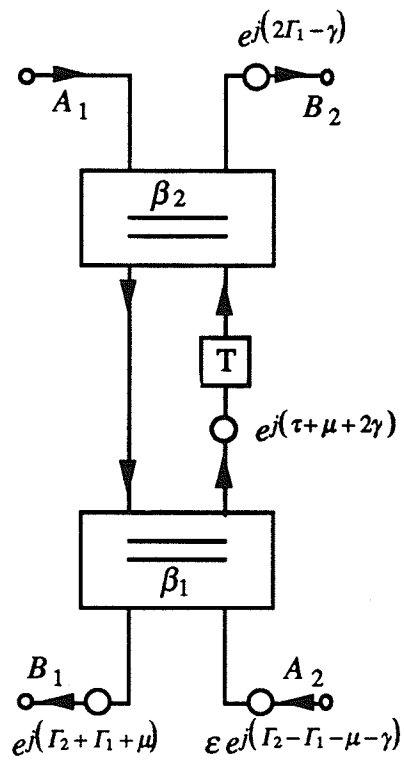

Figure 5.22: Equivalent of the canonic cascade section using real two-port adaptors.

Notice that the section requires two real two-port adaptors and four unimodular multipliers. The number of unimodular multipliers will be reduced by two in the following section. The respective port impedances are known after the decomposition from the discussion of the factorization of the complex two-port adaptor found in Section 4.6.4.

5.3.6 Minimum Multiplier Realization of CWD Filters

The section given above in Figure 5.22 is the most convenient form to use for the actual implementation of the dynamic sections given in Tables 5.1-5.8. The section can be simplified by taking advantage of the properties of linear flow graphs. However, since the form given in Figure 5.22 is inconvenient to use for this discussion, consider the general form of the section as given in the following figure as a function of four general unimodular multipliers with angles labelled θ_k, k=1(1)4.

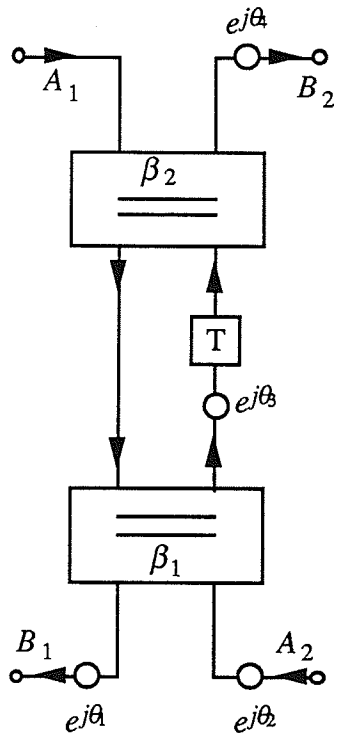

Figure 5.23: General form of the canonic cascade section using real two-port adaptors.

The canonic polynomials for this section are given by

$$f = z^{-1} - \frac{\cos\beta_1}{\cos\beta_2} e^{-j\theta_3}$$

$$h = \sin\beta_1 \tan\beta_2 e^{j(\theta_1 - \theta_3 - \theta_4)}$$

$$g = \frac{e^{-j(\theta_3 + \theta_4)}}{\cos\beta_2} - \cos\beta_1 e^{-j\theta_4} z^{-1}$$

$$\sigma = -e^{j(\theta_1 + \theta_2 - \theta_3 - \theta_4)} \qquad (5.11a,b,c,d)$$

Notice that the location of the transmission zero is defined by the unimodular multiplier associated with the delay (which gives the angle of the transmission zero) and the ratio of the multipliers of the two real two-port adaptors (which gives the magnitude of the transmission zero).

Consider the general section given above as a reciprocal section as shown in the following figure:

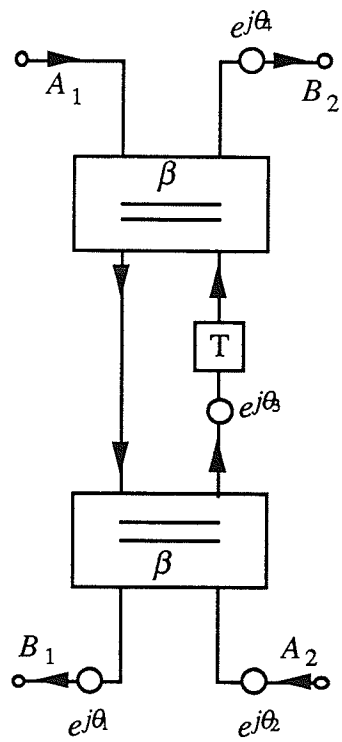

Figure 5.24: Reciprocal form of the canonic cascade section using real 2-port adaptors.

with the following canonic polynomials

$$f = z^{-1} - e^{-j\theta_3}$$

$$h = \sin\beta \tan\beta\, e^{j(\theta_1 - \theta_3 - \theta_4)}$$

$$g = \frac{e^{-j(\theta_3 + \theta_4)}}{\cos\beta} - \cos\beta\, e^{-j\theta_4} z^{-1}$$

$$\sigma = -e^{j(\theta_1 + \theta_2 - \theta_3 - \theta_4)} \qquad (5.12a,b,c,d)$$

Notice that the location of the transmission zero is now uniquely defined as the value of the unimodular multiplier associated with the delay.

Using either of the sections given in Figures 5.22-23, the four angles θ_k, k=1(1)4 can be determined for each dynamic section in a CWD realization by simply equating the values found in Figures 5.22 and 5.23. Let the angles of the lth section be labelled as θ_k^l.

The unimodular multiplier represented by θ_4^l (the top most unimodular multiplier in

Figure 5.23) can be drawn-through the remainder of the network to the right, in order to form an ideal complex transformer, with a turns ratio that is unimodular, as the last element to the right (that is, to the right of the last complex two-port adaptor associated with the constant section). This process will also introduce a contribution from θ_4^l into θ_2^l. Thus one unimodular multiplier per section can be removed.

Now consider two adjacent cascade sections labelled as the lth and the $(l+1)^{\text{th}}$ sections connected as described earlier. The θ_2^l angle from the lth section can be combined with the θ_1^{l+1} angle from the $(l+1)^{\text{th}}$ section for each of the dynamic sections of the network. The θ_1^1 angle from the first section will not change, and the θ_2^N angle from the last dynamic section can be combined with the constant section shown in Figure 5.21. This process will further remove one unimodular multiplier per section.

Thus, after the above simplifications, each dynamic section is a function of the canonic number of real parameters (that is, three and four parameters for reciprocal and non-reciprocal sections, respectively). The real parameters are found in the real angles β_1 and β_2 of the normalized two-port adaptors (for reciprocal sections the angles are equal removing one degree of freedom), and the two angles $\tilde{\theta}_1^l$ and θ_3^l are associated with the unimodular multipliers.

The remaining dynamic section will hereafter be known as the minimal characterization and is shown along with the final ideal complex transformer in the Figure 5.25. The unimodular angle becomes

$$\tilde{\theta}_1^l = \theta_1^l + \theta_2^{l-1} + \theta_4^{l-1}, \qquad l = 1(1)N \tag{5.13}$$

where

$$\theta_2^0 = \theta_4^0 = 0 \tag{5.14}$$

The angle of the complex ideal transformer is given by

$$\theta_T = -\left(\sum_{k=1}^{N} \theta_4^k\right) \tag{5.15}$$

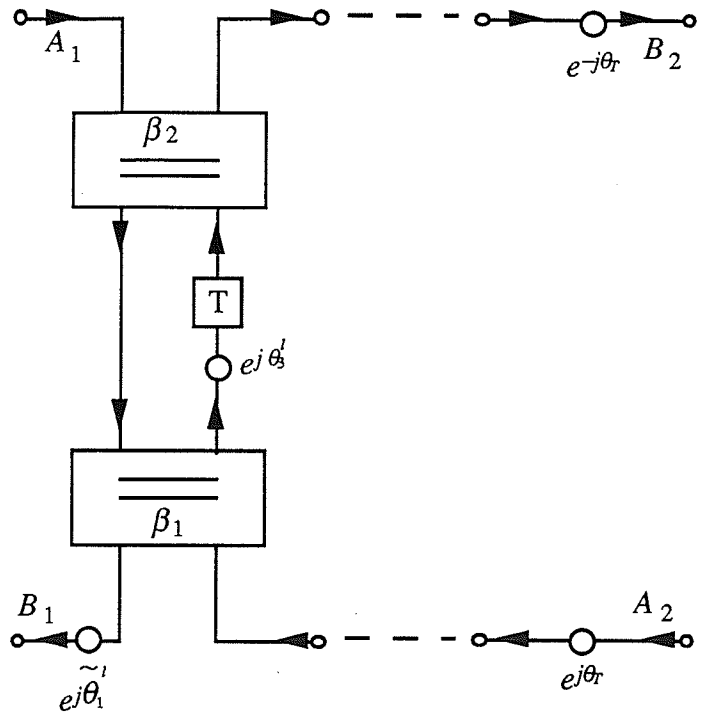

Figure 5.25: Minimal realization of the canonic cascade section.

The minimal form of the complex cascade section reduces in a simple manner to the real section given in [16] if all quantities are real, and thus the canonic cascade section is the most general form of a first-order section.

Now consider the last constant section as given in Figure 5.21. The section after the simplifications discussion above is shown in the following figure:

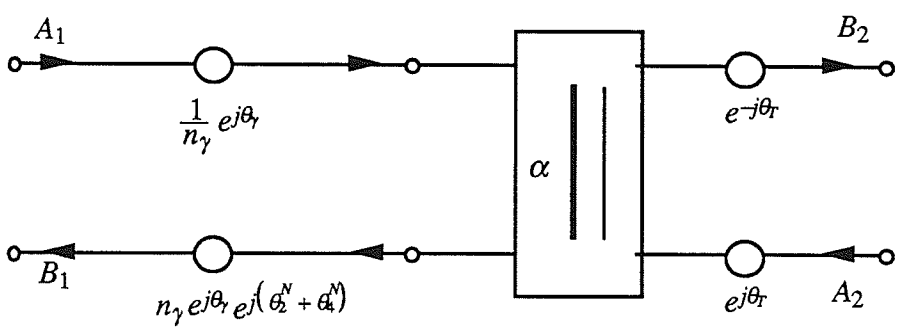

Figure 5.26: The last constant section in a CWD network.

where the turns ratio n_γ is real as defined from

$$\gamma = n_\gamma e^{j\theta_\gamma} \tag{5.16}$$

Notice that the unimodular multipliers from the last dynamic section as well as the last complex ideal transformer have been combined with this section. Now consider the real transformer on the left of the section in Figure 5.26 as well as the top unimodular multiplier, drawn through the section toward the right. This process will remove one multiplier from the section, leaving the following constant section in the minimal characterization.

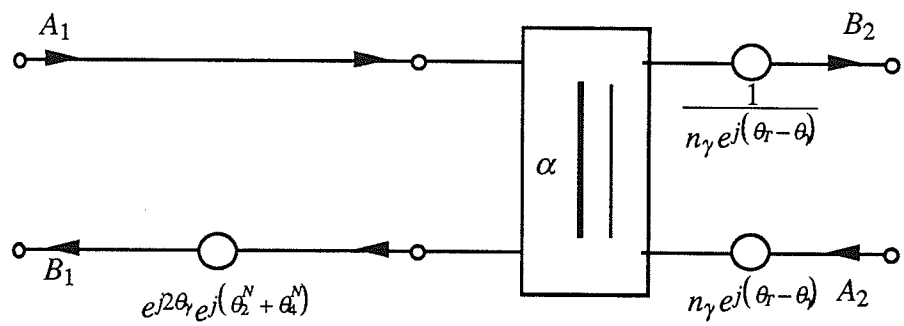

Figure 5.27: Minimal form of the last constant section in a CWD network.

where the last transformer on the right has a complex turns ratio of

$$n_{N+1} = n_\gamma e^{j(\theta_r - \theta_\gamma)} \tag{5.17}$$

Notice that the minimal form of the section contains three complex multipliers, however, ordinarily at least one can be ignored since the input at port two is usually zero when realizing a transmittance (however, this need not be the case).

The output of the voltage wave complex two-port adaptor can be efficiently computed using

$$X = A_1 - A_2$$

$$B_2 = (1-\alpha)X + A_2$$

$$B_1 = B_2 - \frac{(1-\alpha)}{(1-\alpha^*)}X \tag{5.18a,b,c}$$

which involves two complex multiplications and three complex additions/subtractions.

5.3.7 Quantization of the Minimal Form CWD Realization

Once the CWD network has been reduced to the minimal form as described above, the only elements that remain are terms involving sines and cosines (except the last two-port adaptor). They arise from the real normalized two-port adaptors associated with the dynamic sections and the real and imaginary parts of unimodular multipliers. Thus the quantization process involves the binary representation of sines and cosines. Note that the comments given in Section 5.1.3 about quantization also apply to this discussion.

Since the quantized form of a unimodular multiplier cannot have a magnitude of unity in general, the quantized form of a unimodular multiplier is passive and not lossless. A similar argument holds for the real normalized two-port adaptors [16]. From (5.18), the quantized form of the complex two-port adaptor involves two quantizations.

5.4 Design Examples Using the Minimal Form of the First-Order Sections

The following presents three design examples of lowpass Elliptical filters that are realized using the minimal form of the canonic cascade section. The finite transmission zeros for all examples are realized using the CC1_$j\phi$ first-order complex section. Note that the complex filter output for a real transfer function is real under nominal conditions.

The examples were generated by a computer program written by the author in the PASCAL computer language for the Macintosh computer. The program is capable of determining the quantized form of a CWD network which meets a set of frequency specifications. As with the examples given in Section 5.2, all attenuation plots are given as a function of the normalized frequency. That is, the frequency range plotted is from -0.5 to 0.5 (instead of $-\pi$ to π). Any frequency independent vertical shifts are removed in order to compare the shape of the plot to the nominal plot.

5.4.1 Elliptic Filter of Order Four

The 4th order Elliptic filter as given in Appendix A was quantized to the same frequency specifications (a passband ripple of 1.5 dB) as the example given in Sections 5.2.2.1 and 5.2.2.2. The two realizations given earlier required 7 bits (series adaptors) and 10 or 12 bits (parallel adaptors), while for this example using the cascade section throughout 6 bits are required. This implies that the cascade section is less sensitive than the realization method employing complex three-port adaptors.

The stopband and passband attenuation plots are shown in Figures 5.28 and 5.29, respectively. With the larger number of bits used for the earlier examples, both the stopband and passband plots appear to deviate less from the nominal plot than the example given here. Notice the quantized stopband plot is very close to the nominal, except the large nominal attenuation is not achieved. The quantized passband plot deviates from the nominal to the extent that the plot does not appear Elliptic in nature. This is a result of the low number of bits used.

This example was regenerated using 8 bits, which is a rough average of the bits required for the examples given in Sections 5.2.2.1 and 5.2.2.2, in order to compare the realizations. The stopband and passband attenuation plots are shown in Figures 5.30 and 5.31, respectively. Clearly, the quantized and nominal attenuation plots are difficult to distinguish in the stopband. The passband attenuation plot shows an improvement over the earlier examples. This again implies the cascade section is less sensitive than the realization using complex three-port adaptors.

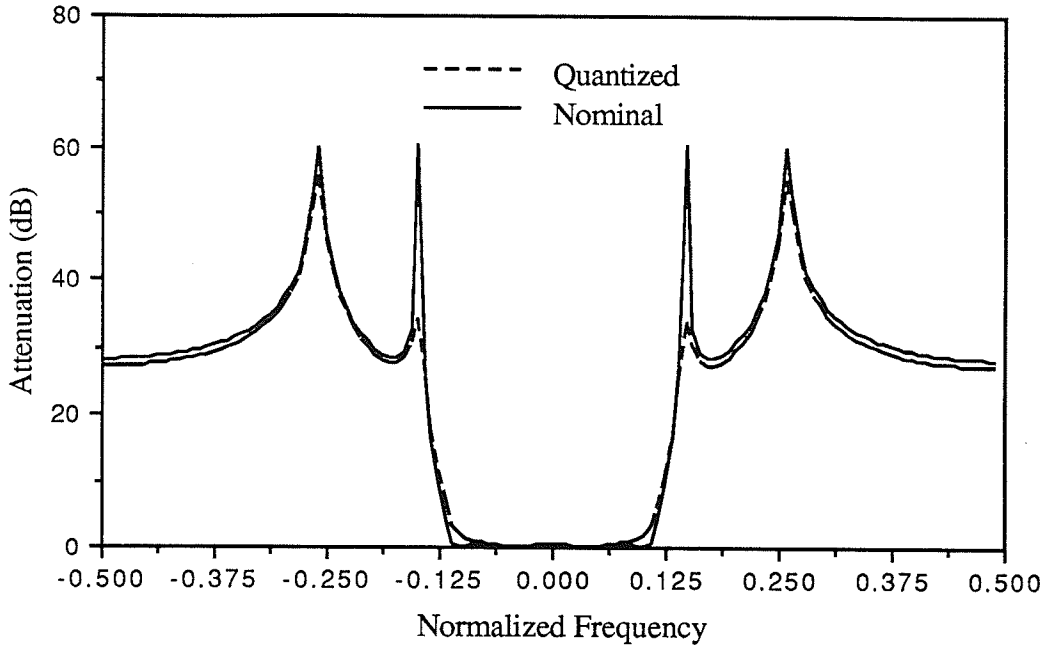

Figure 5.28: Stopband attenuation plot of the 4th order Elliptic filter using 6 bits.

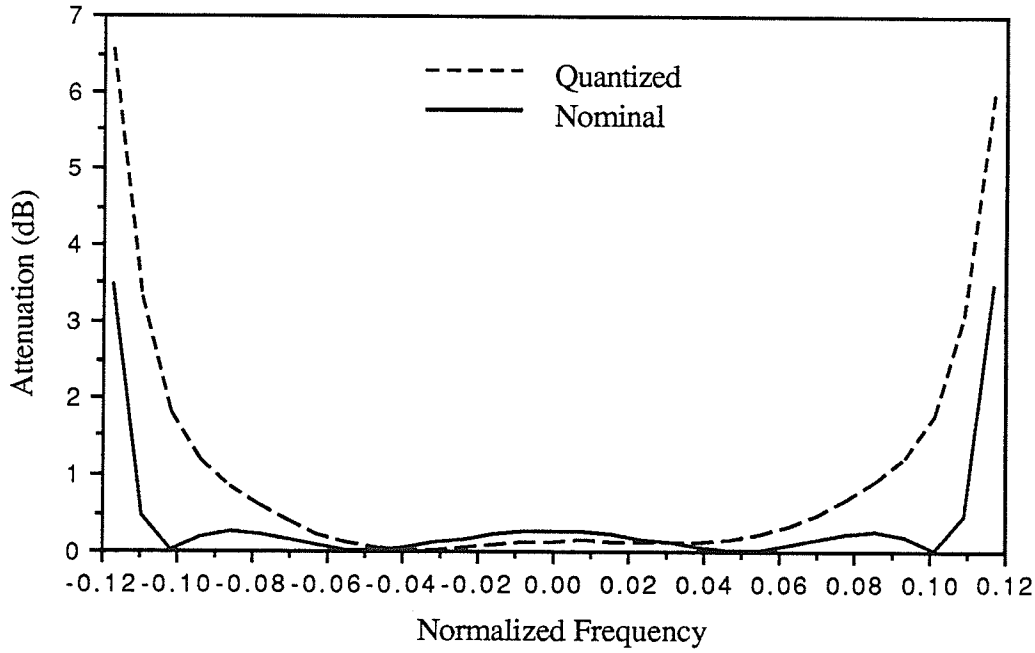

Figure 5.29: Passband attenuation plot of the 4th order Elliptic filter using 6 bits.

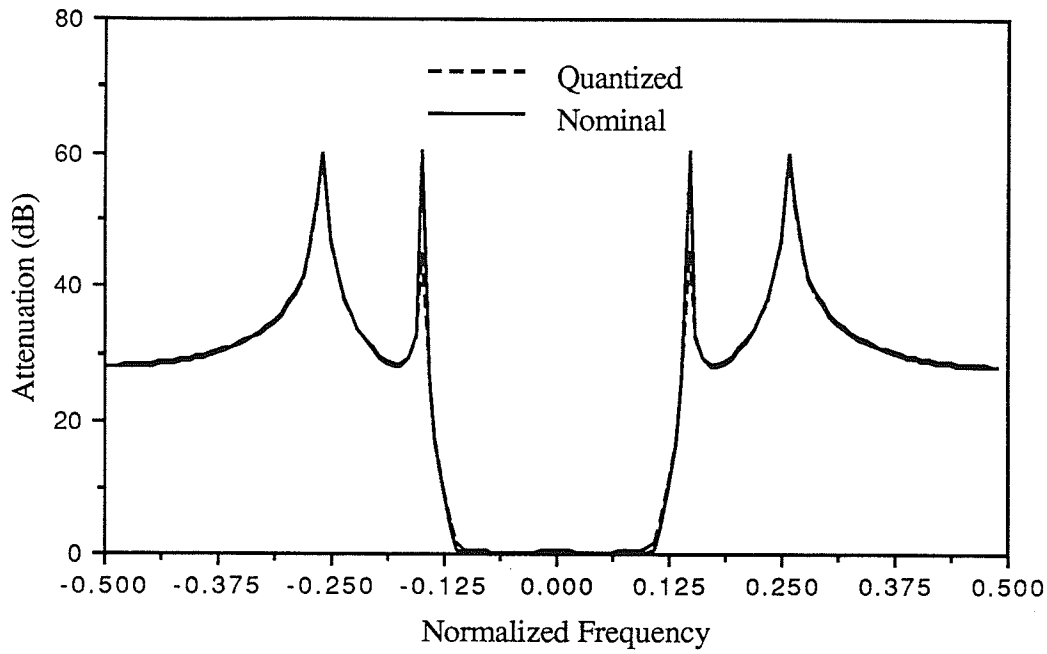

Figure 5.30: Stopband attenuation plot of the 4th order Elliptic filter using 8 bits.

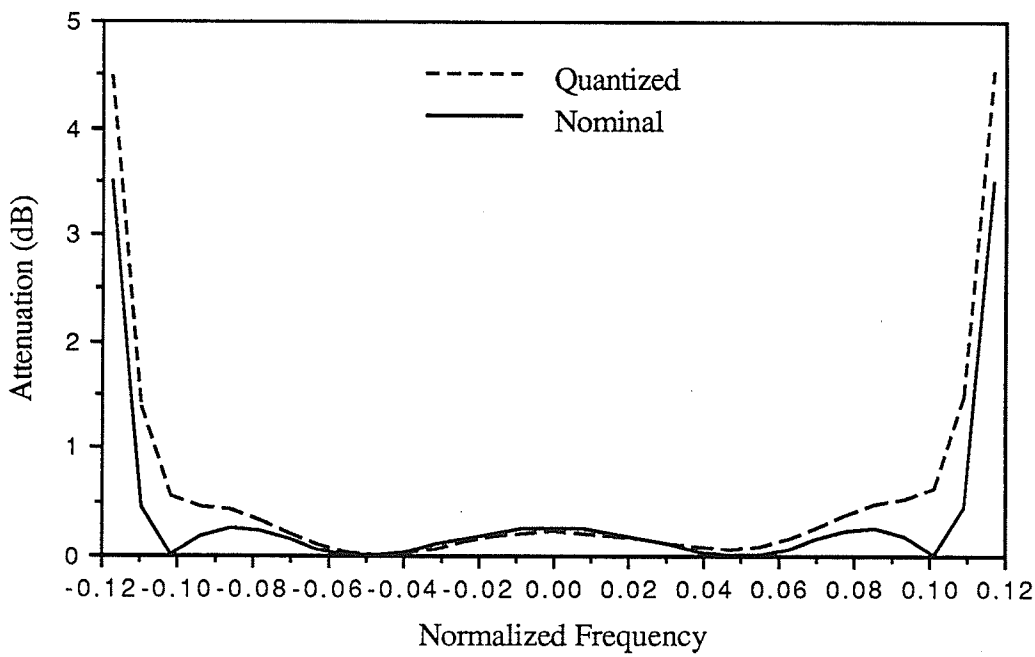

Figure 5.31: Passband attenuation plot of the 4th order Elliptic filter using 8 bits.

5.4.2 Elliptic Filter of Order Five

The 5th order Elliptic filter as given in Appendix A was quantized to the same frequency specifications (a passband ripple of 1.5 dB) as the example given in Section 5.2.2.4. Whereas the earlier example based on either the series or parallel three-port adaptor realization required 9 bits, this example based on the cascade section required 7 bits for the quantization. Again, this implies the insensitivity found earlier.

The stopband and passband attenuation plots are shown in Figures 5.32 and 5.33, respectively. With the larger number of bits used for the earlier example, both the stopband and passband plots appear to deviate less from the nominal plot than the example given here. Notice the quantized stopband plot is identical to the nominal. The quantized passband plot deviates from the nominal at the edges of the passband.

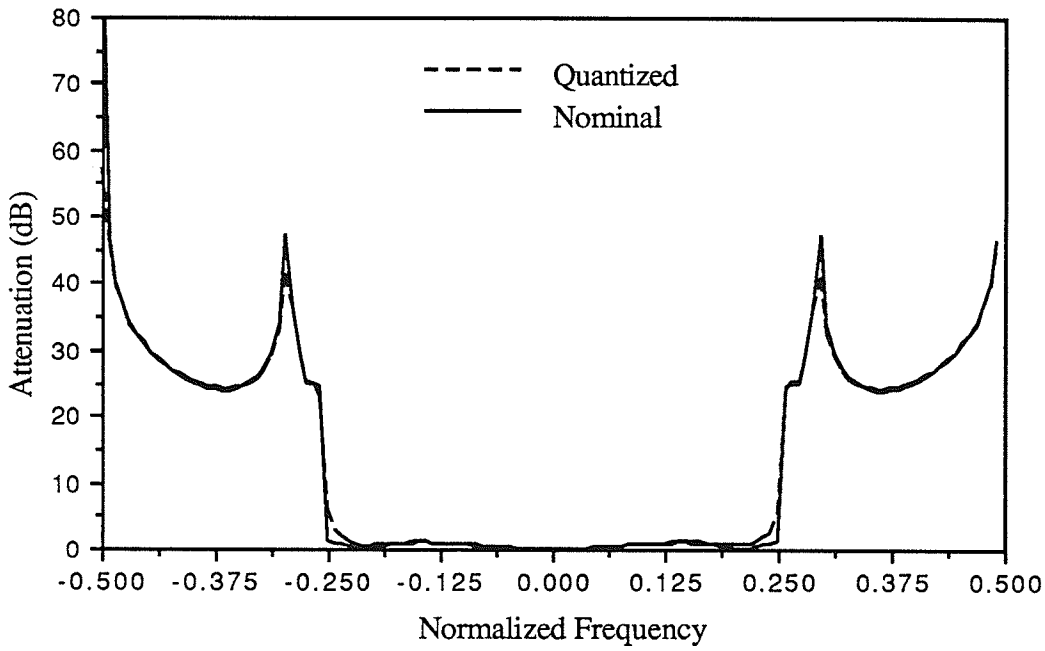

Figure 5.32: Stopband attenuation plot of the 5th order Elliptic filter using 7 bits.

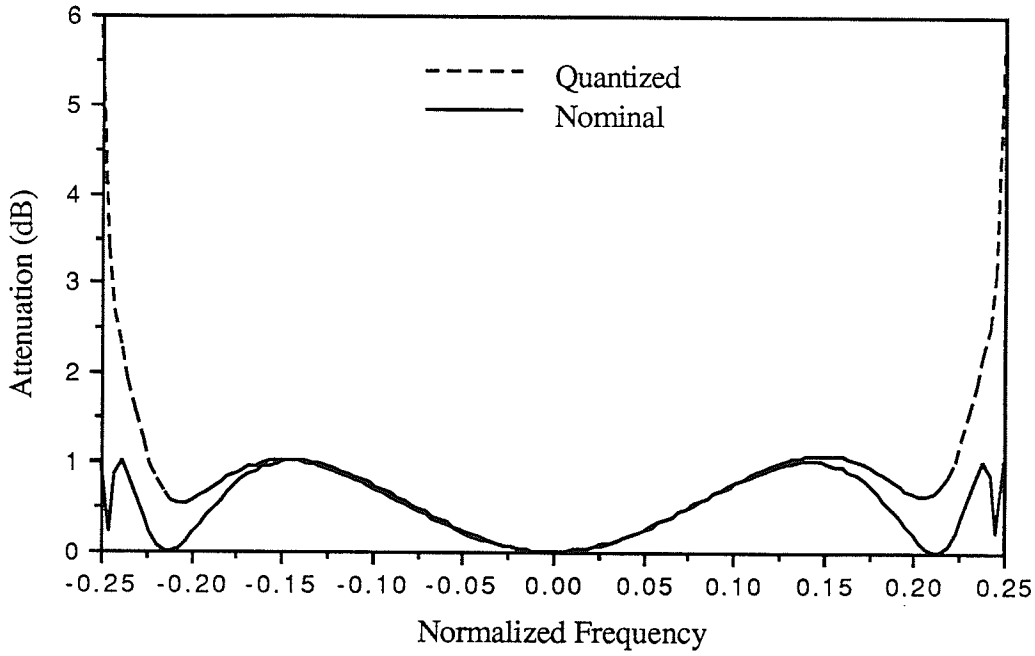

Figure 5.33: Passband attenuation plot of the 5th order Elliptic filter using 7 bits.

5.4.3 Elliptic Filter of Order Eight

The 8th order Elliptic filter as given in Appendix A was quantized to 9 bits in order to satisfy a passband ripple of 1.5 dB. The stopband and passband attenuation plots are shown in Figures 5.34 and 5.35, respectively.

From the stopband attenuation plot it is clear that the quantized and nominal plots are similar since the stopband attenuation is achieved. However, the locations of the transmission zeros have shifted slightly. The quantized passband attenuation plot is very similar to the nominal plot, except at the corners of the passband.

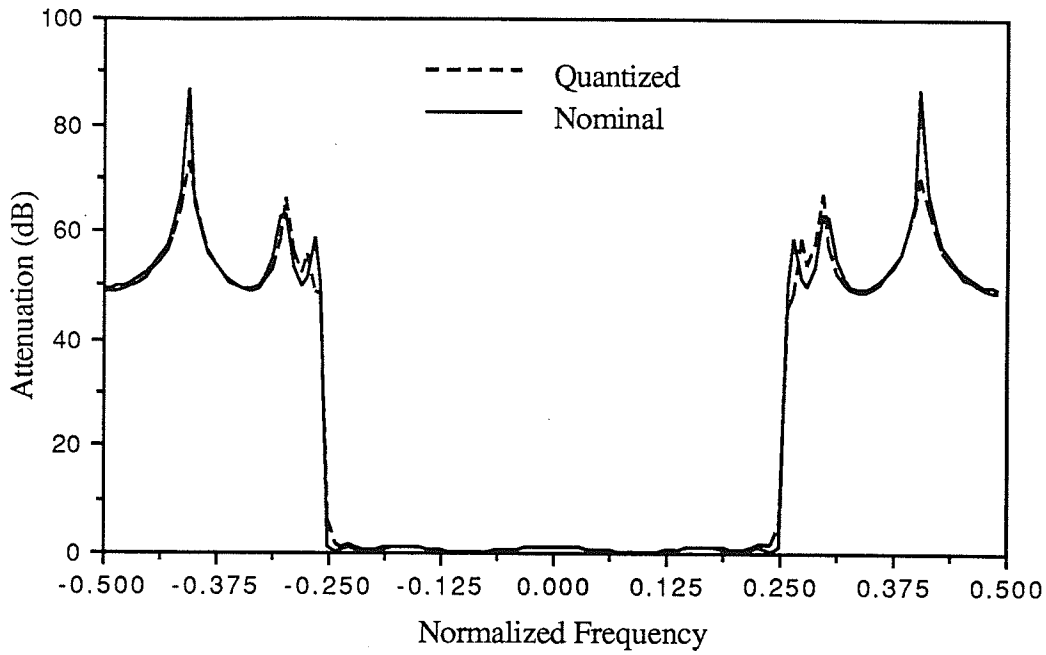

Figure 5.34: Stopband attenuation plot of the 8th order Elliptic filter using 9 bits.

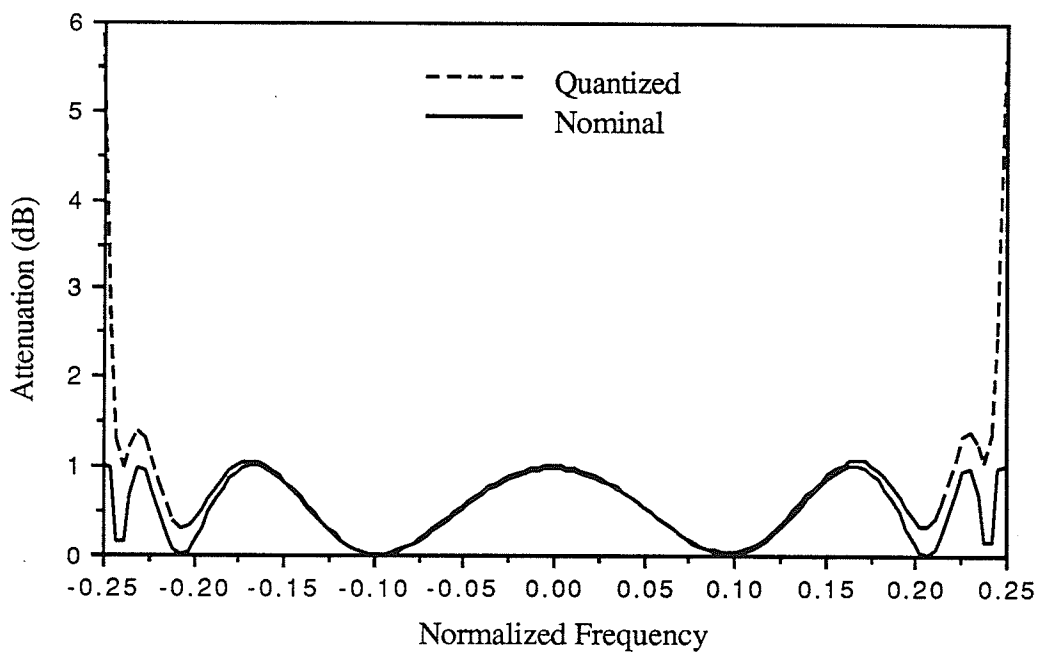

Figure 5.35: Passband attenuation plot of the 8th order Elliptic filter using 9 bits.

5.5 Comparison of the Two Realization Methods

Several observations can be made when comparing the complex first-order section realization methods using either the three-port adaptor or the cascade section. The two realization methods discussed in Sections 5.1 and 5.3 are capable of realizing the same reciprocal ladder filter. However, nonreciprocal filters must be realized using the cascade section. Thus the comparison of the two realization methods will be limitted to reciprocal networks. Notice that for this discussion either the series or the parallel three-port adaptor realization can be considered equivalent with respect to the number of calculations required and the number of independent quantizations needed. Thus the discussion of the three-port adaptor method applies to either adaptor type.

The networks derived from the three-port adaptor approach must be scaled after the construction of the network with real scaling transformers. This requires additional computations. However, the cascade section is composed of normalized elements and thus external scaling is not required.

The realization method using the three-port adaptor approach is based on the element-by-element transformation of one of the two sections shown in Figure 5.36,

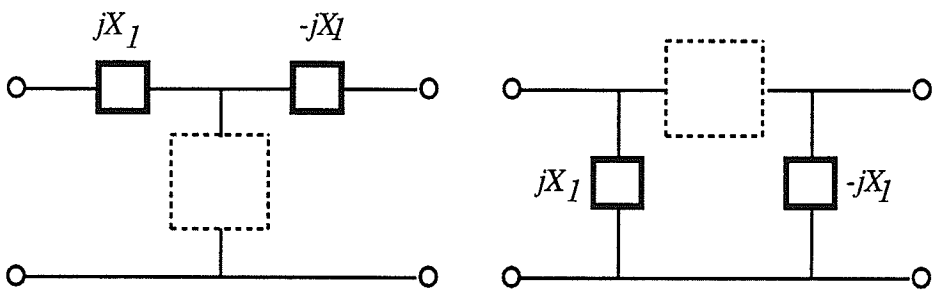

Figure 5.36: General first-order complex sections.

where the dashed box represents a one-port dynamic element possibly in combination with an imaginary resistor. If both sections realize the same transmission zero, the section on the left is usually the dual of the section on the right. Regardless of which section is used to realize a transmission zero, the mapping presented in Figures 5.3-4 and the equivalences between the three-port adaptors and combinations of two-port adaptors possibly with external multipliers given in Section 4.6.6, lead to the general form of the CWD section shown in Figure 5.37a). Note that it is assumed that the three-port adaptors were normalized before the adaptor equivalences were applied.

The section shown in Figure 5.37a) represents the direct transformation of a first-order section after making use of the adaptor equivalences. The complex multipliers can be expressed in polar form as $\gamma_1 = n_1 e^{j\theta_1}$ and $\gamma_2 = n_2 e^{j\theta_2}$, creating two constant two-port sections on each side of the central section containing the real two-port adaptors. Since the two sections consist of a real transformer and a section with equal unimodular multipliers,

the section shown in Figure 5.37b) can be derived from a). Note that the real transformer on the left is combined with the transformer on the right. By applying suitable flowgraph transformations on Figure 5.37b), the flowgraph resulting from the three-port adaptor approach can be made similar to the canonic section flowgraph (the ideal transformer on the right can be ignored since it represents scaling).

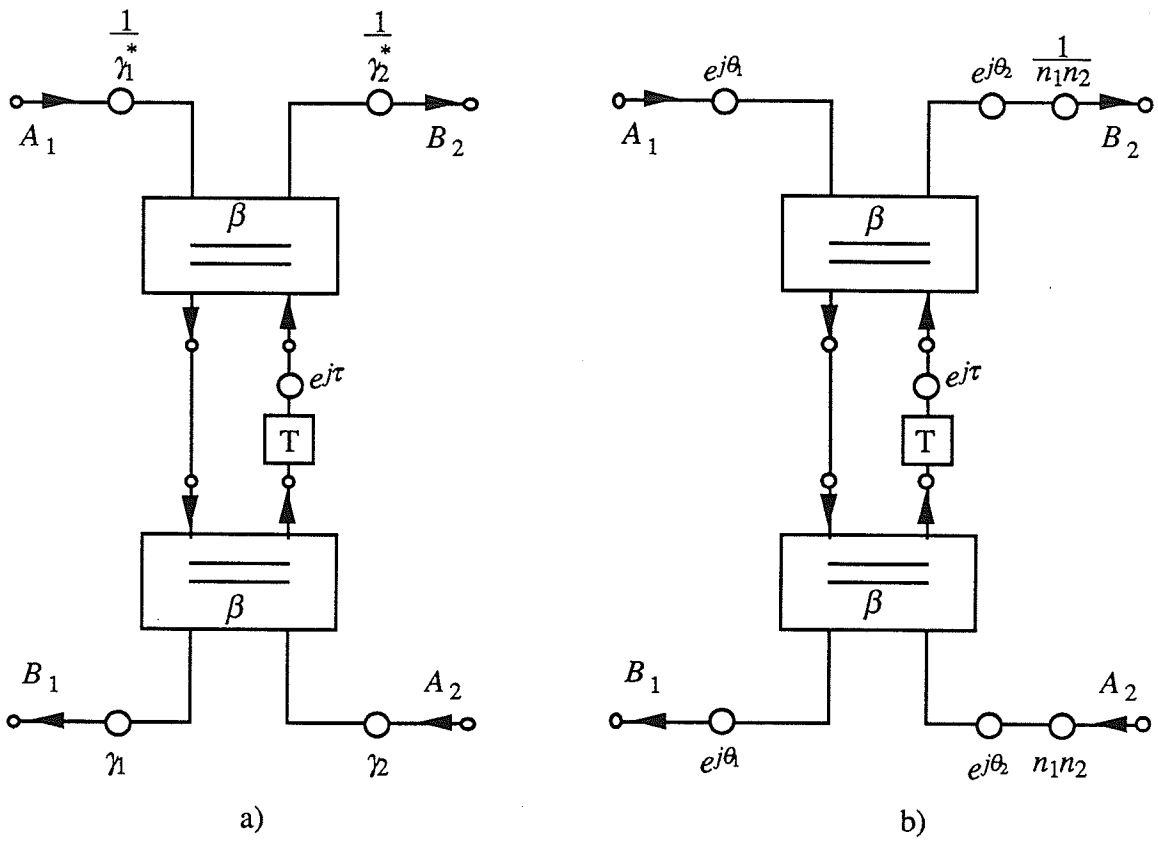

Figure 5.37: General form of the transformation of a complex first-order section, a) Direct transformation, b) Equivalent of the direct transformation.

The number of computations required for each approach can be compared. For the comparison, assume that the three-port and two-port adaptor equivalences are not applied. In the following, assume that all signals that are processed are complex. Also, assume that a complex multiplication requires four real multiplications and two real additions (the number of multiplications can be reduced to three at the expense of more additions). Similarly, assume that a complex addition requires two real additions.

The three-port adaptor method of realization using unnormalized adaptors requires five complex multiplications, one real multiplication and four complex additions operating on complex signals. This is equivalent to 22 real multiplications and eight real additions. The canonic cascade section in the minimal characterization requires two complex

multiplications, eight real multiplications and four complex additions. This is equivalent to 24 real multiplications and eight real additions. Thus, it is clear that the cascade section requires two more real multiplications than the method using three-port adaptors. The added computations from the scaling of the three-port adaptors was not included in this analysis. Note that if the normalized form of the cascade section is not used, the series three-port adaptor with a reflection-free port (a function of one real multiplier) can be used to replace the two two-port adaptors in Figure 5.24 in order to decrease the number of required computations.

The number of independent real quantizations for both methods are given by six and 11 for the cascade and three-port adaptor realization methods, respectively (note that the cascade section was assumed to be reciprocal for the comparison). Thus the cascade section requires nearly half the number of independent quantizations that the three-port adaptor method requires, which leads to the lower sensitivity that was observed in the examples in Section 5.3.

The preferred realization method uses the canonic cascade section because of the fewer real independent quantizations that are required and the uniformity of the sections. That is, a basic block structure that is, in general, a function of four real parameters is capable of realizing any of the real or complex first-order elementary sections. The preferred method of realization for a particular application will of course depend on the constraints placed on the operation of the implemented network.

The above discussion shows by construction that it is possible to realize a general complex filter without alteration (to make it one-real) using complex port impedances and the related structures. This gives the sufficiency of Theorem 1.1 in Chapter I of allowing complex port impedances and thus completes the proof. Thus, the imaginary part of the port impedance can be used simultaneously to guarantee computability of the complex WD network and to simplify the CWD elements (real port impedances with complex networks do not allow this freedom). Also, the port impedances of a WD structure based on port impedances are necessarily complex, unless the network is one-real.

Chapter VI

Conclusion

This thesis has developed a new theory for complex wave digital (WD) filters allowing the realization of general complex reference networks without alteration (the networks do not require the property of one-realness). A port reference impedance is now allowed to be complex, containing a positive resistance and an imaginary resistance, or constant reactance. The voltage wave incident and reflected wave variables, A and B, are redefined and the familiar concept of the WD mapping of analog networks is preserved. The generalization reduces to the known theory of real WD filters if all quantities are real, and a stability theory exists. The resulting definition of power and the power-wave description are the same as suggested by Fettweis. A motivation for the generalization is found in the additional degree of freedom in the choice of the imaginary part of the port reference (that is, there is an additional parameter) which can be used simultaneously to guarantee computability of the complex WD network and to simplify the CWD elements (real port references with complex networks do not allow this freedom).

The new definitions of the incident and reflected wave variables lead to new definitions for the complex n-port series and parallel adaptors which allow complex port references. The complex series three-port adaptor with a reflection-free port has the same scattering matrix as the real case. Thus, no extra computations are needed, that is, no penalty is imposed for having free parameters in the port references. The complex three-port parallel adaptor is more complicated than the series adaptor. Equivalences between the three-port adaptors exist only when each adaptor contains a reflection-free port.

Many useful complex dynamic and non-dynamic one-ports, as well as non-dynamic two-ports that do not have a real WD equivalent are now defined. The analog series connected imaginary resistor when viewed as a two-port has a straight forward complex WD equivalent of a simple pass through connection. Similarly, the analog parallel connected imaginary resistor when viewed as a two-port has a WD equivalent of inverse conjugate multipliers in the signal paths which is a hybrid form of scaling. Thus the definition of the voltage waves have a bias towards series connections. Similarly, the dual definition of complex current waves have a bias towards parallel connections.

The complex reference networks are designed using the new generalization to the complex domain of the synthesis algorithm given in [16]. The algorithm is novel since it

does not require the use of zero-finding or polynomial manipulation routines associated with the determination of intermediate polynomials, namely, it is based entirely on polynomial evaluations. Complex networks are derived by using general first-order complex sections which are capable of independently realizing a transmission zero anywhere in the complex plane. It is found that a more judicious representation for a complex elementary section, from the viewpoint of network synthesis, are the canonic parameters rather than the lumped-element parameters. The canonic parameters completely characterize a section and are given by the location of the transmission zero, the reflectance evaluated at the transmission zero, and for reciprocal sections, the return group delay (or simply the delay) evaluated at the transmission zero.

A complex WD ladder network is realized from a complex reference filter using one of two methods. The first method maps a complex reciprocal reference network to the equivalent CWD network on an element-by-element basis. This inherently requires the use of complex three-port series and parallel adaptors. The second method maps a complex reciprocal or non-reciprocal elementary section as a dynamic two-port to the CWD equivalent. This method requires at most two real normalized two-port adaptors and two unimodular multipliers for each dynamic section, which is referred to as the canonic cascade section. From the examples presented, the realization method using the cascade section appears less sensitive to binary quantizations than the method using three-port adaptors.

Appendix A

Complex Analog Design Examples

Few examples of complex analog networks exist in the literature, and no examples exist for either the realizations of frequency shifted networks or the realizations of networks with the phase of the h polynomial scaled by an arbitrary real constant. In order to give examples of complex analog networks and to support the observations made in this thesis, the following Appendix contains five examples of classical filters: Elliptic filters of orders 4, 5, 8, 14, and a Chebyshev filter of order 5.

Each filter is realized using the following:

a) real sections throughout.
b) real sections with each dynamic section having port two reflection-free (RF).
c) complex sections throughout
d) complex sections with each dynamic section having port two reflection-free.

In addition, the 4th order Elliptic filter and the 5th order Chebyshev filter are realized with four different phase shifts of the h polynomial, namely 45°, 90°, 135°, and 180°. The 5th order Elliptic is realized an additional four times with each of the four first-order reciprocal sections CA1_jw, CB1_jw, CC1_jw and CD1_jw. Also, realizations are given for four different $j\phi$ axis shifts for the 5th and 8th order Elliptic examples, namely -j2, -j1, +j1 and +j2. The 8th order Elliptic is realized a final time with the f and h polynomials exchanged in order to create a network with non-reciprocal sections.

For each type of filter, the canonic polynomials and the attenuation stopband plots are given, where the frequency axis of the attenuation plots has a range of 2π (digital frequencies). The passband plot is also given for the 14th order Elliptic example from [16] since it is a very narrow band filter and the passband cannot be detected in the stopband plot.

For all cases, both the canonic parameters and the lumped element values are given. The canonic parameters are given with a sufficient accuracy to calculate the lumped element values to a higher accuracy than the one presented if this becomes necessary.

Description: 4 order Elliptic canonic polynomials		
	g	
K	2.6000000000000000000000e+1	+j0.0000000000000000000000e+0
zeros	-4.5788990000000000000000e-2	+ j3.7160221000000000000000e-1
	-4.5788990000000000000000e-2	- j3.7160221000000000000000e-1
	-1.9994624000000000000000e-1	+ j2.0762199000000000000000e-1
	-1.9994624000000000000000e-1	- j2.0762199000000000000000e-1
	h	
K	2.5980762113533159400000e+1	+j 0.0000000000000000000000e+0
zeros	-6.1870506475141583520000e-2	+j 1.6294482941800889330000e-1
	-6.1870506475141583520000e-2	-j 1.6294482941800889330000e-1
	1.6462049838829611380000e-2	+j 3.3884235499294729630000e-1
	1.6462049838829611380000e-2	-j 3.3884235499294729630000e-1
	f	
K	1.0000000000000000000000e+0	+j 0.0000000000000000000000e+0
zeros	0.0000000000000000000000e+0	+j 5.0425225000000000000000e-1
	0.0000000000000000000000e+0	-j 5.0425225000000000000000e-1
	0.0000000000000000000000e+0	+j 1.0658983300000000000000e+0
	0.0000000000000000000000e+0	-j 1.0658983300000000000000e+0

Table A.1: 4th order Elliptic canonic polynomials.

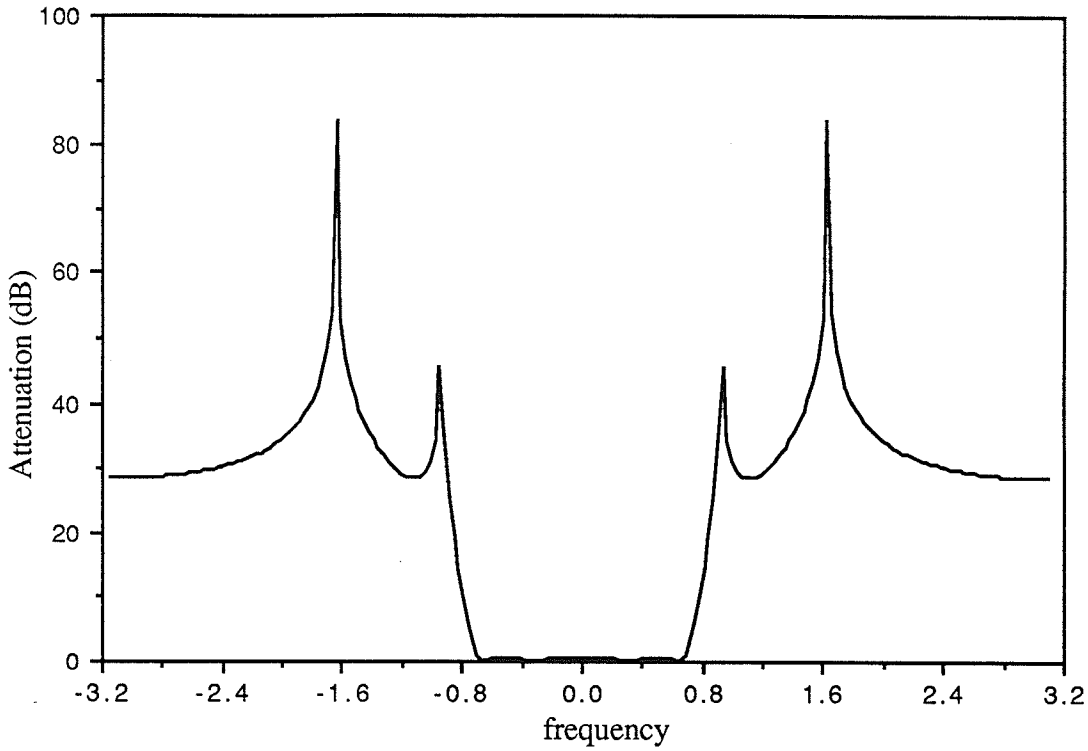

Figure A.1: 4th order Elliptic fullband plot.

Description: 4 Elliptic Canonic Parameters				
	Section	$\lvert\rho\rvert$	Arg$\{\rho\}$	d
1	BRUNE2	1.000000000000000	1.098456804919560	4.279780320238098
2	BRUNE2	1.000000000000000	0.232172253166848	0.244918865281266

Table A.2: 4th order Elliptic canonic parameters with real sections.

Description: 4 Elliptic Canonic Parameters RF port 2				
	Section	$\lvert\rho\rvert$	Arg$\{\rho\}$	d
1	BRUNE2	1.000000000000000	1.098456804919560	4.279780320238098
2	BRUNE2	1.000000000000000	0.086764297935227	0.092239444290098

Table A.3: 4th order Elliptic canonic parameters with real sections and port 2 RF.

Description: 4 Elliptic Canonic Parameters				
	Section	$\lvert\rho\rvert$	Arg $\{\rho\}$	d
1	CC1_jw	1.00000000	1.09845680	4.27978032
2	CC1_jw	1.00000000	-0.49838743	2.29731862
3	CC1_jw	1.00000000	0.04031452	0.04290071
4	CC1_jw	1.00000000	-0.00254213	0.00270594

Table A.4: 4th order Elliptic canonic parameters with complex sections.

Description: 4 Elliptic Canonic Parameters RF port 2				
	Section	$\lvert\rho\rvert$	Arg $\{\rho\}$	d
1	CC1_jw	1.00000000	1.09845680	4.27978032
2	CC1_jw	1.00000000	-0.84451750	2.45619364
3	CC1_jw	1.00000000	-0.00108656	0.09223944
4	CC1_jw	1.00000000	-0.14432050	0.12629905

Table A.5: 4th order Elliptic canonic parameters with complex sections and port 2 RF.

Description: 4 Elliptic Canonic Parameters h 45				
	Section	$\lvert\rho\rvert$	Arg $\{\rho\}$	d
1	CC1_jw	1.00000000	1.88385497	4.27978032
2	CC1_jw	1.00000000	0.28701073	2.29731862
3	CC1_jw	1.00000000	0.82571268	0.04290071
4	CC1_jw	1.00000000	0.78285603	0.00270594

Table A.6: 4th order Elliptic canonic parameters with h polynomial scaled by 45 °.

Description: 4 Elliptic Canonic Parameters h 90				
	Section	$\lvert\rho\rvert$	Arg $\{\rho\}$	d
1	CC1_jw	1.00000000	2.66925313	4.27978032
2	CC1_jw	1.00000000	1.07240890	2.29731862
3	CC1_jw	1.00000000	1.61111085	0.04290071
4	CC1_jw	1.00000000	1.56825419	0.00270594

Table A.7: 4th order Elliptic canonic parameters with h polynomial scaled by 90 °.

Description: 4 Elliptic Canonic Parameters h 135				
	Section	$\lvert\rho\rvert$	Arg $\{\rho\}$	d
1	CC1_jw	1.00000000	-2.82853401	4.27978032
2	CC1_jw	1.00000000	1.85780706	2.29731862
3	CC1_jw	1.00000000	2.39650901	0.04290071
4	CC1_jw	1.00000000	2.35365236	0.00270594

Table A.8: 4th order Elliptic canonic parameters with h polynomial scaled by 135 °.

Description: 4 Elliptic Canonic Parameters h 180				
	Section	$\lvert\rho\rvert$	Arg $\{\rho\}$	d
1	CC1_jw	1.00000000	-2.04313585	4.27978032
2	CC1_jw	1.00000000	2.64320522	2.29731862
3	CC1_jw	1.00000000	-3.10127813	0.04290071
4	CC1_jw	1.00000000	3.13905052	0.00270594

Table A.9: 4th order Elliptic canonic parameters with h polynomial scaled by 180 °.

Description: 4 order Elliptic Lumped Element Values				
	Section	L	C	n
1	BRUNE2	1.89293934	0.86386147	2.40504666
2	BRUNE2	7.53813225	0.00736179	15.86067023
3	T0	-	-	1.36269167

Table A.10: 4th order Elliptic lumped element values with real sections.

Description: 4 order Elliptic Lumped Element Values RF port 2				
	Section	L	C	n
1	BRUNE2	1.89293934	0.86386147	2.40504666
1	T0	-	-	0.61013108
2	BRUNE2	20.24964667	0.00274050	15.86067023
2	T0	-	-	1.16993751
3	T0	-	-	1.90902573

Table A.11: 4th order Elliptic lumped element values with real sections and port 2 RF.

Description: 4 order Elliptic Lumped Element Values					
	Section	*C*	*X1*	*X2*	*n*
1	CC1_jw	2.94148863	1.63386926	0.67419415	-
2	CC1_jw	1.22304846	-3.92953181	-1.62146840	-
3	CC1_jw	0.02145907	49.60319911	43.71930500	-
4	CC1_jw	0.00135297	-786.73998336	-693.41747924	-
5	T0	-	-	-	51.98076211

Table A.12: 4th order Elliptic lumped element values with complex sections.

Description: 4 order Elliptic Lumped Element Values RF port 2					
	Section	*C*	*X1*	*X2*	*X3*
1	CC1_jw	2.94148863	1.63386926	0.67419415	-
1	C0Pi	-	-0.97376318	0.11613691	0.77049151
2	CC1_jw	1.47599622	-2.22576122	-1.34359046	-
2	C0Pi	-	0.64962572	-0.13581892	-0.47214844
3	CC1_jw	0.04611974	-1840.673358	20.34217602	-
3	C0Pi	-	0.25969432	-0.20155609	-0.05524646
4	CC1_jw	0.06347949	-13.83398363	-14.77919435	-
4	C0Pi	-	0.06326706	-0.04735778	-0.01586175
5	C0Pi	-	-0.01620919	0.00771929	0.00849377

Table A.13: 4th order Elliptic lumped element values with complex sections and RF port 2.

Description: 4 order Elliptic Lumped Element Values *h* 45					
	Section	*C*	*X1*	*X2*	*X3*
1	CC1_jw	6.18438600	0.72738367	0.32066796	-
2	CC1_jw	1.17264316	6.92047958	-1.69116617	-
3	CC1_jw	0.02556607	2.28294161	36.69613287	-
4	CC1_jw	0.00158344	2.42291967	-592.49223487	-
5	C0Pi	-	2.77140635	18.37117307	0.42358027

Table A.14: 4th order Elliptic lumped element values with *h* polynomial scaled by 45°.

Description: 4 order Elliptic Lumped Element Values *h* 90					
	Section	*C*	*X1*	*X2*	*X3*
1	CC1_jw	39.08700486	0.24066087	0.05073641	-
2	CC1_jw	1.55433252	1.68270295	-1.27587528	-
3	CC1_jw	0.04470238	0.96047681	20.98715606	-
4	CC1_jw	0.00269908	1.00254537	-347.59068052	-
5	C0Pi	-	1.03923048	25.98076211	1.03923048

Table A.15: 4th order Elliptic lumped element values with *h* polynomial scaled by 90 °.

Description: 4 order Elliptic Lumped Element Values *h* 135					
	Section	*C*	*X1*	*X2*	*X3*
1	CC1_jw	88.05416979	-0.15782037	0.02252175	-
2	CC1_jw	3.20445722	0.74749004	-0.61886750	-
3	CC1_jw	0.16190853	0.39079026	5.79448015	-
4	CC1_jw	0.00918224	0.41570350	-102.17282528	-
5	C0Pi	-	0.42358027	18.37117307	2.77140635

Table A.16: 4th order Elliptic lumped element values with *h* polynomial scaled by 135 °.

Description: 4 order Elliptic Lumped Element Values *h* 180					
	Section	*C*	*X1*	*X2*	*n*
1	CC1_jw	7.85238847	-0.61204408	0.25255175	-
2	CC1_jw	18.88536070	0.25448324	-0.10500908	-
3	CC1_jw	52.79956474	-0.02015999	0.01776863	-
4	CC1_jw	837.43648455	0.00127107	-0.00112029	-
5	T0	-	-	-	0.01923789

Table A.17: 4th order Elliptic lumped element values with *h* polynomial scaled by 180 °.

Description: 5 order Chebyshev canonic polynomials		
	g	
K	8.141554238553398	+j 0.000000000000000
zeros	-0.089458362200190	+j 0.990107112003389
	-0.234205032817997	+j 0.611919847721094
	-0.289493341235613	+j 0.000000000000000
	-0.234205032817997	-j 0.611919847721094
	-0.089458362200190	-j 0.990107112003389
	h	
K	8.141554238553398	+j 0.000000000000000
zeros	0.000000000000000	+j 0.000000000000000
	0.000000000001143	+j 0.951056515795481
	0.000000000001044	-j 0.951056516783792
	-0.000000000002476	+j 0.587785251278035
	0.000000000000431	-j 0.587785253230156
	f	
K	1.000000000000000	+j 0.000000000000000

Table A.18: 5th order Chebyshev canonic polynomials.

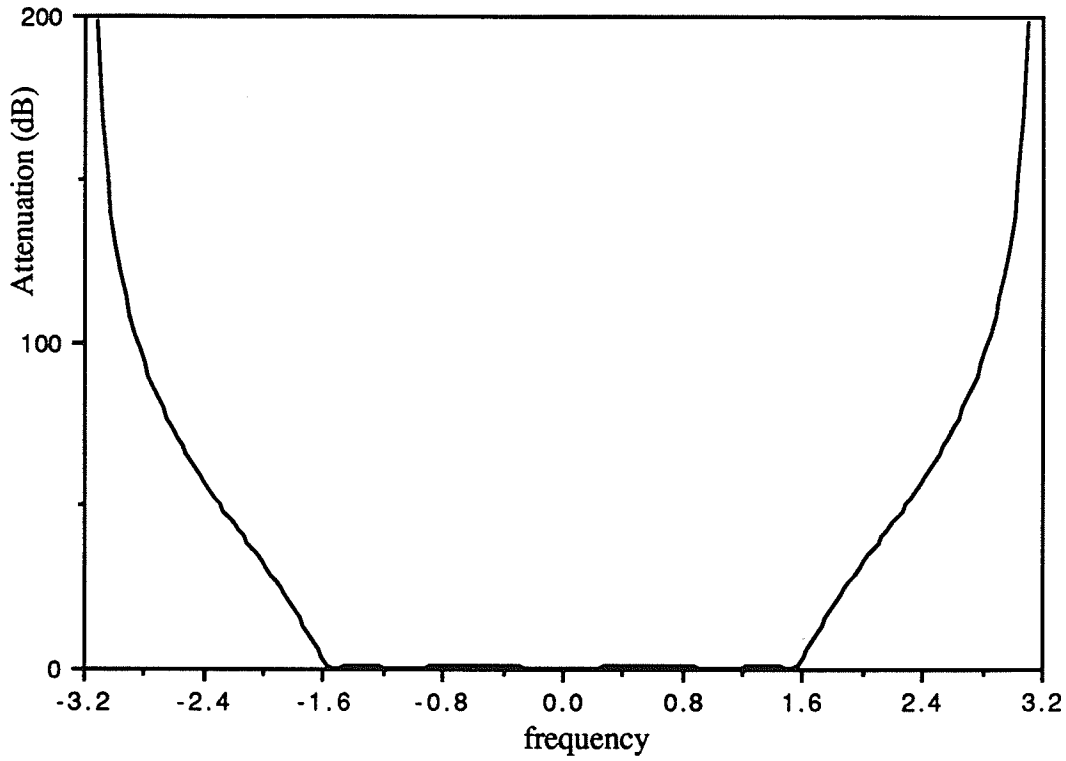

Figure A.2: 5th order Chebyshev fullband plot.

Description: 5 Chebyshev Canonic Parameters				
	Section	$\lvert\rho\rvert$	Arg $\{\rho\}$	d
1	A1	1.00000000	-0.00000000	0.93682013
2	B1	1.00000000	3.14159265	1.83300031
3	A1	1.00000000	0.00000001	0.66646164
4	B1	1.00000000	3.14159264	1.83300031
5	A1	0.99995099	0.00125347	0.93681333

Table A.19: 5th order Chebyshev canonic parameters with real sections.

Description: 5 Chebyshev Canonic Parameters RF 2				
	Section	$\lvert\rho\rvert$	Arg$\{\rho\}$	d
1	A1	1.00000000	-0.00000000	0.93682013
2	B1	1.00000000	3.14159265	0.58471119
3	A1	1.00000000	0.00000000	0.47263477
4	B1	1.00000000	3.14159265	0.49405776
5	A1	0.99996398	0.00092123	0.68850828

Table A.20: 5th order Chebyshev canonic parameters with real sections and port 2 RF.

Description: 5 Chebyshev Canonic Parameters h 45				
	Section	$\lvert\rho\rvert$	Arg$\{\rho\}$	d
1	CB1_INF	1.00000000	0.78539816	0.93682013
2	CB1_INF	1.00000000	-2.35619450	1.83300031
3	CB1_INF	1.00000000	0.78539816	0.66646164
4	CB1_INF	1.00000000	-2.35619450	1.83300031
5	CB1_INF	0.99994945	0.78539822	0.93681370

Table A.21: 5th order Chebyshev canonic parameters with h polynomial scaled by 45 °.

Description: 5 Chebyshev Canonic Parameters h 90				
	Section	$\lvert\rho\rvert$	Arg$\{\rho\}$	d
1	CB1_INF	1.00000000	1.57079633	0.93682013
2	CB1_INF	1.00000000	-1.57079633	1.83300031
3	CB1_INF	1.00000000	1.57079632	0.66646164
4	CB1_INF	1.00000000	-1.57079633	1.83300031
5	CB1_INF	0.99994945	1.57079639	0.93681370

Table A.22: 5th order Chebyshev canonic parameters with h polynomial scaled by 90 °.

Description: 5 Chebyshev Canonic Parameters h 135				
	Section	$\lvert\rho\rvert$	Arg$\{\rho\}$	d
1	CB1_INF	1.00000000	2.35619449	0.93682013
2	CB1_INF	1.00000000	-0.78539817	1.83300031
3	CB1_INF	1.00000000	2.35619449	0.66646164
4	CB1_INF	1.00000000	-0.78539817	1.83300031
5	CB1_INF	0.99994945	2.35619455	0.93681370

Table A.23: 5th order Chebyshev canonic parameters with h polynomial scaled by 135 °.

Description: 5 Chebyshev Canonic Parameters h 180				
	Section	$\lvert\rho\rvert$	Arg$\{\rho\}$	d
1	B1	1.00000000	3.14159265	0.93682013
2	A1	1.00000000	-0.00000001	1.83300031
3	B1	1.00000000	-3.14159265	0.66646164
4	A1	1.00000000	-0.00000001	1.83300031
5	B1	0.99995099	-3.14033918	0.93681333

Table A.24: 5th order Chebyshev canonic parameters with h polynomial scaled by 180 °.

Description: 5 Chebyshev Lumped Element Values				
	Section	L	C	n
1	A1	2.13488154	-	-
2	B1	-	1.09110729	-
3	A1	3.00092291	-	-
4	B1	-	1.09110729	-
5	A1	2.13489704	-	-
6	T0	-	-	0.99973870

Table A.25: 5th order Chebyshev lumped element values.

Description: 5 Chebyshev Lumped Element Values RF 2				
	Section	*L*	*C*	*n*
1	A1	2.13488154	-	-
1	T0	-	-	1.77055967
2	B1	-	3.42049210	-
2	T0	-	-	0.47562502
3	A1	4.23159723	-	-
3	T0	-	-	2.28726851
4	B1	-	4.04810971	-
4	T0	-	-	0.44507747
5	A1	2.90483070	-	-
5	T0	-	-	1.97606445
6	T0	-	-	0.59014317

Table A.26: 5th order Chebyshev lumped element values and port 2 RF.

Description: 5 Chebyshev Lumped Element Values *h* 45				
	Section	*C*	*X1*	*n*
1	CB1_INF	0.31264616	2.41421356	-
2	CB1_INF	0.93131833	-0.41421356	-
3	CB1_INF	0.43947498	2.41421357	-
4	CB1_INF	0.93131833	-0.41421356	-
5	CB1_INF	0.31264835	2.41421336	-
6	T0	-	-	0.99822999

Table A.27: 5th order Chebyshev lumped element values with *h* polynomial scaled by 45°.

Description: 5 Chebyshev Lumped Element Values *h* 90				
	Section	*C*	*X1*	*n*
1	CB1_INF	1.06744077	1.00000000	-
2	CB1_INF	0.54555365	-0.99999999	-
3	CB1_INF	1.50046145	1.00000000	-
4	CB1_INF	0.54555365	-0.99999999	-
5	CB1_INF	1.06744816	0.99999994	-
6	T0	-	-	0.99768900

Table A.28: 5th order Chebyshev lumped element values with *h* polynomial scaled by 90°.

Description: 5 Chebyshev Lumped Element Values *h* 135				
	Section	*C*	*X1*	*n*
1	CB1_INF	1.82223537	0.41421356	-
2	CB1_INF	0.15978897	-2.41421354	-
3	CB1_INF	2.56144792	0.41421356	-
4	CB1_INF	0.15978897	-2.41421354	-
5	CB1_INF	1.82224794	0.41421353	-
6	T0	-	-	0.99843263

Table A.29: 5th order Chebyshev lumped element values with *h* polynomial scaled by 135°.

Description: 5 Chebyshev Lumped Element Values *h* 180				
	Section	*L*	*C*	*n*
1	B1	-	2.13488154	-
2	A1	1.09110729	-	-
3	B1	-	3.00092291	-
4	A1	1.09110729	-	-
5	B1	-	2.13489704	-
6	T0	-	-	1.00002527

Table A.30: 5th order Chebyshev lumped element values with *h* polynomial scaled by 180°.

Description: 5 order Elliptic canonic polynomials		
	g	
K	5.08797927494456309800	+j 0.00000000000000000000
zeros	-0.02355908935830095100	-j 1.00116432437774274600
	-0.18118541125878269200	-j 0.85848241403329607900
	-0.51179432488142946200	+j 0.00000000000000000000
	-0.18118541125878269200	+j 0.85848241403329607900
	-0.02355908935830095100	+j 1.00116432437774274600
	h	
K	5.08797927494456309800	+j 0.00000000000000000000
zeros	-0.00000000000000182050	-j 0.98626463252163675090
	-0.00000000000000182050	+j 0.98626463252163675090
	-0.00000000000003074655	-j 0.78839627515963330840
	-0.00000000000003074655	+j 0.78839627515963330840
	0.00000000000000000000	+j 0.00000000000000000000
	f	
K	1.00000000000000000000	+j 0.00000000000000000000
zeros	0.00000000000000000000	+j 1.06462295875831567000
	0.00000000000000000000	-j 1.06462295875831567000
	0.00000000000000000000	+j 1.33181775809400546300
	0.00000000000000000000	-j 1.33181775809400546300

Table A.31: 5th order Elliptic canonic polynomials.

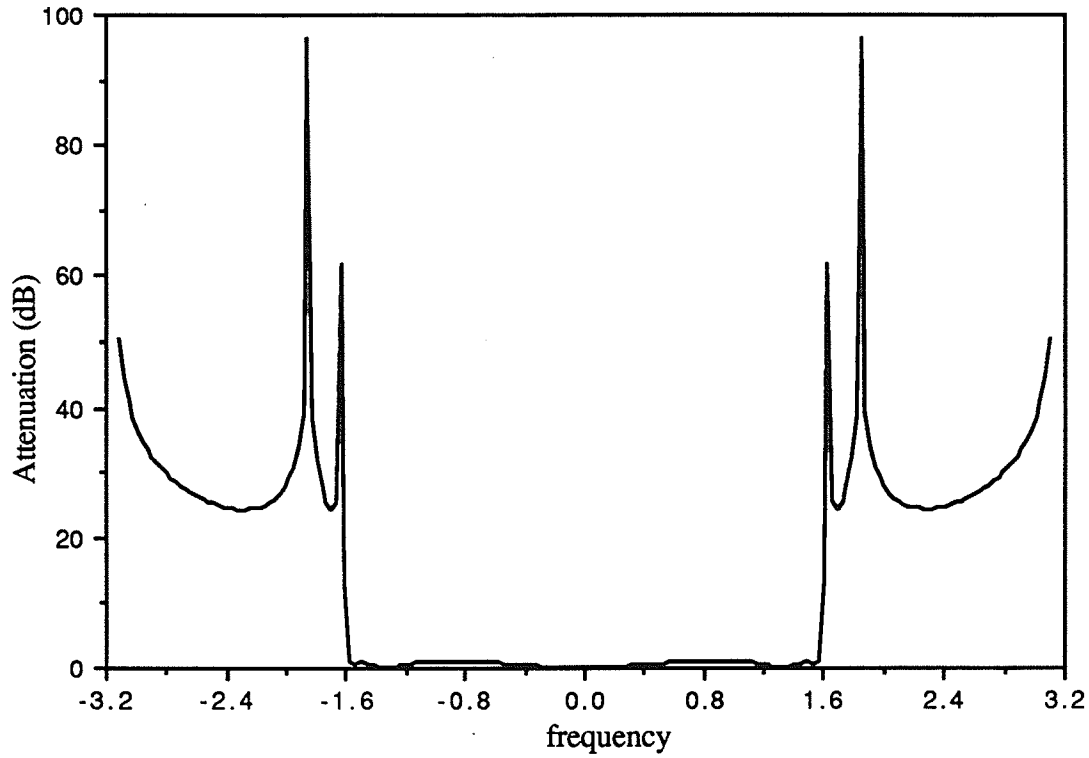

Figure A.3: 5th order Elliptic fullband plot.

Description: 5 Elliptic Canonic Parameters				
	Section	$\lvert\rho\rvert$	Arg$\{\rho\}$	d
1	BRUNE2	0.999999962782041	1.629991081405960	7.967967818455033
2	BRUNE2	0.999999726175078	0.643262157328017	0.783925157938231
3	A1	1.000000000000596	-0.000000000000000	0.921283326122010

Table A.32: 5th order Elliptic canonic parameters with real sections.

Description: 5 Elliptic Canonic Parameters RF port 2				
	Section	$\lvert\rho\rvert$	Arg$\{\rho\}$	d
1	BRUNE2	0.999999962782041	1.629991081405960	7.967967818455033
2	BRUNE2	0.999999775238420	0.514771985615197	0.643463173254037
3	A1	1.000000000000421	-0.000000000000000	0.650211580273026

Table A.33: 5th order Elliptic canonic parameters with real sections and port 2 RF.

Description: 5 Elliptic Canonic Parameters				
	Section	$\lvert\rho\rvert$	Arg$\{\rho\}$	d
1	CA1_jw	0.99999996	1.62999108	7.96796782
2	CA1_jw	0.99999996	1.27933203	7.64530258
3	CA1_jw	0.99999973	0.64326216	0.78392515
4	CA1_jw	0.99999934	1.36287977	1.27881054
5	A1	1.00000000	-0.00000000	0.92128333

Table A.34: 5th order Elliptic canonic parameters with complex section CA1_jw.

Description: 5 Elliptic Canonic Parameters				
	Section	$\lvert\rho\rvert$	Arg$\{\rho\}$	d
1	CB1_jw	0.99999996	1.62999108	7.96796782
2	CB1_jw	0.99999996	1.27933203	7.64530258
3	CB1_jw	0.99999973	0.64326216	0.78392515
4	CB1_jw	0.99999934	1.36287977	1.27881054
5	A1	1.00000000	-0.00000000	0.92128333

Table A.35: 5th order Elliptic canonic parameters with complex section CB1_jw.

Description: 5 Elliptic Canonic Parameters				
	Section	$\lvert\rho\rvert$	Arg$\{\rho\}$	d
1	CC1_jw	0.99999996	1.62999108	7.96796782
2	CC1_jw	0.99999996	-1.39449463	7.85822055
3	CC1_jw	0.99999982	0.40947587	0.52033748
4	CC1_jw	0.99999992	-0.11211207	0.14621906
5	A1	1.00000000	0.00000000	0.04192916

Table A.36: 5th order Elliptic canonic parameters with complex section CC1_jw.

Description: 5 Elliptic Canonic Parameters				
	Section	$\lvert\rho\rvert$	Arg$\{\rho\}$	d
1	CD1_jw	0.99999996	1.62999108	7.96796782
2	CD1_jw	0.99999996	-1.39449463	7.85822055
3	CD1_jw	0.99999982	0.40947587	0.52033748
4	CD1_jw	0.99999992	-0.11211207	0.14621906
5	A1	1.00000000	0.00000000	0.04192916

Table A.37: 5th order Elliptic canonic parameters with complex section CD1_jw.

Description: 5 Elliptic Lumped Element Values				
	Section	*L*	*C*	*n*
1	BRUNE2	0.18641882	3.73619040	1.26674615
2	BRUNE2	1.64448143	0.09264724	3.70040242
3	A1	2.17088483	-	-
4	T0	-	-	1.00000703

Table A.38: 5th order Elliptic lumped element values with real sections.

Description: 5 Elliptic Lumped Element Values RF port 2				
	Section	*L*	*C*	*n*
1	BRUNE2	0.18641882	3.73619040	1.26674615
1	T0	-	-	0.88881273
2	BRUNE2	2.08165351	0.07319021	3.70040239
2	T0	-	-	0.94519296
3	A1	3.07592184	-	-
3	T0	-	-	2.01889124
4	T0	-	-	0.58960259

Table A.39: 5th order Elliptic lumped element values with real sections and port 2 RF.

Description: 5 order Elliptic Lumped Element Values						
	Section	*L*	*C*	*X1*	*X2*	*n*
1	CA1_jw	0.10417811	-	0.94249058	-0.11091040	-
2	CA1_jw	0.14856346	-	1.34404118	0.15816407	-
3	CA1_jw	1.29462172	-	3.00119519	-1.72420019	-
4	CA1_jw	0.53186739	-	1.23297626	0.70835043	-
5	A1	2.17088483	-	-	-	-
6	T0	-	-	-	-	1.00000703

Table A.40: 5th order Elliptic lumped element values with complex section CA1_jw.

Description: 5 order Elliptic Lumped Element Values						
	Section	*L*	*C*	*X1*	*X2*	*n*
1	CB1_jw	-	0.11727959	0.94249058	8.00906374	-
2	CB1_jw	-	0.08224071	1.34404118	-11.42134645	-
3	CB1_jw	-	0.14373231	3.00119519	5.22397145	-
4	CB1_jw	-	0.34985971	1.23297626	-2.14615590	-
5	A1	2.17088483	-	-	-	-
6	T0	-	-	-	-	1.00000703

Table A.41: 5th order Elliptic lumped element values with complex section CB1_jw.

Description: 5 order Elliptic Lumped Element Values						
	Section	*L*	*C*	*X1*	*X2*	*n*
1	CC1_jw	-	8.46899519	0.94249058	0.11091040	-
2	CC1_jw	-	6.68562933	-1.19389631	-0.14049533	-
3	CC1_jw	-	0.27138655	4.81585526	2.76673059	-
4	CC1_jw	-	0.07333974	-17.82060242	-10.23801657	-
5	A1	47.69950569	-	-	-	-
6	T0	-	-	-	-	4.68750344

Table A.42: 5th order Elliptic lumped element values with complex section CC1_jw.

Description: 5 order Elliptic Lumped Element Values						
	Section	*L*	*C*	*X1*	*X2*	*n*
1	CD1_jw	7.52291097	-	0.94249058	-8.00906374	-
2	CD1_jw	9.52961848	-	-1.19389631	10.14545063	-
3	CD1_jw	6.29412230	-	4.81585526	-8.38262384	-
4	CD1_jw	23.29078535	-	-17.82060242	31.01908153	-
5	A1	47.69950569	-	-	-	-
6	T0	-	-	-	-	4.68750344

Table A.43: 5th order Elliptic lumped element values with complex section CD1_jw.

Description: 5 Elliptic Canonic Parameters RF port 2				
	Section	$\lvert\rho\rvert$	Arg $\{\rho\}$	d
1	CC1_jw	0.99999996	1.62999108	7.96796782
2	CC1_jw	0.99999997	-1.51254380	7.03016818
3	CC1_jw	0.99999978	0.50003614	0.64346317
4	CC1_jw	0.99999970	-0.55475288	0.57337790
5	CB1_INF	1.00000000	-0.07233405	0.65021158

Table A.44: 5th order Elliptic canonic parameters with complex sections and port 2 RF.

Description: 5 order Elliptic Lumped Element Values RF port 2						
	Section	*L*	*C*	*X1*	*X2*	*X3*
1	CC1_jw	-	8.46899519	0.94249058	0.11091040	-
1	C0Pi	-	-	-1.27128535	0.06224604	1.12038080
2	CC1_jw	-	6.64339262	-1.06001759	-0.14138855	-
2	C0Pi	-	-	1.01916438	-0.06317338	-0.89816358
3	CC1_jw	-	0.34271148	3.91602220	2.19092010	-
3	C0Pi	-	-	-0.02741367	0.01241781	0.01499076
4	CC1_jw	-	0.30992887	-3.51227234	-2.42266389	-
4	C0Pi	-	-	0.15091498	-0.07158789	-0.07847923
5	CB1_INF	-	0.00402172	-27.63743824	-	-
5	C0Pi	-	-	0.10952143	-0.05505495	-0.05414003
6	C0Pi	-	-	0.08824736	0.06132842	-0.14929640

Table A.45: 5th order Elliptic lumped element values with complex sections and port 2 RF.

Description: 5 Elliptic Canonic Parameters shift -j2				
	Section	$\lvert\rho\rvert$	Arg $\{\rho\}$	d
1	CC1_jw	0.99999996	1.62999108	7.96796782
2	CC1_jw	0.99999996	-1.39449463	7.85822055
3	CC1_jw	0.99999982	0.40947587	0.52033748
4	CC1_jw	0.99999992	-0.11211208	0.14621906
5	A1	1.00000000	0.00000000	0.04192916

Table A.46: 5th order Elliptic canonic parameters with all polynomials shifted by -j2.

Description: 5 Elliptic Canonic Parameters shift -j1				
	Section	$\lvert\rho\rvert$	Arg $\{\rho\}$	d
1	CC1_jw	0.99999996	1.62999108	7.96796782
2	CC1_jw	0.99999996	-1.39449463	7.85822055
3	CC1_jw	0.99999982	0.40947587	0.52033748
4	CC1_jw	0.99999992	-0.11211208	0.14621906
5	A1	1.00000000	0.00000000	0.04192916

Table A.47: 5th order Elliptic canonic parameters with all polynomials shifted by -j1.

Description: 5 Elliptic Canonic Parameters shift j1				
	Section	$\lvert\rho\rvert$	Arg $\{\rho\}$	d
1	CC1_jw	0.99999996	1.62999108	7.96796782
2	CC1_jw	0.99999996	-1.39449463	7.85822055
3	CC1_jw	0.99999982	0.40947587	0.52033748
4	CC1_jw	0.99999992	-0.11211208	0.14621906
5	A1	1.00000000	-0.00000000	0.04192916

Table A.48: 5th order Elliptic canonic parameters with all polynomials shifted by j1.

Description: 5 Elliptic Canonic Parameters shift j2				
	Section	$\lvert\rho\rvert$	Arg $\{\rho\}$	d
1	CC1_jw	0.99999996	1.62999108	7.96796782
2	CC1_jw	0.99999996	-1.39449463	7.85822055
3	CC1_jw	0.99999982	0.40947587	0.52033748
4	CC1_jw	0.99999992	-0.11211208	0.14621906
5	A1	1.00000000	-0.00000000	0.04192916

Table A.49: 5th order Elliptic canonic parameters with all polynomials shifted by j2.

Description: 5 order Elliptic Lumped Element Values shift -j2						
	Section	*L*	*C*	*X1*	*X2*	*n*
1	CC1_jw	-	8.46899519	0.94249058	-0.12623547	-
2	CC1_jw	-	6.68562933	-1.19389631	-0.04880684	-
3	CC1_jw	-	0.27138656	4.81585525	-5.51463461	-
4	CC1_jw	-	0.07333974	-17.82060228	-4.09241234	-
5	A1	47.69950520	-	-	-	-
6	C0_1	-	-	95.39965134	-	4.68750196

Table A.50: 5th order Elliptic lumped element values with all polynomials shifted by -j2.

Description: 5 order Elliptic Lumped Element Values shift -j1						
	Section	*L*	*C*	*X1*	*X2*	*n*
1	CC1_jw	-	8.46899519	0.94249058	1.82717976	-
2	CC1_jw	-	6.68562933	-1.19389631	-0.07244642	-
3	CC1_jw	-	0.27138656	4.81585525	11.10483338	-
4	CC1_jw	-	0.07333974	-17.82060228	-5.84744330	-
5	A1	47.69950520	-	-	-	-
6	C0_1	-	-	47.69982568	-	4.68750196

Table A.51: 5th order Elliptic lumped element values with all polynomials shifted by -j1.

Description: 5 order Elliptic Lumped Element Values shift j1						
	Section	*L*	*C*	*X1*	*X2*	*n*
1	CC1_jw	-	8.46899519	0.94249058	0.05719096	-
2	CC1_jw	-	6.68562933	-1.19389631	-2.31457292	-
3	CC1_jw	-	0.27138656	4.81585525	1.58021822	-
4	CC1_jw	-	0.07333974	-17.82060228	-41.09235201	-
5	A1	47.69950520	-	-	-	-
6	C0_1	-	-	-47.69982568	-	4.68750196

Table A.52: 5th order Elliptic lumped element values with all polynomials shifted by j1.

Description: 5 order Elliptic Lumped Element Values shift j2						
	Section	*L*	*C*	*X1*	*X2*	*n*
1	CC1_jw	-	8.46899519	0.94249058	0.03852930	-
2	CC1_jw	-	6.68562933	-1.19389631	0.15990830	-
3	CC1_jw	-	0.27138656	4.81585525	1.10593711	-
4	CC1_jw	-	0.07333974	-17.82060228	20.40636710	-
5	A1	47.69950520	-	-	-	-
6	C0_1	-	-	-95.39965134	-	4.68750196

Table A.53: 5th order Elliptic lumped element values with all polynomials shifted by j2.

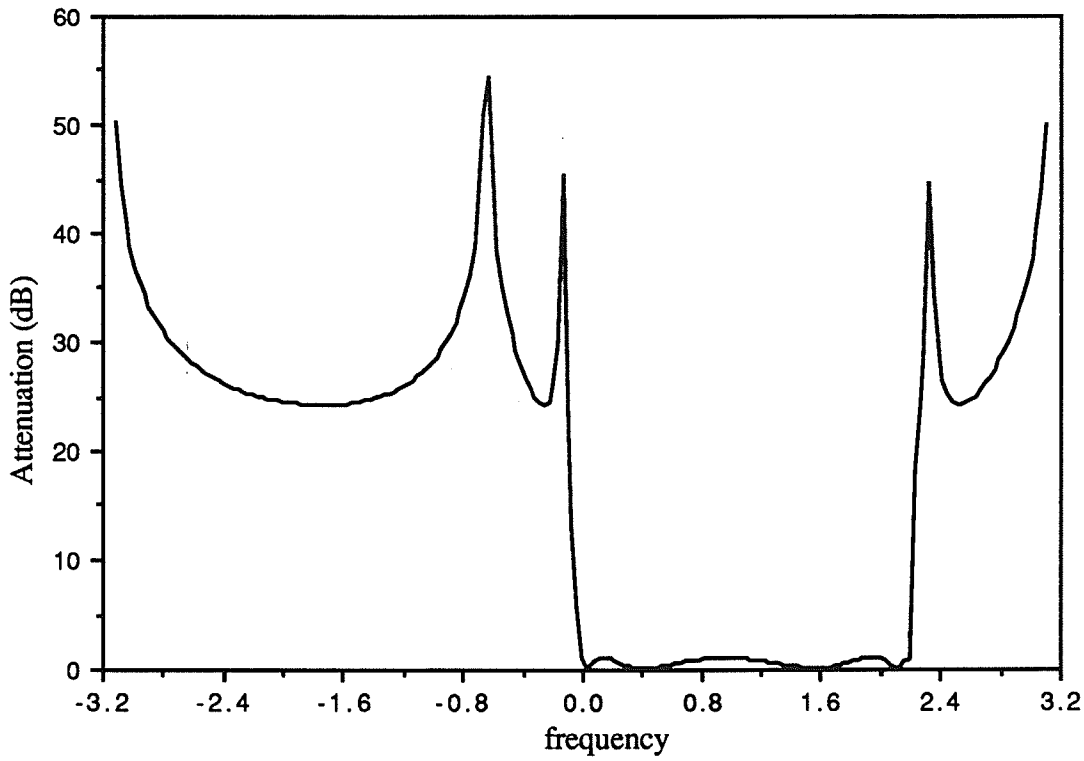

Figure A.4: 5th order Elliptic fullband plot shifted by j1.

Description: 8 order Elliptic canonic polynomials		
	g	
K	2.92790000000000000000e+2	+j 0.00000000000000000000e+0
zeros	-9.10240618156253600000e-3	-j 9.99652231595446578100e-1
	-4.22617940201533620000e-2	-j 9.53923074436400031100e-1
	-1.30371309992933478000e-1	-j 7.89531875177395705000e-1
	-2.74078495771746945000e-1	-j 3.41142083398673628000e-1
	-2.74078495771746945000e-1	+j 3.41142083398673628000e-1
	-1.30371309992933478000e-1	+j 7.89531875177395705000e-1
	-4.22617940201533620000e-2	+j 9.53923074436400031100e-1
	-9.10240618156253600000e-3	+j 9.99652231595446578100e-1
	h	
K	2.92788292286423228900e+2	+j 0.00000000000000000000e+0
zeros	3.92154713768187589800e-3	-j 3.15923479582966877900e-1
	3.92154713768187589800e-3	+j 3.15923479582966877900e-1
	-1.94027679462498836900e-3	-j 7.60528437821750798200e-1
	-1.94027679462498836900e-3	+j 7.60528437821750798200e-1
	-6.44621471045942805800e-4	-j 9.41747166596645102700e-1
	-6.44621471045942805800e-4	+j 9.41747166596645102700e-1
	1.39964140855393075300e-4	+j 9.94886738430446074100e-1
	1.39964140855393075300e-4	-j 9.94886738430446074100e-1
	f	
K	1.00000000000000000000e+0	+j 0.00000000000000000000e+0
zeros	0.00000000000000000000e+0	+j 1.05539762344694012000e+0
	0.00000000000000000000e+0	-j 1.05539762344694012000e+0
	0.00000000000000000000e+0	+j 1.11495205683218050400e+0
	0.00000000000000000000e+0	-j 1.11495205683218050400e+0
	0.00000000000000000000e+0	+j 1.38063010780515952200e+0
	0.00000000000000000000e+0	-j 1.38063010780515952200e+0
	0.00000000000000000000e+0	+j 3.32364350474930916300e+0
	0.00000000000000000000e+0	-j 3.32364350474930916300e+0

Table 54: 8th order Elliptic canonic polynomials.

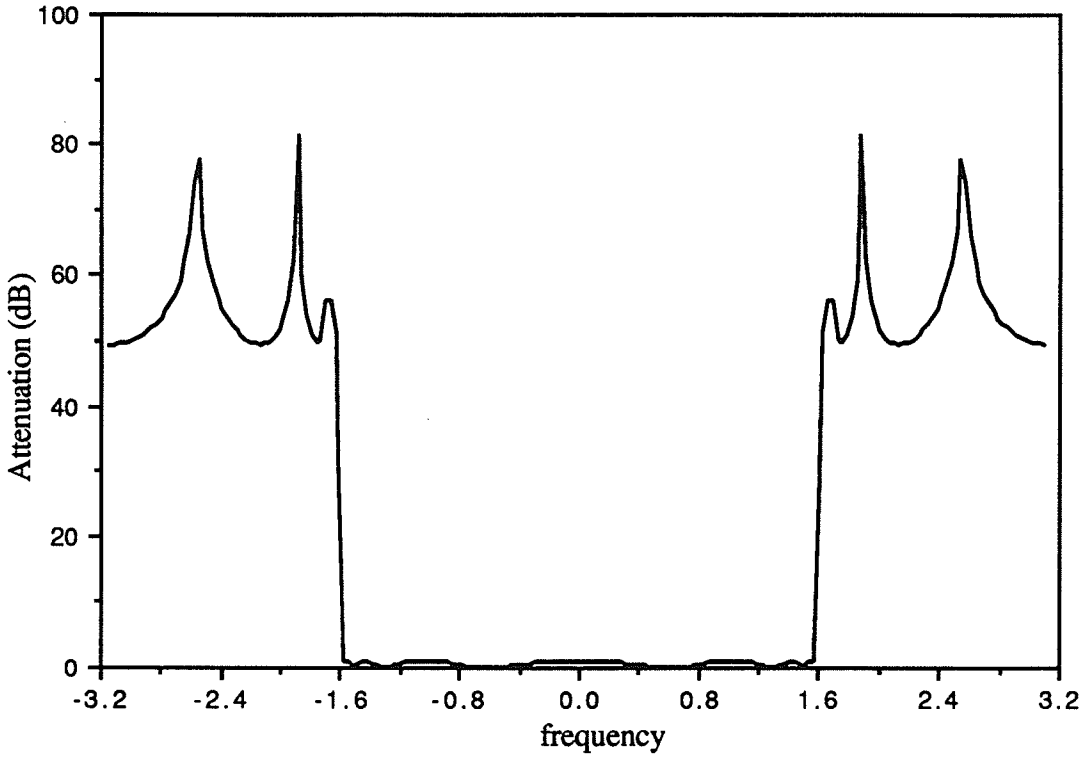

Figure A.5: 8th order Elliptic fullband plot.

Description: 8 Elliptic Canonic Parameters				
	Section	$\lvert\rho\rvert$	Arg $\{\rho\}$	d
1	BRUNE2	1.000000000000000	1.665495050179896	8.466398144178332
2	BRUNE2	1.000000000000000	0.874372974427579	1.812421205592946
3	BRUNE2	1.000000000000000	0.541347707654213	0.558791472457098
4	BRUNE2	1.000000000000000	0.205168413833498	0.066261697254630

Table A.55: 8th order Elliptic canonic parameters with real sections.

Description: **8 Elliptic Canonic Parameters** RF port 2				
	Section	$\lvert\rho\rvert$	Arg $\{\rho\}$	d
1	BRUNE2	1.000000000000000	1.665495050179896	8.466398144178332
2	BRUNE2	1.000000000000000	0.709804007639389	1.539648224519777
3	BRUNE2	1.000000000000000	0.366760710683859	0.388865297197562
4	BRUNE2	1.000000000000000	0.139262839140198	0.045147504946848

Table A.56: 8th order Elliptic canonic parameters with real sections and port two RF.

Description: 8 Elliptic Canonic Parameters				
	Section	$\lvert\rho\rvert$	Arg $\{\rho\}$	d
1	CC1_jw	1.00000000	1.66549505	8.46639814
2	CC1_jw	1.00000000	-1.44223808	8.43432203
3	CC1_jw	1.00000000	0.58059629	1.29592012
4	CC1_jw	1.00000000	-0.26706452	0.62348356
5	CC1_jw	1.00000000	0.07169814	0.07768417
6	CC1_jw	1.00000000	-0.01428074	0.01548577
7	CC1_jw	1.00000000	0.00105485	0.00034308
8	CC1_jw	1.00000000	-0.00004105	0.00001335

Table A.57: 8th order Elliptic canonic parameters with complex sections.

Description: 8 Elliptic Canonic Parameters RF port 2				
	Section	$\lvert\rho\rvert$	Arg $\{\rho\}$	d
1	CC1_jw	1.00000000	1.66549505	8.46639814
2	CC1_jw	1.00000000	-1.54573012	7.52655809
3	CC1_jw	1.00000000	0.69672652	1.53964822
4	CC1_jw	1.00000000	-0.73673516	1.32237806
5	CC1_jw	1.00000000	0.29621996	0.38886530
6	CC1_jw	1.00000000	-0.43382111	0.39443635
7	CC1_jw	1.00000000	0.07562326	0.04514750
8	CC1_jw	1.00000000	-0.14396483	0.06487300

Table A.58: 8th order Elliptic canonic parameters with complex sections and port two RF.

Description: 8 Elliptic Canonic Parameters shift -j2				
	Section	$\lvert\rho\rvert$	Arg $\{\rho\}$	d
1	CC1_jw	1.00000000	1.66549505	8.46639814
2	CC1_jw	1.00000000	-1.44223808	8.43432203
3	CC1_jw	1.00000000	0.58059629	1.29592012
4	CC1_jw	1.00000000	-0.26706452	0.62348356
5	CC1_jw	1.00000000	0.07169814	0.07768417
6	CC1_jw	1.00000000	-0.01428074	0.01548577
7	CC1_jw	1.00000000	0.00105485	0.00034308
8	CC1_jw	1.00000000	-0.00004105	0.00001335

Table A.59: 8th order Elliptic canonic parameters with all polynomials shifted by -j2.

Description: 8 Elliptic Canonic Parameters shift -j1				
	Section	$\lvert\rho\rvert$	Arg $\{\rho\}$	d
1	CC1_jw	1.00000000	1.66549505	8.46639814
2	CC1_jw	1.00000000	-1.44223808	8.43432203
3	CC1_jw	1.00000000	0.58059629	1.29592012
4	CC1_jw	1.00000000	-0.26706452	0.62348356
5	CC1_jw	1.00000000	0.07169814	0.07768417
6	CC1_jw	1.00000000	-0.01428074	0.01548577
7	CC1_jw	1.00000000	0.00105485	0.00034308
8	CC1_jw	1.00000000	-0.00004105	0.00001335

Table A.60: 8th order Elliptic canonic parameters with all polynomials shifted by -j1.

Description: 8 Elliptic Canonic Parameters shift j1				
	Section	$\lvert\rho\rvert$	Arg $\{\rho\}$	d
1	CC1_jw	1.00000000	1.66549505	8.46639814
2	CC1_jw	1.00000000	-1.44223808	8.43432203
3	CC1_jw	1.00000000	0.58059629	1.29592012
4	CC1_jw	1.00000000	-0.26706452	0.62348356
5	CC1_jw	1.00000000	0.07169814	0.07768417
6	CC1_jw	1.00000000	-0.01428074	0.01548577
7	CC1_jw	1.00000000	0.00105485	0.00034308
8	CC1_jw	1.00000000	-0.00004105	0.00001335

Table A.61: 8th order Elliptic canonic parameters with all polynomials shifted by j1.

Description: 8 Elliptic Canonic Parameters shift j2				
	Section	$\lvert\rho\rvert$	Arg $\{\rho\}$	d
1	CC1_jw	1.00000000	1.66549505	8.46639814
2	CC1_jw	1.00000000	-1.44223808	8.43432203
3	CC1_jw	1.00000000	0.58059629	1.29592012
4	CC1_jw	1.00000000	-0.26706452	0.62348356
5	CC1_jw	1.00000000	0.07169814	0.07768417
6	CC1_jw	1.00000000	-0.01428074	0.01548577
7	CC1_jw	1.00000000	0.00105485	0.00034308
8	CC1_jw	1.00000000	-0.00004105	0.00001335

Table A.62: 8th order Elliptic canonic parameters with all polynomials shifted by j2.

Description: 8 Elliptic Lumped Element Values				
	Section	L	C	n
1	BRUNE2	0.17277651	4.15439481	1.25076381
2	BRUNE2	1.05616319	0.34248781	2.22388064
3	BRUNE2	2.09057226	0.04996251	5.02268395
4	BRUNE2	2.80892386	0.00125413	25.69746469
5	T0	-	-	1.63106797

Table A.63: 8th order Elliptic lumped element values with real sections.

Description: 8 Elliptic Lumped Element Values RF port 2				
	Section	L	C	n
1	BRUNE2	0.17277651	4.15439481	1.25076381
1	T0	-	-	0.89048952
2	BRUNE2	1.33190545	0.27158310	2.22388064
2	T0	-	-	0.91808355
3	BRUNE2	3.12783003	0.03339384	5.02268395
3	T0	-	-	1.00679049
4	BRUNE2	4.14609948	0.00084965	25.69746469
4	T0	-	-	1.15735286
5	T0	-	-	1.71220651

Table A.64: 8th order Elliptic lumped element values with real sections and port two RF.

Description: 8 order Elliptic Lumped Element Values					
	Section	*C*	*X1*	*X2*	*n*
1	CC1_jw	9.35056149	0.90951792	0.10133190	-
2	CC1_jw	7.47588106	-1.13759210	-0.12674228	-
3	CC1_jw	0.70578667	3.34742029	1.27077995	-
4	CC1_jw	0.31736716	-7.44426316	-2.82606292	-
5	CC1_jw	0.03889205	27.88277689	18.62352400	-
6	CC1_jw	0.00774328	-140.04637597	-93.54007508	-
7	CC1_jw	0.00017154	1895.99667516	1753.96096522	-
8	CC1_jw	0.00000668	-48722.30760634	-45072.34996735	-
9	T0	-	-	-	585.57828356

Table A.65: 8th order Elliptic lumped element values with complex sections.

Description: 8 order Elliptic Lumped Element Values RF port 2					
	Section	*C*	*X1*	*X2*	*X3*
1	CC1_jw	9.35056149	0.90951792	0.10133190	-
1	C0Pi	-	-1.36927240	0.06077935	1.20796222
2	CC1_jw	7.34252801	-1.02538570	-0.12904414	-
2	C0Pi	-	1.08766736	-0.06152806	-0.96177530
3	CC1_jw	0.87136077	2.75349523	1.02930908	-
3	C0Pi	-	-0.12351690	0.03525460	0.08787963
4	CC1_jw	0.75969659	-2.59076519	-1.18060232	-
4	C0Pi	-	0.21354984	-0.06643184	-0.14506010
5	CC1_jw	0.19876099	6.70229716	3.64411020	-
5	C0Pi	-	0.11867603	-0.06578904	-0.05247728
6	CC1_jw	0.20679634	-4.53766392	-3.50251344	-
6	C0Pi	-	0.09992502	-0.05517509	-0.04450456
7	CC1_jw	0.02260606	26.43428522	13.30946931	-
7	C0Pi	-	0.23834505	-0.19747879	-0.03902923
8	CC1_jw	0.03260515	-13.86827977	-9.22782561	-
8	C0Pi	-	-0.16565683	0.13132347	0.03360235
9	C0Pi	-	0.03558878	-0.01481013	-0.02081081

Table A.66: 8th order Elliptic lumped element values with complex sections and port two RF.

Description: 8 order Elliptic Lumped Element Values shift -j2					
	Section	*C*	*X1*	*X2*	*n*
1	CC1_jw	9.35056149	0.90951792	-0.11321743	-
2	CC1_jw	7.47588106	-1.13759210	-0.04377941	-
3	CC1_jw	0.70578667	3.34742029	-1.60088358	-
4	CC1_jw	0.31736716	-7.44426316	-1.01154837	-
5	CC1_jw	0.03889205	27.88277689	-41.51347728	-
6	CC1_jw	0.00774328	-140.04637597	-38.20123463	-
7	CC1_jw	0.00017154	1895.99667516	4404.16241135	-
8	CC1_jw	0.00000668	-48722.30760632	-28139.45431888	-
9	T0	-	-	-	585.57828868

Table A.67: 8th order Elliptic lumped element values with all polynomials shifted by -j2.

Description: 8 order Elliptic Lumped Element Values shift -j1					
	Section	*C*	*X1*	*X2*	*n*
1	CC1_jw	9.35056149	0.90951792	1.93050609	-
2	CC1_jw	7.47588106	-1.13759210	-0.06507913	-
3	CC1_jw	0.70578667	3.34742029	12.32564912	-
4	CC1_jw	0.31736716	-7.44426316	-1.48983267	-
5	CC1_jw	0.03889205	27.88277689	67.55166609	-
6	CC1_jw	0.00774328	-140.04637597	-54.24792517	-
7	CC1_jw	0.00017154	1895.99667516	2508.79317664	-
8	CC1_jw	0.00000668	-48722.30760638	-34647.72778801	-
9	T0	-	-	-	585.57828715

Table A.68: 8th order Elliptic lumped element values with all polynomials shifted by -j1.

Description: 8 order Elliptic Lumped Element Values shift j1					
	Section	*C*	*X1*	*X2*	*n*
1	CC1_jw	9.35056149	0.90951792	0.05203151	-
2	CC1_jw	7.47588106	-1.13759210	-2.41460715	-
3	CC1_jw	0.70578667	3.34742029	0.66992475	-
4	CC1_jw	0.31736716	-7.44426316	-27.41077241	-
5	CC1_jw	0.03889205	27.88277689	10.80058505	-
6	CC1_jw	0.00774328	-140.04637597	-339.29066907	-
7	CC1_jw	0.00017154	1895.99667516	1348.29362394	-
8	CC1_jw	0.00000668	-48722.30760632	-64469.62406297	-
9	T0	-	-	-	585.57829544

Table A.69: 8th order Elliptic lumped element values with all polynomials shifted by j1.

Description: 8 order Elliptic Lumped Element Values shift j2					
	Section	*C*	*X1*	*X2*	*n*
1	CC1_jw	9.35056149	0.90951792	0.03500214	-
2	CC1_jw	7.47588106	-1.13759210	0.14160826	-
3	CC1_jw	0.70578667	3.34742029	0.45485731	-
4	CC1_jw	0.31736716	-7.44426316	3.56017399	-
5	CC1_jw	0.03889205	27.88277689	7.60574127	-
6	CC1_jw	0.00774328	-140.04637597	208.50907604	-
7	CC1_jw	0.00017154	1895.99667516	1095.02842639	-
8	CC1_jw	0.00000668	-48722.30760635	-113175.80804067	-
9	T0	-	-	-	585.57829285

Table A.70: 8th order Elliptic lumped element values with all polynomials shifted by j2.

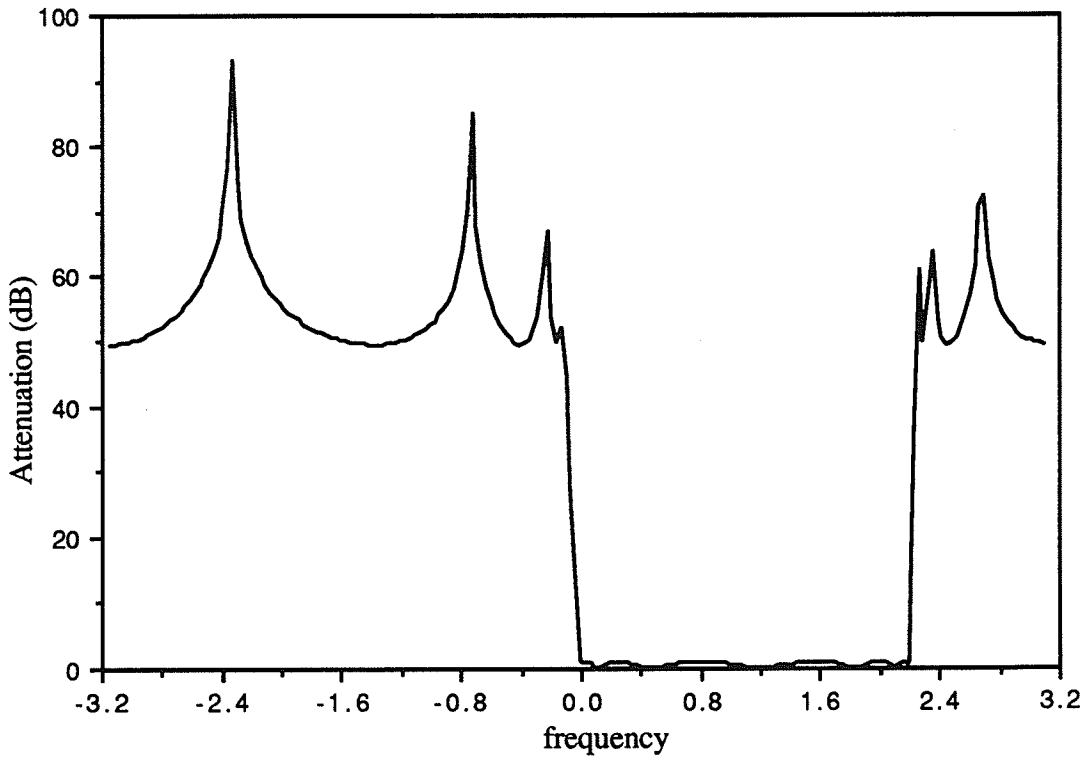

Figure A.6: 8th order Elliptic fullband plot shifted by j1.

Description: 8 Elliptic Canonic Parameters after exchanging the f and h polynomials			
	Section	$\lvert\rho\rvert$	Arg $\{\rho\}$
1	CF1	0.980742178206472	1.274331742082993
2	CF1	0.988066221429816	-2.509997017723201
3	CF1	1.014040586647902	0.127316376085360
4	CF1	1.014707564677322	-0.133355859515346
5	CF1	1.013894267484888	-2.518850656412622
6	CF1	1.014559363421499	2.484287647890324
7	CF1	0.986094488786269	-0.957578854867896
8	CF1	0.985964558905910	0.971081676793818

Table A.71: 8th order Elliptic canonic parameters with f and h polynomials exchanged.

Description: 8 Elliptic Lumped Element Values after exchanging the f and h polynomials						
	Section	C	$X1$	$X2$	R	n
1	CF1	3.83724406	1.35127907	-0.82489500	66.45430766	-
2	CF1	15.86391307	-0.32685426	0.19952980	16.07430627	-
3	CF1	3.60756671	15.68843869	-0.36447704	-142.86371534	-
4	CF1	3.77917706	-14.97603532	0.34792634	-136.37635260	-
5	CF1	113.97752982	-0.32200307	-0.00931636	-13.61055994	-
6	CF1	107.56766659	0.34119095	0.00987152	-14.42160131	-
7	CF1	63.50028264	-1.92663070	0.01582890	112.51425761	-
8	CF1	64.55234314	1.89523088	-0.01557092	110.68052394	-
9	T0	-	-	-	-	1.00342127

Table A.72: 8th order Elliptic lumped element values with f and h polynomials exchanged.

Table A.73: 14th order Elliptic canonic polynomials from [16].

Description: 14 order Elliptic canonic polynomials

	g	h	f
K	3035.622365841900 +j 0.000000000000000	-3035.622365841900 +j 0.000000000000000	1.000000000000000 +j 0.000000000000000
zeros	-0.000011552342827 +j 0.899770211508410	0.899862491900000 +j 0.000000000000000	0.000000000000000 +j 0.899242418100000
	-0.000011552342827 -j 0.899770211508410	-0.899862491900000 +j 0.000000000000000	0.000000000000000 -j 0.899242418100000
	-0.000019199339335 +j 0.899826351481760	0.000000000000000 +j 0.899745096600000	0.000000000000000 +j 0.900482581900000
	-0.000019199339335 -j 0.899826351481760	0.000000000000000 -j 0.899745096600000	0.000000000000000 -j 0.900482581900000
	-0.000019199339335 +j 0.899898648518240	0.000000000000000 +j 0.899771435800000	0.000000000000000 +j 0.899621009700000
	-0.000019199339335 -j 0.899898648518240	0.000000000000000 +j 0.899827047400000	0.000000000000000 -j 0.899621009700000
	-0.000011552342827 +j 0.899954788491590	0.000000000000000 -j 0.899827047400000	0.000000000000000 +j 0.900103990300000
	-0.000011552342827 -j 0.899954788491590	0.000000000000000 +j 0.899897952600000	0.000000000000000 -j 0.900103990300000
	-0.000003493661824 +j 0.899980921048840	0.000000000000000 -j 0.899897952600000	0.000000000000000 +j 0.899675186300000
	-0.000003493661824 -j 0.899980921048840	0.000000000000000 +j 0.899953564200000	0.000000000000000 -j 0.899675186300000
	-0.000003493661824 +j 0.899744078951160	0.000000000000000 -j 0.899953564200000	0.000000000000000 +j 0.900049813700000
	-0.000003493661824 -j 0.899744078951160	0.000000000000000 +j 0.899979903400000	0.000000000000000 -j 0.900049813700000
	-0.899697796104650 +j 0.000000000000000	0.000000000000000 -j 0.899979903400000	0.000000000000000 +j 0.000000000000000
	-0.900027217844070 +j 0.000000000000000		

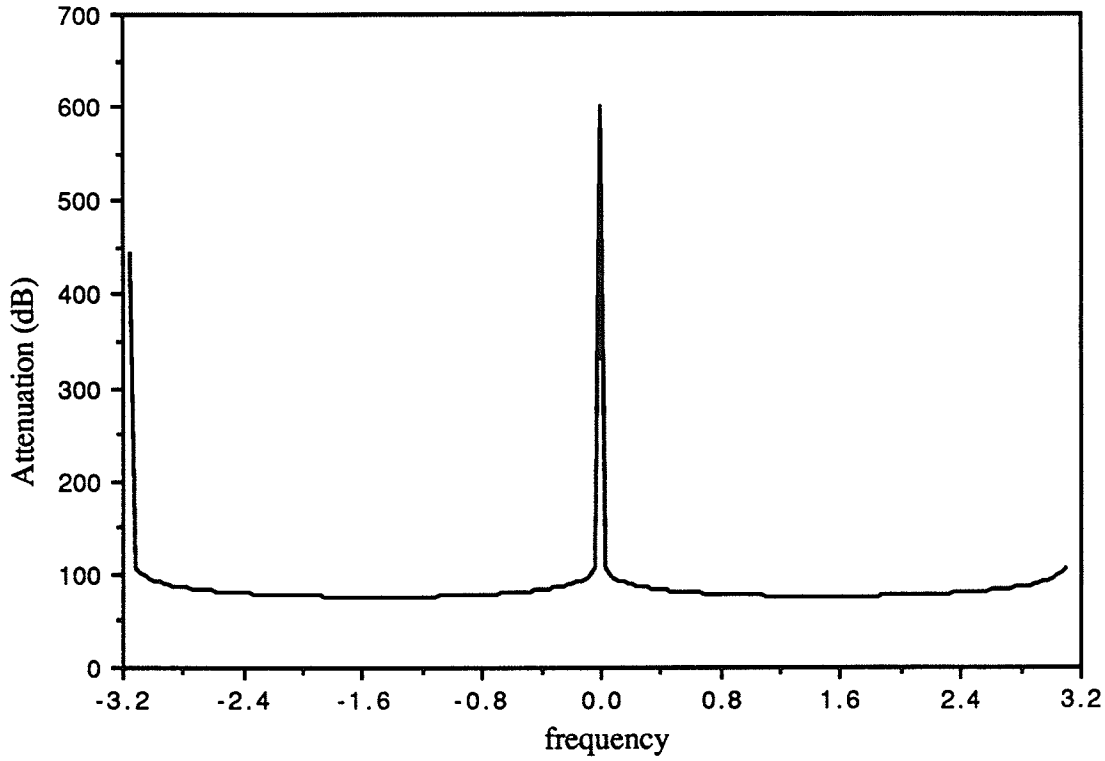

Figure A.7: 14th order Elliptic fullband plot.

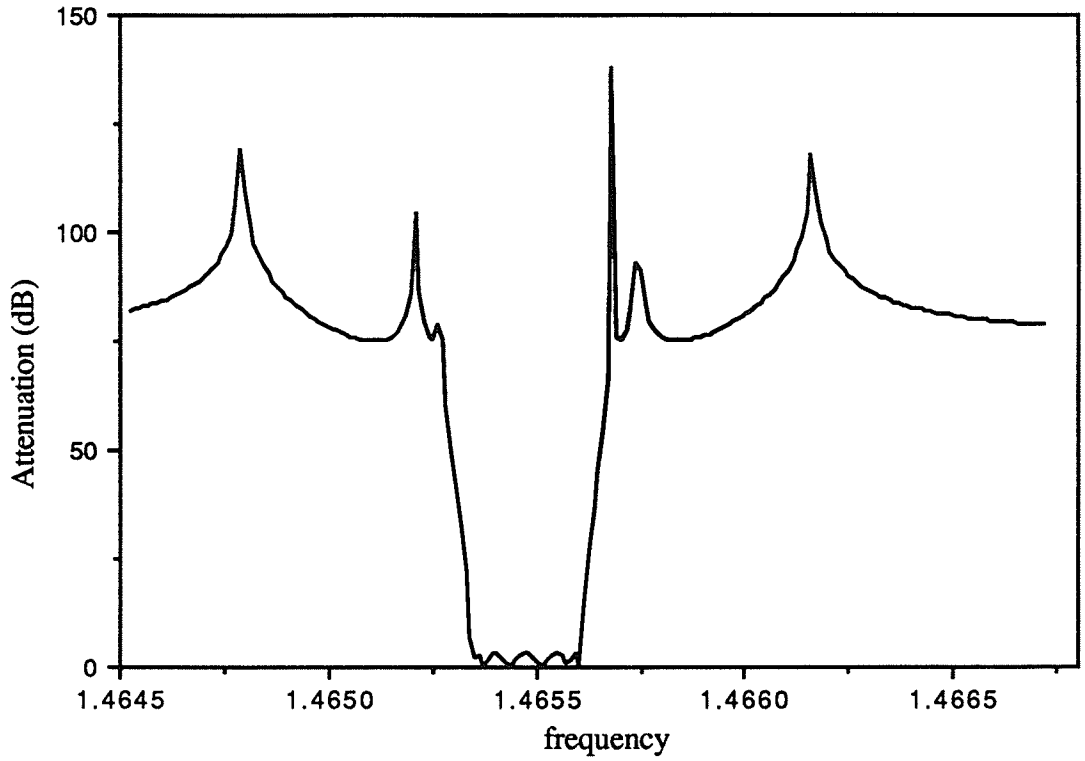

Figure A.8: 14th order Elliptic passband plot.

Description: 14 Elliptic Canonic Parameters				
	Section	$\lvert\rho\rvert$	Arg $\{\rho\}$	d
1	BRUNE2	1.000000000002052	-1.681979728735969	186.399961283533143
2	BRUNE2	1.000000000000619	-1.556678547494451	3.778343341720900
3	BRUNE2	1.000000000000599	-0.989025057559922	1.278142565519755
4	BRUNE2	1.000000000000233	-0.170329074732248	0.223008665527554
5	BRUNE2	1.000000000000475	-0.014400551215495	0.022045889552428
6	BRUNE2	1.000000000000172	-0.002285924171847	0.003750586580709
7	C1	0.999999999999998	-0.000000000000000	0.000489079488471
8	B1	0.999999999988544	3.141592653581955	1.245315419309203

Table A.74: 14th order Elliptic canonic parameters with real sections.

Description: 14 Elliptic Canonic Parameters RF port 2				
	Section	$\lvert\rho\rvert$	Arg $\{\rho\}$	d
1	BRUNE2	1.000000000002052	-1.681979728735969	186.399961283533143
2	BRUNE2	1.000000000000619	-1.568474945067798	3.778709725593045
3	BRUNE2	1.000000000000717	-1.619096743661874	1.528026628888073
4	BRUNE2	1.000000000001370	-1.667257190505580	1.309517521340930
5	BRUNE2	1.000000000032757	-1.675200234594504	1.522622582698051
6	BRUNE2	1.000000000076473	-1.676163956428675	1.631634713196574
7	C1	0.999999999989135	-0.000000000000002	2.470020892415707
8	B1	0.999999999999999	3.141592653589792	0.000136253597376

Table A.75: 14th order Elliptic canonic parameters with real sections and port two RF.

Description: 14 Elliptic Canonic Parameters				
	Section	$\lvert\rho\rvert$	Arg $\{\rho\}$	d
1	CC1_jw	1.000000000002052	-1.681979728735969	186.399961283533143
2	CC1_jw	1.000000000002049	1.693756792492627	186.141954883242989
3	CC1_jw	1.000000000000619	-1.580394540979185	3.778545849694890
4	CC1_jw	1.000000000000567	2.150525283719941	3.161319234433814
5	CC1_jw	1.000000000000600	-2.152262001787222	1.278399400017669
6	CC1_jw	1.000000000000258	2.971192819214553	0.259419809646930
7	CC1_jw	1.000000000000233	-2.971184063883335	0.223111763543324
8	CC1_jw	1.000000000000069	3.127186465078518	0.018952609545458
9	CC1_jw	1.000000000000475	-3.127187582731513	0.022052808070412
10	CC1_jw	1.000000000000160	3.139306059152389	0.003500678895454
11	CC1_jw	1.000000000000176	-3.139306106354442	0.003751613183988
12	CC1_jw	1.000000000000075	3.141152521070623	0.000722143061231
13	CC1_0	0.999999955571538	0.021788480795309	10100.4227611202154
14	B1	1.000000000000000	3.141592653589793	0.000000060292790

Table A.76: 14th order Elliptic canonic parameters with complex sections.

Description: 14 Elliptic Canonic Parameters RF port 2				
	Section	$\lvert\rho\rvert$	Arg$\{\rho\}$	d
1	CC1_jw	1.000000000002052	-1.681979728735969	186.399961283533143
2	CC1_jw	1.000000000002040	1.687237572536880	185.295426511457036
3	CC1_jw	1.000000000000619	-1.568506556262263	3.778709725593082
4	CC1_jw	1.000000000000479	1.845623650424720	2.670241225399191
5	CC1_jw	1.000000000000717	-1.696704350894683	1.528026628888250
6	CC1_jw	1.000000000000415	2.058829601494008	0.417302577419850
7	CC1_jw	1.000000000001370	-2.223081557458250	1.309517521350613
8	CC1_jw	1.000000000000742	1.641229977229385	0.203622222271528
9	CC1_jw	1.000000000032792	-2.872610798183983	1.522622570830383
10	CC1_jw	1.000000000019004	0.949048004133102	0.417142054182997
11	CC1_jw	1.000000000076431	2.932416063605692	1.631634700820653
12	CC1_jw	1.000000000045608	0.449049615099089	0.526752783294113
13	CC1_0	0.999999999989135	-2.090412649781115	2.470020892369623
14	CB1_INF	0.999999999999999	1.051179929809550	0.000136253585757

Table A.77: 14th order Elliptic canonic parameters with complex sections and port two RF.

Description: 14 order Elliptic Lumped Element Values				
	Section	L	C	n
1	BRUNE2	0.01186690	105.45305976	0.98821173
2	BRUNE2	0.93754423	2.41034655	0.54573036
3	BRUNE2	10.95835391	0.71211679	0.15833768
4	BRUNE2	141.29297841	0.10358137	0.08433588
5	BRUNE2	818.13543384	0.00951342	0.15873271
6	BRUNE2	4078.0170209	0.00157259	0.19248719
7	C1	-	0.00024454	-
8	B1	-	1.60601882	-
9	T0	-	-	0.83180234

Table A.78: 14th order Elliptic canonic parameters with real sections.

Description: 14 order Elliptic Lumped Element Values RF port 2				
	Section	*L*	*C*	*n*
1	BRUNE2	0.01186690	105.45305976	0.98821173
1	T0	-	-	1.00591586
2	BRUNE2	0.92654913	2.43894946	0.54573036
2	T0	-	-	1.38693586
3	BRUNE2	5.63001114	1.38607679	0.15833768
3	T0	-	-	2.57457448
4	BRUNE2	10.95149963	1.33637596	0.08433588
4	T0	-	-	3.45708862
5	BRUNE2	5.30587711	1.46691481	0.15873271
5	T0	-	-	2.51115044
6	BRUNE2	4.19405394	1.52907864	0.19248774
6	T0	-	-	2.27904671
7	C1	-	1.23501045	-
7	T0	-	-	1.34525453
8	B1	-	4678.51152935	-
8	T0	-	-	0.00825361
9	T0	-	-	1.05340742

Table A.79: 14th order Elliptic canonic parameters with real sections and port two RF.

Description: 14 order Elliptic Lumped Element Values					
	Section	*C*	*X1*	*X2*	*n*
1	CC1_jw	209.66301014	-0.89456905	0.00530397	-
2	CC1_jw	212.16405783	0.88402363	-0.00524145	-
3	CC1_jw	3.81516405	-0.99044756	0.29107940	-
4	CC1_jw	6.99093245	0.54051730	-0.15885086	-
5	CC1_jw	2.83615641	-0.53939576	0.39193156	-
6	CC1_jw	17.91207510	0.08540667	-0.06205753	-
7	CC1_jw	15.40354615	-0.08541108	0.07212513	-
8	CC1_jw	182.64523037	0.00720322	-0.00608274	-
9	CC1_jw	212.55464763	-0.00720266	0.00522930	-
10	CC1_jw	1339.07276125	0.00114330	-0.00083006	-
11	CC1_jw	1435.11889809	-0.00114327	0.00077419	-
12	CC1_jw	7455.66404259	0.00022007	-0.00014902	-
13	CC1_0	5050.81080967	91.78799087	-	-
14	B1	33171462.09165	-	-	-
15	T0	-	-	-	2.29036542

Table A.80: 14th order Elliptic canonic parameters with complex sections.

Description: 14 order Elliptic Lumped Element Values RF port 2					
	Section	*C*	*X1*	*X2*	*X3*
1	CC1_jw	209.66301014	-0.89456905	0.00530397	-
1	C0Pi	-	-0.89231314	-0.00265201	0.89708804
2	CC1_jw	209.65249598	0.88984742	-0.00530424	-
2	C0Pi	-	0.88294098	0.00265210	-0.88767170
3	CC1_jw	3.77007712	-1.00229240	0.29456046	-
3	C0Pi	-	-1.22875493	-0.14115067	1.65735687
4	CC1_jw	3.66479640	0.75702898	-0.30302247	-
4	C0Pi	-	0.75451695	0.15363393	-1.02722635
5	CC1_jw	1.74746572	-0.88140151	0.63610930	-
5	C0Pi	-	-1.06284473	-0.30077888	2.00438925
6	CC1_jw	0.78571731	0.60130911	-1.41473172	-
6	C0Pi	-	0.68360233	0.68432309	-2.57034557
7	CC1_jw	3.33214007	-0.49452192	0.33341418	-
7	C0Pi	-	-0.39174684	-0.18053803	0.61584030
8	CC1_jw	0.21903705	0.93193523	-5.07212250	-
8	C0Pi	-	1.31342506	1.40473829	3.21669102
9	CC1_jw	42.34443556	-0.13530772	0.02624931	-
9	C0Pi	-	0.19631552	0.08418201	-0.28521099
10	CC1_jw	0.26360401	1.94677375	-4.21659853	-
10	C0Pi	-	23.93515018	0.87211038	1.24822102
11	CC1_jw	74.85328933	0.10497132	0.01484303	-
11	C0Pi	-	0.71231523	0.23145561	-1.13008766
12	CC1_jw	0.27711287	4.37875649	-4.00937580	-
12	C0Pi	-	-1.79301943	0.54657479	0.62951138
13	CC1_0	4.90616120	-0.58000830	-	-
13	C0Pi	-	-1.34834114	-0.26122787	2.48476283
14	CB1_INF	3694.96915594	1.72411341	-	-
14	C0Pi	-	1.78206553	52.58002977	0.58642367
15	C0Pi	-	-1.53780038	0.80775922	-1.71309990

Table A.81: 14th order Elliptic canonic parameters with complex sections and port two RF.

Appendix B

Computer Software

CSYN, CANAL, CLAD and CWD

The computer programs that were used to generate the examples given in the thesis will be discussed in the following. Note that all software was written in the PASCAL computer language for the Macintosh computer using the LightSpeed Pascal compiler. Since the total length of the written code exceeds 20,000 lines, the software listing will not be supplied.

For each program, the required input files, the method of running the program, the options available and the output files generated will be outlined. The four programs that will be discussed are:

- CSYN - complex synthesis of lossless two-port networks using the algorithm given in Chapter III based on the sample characterization.
- CANAL - complex analysis of the *f*, *h*, and *g* polynomials of the sections generated by CSYN.
- CLAD - complex ladder simulation program based on the complex three-port adaptor approach (element-by-element transformation to the complex wave digital domain).
- CWD - complex ladder simulation program based on the canonic cascade section approach (dynamic two-port transformation to the complex wave digital domain).

Note that for all programs, the files representing a particular design are assumed to occupy their own unique folder (directory). Also, by convention, *all files* within a particular folder have the following form

Order FilterType.FileName

where *Order* is the filter order, *FilterType* is the filter type (either Butterworth (butt), Chebyshev (cheb), or Elliptic (ell)), and *FileName* is a particular input or output file. Notice that *FileName* is separated from the remaining part of the complete filename by a period.

All of the various input and output files are identified by *FileName*, for example,

4 ell.CWDFreqResp

refers to a fourth order Elliptic filter frequency response generated by the CWD program. By double clicking on any file within the folder when either of the programs begin running, all of the relevant files will automatically be loaded if they exist.

All frequency response files contain four columns, and they are: the normalized frequency (from -0.5 to 0.5), the actual frequency (from $-\pi$ to $+\pi$), a particular response of the ladder filter (either infinite-precision, scaled, minimal characterization, quantized, etc.), and finally the nominal response generated from the original f and g polynomials. All responses are given as an attenuation, that is

$$- 20.0 * \log_{10} (\text{response} + 1.0\text{e-}30)$$

The quantization process explicitly assumes that all filters are of the type lowpass, however, other filter types can easily be implemented. The four programs will be discussed in the following.

B.1 CSYN - Complex Synthesis of Lossless Two-port Networks

This program generates a real or complex lossless two-port network from the original f, h and g polynomials. The synthesis algorithm outlined in Chapter III is implemented using the sample characterization. All of the elementary first and second order sections given in the tables in Chapter II are realizable sections. The user has the freedom of specifying the h polynomial phase shift and the imaginary axis polynomial shift.

Input Files:

Order FilterType <No FileName>: the nominal polynomial file containing the g, h, and f polynomials (in the order given) of the overall network. The representation of each polynomial is given by

poly. order
poly. complex gain
poly. complex zeros

Order FilterType.dir: the synthesis directives file containing information needed in order to realize a lossless two-port network. The file contains the following:

1. Finite-zero ordering: if finite transmission zeros exist, then the ordering gives the order of the sections realizing

the transmission zeros as referenced to the order given in the *f* polynomial. For example, if a tenth order Elliptic filter is to be realized with 5 Brune sections, then the ordering could be

1 2 3 4 5

(note that the zeros of the *f* polynomial must be ordered in complex conjugate pairs). However, if the filter is to be realized using complex first-order sections, then the following ordering can be used

1 2 3 4 5 6 7 8 9 10

(note that now the zeros of the *f* polynomial do not have to come in complex conjugate pairs). If no finite zeros exist, then this line is not included.

2. The remainder of the file specifies the sections to be used. A separate line is used for each section. Each line consists of an ordered sequence of control codes (separated by spaces) as given in the following:

   The order of the section: this must be given for all sections (either 1 or 2) and it must appear first on a line.

   Transmission zero at infinity: specified by the character 'I'. Any of the following codes may come after this code.

   Capacitor section: specified by the character 'C', this chooses a dynamic section containing a capacitor if a choice between sections is appropriate. A number code follows the 'C' for reciprocal finite transmission zeros with 1=CC1 and 2=CB1 sections. The default is the CC1 section. The 'L' code can not follow this code.

   Inductor section: specified by the character 'L', this chooses a dynamic section containing an inductor if a choice between sections is appropriate. A number code follows the 'L' for reciprocal finite transmission zeros with 1=CD1 and 2=CA1 sections. The default is the CD1 section. The 'C' code can not follow this code.

Reflection-free port: specified by the character 'R', and followed by the port to be made reflection-free (1 or 2). This code can follow any of the other codes.

Output Files:

Order FilterType.sect: contains all information about all of the sections.
Order FilterType.cir: the definition of the synthesized network used by the CLAD ladder simulation program.
Order FilterType.nom: the definition of the nominal network used by the CLAD ladder simulation program.
Order FilterType.anal: information about the sections used by the CANAL analysis program
Order FilterType.CWD: the definition of the synthesized network used by the CWD ladder simulation program.
Order FilterType.CanParm: contains a summary of the canonic parameters for all of the sections.
Order FilterType.LumpParm: contains a summary of the lumped element parameters for all of the sections.
Order FilterType.SDomainPolys: contains a summary of the section analog domain f, h, and g polynomials and, if they exist, the reflection-free polynomials based on the method outlined in Section 2.5 .
Order FilterType.RF_polys: contains a summary of the section analog domain f, h, and g reflection-free polynomials based on the equations given in the tables of Chapter II for the first-order complex sections.

B.2 CANAL - Complex Analog Domain Analysis

The CANAL program analyzes the canonic polynomials of the sections generated by CSYN. The program recombines the polynomials of the sections in order to reconstruct the original f, h, and g polynomials. This is achieved by multiplying the transfer matrices of all of the sections. This operation is performed using the summation form of the polynomials, and thus for higher order systems the reconstructed polynomials will lose accuracy. However, the polynomials give an indication of the validity of the design.

Input Files:

Order FilterType <No FileName>: the nominal polynomial file containing the g, h, and f polynomials (in the order given) of the overall network. The representation of each polynomial is given by

poly. order
poly. complex gain
poly. complex zeros

Order FilterType.anal: the canonic polynomials of each section as derived by the CSYN program.

Output Files:

Order FilterType.anal_data: contains a summary of the canonic polynomials derived.

B.3 CLAD - Complex Ladder Simulation Using Complex 3-port Adaptors

The CLAD program designs and simulates the complex WD realization of the analog network derived using CSYN based on the lumped elements composing the network. The program also determines the quantized network that meets a given set of frequency specifications. Note that only reciprocal networks can be realized, however, they can be non-canonic (for example, a real Elliptic filter without coupled coils).

A network can be scaled for either power waves or voltage waves, however, power wave scaling is recommended. After the values of the real scaling transformers have been determined, the user has the option of either absorbing the transformers into the associated scattering matrices or leaving them external. If the scaling transformers are not absorbed, they will be quantized to the nearest power of two. The user also has the option of absorbing all external multipliers into the associated scattering matrices (shrink the network). At each stage, the user can generate the nominal frequency response if this is desired. After the final nominal version of the Network is derived, the design can be quantized using the frequency specifications and the quantization directives discussed below. The frequency response of the quantized network is generated automatically if a solution is found.

The non-linear optimization procedure used to quantize the network allows the integer denominators of the quantized sections to be different from section to section. All denominators can also be equal, which is perhaps more appropriate for the implementation on a digital signal processor (DSP).

Input Files:

Order FilterType.nom: the nominal polynomial file containing the g and f polynomials (in the order given) of the overall network as well as the number of points used to generate the frequency response. The first line of the file contains the number of frequency points. The second line contains the representation used by the polynomials, either 'zeros' or 'coefficient'. In either case, the representation of the polynomial is first given by the order, and then the gain (for both cases). If the zero form is used, the actual complex zeros are then given. If the coefficient form is used, the complex coefficients are given from the constant term to the higher order term.

Order FilterType.cir: the lossless network lumped element description of the network as derived by CSYN. The first line contains the polynomial imaginary axis shift (usually zero). The second and third lines contain the port one and port two reference impedances as given as complex numbers (usually unity), respectively. The network description starts on line four as discussed below. Each component starts on a new line unless specified otherwise.

1. Connection: this gives the type of connection of the element, either

   'parallel'
   'series'
   'series/parallel' (series connection of elements in parallel)
   'parallel/series' (parallel connection of elements in series)
   'transformer'
   '*'

   The '*' represents the end of the file. Directly following the type of connection is the actual element (unless the connection was a transformer, when the complex turns ratio would follow.
2. Element: this gives the type of element that is connected, either,

   'imag res' (imaginary resistor)
   'inductor'

'capacitor'
'inductor series imag res'
'inductor parallel imag res'
'capacitor series imag res'
' capacitor parallel imag res'

3. Value: this follows the element type. Either one or two real numbers are specified and separated by a space. For the first three choices given above, one real number is needed, while for the remaining choices, two real numbers are given.

Order FilterType.qfre: gives the frequency specifications to be used for the quantization process. More than one set of passband and stopband specifications can be given in order to generate a set of *staircase* specifications. The frequency range under consideration ranges from $-\pi$ to $+\pi$, thus the stopband for a lowpass filter is separated. For this reason the stopband specifications are given in terms of the positive frequencies and the negative frequencies. The form of the file is given below.

1. Passband: the first line gives the number of passband specifications that will be given (usually one). The next line gives the starting freq, the ending frequency, and the maximum attenuation in dB all separated by spaces.
2. Positive Stopband: the number of positive stopband specifications is given (zero is allowed), followed on the next line by the starting frequency and the minimum attenuation that must be achieved between the starting frequency and $+\pi$.
3. Negative Stopband: the number of negative stopband specifications is given (zero is allowed), followed on the next line by the starting frequency and the minimum attenuation that must be achieved between the starting frequency and $-\pi$.

Order FilterType.qdir: gives the quantization directives to be used during the non-linear optimization of the design. The file contains the following,

all_den_equal : boolean
fix_passive_with_wordlength : boolean
number_pass : integer
number_stop_pos : integer

number_stop_neg : integer
number_solutions : integer
maximum_bit_iden.re maximum_bit_iden.im : integer
start_bit_iden : integer
max_bits : integer

1. *all_den_equal*: if true, all integer denominators are equal.
2. *fix_passive_with_wordlength*: if a block of the quantized design is not passive, then if fix_passive_with_wordlength is true the wordlength will be increased in order to facilitate a passive design.
3. *number_pass*: the number of frequency points to check in the passband.
4. *number_stop_pos*: the number of frequency points to check in the positive stopband.
5. *number_stop_neg*: the number of frequency points to check in the negative stopband.
6. *number_solutions*:
7. *maximum_bit_iden.re, maximum_bit_iden.im*: the maximum number of bits that is allowed. Set maximum_bit_iden.im to zero.
8. *start_bit_iden*: the number of bits to use to start the quantization process.
9. *max_bits*: if all_den_equal is false, max_bits gives the maximum difference in bits from the highest bit block to the lowest bit block. If if all_den_equal is true this is ignored.

<u>*Output Files*:</u>

Order FilterType.Adap: the nominal blocks that realize the network, including complex 3-port adaptors and non-dynamic two-ports.
Order FilterType.ScAdap: the nominal scaled network blocks.
Order FilterType.ShAdap: the nominal shrunk network blocks (all external multipliers absorbed).
Order FilterType.QuAdap: the quantized network blocks.
Order FilterType.Resp: the nominal attenuation response.
Order FilterType.ScResp: the nominal scaled attenuation response.
Order FilterType.ShResp: the nominal shrunk attenuation response.
Order FilterType.QuResp: the quantized attenuation response.

B.4 CWD - Complex Ladder Simulation Using the Cascade Section

The CWD program designs and simulates the complex WD realization of the analog network derived using CSYN based on the canonic parameters. The program also determines the quantized network that meets a given set of frequency specifications. Note that reciprocal or non-reciprocal networks can be realized, however, they must be canonic. The user has the option of generating the frequency response of the nominal design based on the cascade section, the representation involving real adaptors and four unimodular multipliers, the minimal characterization and the quantized characterization.

The network can be quantized using the non-linear optimization technique implemented which assumes that the integer denominator of the quantized sections are all equal. The frequency range is assumed to extend from 0.0 to 2π (instead of $-\pi$ to $+\pi$ as will the CLAD program). Thus, in this case the passband is separated into two frequency ranges, which will be referred to as the positive passband (within 0.0 to π) and the negative passband (within 0.0 to π). The stopband is not affected. Again, several sets of frequency specifications can be given in order to form a set of *staircase* specifications.

During the simulation of the quantized filter, the user has the option of using either floating-point signals or binary signals (in which case the number of bits used for the signals must be specified). Note that for comparison purposes, floating-point signals are usually preferred.

The object of the simulation is usually to find the impulse response. The simulation will continue to generate output until the total energy in the states decreases past a constant set by the user. The simulation can also continue past this point to the next integer power of two if the user wishes (in order to generate the frequency response using the FFT).

Input Files:

Order FilterType <no file name>: the nominal polynomial file containing the *g*, *h*, and *f* polynomials (in the order given) of the overall network. The representation of each polynomial is given by

poly. order
poly. complex gain
poly. complex zeros

Order FilterType.CWD: contains the canonic parameters generated from the CSYN program that describe the sections as well as the sections used. The first and the second lines contain the *h* polynomial phase shift and the imaginary axis polynomial shift. The remainder of the file contains the sections. The end of the file is

signified with the character 'N'.

Order FilterType.FreqSpecs: contains the frequency specifications for the quantized network. The file contains information on the positive passband, the negative passband, and the stopband as given in the following.

1. *Positive Passband*: the first line contains the number of positive passband frequency specifications (zero is allowed). The following lines contain the starting frequency, the ending frequency and the maximum attenuation between the frequencies.
2. *Negative Passband*: the first line contains the number of negative passband frequency specifications (zero is allowed). The following lines contain the starting frequency, the ending frequency and the maximum attenuation between the frequencies.
3. *Stopband*: the first line contains the number of stopband frequency specifications. The following lines contain the starting frequency, the ending frequency and the minimum attenuation between the frequencies.

Order FilterType.QuantSpecs: contains the quantization directives to be used during the non-linear optimization process. The file contains the following,

PowerOfTwoWithEnergy : boolean
BinaryCoeff : boolean
LSBitsCoeff : integer
MSBitsCoeff : integer
BinarySignals : boolean
LSBitsSignals : integer
MSBitsSignals : integer
UnderFlowType (set to Truncation)
OverFlowType (set to Saturation)
FreqPointsPerRange : integer
MaxWordLength : integer
MaxEnergy : extended

1. *PowerOfTwoWithEnergy*: if true, the simulation will continue past the MaxEnergy constant to the next integer power of two.
2. *BinaryCoeff*: for quantization purposes, set this to true
3. *LSBitsCoeff*: the starting value of the number of least

significant bits to use for the coefficients.

4. *MSBitsCoeff*: the starting value of the number of most significant bits (in front of the decimal place) to use for the coefficients.
5. *BinarySignals*: if true, the signals will be binary.
6. *LSBitsSignals*: if binary signals is true, this gives the starting value of the number of least significant bits to use for the signals.
7. *MSBitsSignals*: if binary signals is true, this gives the starting value of the number of most significant bits (in front of the decimal place) to use for the signals.
8. *UnderFlowType*: set to Truncation.
9. *OverFlowType*: set to Saturation.
10. *FreqPointsPerRange*: the number of frequency points to check for the frequency specifications for the quantization process in each of the three frequency ranges.
11. *MaxWordLength*: the maximum number of bits that can be used.
12. *MaxEnergy*: the energy required in the states of the filter in order to stop the simulation (around 1.0e-8 for an accurate output).

<u>*Output Files*:</u>

Order FilterType.CWDSect: the nominal sections that realize the network based on the canonic cascade section.

Order FilterType.CWDReSect: the nominal sections that realize the network based on the canonic cascade section composed of two real 2-port adaptors and four unimodular multipliers.

Order FilterType.CWDMinSect: the nominal sections that realize the network based on the minimal characterization of the canonic cascade section.

Order FilterType.CWDQuantSections: the quantized sections that realize the network.

Order FilterType.CWDTimeImpResp: the time domain nominal impulse response of the filter.

Order FilterType.CWDTimeRespNorms: the L_2-norms and the L_∞-norms at the significant signal nodes of the nominal impulse response.

Order FilterType.CWDResp: the nominal attenuation response based on the transfer matrix multiplication.

Order FilterType.CWDMinResp: the nominal attenuation response from the minimal characterization based on the transfer matrix multiplication.

Order FilterType.CWDPartResp: the partial frequency range nominal attenuation response from the minimal characterization based on the transfer matrix multiplication.

Order FilterType.CWDTimeResp: the nominal attenuation response from the minimal characterization based on the FFT of the impulse response.

Order FilterType.CWDPartTimeResp: the partial frequency range nominal attenuation response from the minimal characterization based on the FFT of the impulse response.

Order FilterType.CWDQuantFreqResp: the attenuation response from the quantized network based on the FFT of the impulse response from the quantized simulation.

Order FilterType.CWDQuantNorms: the L_2-norms and the L_∞-norms at the significant signal nodes of the quantized impulse response.

Order FilterType.CWDQuantBitsUsed: a record of the bits used during the quantization process, where the frequency specification were not met and by how much.

Order FilterType.zInvDomainPolys: the canonic polynomials for each section in the z^{-1} domain.

References

[1] A. Fettweis, "Digital filter structures related to classical filter networks," *Arch. Elek. Übertragung*, vol. 25, pp. 79-89, Feb. 1971.

[2] A. Fettweis, "Some principles of designing digital filters imitating classical filter structures," *IEEE Trans. Circuit Theory*, vol. CT-18, pp. 314-316, Mar. 1971.

[3] A. Fettweis, "Pseudopassivity, sensitivity, and stability of wave digital filters," *IEEE Trans. Circuit Theory*, vol. CT-19, pp. 668-673, Nov. 1972.

[4] A. Sedlmeyer and A. Fettweis, "Digital filters with true ladder configuration," *Int. J. Circuit Theory Appl.*, vol. 1, pp. 5-10, Mar. 1973.

[5] A. Fettweis and K. Meerkötter, "Suppression of parasitic oscillations in wave digital filters," *IEEE Trans. Circuits Syst.*, vol. CAS-22, pp. 239-246, Mar. 1975.

[6] A. Fettweis, "Wave digital filters: theory and practise," *Proc. IEEE*, vol.74, pp. 270-327, Feb. 1986.

[7] K. Meerkötter, "Incremental pseudopassivity of wave digital filters," in *Proc. 1st European Signal Processing Conf.* (EUSIP-CO-80), (Lausanne, Switzerland, Sept. 1980), pp. 27-32

[8] A. Fettweis and K. Meerkötter, "On parasitic oscillations in wave digital filters under looped conditions," *IEEE Trans. Circuits Syst.*, vol. CAS-24, pp.475-481, Sept. 1977.

[9] A. Fettweis, "On the connection between muliplier work length limitation and roundoff noise in digital filters," *IEEE Trans. Circuit Theory*, vol. CT-19, pp. 486-491, Sept. 1972.

[10] A. Fettweis, "Roundoff noise and attenuation sensitivity in digital filters with fixed-point arithmetic," *IEEE Trans. Circuit Theroy*, vol. CT-20, pp. 174-175, Mar. 1973.

[11] A. Fettweis, "On the evaluation of roundoff noise in digital filters," *IEEE Trans. Circuits Syst.*, vol. CAS-22, pp. 896, Nov. 1975.

[12] A. Fettweis and K. Meerkötter, "On Adaptors for wave digital filters," *IEEE Trans. Acoust., Speech, Singal Processing*, vol. ASSP-23, pp. 515-525, Dec. 1975.

[13] G. O. Martens and K. Meerkötter, "On n-port adaptors for wave digital filters with applications to bridged-T filters," in *Proc. 1976 IEEE Int. Symp. on Circuits and Systems* (Munich, W. Germany, Apr. 1976), pp. 514-517.

[14] A. Fettweis, "Canonic realization of ladder wave digital filters," *Int. J. Circuit Theory Appl.*, vol. 5, no. 4, pp. 321-332, Dec. 1975.

[15] A. Fettweis, "On sensitivity and roundoff noise in wave digital filters," *IEEE Trans. Acoust., Speech, Singal Processing*, vol. ASSP-22, no. 5, pp. 383-384, Oct. 1974.

[16] M. Jarmasz, "A simplified synthesis of lossless two-port wave digital and analog networks", *Ph. D. Thesis*, University of Manitoba, Winnipeg, Canada, 1990.

[17] C. T. Mullis and R. A. Roberts, "Synthesis of minimum roundoff noise fixed point digital filters." *IEEE Trans. Circuits and Syst.*, vol. CAS-23, pp. 551-562, Sept. 1976.

[18] A. Fettweis, "Passivity and losslessness in digital filtering", *Archiv Für Elektronik und Übertragungstechnik*, vol. 42, no. 1, pp. 1-8, Jan./Feb. 1988.

[19] A. Fettweis, H. Levin, and A. Sedlmeyer, "Wave digital lattice filters," *Int. J. Circuit Theory Appl.*, vol. 2, pp. 203-211, June 1974.

[20] W. Wegener, "On the design of wave digital lattice filters with short coefficient word length and optimal dynamic range," *IEEE Trans. Circuits and Syst.*, vol. CAS-2, pp. 1091-1098, Dec. 1978.

[21] G. O. Martens and M. R. Jarmasz, "Design of digital filters with a diagonal Lyapunov function based on elliptic reference filters," *IEEE Int. Symp. on Circuits and Systems* (Rome, Italy, May 1982), vol. 2, pp. 527-530.

[22] G. O. Martens and H. H. Lê, "Wave digital adaptors for reciprocal second-order sections," *IEEE Trans. Circuits and Syst.*, vol. CAS-25, no. 12, pp. 1077-1083, Dec. 1978.

[23] G. O. Martens, "Voltage scattering matrix analysis of n-ports with application to wave digital filters," in *Proc. 1980 Int. Conf. on Circuits and Computers* (Port Chester, NY, USA, Oct 1980), pp. 1180-1183.

[24] L. Gazsi, "Explicit formulas for lattice wave digital filters," *IEEE Trans. Circuits and Syst.*, vol. CAS-32, pp. 68-88, Jan. 1985.

[25] P. R. Moon and G. O. Martens, "A digital filter structure requiring only m-bit delays, shifters, inverters, and m-bit adders plus simple logic circuitry," *IEEE Trans. Circuits and Syst.*, vol. CAS-27, no. 10, pp. 901-908, Oct. 1980.

[26] A. Fettweis, "Principles of complex wave digital filters," *Int. J. Circuit Theory Appl.*, vol. 9, pp. 119-134, Apr. 1981.

[27] K. Meerkötter, "Complex passive networks and wave digital filters," in *Proc. Eur. Conf. on Circuit Theory and Design* (Warsaw, Poland, Sept. 1980), vol. 2, pp.24-35.

[28] K. Meerkötter, "Antimetric wave digital filters derived from complex reference filters," in *Proc. Eur. Conf. on Circuit Theory and Design* (Stuttgart, W. Germany, Sept. 1983).

[29] P. P. Regalia, S. K. Mitra, and P. P. Vaidyanathan, "The digital allpass filter: a versatile signal processing building block," *Proc. IEEE*, vol. 76, no. 1, pp. 19-37 Jan. 1988.

[30] P. P. Vaidyanathan, P. P. Regalia, and S. K. Mitra, "Design of doubly-complemenary IIR digital filters using a single complex allpass filter, with multirate applications," *IEEE Trans. Circuits and Syst.*, vol. CAS-34, no. 4, pp. 378-389, Apr. 1987.

[31] P. P. Regalia and S. K. Mitra, "Low sensitivity active filter realization using a complex allpass filter," *IEEE Trans. Circuits and Syst.*, vol. CAS-34, no. 4, pp. 390-399, Apr. 1987.

[32] P. I. Richards, "Resistor-transmission-line circuits," *Proc. IRE*, vol. 36, no. 2, pp. 217-220, Feb. 1948.

[33] H. K. Kwan, "Amplitude scaling of arbitrary linear digital networks," *IEEE Trans. Acoust., Speech, Singal Processing*, vol. ASSP-32, pp. 1240-1242, Dec. 1984.

[34] H. J. Orchard, "Loss sensitivities in singly and doubly terminated filters", *IEEE Trans. Circuits and Syst.*, vol. CAS-26, no. 5, pp. 293-297, May 1979.

[35] R. F. Baum, "Design of unsymmetrical band-pass filters", *Proc. IRE*, vol. CT-4, no. 2, pp. 33-40, June 1957.

[36] K.S. Prasad and C. Eswaran, "Limit-cycle free complex biquad recursive digital filters", *IEEE Trans. Circuits and Syst,* vol. CAS-36, no. 2, pp. 280-285, Feb, 1989.

[37] A. Fettweis, "Reciprocity, inter-reciprocity and transposition in wave digital filters", *IEEE Trans. Circuit Theory and Appl.*, vol. 1, pp. 323-337, 1973.

[38] C. Barnes and A. Fam, "Minimum norm recursive digital filters that are free of overflow limit cycles," *IEEE Trans. Circuits and Syst.*, vol. CAS-24, no. 10, pp. 569-574, Oct. 1977.

[39] K. Erichson and A. Michel, "Stability analysis of fixed-point digital filters using computer generated Lyapunov functions - part II: wave digital filters and lattice digital filters," *IEEE Trans. Circuits and Syst.*, vol. CAS-32, no. 2, pp. 132-142, Feb. 1985.

[40] V. Belevitch, *Classical Network Theory*, San Francisco, CA: Holden-Day, 1968.

[41] A. Antoniou, *Digital Filters: Analysis and Design*, New York, NY: McGraw-Hill, 1979.

[42] Z. Nehari, *Conformal Mapping*, New York, NY: McGraw-Hill, 1952.

[43] D. Humphery, *The Analysis, Design, and Synthesis of Electrical Filters*, Englewood Cliffs, NJ: Prentice-Hall, 1970.

[44] C. Chen, *One-Dimensional Digital Signal Processing*, New York, NY: Marcel

Dekker, 1979.

[45] E. Kuh and R. Rohrer, *Theory of Linear Active Networks*, London, EN: Holden-Day, 1969.

[46] R. Newcomb, *Linear Multiport Synthesis*, New York, NY: McGraw-Hill, 1966.

[47] G. Temes and S. K. Mitra, *Modern Filter Theory and Design*, London, EN: John Wiley and Sons, 1973.

[48] P. Saeks, *Generalized Networks*, New York, NY: Holt, Rinehart and Winston, 1972.

[49] M. E. Van Valkenburg, *Introduction to Modern Network Synthesis*, New York, NY: John Wiley and Sons, 1965.

[50] R. A. Roberts and C. T. Mullis, *Digital Signal Processing*, Reading, Massachusetts: Addison-Wesley, 1987.

[51] A. V. Oppenheim and R. W. Schafer, *Digital Signal Processing*, Englewood Cliffs, NJ: Prentice-Hall, 1975.

[52] R. V. Churchill, *Complex Variables and Applications*, New York, NY: McGraw-Hill, 1960.

[53] G. Scarth, "Complex wave digital networks including the implementation of even-order filters", *M.Sc. Thesis*, University of Manitoba, Winnipeg, Canada, 1988.

[54] G. Scarth and G. O. Martens, "Complex wave digital networks using complex port references", in *Proc. IEEE Inter. Conf. on ASSP*, (Glasgow, Scotland, May. 1989), vol. 2, pp. 841-844.

[55] K. Chan, "Cascade synthesis of real and complex lossless two-port networks using transfer scattering matrix factorization", *M.Sc. Thesis*, University of Manitoba, Winnipeg, Canada, 1989.

[56] H. Schutte, "On adaptors for complex wave digital filters", in *Proc. IEEE Inter. Symp. on Circuits and Systems*, (Portland, Oregon, May. 1989), vol. 3 pp. 1644-1647.

[57] private communication.

[58] H. Baher, *Synthesis of Electrical Networks*, New York, John Wiley & Sons, 1984.

[59] A. Fettweis, "Factorization of transfer matrices of lossless two-ports", *IEEE Trans. Circuit Theory*, vol. CT-17, pp. 86-94, Feb. 1970.

[60] A. Fettweis, "Cascade synthesis of lossless two-ports by transfer matrix factorization", in *Proc. Nat. Advanced Study Institute in Network Theory*, R. Boite (Ed), Gordon and Breach, New York, 1972.

[61] J. Williamson, "Transfer matrix factorization using product-form polynomial scattering parameters", *M.Sc. Thesis*, University of Manitoba, Winnipeg, Canada, 1987.

[62] E. Kreyzig, *Advanced Engineering Mathematics*, John Wiley & Sons, 1983.

[63] R. Maruta, A. Kanemasa, H. Sakaguchi, M. Hibino, K. Nakayama, "24 and 120 - channel transmultiplexer built with new digital signal processing LSI's", *IEEE Trans. Com.*, vol. COM-30, July 1982, pp. 1528-1539.

[64] T.J.M. Rossiter, S. Chitsaz, M.J. Gingell, L.D. Humphrey, "A modular transmultiplexer system using custom LSI devices", *IEEE Trans. Com.*, vol. COM-30, July 1982, pp. 1540-1551.

[65] R. Plaruta, A. Tomozawa, "An improved method of digital SSB-FDM modulation and demodulation", *IEEE Trans. Com.*, vol. COM-26, May 1978, pp. 720-725.

[66] T. Aoyama, F. Mano, K. Watabayashi, R. Maruta, A. Tomozawa, "120 channel transmultiplexer design and performance", *IEEE Trans. Com.*, vol. COM-28, Sept. 1980, pp. 1709-1717.

[67] C. Webb, " Design of Wave-State-Variable Lattice Filters", M. Sc. Thesis, University of Manitoba, Winnipeg, Manitoba, Canada, 1988.

[68] P. R. Moon, "On the Reduction of Finite-Wordlength Effects in State-Variable Digital Filters," Ph. D. Thesis, University of Manitoba, Winnipeg, Manitoba, Canada, 1983.

[69] A. Fettweis, "The role of passivity and losslessness in multidimensional digital signal processing- new challenges", in *Proc. IEEE International Symposium on Circuits and System*, (Singapore, June 1991), vol. 1, pp. 112-115.

[70] G. Scarth and G.O. Martens, "Complex wave digital ladder filters using complex port references", in *Proc. IEEE International Symposium on Circuits and System*, (Singapore, June 1991), vol. 5, pp. 2447-2450.

[71] Balabanian and Brickart, *Electrical Network Theory*, New York, NY: John Wiley and Sons, Inc., 1969.

[72] M. Wohlers, *Lumped and Distributed Passive Networks*, New York, NY: Academic Press, 1969.

[73] A. Fettweis, "Realizability of digital filter networks," *Arch. Elek. Übertragung*, vol. 30, pp. 90-96, 1976.

[74] G. Scarth, "Cascade (ladder) realization of complex networks using complex wave digital networks", *Ph.D. Candidacy*, University of Manitoba, Winnipeg, Canada, 1991.

[75] L.E. Franks, *Signal Theory*, Englewood Cliffs, N.J., Prentice-Hall, 1969.

[76] G. Scarth, "Discrete optimization of complex wave digital filters", *Graduate Project*, University of Manitoba, Winnipeg, Canada, 1990.

[77] J. I. Acha and F. Torres,"Realization of complex digital filters based on the LBC two-pair extraction procedure", *Inter. Journal of Circuit Theory and Applications*, vol. 18, pp. 563-575, 1990.